

**Investigation of multiple sclerosis spinal cord using high field MRI with  
multi-transmit technology**

**Hugh Kearney, MB BCh BAO MRCPI**

NMR Research Unit

Queen Square MS Centre

UCL Institute of Neurology

**Thesis submitted for:**

Doctor of Philosophy

Neurology

UCL

**Date of Submission**

**July 2014**

## **Declaration**

I, Hugh Kearney, confirm that the work presented in this thesis is my own.

Where work has been derived from other sources, I confirm that this has been indicated in my thesis.

I obtained the images and clinical data for chapter four from several European centres participating in the MAGNIMS (MAGNetic Imaging in Multiple Sclerosis) collaborative group.

Spinal cord lesion classification in chapter six was done with assistance from Dr Katherine Miszkiel (Consultant Neuroradiologist, National Hospital for Neurology and Neurosurgery, London, UK). Statistical analysis was performed by Dr Daniel R. Altmann (Medical Statistics Department, London School of Hygiene and Tropical Medicine, London, UK).

## **Abstract**

This thesis explores abnormalities in the multiple sclerosis (MS) spinal cord and their relationship with physical disability through the use of conventional and quantitative magnetic resonance imaging (MRI).

Firstly, an hypothesis was tested that spinal cord atrophy would be associated with disability, independently from brain atrophy and lesion load, in long disease duration MS. The results presented confirm that cord atrophy is significantly associated with higher levels of physical disability after more than twenty years of MS.

Following this observation, the next experiment investigated whether a combination of an active surface model (ASM) and high resolution axial images, would provide a more reproducible measure of spinal cord cross-sectional area; compared to previously described methodologies. The results presented show the superior reproducibility of the ASM combined with axial images for the measurement of cord area in MS, which may be of relevance to future clinical trials utilising cord atrophy as an outcome measure.

The pathology of MS in the spinal cord was also explored in several ways using MRI. Firstly, spinal cord lesion morphology was studied, to investigate whether focal lesions, that traversed two or more spinal cord columns and involved the grey matter, would be associated with progressive MS. The results presented confirm this association and also that diffuse abnormalities are more frequently seen in progressive disease.

Secondly, spinal cord lesion load was measured quantitatively on axial images, to investigate if this measure would be associated with disability independently from cord atrophy. The functional importance of focal lesions in MS is highlighted by demonstrating an independent association between lesion load and disability.

Thirdly, magnetisation transfer ratio (MTR) measures of the outer spinal cord were obtained, in an area expected to contain the pia mater and subpial tissue, to investigate whether outer cord abnormalities could be seen in MS compared to healthy controls and if such abnormalities would be associated with cord atrophy. The results presented show that significant decreases in MTR occur in the outer cord early in the disease course, prior to the development of cord atrophy and further decreases in MTR were seen in progressive MS.

Furthermore, an independent association is presented between outer cord MTR and cord atrophy, suggesting that spinal cord meningeal inflammation may be associated with axonal loss in MS.

Lastly, diffusion tensor imaging was used in the spinal cord grey matter, in order to investigate whether microstructural abnormalities in this structure would be associated with physical disability. The results of this study identified an association between grey matter radial diffusivity and disability, independently from cord atrophy, suggesting a significant contribution of spinal cord grey matter pathology to clinical dysfunction.

In summary, this thesis shows that MS spinal cord abnormalities may be visualised and quantified using high field MRI, and are significantly associated with disability. The observations presented may of relevance to future MRI

studies and clinical trials in MS that aim to understand and potentially prevent the pathological processes underlying irreversible physical disability.

## **Acknowledgements**

I would like to express my sincere gratitude to all of the people with multiple sclerosis and healthy controls who volunteered their time to participate in this study.

I would also like to thank the radiographers Marios Yiannakas, Alaine Berry, Luke Hoy and Chichi Ugorji. I would like to acknowledge their assistance, patience and compassion towards all those who participated in this study.

I am indebted to Nils Muhlert, Varun Sethi, David Paling, Rhian Raftopoulos, Moreno Pasin, Frank Riemer, Marie Braisher and Ifrah Iidow for their assistance in image analysis, recruitment and moral support during this study.

The statistical analysis for this study would not have been possible without the ongoing assistance and support from Dr. Daniel Altmann. The recording of spinal cord lesions was also made possible by the expertise and assistance of Dr. Katherine Miszkziel. I also wish to thank Jon Steel for his assistance in answering and addressing the very frequent questions I had about my computer.

The technical aspects of the image analysis also required a large input from the physics team and I would like to thank Drs. Claudia Wheeler Kingshott, Becky Samson, Dan Tozer and Torben Schneider for their support and expertise.

The long duration MAGNIMS study was supervised by Dr. Declan Chard and I would also like to acknowledge the assistance of the other collaborators for their input in this study including: Drs. Rocca, Valsasina, Balk, Sastre-Garriga,

Reinhardt, Ruggieri, Stippich, Sprenger, Tortorella, Gasperini as well as Professors Rovira, Kappos, Polman, Barkhof and Filippi.

I would particularly like to acknowledge the support and help of my two supervisors Dr. Ciccarelli and Professor Miller. An often used Irish expression says that: 'is fada an bóthar nach mbíonn casadh ann' (it's a long road without a turn) and I would like to thank both supervisors, who in their own ways supported me unconditionally through the many twists and turns I encountered in completing this thesis.

## **Publications associated with this thesis**

Kearney H., et al. *Improved MRI quantification of spinal cord atrophy in multiple sclerosis.* J Magn Reson Imaging 2013 2014; 39:617-23

Kearney H., et al. *A pilot MRI study of white and grey matter involvement by multiple sclerosis spinal cord lesions.* Multiple Sclerosis and Related Disorders Volume 2, Issue 2, April 2013:103–108

Kearney H., et al. *Magnetic resonance imaging correlates of physical disability in relapse onset multiple sclerosis of long disease duration.* Mult Scler. 2014 Jan;20(1):72-80

Kearney H., et al. *Investigation of magnetisation transfer ratio-derived pial and subpial abnormalities in the multiple sclerosis spinal cord.* Brain 2014 Sep;137(Pt 9):2456-68.

Kearney H., et al. *Spinal cord grey matter abnormalities are associated with secondary progression and physical disability in multiple sclerosis.* J Neurol Neurosurg Psychiatry 2014 [Epub ahead of print]

Kearney H, et al. *Cervical cord lesion load is associated with disability independently from atrophy in MS.* Neurology 2014 [In press]

## TABLE OF CONTENTS

Declaration

Abstract

Acknowledgements

Publications associated with this thesis

Table of contents

List of tables

List of figures

### 1. The spinal cord and multiple sclerosis

#### 1.1 The spinal cord

1.1.1 External structure

1.1.2 Internal structure

1.1.3 Physiology

#### 1.2 Multiple sclerosis

1.2.1 Natural history

1.2.2 Environmental factors

1.2.3 Genetics

1.2.4 Pathology

1.2.5 Diagnosis

1.2.6 Differential diagnosis

### 2. Magnetic Resonance Imaging

#### 2.1 Magnetic resonance imaging principles

2.2 T1 – longitudinal relaxation

2.3 T2 – transverse relaxation

2.4 Pulse sequences

2.5 Spin Echo sequences

## 2.6 Gradient Echo sequences

## 2.7 Image contrast

### 2.7.1 T-weighted imaging

### 2.7.2 T2-weighted imaging

### 2.7.3 Proton density imaging

## 3. Spinal cord magnetic resonance imaging in multiple sclerosis

### 3.1 Introduction

#### 3.1.1 Spinal cord imaging in clinically isolated syndrome

### 3.2 Utility of spinal cord MRI in diagnosis

### 3.3 Spinal cord atrophy on MRI

### 3.4 Association between spinal cord MRI abnormalities and disability

### 3.5 Inversion recovery MRI in the spinal cord

#### 3.5.1 Short T1 inversion recovery

#### 3.5.2 Phase sensitive inversion recovery

#### 3.5.3 Double inversion recovery imaging

### 3.6 Quantitative spinal cord MRI

#### 3.6.1 Magnetic resonance spectroscopy

#### 3.6.2 Magnetisation transfer imaging

#### 3.6.3 Diffusion weighted imaging

## 4. Spinal cord atrophy in long disease duration multiple sclerosis

### 4.1 Introduction

### 4.2 Methods

#### 4.2.1 Patients

#### 4.2.2 MRI acquisition

#### 4.2.3 Image analysis

#### 4.2.4 Statistical analysis

### 4.3 Results

- 4.3.1 Correlations between MRI features
- 4.3.2 MRI features and clinical subgroups
- 4.3.3 MRI features and physical disability (EDSS)

#### 4.4 Discussion

### 5. Evaluation of methodologies for improved quantification of spinal cord atrophy

#### 5.1 Introduction

#### 5.2 Methods

##### 5.2.1 Subjects

##### 5.2.2 MRI Protocol

##### 5.2.3 Image Analysis

###### 5.2.3.1 Calculation of relative contrast

###### 5.2.3.2 Reproducibility

##### 5.2.4 Statistics

###### 5.2.4.1 Reproducibility

###### 5.2.4.2 Change in cord area over six months and correlation with disability at baseline

###### 5.2.4.3 Sample size calculation for clinical trials

#### 5.3 Results

##### 5.3.1 Comparison of relative contrast between PSIR and 3D-TFE

##### 5.3.2 Differences between groups at baseline

##### 5.3.3 Reproducibility

##### 5.3.4 Change in cord area over six month follow up and correlation with disability at baseline

##### 5.3.5 Sample size calculations

#### 5.4 Discussion

##### 5.4.1 Limitations and future directions

6. Spinal cord lesion identification:

(i) A Pilot study to evaluate two high resolution axial sequences for spinal cord lesion detection in multiple sclerosis

6.1 Introduction

6.2 Methods

6.2.1 Subjects

6.2.2 MRI protocol

6.2.3 Image analysis

6.2.3.1 Lesion identification and location

Lesion area and length

6.3 Results

6.4 Discussion

(ii) An investigation of cervical spinal cord lesion location and extent in subtypes of multiple sclerosis

6.5 Introduction

6.6 Methods

6.6.1 Subjects

6.6.2 MRI protocol

6.6.2.1 Spinal cord acquisitions

6.6.2.2 Brain acquisition

6.6.3 Image analysis

6.6.3.1 Focal lesions

6.6.3.2 Diffuse abnormalities

6.6.4 Statistical analysis

6.6.4.1 Comparison of focal lesion characteristics, GM involvement and diffuse abnormalities between CIS and MS subtypes

6.6.4.2 Investigation of independent associations between spinal cord lesion characteristics and physical disability

## 6.7 Results

6.7.1 Demographics of CIS and MS groups

6.7.2 Number of spinal cord lesions recorded

6.7.3 Lesion characteristics by MS subtype

6.7.4 Independent associations between EDSS and spinal cord lesion characteristics

## 6.8 Discussion

6.8.1 Association of more extensive focal lesions and diffuse abnormalities with progressive MS

6.8.2 Lesions involving lateral columns and grey matter are independently associated with disability

6.8.3 Limitations and future directions

6.8.4 Conclusions

## 7. Investigation of associations between spinal cord lesion load, magnetisation transfer ratio and physical disability

### 7.1 Introduction

### 7.2 Methods

7.2.1 Subjects

7.2.2 MRI protocol

7.2.3 Image analysis

7.2.3.1 Upper cervical cord lesion load and cross-sectional area

7.2.3.2 MTR analysis

7.2.3.3 Brain image analysis

7.2.4 Statistical analysis

### 7.3 Results

- 7.3.1 Subjects and MRI measures
- 7.3.2 Reproducibility analysis
- 7.3.3 Comparison of MRI parameters between MS and controls
- 7.3.4 Associations between MRI measures and disability
- 7.3.5 Associations with disability in MS patients with EDSS  $\leq 6$

## 7.4 Discussion

- 7.4.1 Association of cord lesion-load with progressive MS and disability
- 7.4.2 Associations between other MRI measures and disability
- 7.4.3 Association of demographic features and disability
- 7.4.4 Spinal cord MRI findings in primary and secondary progressive MS
- 7.4.5 Study limitations
- 7.4.6 Conclusions

## 8. Investigation of magnetisation transfer ratio-derived pial and subpial abnormalities in the multiple sclerosis spinal cord

### 8.1 Introduction

### 8.2 Methods

- 8.2.1 Subjects
- 8.2.2 MRI protocol
- 8.2.3 Image analysis
  - 8.2.3.1 MTR values
  - 8.2.3.2 Spinal cord area
  - 8.2.3.3 Brain scan analysis
- 8.2.4 Statistical analysis

### 8.3 Results

- 8.3.1 Subjects and their clinical and conventional MRI characteristics
- 8.3.2 Comparison of cord area and brain volume between groups

- 8.3.3 Comparison of outer spinal cord WM MTR values within each subject group
- 8.3.4 Comparison of spinal cord WM and GM MTR values within each subject group
- 8.3.5 Outer spinal cord MTR in controls versus patient subgroups
- 8.3.6 Spinal cord WM and GM MTR in controls versus patient subgroups
- 8.3.7 Outer spinal cord MTR: comparison between patient subgroups
- 8.3.8 Univariate correlations and associations between MTR measures and cord area in all MS patients combined
- 8.3.9 Univariate correlations between MRI parameters and disability in all MS patients combined
- 8.3.10 Independent associations between MRI parameters and disability in all MS patients combined

#### 8.4 Discussion

- 8.4.1 The outer spinal cord MTR measure and what it reflects anatomically
- 8.4.2 Higher outer than WM spinal cord MTR in healthy controls
- 8.4.3 Outer spinal cord MTR abnormalities in CIS and RRMS in the absence of cord atrophy
- 8.4.4 Association of outer spinal cord MTR with cord atrophy and progressive MS
- 8.4.5 Associations between spinal cord MRI and disability measures
- 8.4.6 Limitations and future directions

### 9. Spinal cord grey matter abnormalities are associated with secondary progression and physical disability in multiple sclerosis

#### 9.1 Introduction

#### 9.2 Methods

- 9.2.1 Subjects
- 9.2.2 MRI protocol
- 9.2.3 Image analysis

9.2.3.1 Diffusion tensor imaging (DTI) analysis

9.2.3.2 Conventional MRI analysis

9.2.4 Statistical analysis

9.3 Results

9.3.1 Demographics and conventional MRI scans

9.3.2 Reproducibility of spinal cord GM segmentation and white matter region of interest placement

9.3.3 DTI measures in controls versus patient subgroups

9.3.4 Linear trend test analysis of standardised DTI measures across CIS, RRMS and SPMS subgroups

9.3.5 Univariable correlations with disability

9.3.6 Independent associations with physical disability

9.4 Discussion

9.4.1 Spinal cord grey matter findings

9.4.2 Spinal cord white matter findings

9.4.3 Study limitations

9.4.4 Conclusions

10. Summary

10.1 Atrophy

10.2 Lesions

10.3 Lesion load

10.4 Meningeal and subpial abnormality (MTR)

10.5 Grey matter (DTI)

10.6 Future questions

10.7 Conclusions

## LIST OF TABLES

- 3.1 McDonald MRI criteria to demonstrate dissemination of lesions in time
- 3.2 McDonald MRI criteria to demonstrate brain abnormalities and demonstration of dissemination in space
- 3.3 The 2010 McDonald criteria for diagnosis of multiple sclerosis
- 4.1 MRI parameters in each participating centre
- 4.2 Patient demographics by centre
- 4.3 Patient demographics by EDSS category
- 4.4 MRI parameters in benign and 'non-benign' RRMS and SPMS
- 4.5 Comparison of MRI parameters between benign and 'non-benign' RRMS and SPMS using ANOVA
- 5.1 Intra-observer reproducibility in all subjects (COV: coefficient of variation)
- 5.2 Inter-observer reproducibility in all subjects
- 5.3 Scan-rescan reproducibility in all subjects
- 5.4 Longitudinal cord area measures in patients
- 5.5 Longitudinal cord area measures in controls
- 5.6 Correlation with EDSS at baseline (15 patients)
- 5.7 Calculation of differences between longitudinal changes in patients and controls to estimate treatment effect
- 5.8 Estimated sample sizes per arm for six month (m) and 12 month placebo-controlled treatment trials
- 6.1 Spinal cord lesion number and location in all MS patients and clinical subgroups
- 6.2 Mean ( $\pm$ SD) Lesion area and length in white matter columns
- 6.3 Classification system used for focal spinal cord lesions identified on axial scans
- 6.4 A list of all MRI variables that were tested prior to construction of the final regression model investigating independent associations between spinal cord lesion variables with EDSS
- 6.5 6.5 Demographics of all CIS and MS patients recruited for this study. Data represents mean  $\pm$  standard deviation (SD).

- 6.6a Number (percentage) of lesion types I-IV recorded in each clinical subgroup
- 6.6b The number (percentage) of lesions involving the spinal cord grey matter and each column of the spinal cord in each clinical subgroup. Note: the numbers in this table do not add to the total number of lesions, since some lesions seen involved more than one column e.g. extension into the lateral and posterior column by the same lesion
- 6.7a Number (percentage) of people with CIS or MS with spinal cord lesions, each lesion type, spinal cord grey matter involvement and diffuse abnormalities
- 6.7b Mean, median (range) of the number of spinal cord lesions in each category and involving the grey matter seen in each person with CIS and MS
- 7.1 Demographics of cohort studied presented as mean  $\pm$  standard deviation
- 7.2 Mean  $\pm$  standard deviation of MRI parameters in each group studied.
- 8.1 Demographics and conventional magnetic resonance imaging parameters in healthy controls, CIS and MS.
- 8.2 Mean MTR values ( $\pm$  standard deviation) of spinal cord region subtypes (outer cord, white matter, grey matter) in the control group and in each patient group. The CIS cohort is presented with and without the two cases of myelitis included
- 8.3 Comparison of MTR values between patient and control groups using a linear regression model adjusted for age, gender and cord area
- 8.4 Significant ( $p < 0.01$ ) univariate correlations between MRI parameters and disability measure in all MS patients combined
- 8.5 Summary of MRI parameters significantly associated with disability measures from linear regression models using disability as dependent variable
- 9.1 Demographic and conventional MRI features of all participants. Presented as mean  $\pm$  standard deviation
- 9.2 Mean  $\pm$  standard deviation of DTI measures in patients and controls. Significantly different from controls, ANOVA with post hoc Bonferonni correction: \*  $p < 0.05$ ; \*\*  $p < 0.01$ ; \*\*\*  $p < 0.001$
- 9.3 Univariable correlations (r values presented) between DTI metrics and physical disability, significant correlations are highlighted in bold font: \*  $p < 0.05$ ; \*\*  $p < 0.01$ ; \*\*\*  $p < 0.001$ . (EDSS: expanded disability status scale, 25ft TWT: 25 foot timed walk test, 9-HPT: 9 hole peg test)
- 9.4 Significant univariable correlations between DTI metrics and physical disability. Significant correlations are highlighted in the table in bold font: \*  $p < 0.05$ ; \*\*  $p < 0.01$ ; \*\*\*  $p < 0.001$ . (ASIA: American spinal injury association)

## FIGURES

- 2.1 T1 relaxation of brain grey and white matter (image from [www.mcauslander.sc.edu](http://www.mcauslander.sc.edu))
- 2.2 T2 (transverse relaxation) of grey matter, white matter, blood and CSF (image from [www.mcauslander.sc.edu](http://www.mcauslander.sc.edu))
- 3.1 Sagittal T2-weighted T2 MRI of cervical cord with MS lesion
- 3.2 Axial T2-weighted MRI of the cervical spinal cord with MS lesion
- 3.3 Sagittal 3D T1-weighted cervical spine MRI: used in calculating spinal cord area in MS
- 3.4 Sagittal STIR image of cervical spine showing MS lesion in the cervical cord
- 3.5 Axial PSIR of healthy cervical spinal cord at the level of C2/C3
- 3.6 Axial PSIR of MS cervical spinal cord with lesion visible in the lateral column of the white matter
- 3.7 MTR imaging in healthy cervical spinal cord
- 4.1 Graphs of spinal cord area (A), T2 lesion volume (B), white matter fraction (C) and grey matter fraction (D) against EDSS
- 5.1 3D-TFE  $1 \times 1 \times 1 \text{mm}^3$  voxels 6min 30secs 16 channel NV coil. A: sagittal view. B: Axial 3D-TFE reconstruction at C2/C3
- 5.2 PSIR  $0.5 \times 0.5 \times 3 \text{mm}^3$  acquired with 16 channel NV coil
- 5.3 Spinal cord outlined using ASM. A: axially reformatted 3D-TFE B: PSIR
- 5.4 Calculation of CNR with ROI placed in CSF and on spinal cord. A: PSIR B: 3D-TFE
- 6.1 Survey image demonstrating coverage of axial images acquired in this study
- 6.2 Axial cervical cord MRI (A) FFE and (B) PSIR in a healthy control showing central grey matter and white matter columns. (C) Sagittal T2 weighted image
- 6.3 Axial cervical cord MRI (A) FFE and (B) PSIR in a MS patient showing (i) a WM-GM lesion involving the anterior column lesion and ventral horn of GM and (ii) a GM-WM lesion in the left lateral column and extending to adjacent dorsal horn and posterior column. (C) Sagittal T2 weighted image
- 6.4 Axial cervical cord MRI (A) FFE and (B) PSIR in a MS patient showing a WM-GM lesion involving the left lateral column and adjacent dorsal horn GM. (C) Sagittal T2 weighted image

- 6.5 Axial cervical cord MRI (A) FFE and (B) PSIR demonstrating diffuse changes seen in both lateral columns and posterior column on the FFE sequence. These were seen on 3 consecutive FFE slices at the C2/C3 level in the absence of focal lesions at the same level. (C) Sagittal T2 weighted image shows a focal lesion at C3-4 only
- 6.6 Axial cervical cord MRI (A) FFE and (B) PSIR in a MS patient showing a WM-only lesion in the right lateral column. (C) Sagittal T2 weighted image
- 6.7 Axial cervical cord MRI (A) FFE and (B) PSIR in a MS patient showing a WM-GM lesion involving posterior column and adjacent left dorsal horn GM; the GM involvement is more clearly evident on PSIR. (C) Sagittal T2 weighted image
- 6.8 Axial cervical cord MRI (A) FFE and (B) PSIR in a MS patient showing a WM-only lesion in the posterior column. (C) Sagittal T2 weighted image
- 6.9 Three cases of lesions involving a single spinal cord column restricted to the white matter (Type I lesions). 1A-C: 3D-FFE 0.5 x 0.5 mm<sup>2</sup> in plane resolution, 1D-F: 3D-PSIR 0.5 x 0.5 mm<sup>2</sup> in plane resolution. Focal lesions are marked may yellow single chevron and are located in the left lateral column (Figures A/D and C/F) and in the right lateral column (Figures B/E and C/F)
- 6.10 Three cases of lesions involving a single spinal cord column also involving the grey matter (Type II lesions). 2A-C: 3D-FFE 0.5 x 0.5 mm<sup>2</sup> in plane resolution, 2D-F: 3D-PSIR 0.5 x 0.5 mm<sup>2</sup> in plane resolution. Diffuse abnormalities are demonstrated on the 3D-FFE images 2B and 2C in the right lateral column indicated by a double chevron. Focal lesions involving the grey matter are demonstrated in the left lateral column by a single chevron in all images and a separate focal lesion is demonstrated in the posterior column (Figure B and E).
- 6.11 Three cases of focal lesions (indicated by single chevrons) involving two spinal cord columns and the grey matter (Type III lesions). 3A-C: 3D-FFE 0.5 x 0.5 mm<sup>2</sup> in plane resolution, 3D-F: 3D-PSIR 0.5 x 0.5 mm<sup>2</sup> in plane resolution. A focal lesion crossing from the anterior to posterior column is demonstrated in Figures A and D. Figure B and E demonstrate lesions crossing from the lateral to the posterior column and a separate focal lesion in the left lateral column. Figure A also shows diffuse abnormalities in the right lateral column (indicated by double chevron). A focal lesion crossing from the lateral to the anterior column is demonstrated in Figure C and F.
- 6.12 Three cases of lesions involving three spinal cord columns and the grey matter (Type IV lesions). 4A-C: 3D-FFE 0.5 x 0.5 mm<sup>2</sup> in plane resolution, 4D-F: 3D-PSIR 0.5 x 0.5 mm<sup>2</sup> in plane resolution. Focal lesions are shown in all images by a single chevron.
- 6.13 Images demonstrating diffuse abnormalities on 3D-FFE images (A and B) shown by double chevrons. Corresponding slices of 3D-PSIR image shown in images C and D.
- 7.1 3D-Phase sensitive inversion recovery image (PSIR); 0.5 x 0.5 mm<sup>2</sup> in plane resolution, centred at C2/C3 intervertebral disc acquired using 16-channel neurovascular coil

- 7.2 Representative 3D-FFE images and MT-off images acquired using 16-channel neurovascular coil
- 7.3 MT-off images;  $0.5 \times 0.5 \text{ mm}^2$  in plane resolution, centred at C2/C3 intervertebral disc acquired using 16-channel neurovascular coil demonstrating the cord outline region of interest acquired using the active surface model
- 8.1 (A) Axial 3D-FFE image (resolution  $0.5 \times 0.5 \times 5 \text{ mm}^3$ ) through the C2/C3 intervertebral disc (B) Following independent linear registration of the MT-on and MT-off to the FFE the MTR-map is created in this space (resolution  $0.5 \times 0.5 \times 5 \text{ mm}^3$ )
- 8.2 (A) Axial 3D-FFE image (resolution  $0.5 \times 0.5 \times 5 \text{ mm}^3$ ) demonstrating the spinal cord outline created using the active surface model (B) Axial 3D-FFE (resolution  $0.5 \times 0.5 \times 5 \text{ mm}^3$ ) demonstrating grey matter region of interest outlined using the fuzzy connector
- 8.3 Graphical representation of voxel layers analysed in the outermost region of the spinal cord
- 8.4 (A) MTR-map (resolution  $0.5 \times 0.5 \times 5 \text{ mm}^3$ ) demonstrating a square shaped region of interest from which (B) was obtained in the periphery of the spinal cord (B) Zoomed image of the periphery of the spinal cord demonstrating from right to left: Cerebrospinal fluid (CSF), (P) Outer exclusion voxel layer - partial volume with CSF (1) inner exclusion layer - interpolation of voxels (2) Outermost spinal cord voxel layer, (WM) spinal cord white matter
- 9.1 A) b0 image with regions of interest displayed in lateral and posterior column B) Average transverse diffusion weighted image optimised displaying grey matter region of interest (see methods for details). Resolution of images  $1 \times 1 \times 5 \text{ mm}^3$
- 9.2 Graphs of standardised DTI measures (FA, RD and MD): the trend lines demonstrated are fitted to the means in each group. Bars on either side of the mean represent the standard error of group means. CIS – clinically isolated syndrome, RR – Relapsing remitting MS, SP – Secondary progressive MS.

## **Chapter 1- The spinal cord and multiple sclerosis**

### **1.1 The spinal cord**

#### **1.1.1 External structure**

The spinal cord (medulla spinalis) extends from the medulla oblongata to the conus medullaris. It extends from cranial border of the atlas to the second lumbar vertebra, although the caudal termination of the cord is variable (Jit *et al.* 1959). Three layers cover the cord: dura, arachnoid and pia, with the cerebrospinal fluid (CSF) contained in the subarachnoid space. The width of the spinal cord depends on the level with enlargements at the cervical and lumbar levels corresponding to the spinal nerves innervating the limbs.

The anterior surface of the spinal cord is marked by the anterior median fissure, which contains perforating blood vessels and dorsally by the posterior median and lateral sulci. The white substance contained between the two posterior sulci is known as the posterior funiculus. The region between the posterolateral sulcus and the anterior median fissure is the anterolateral funiculus. Inferiorly the filum terminale descends to leave the subarachnoid space and extends to the tip of the coccyx.

Along the length of the cord are paired dorsal and ventral roots of spinal nerves, which join in the vertebral foramina to form a spinal nerve. Caudally the spinal nerve roots form a bundle known as the cauda equina.

### **1.1.2 Internal structure**

The spinal cord is divided in cross sections into laminae which contain grey and white matter, with the grey matter forming a central 'H' shaped arrangement, surrounded by the white matter (Schoenen 1973). The white matter is divided into anterior, posterior and lateral columns connected by a central commissure, which contains the central canal. The grey matter contains nerve cells supplying the limbs. The white matter is coloured by myelin, which coats the nerve fibres. The white matter contains the ascending and descending tracts of the spinal cord.

The descending tracts include: corticospinal, vestibulospinal, tectospinal, olivospinal, reticulospinal and rubrospinal (Williams 1980). The ascending tracts include: spinothalamic, dorsal columns and spinocerebellar tracts. Cajal first described the histology of spinal cord motor neurons (Cajal 1908), using Golgi silver stains.

### **1.1.3 Physiology**

The cell bodies of motor neurons that innervate the muscles, that are located in the grey matter in longitudinal columns, and receive both afferent and efferent input. The most important tract for movement and motor control is the corticospinal tract, originating in the precentral gyrus of the frontal lobe. This tract is also known as the pyramidal tract, as the fibres cross at the medulla they are said to form pyramids.

Injury to the spinal cord may result in sphincter and sensory dysfunction, and spastic paraplegia associated with injury to the corticospinal tract.

Many different conditions can result in spinal cord injury including, trauma, tumours and multiple sclerosis (MS).

## **1.2 Multiple sclerosis**

The name multiple sclerosis (MS) is due to the pathological appearance of white matter lesions in the CNS that become sclerotic as they age. MS is potentially the most common cause of neurological disability in young adults (Compston and Coles 2002); it is thought to be the result of infiltration of the central nervous system (CNS) by inflammatory cells in a genetically predisposed individual due to an unknown environmental antigen (Compston and Coles 2008). The result of inflammation of the CNS is a host of neurological symptoms and signs ranging from cognitive impairment to paraplegia depending on the site affected by the disease.

The result of migration of inflammatory cells into the CNS is dysfunction of the oligodendrocytes as well as activation of other inflammatory cells. The oligodendrocyte is responsible for myelination or coating the axons in the CNS, allowing saltatory conduction to occur along the length of the axon. It is estimated that each oligodendrocyte myelinates 30 to 50 axons (Compston *et al.*, 2006). In MS demyelination occurs, resulting in impaired conduction along the axon; this may be manifested as slowing of conduction (where conduction is still possible through sodium channels being distributed along the axonal membrane) or conduction block. Demyelinated axons are susceptible to a rise in temperature (e.g. Uhthoff's phenomenon) and positive phenomena (e.g. tonic

spasms) can also result from transmission between neighbouring axons (Compston and Coles 2002).

The symptoms and signs produced by demyelination often become apparent when a clinically eloquent site, such as the spinal cord, is involved. The involvement of the spinal cord can result in weakness, spasms, stiffness, bladder dysfunction, sexual dysfunction, paraplegia, constipation and sensory dysfunction.

### **1.2.1 Natural history**

MS affects women twice as commonly as it does men and has a lifetime risk of one in 400 in the UK (Compston and Coles 2002). MS typically presents between the ages of 20 and 40, as a relapsing remitting condition (RRMS), where a relapse is defined as 'the rapid appearance of new symptoms or the sudden worsening of old symptoms, lasting longer than 24 hours and occurring at least one month after the preceding relapse' (Confavreux *et al.*, 1980). RRMS is the initial course in about 85% of patients (Compston and Coles. 2002); the remaining 15% have a slowly progressive onset of symptoms and disability and is known as primary progressive MS. The main clinically recognised forms of the disease have been defined by a National Multiple Sclerosis Society of the USA Advisory Committee (Lublin and Reingold 1996): Relapsing remitting MS (RRMS), secondary progressive MS (SPMS), primary progressive MS (PPMS) and progressive relapsing MS (PRMS).

These definitions have recently been modified (Lublin *et al.*, 2014), with the inclusion of two new disease courses: clinically isolated syndrome (CIS) and radiologically isolated syndrome (RIS), which is an incidental imaging finding suggestive of demyelination without a corresponding history or physical examination findings typical for MS. The PRMS disease subtype has also been redefined in the modified criteria as PPMS with accompanying disease activity.

RRMS as described consists of relapses with a course exhibiting partial or complete recovery from the relapse-acquired deficit. About two-thirds to four-fifths of cases of RRMS will at some time enter a secondary progressive phase (Weinshenker *et al.*, 1989), which consists of a gradual and progressive increase in symptoms and disability, with or without occasional relapses, but without a significant reversal of the underlying disability. The mean age of onset of RRMS is about 30 years and there is a 2:1 female to male predominance.

This differs from PPMS where the mean age of onset is about 40 years and equal numbers of males and females are affected. PPMS is often described as a 'chronic progressive myelopathy', since spinal cord involvement, with walking impairment, is the predominant manifestation in 80% of cases. Typically it progresses to quadriparesis with autonomic dysfunction and a substantially worse prognosis than RRMS (Noseworthy *et al.*, 2000), although the course of SPMS (once established) and PPMS are quite similar in their evolution. PRMS differs slightly from PPMS, where although there is progressive disease from onset, there are also superimposed relapses, with or without full recovery. PRMS is less common than PPMS.

As RRMS is the most common subtype it has been extensively studied in natural history studies of MS. Initial symptoms in RRMS consist of: optic neuritis, sensory symptoms, motor deficit of acute or insidious onset, diplopia, vertigo or balance difficulty (Weinshenker *et al.*, 1989). Confavreux *et al.* estimated from a natural history study that the annual relapse frequency is approximately one per year (Confavreux *et al.*, 1980). It was found that more than half of the RRMS cases in this study were severely disabled within fifteen years. The percentage of patients who convert to a progressive form increases steadily with duration of disease.

Given the potential for intervention during the RRMS phase, studies have also focused on what factors determine long-term disability following the initial phase, as there is a disparity between the suppression of relapses and accumulation of disability in clinical trials in MS (Beutler *et al.*, 1996; Coles *et al.*, 1999). Being able to predict the course from an early stage would also be invaluable in counselling patients. Factors that influence disease outcome including frequency of relapses in first two years, interval between relapses and interval between first and second relapse were assessed longitudinally by Weinshenker *et al.* (1989(2)). It was found that the median interval between first and second relapse was two years in an untreated population. High numbers of relapses in the first two years following onset of MS correlated with long-term disability. This study was then extended to 28 years of follow up (Scalfari *et al.*, 2010), where the effect of relapses was reevaluated. It was found that 80% of patients developed SPMS with a median time to progression of 15 years. There was also found to be a variable interval between the first and second relapse, and

patients who had frequent relapses in the first two years were found to be more likely to develop SPMS. A longer interval correlated with a lower probability of developing SPMS. The frequency and the interval of relapses were both found to be important factors in the first two years of the disease. However over the course of the disease the overall number of relapses and location of relapse do not appear to correlate with progression to SPMS (Kremenchtzky *et al.*, 2006).

Given the apparent importance of relapse frequency in the initial phase of the disease and its effect on long-term outcomes investigators have looked at what are possible reasons for an increase in relapse frequency. As MS has a female predominance (Compston *et al.*, 2002) the effect of pregnancy on the course of MS has been assessed in the Pregnancy in Multiple Sclerosis (PRIMS) study (Confavreux *et al.*, 1998). The investigators studied 254 pregnant women with MS and found no increased risk of relapse with breast-feeding or epidural. The relapse rate was affected by pregnancy with a decrease during pregnancy and an increase in the first three months post-partum followed by a return to baseline number of relapses. It was also found that the overall progression in level of disability was not affected by pregnancy, despite the post-partum increase in relapse rate.

Other factors that have been studied to influence relapse rate include vaccination status, as earlier reports suggested a potential link between vaccination and onset of MS. In an observational study, it was shown that commonly administered vaccines do not increase the risk of relapse in patients with MS and some possibly lowered the risk of relapse, including tetanus, poliomyelitis or diphtheria (Confavreux *et al.*, 2001).

### **1.2.2 Environmental factors**

MS has been noted for several years to have a clear distribution based on latitude (Kurtzke 1975). In this study Kurtzke divided areas into: high, medium and low risk, which correlated with latitude. It was noted that there were virtually no cases of MS in the tropics and high-risk zones were identified in northern Europe and USA. Based on other epidemiological studies the effect of migration from high to low risk has shown a reduction in MS risk (Dean 1967). However, the opposite does not appear to be true with migration from Asia to Northern Europe (Dean *et al.*, 1976). In more recent studies the prevalence and incidence of MS has been increasing and in some countries the female to male ratio of MS has also been increasing (Orton *et al.*, 2006).

A number of different hypotheses have arisen from this geographical distribution of what is believed to be an autoimmune disease. The first known as the “poliomyelitis hypothesis” is based on the idea that higher risk is associated with late childhood infection with an unknown virus, whereas infantile infection confers immunity (Poskanzer *et al.*, 1976). The second hypothesis is based on Kurtzke’s studies of British troops and their effect on the prevalence of MS in the Faroe Islands; he concluded that MS is caused by a pathogen (Kurtzke 1993). The third hypothesis is known as the ‘hygiene hypothesis’ based on observations in Israel on sanitation (Leibowitz *et al.*, 1966) and is substantiated by the fact that MS appears to be more prevalent among higher socio-economic groups.

Based on his observations including apparent clustering of MS in areas, Kurtzke concluded that MS is a 'rare late outcome of a specific but unknown infectious disease of adolescence and young adulthood and that this infection could be caused by a thus-far-unidentified virus' (Kurtzke 1993).

A number of different proposed viruses have been suggested as the 'unidentified virus', the most frequently cited being Epstein-Barr virus (EBV). EBV is a ubiquitous virus that infects 90% of the adult population worldwide, this normally occurs asymptotically in the first decade of life, however in industrialised countries later infection also occurs and may result in infectious mononucleosis. EBV is implicated in the pathogenesis of a number of different diseases including: Burkitt's lymphoma, nasopharyngeal carcinoma and EBV-related Hodgkin's disease (Crawford 2001).

Similarities have been noted between the epidemiology of MS and EBV, EBV related diseases have a known geographic distribution (Ascherio *et al.*, 2007). Epidemiological evidence also suggests that there is a greater risk conferred of developing MS in those who had previously been exposed to EBV, whereas the risk of developing MS in seronegative subjects is extremely low (Thacker *et al.*, 2006). EBV has been suggested to be a necessary cofactor for the development of MS with serological levels of immunoglobulin G (IgG) correlating with activity on neuroimaging and progression of disability (Farrell *et al.*, 2009). The basis for EBV as a putative agent in the pathogenesis of MS is strengthened by the fact that T cells derived from MS patients cross react with EBV based on shared epitopes between myelin basic protein and EBV DNA (Lang *et al.*, 2002).

However a number of counter arguments are proposed that EBV may be simply a confounder in epidemiological studies, rather than a causative agent in MS.

Firstly EBV is a ubiquitous virus with the majority of the adult population being exposed, while MS is a relatively rare disease (Ascherio *et al.*, 2007). Secondly antibody titres to EBV and other viruses are raised in MS, which may be a reflection of immune dysregulation rather than being causative factors (Hunter *et al.*, 2000). Furthermore, in a study of acute and chronic MS plaques and CSF, EBV was not found in the B lymphocytes or plasma cells and no intrathecal EBV antibody production was found (Sargsyan *et al.*, 2010). It has therefore been suggested that EBV may combine with other risk factors such as smoking that may increase risk of MS by modulating EBV infection or the host's response to EBV (Simon *et al.*, 2010).

Smoking has also been extensively studied as a contributory factor in the development of MS. It has been shown that cigarette smoking accelerates the transition to SPMS (Hernan *et al.*, 2005); smoking can aggravate MS symptoms (Emre 1992), and an association has been established between age of onset of MS and smoking (Ghadirian *et al.*, 2001). In three large epidemiological studies in women there was found to be an increase in the relative risk of developing MS in those who smoked (Villard-Mackintosh *et al.*, 1993; Thorogood *et al.*, 1998; Hernàn *et al.*, 2001). The mechanisms by which smoking might increase MS risk are uncertain at present but may include neurotoxicity of compounds in cigarettes (Smith *et al.*, 1963), immunomodulatory effects (Sopori *et al.*, 1998) or the increased risk of respiratory infections, which are some researchers suggest may be linked to MS risk (Graham 1990).

The other major environmental factor investigated has been the role of vitamin D in MS. For most people the major source of vitamin D is sunlight (Holick 2004). However for people living beyond the 40<sup>th</sup> parallels north or South the level of sunshine is seasonally low for almost four months of the year with a corresponding reduction in vitamin D levels (Webb *et al.*, 1988). The areas that experience limited amounts of sunshine include Canada, the Northern half of the USA, Northern Europe, Russia, New Zealand and Tasmania (Pierrot-Deseilligny and Souberbielle 2010). These regions are also those with a higher prevalence of MS (Goodin 2009). This association was first noted by Goldberg (Goldberg 1974) and more recent studies have suggested that the month of birth is important in MS risk determination as this determines maternal vitamin D levels during the pregnancy. Births in November have the lowest risk of MS and births in May have the highest risk (Willer CJ *et al.*, 2004).

In experimental autoimmune encephalomyelitis (EAE), mouse model of MS, injection of vitamin D has been shown to prevent pathological signs of disease (Cantorna *et al.*, 1996) and its onset can be delayed by providing vitamin D supplements (Spach *et al.*, 2005). It has also been shown that macrophages and B and T cells contain vitamin D receptors (von Essen *et al.*, 2010), which play a role in autoimmunity in conditions such as MS. In some studies the intake of vitamin D supplements was found to be associated with a lower risk of MS (Kampman and Brustad 2008). Serum vitamin D levels are also found to be low in patients RRMS (Soilu-Hänninen *et al.*, 2008).

It is unlikely that vitamin D alone is responsible for MS alone, as with the other potential environmental factors listed above, none of which appear to be solely

responsible, it is more likely that a complex interaction between these and genetic factors contribute to the pathogenesis of MS.

### **1.2.3 Genetics**

15 to 20% of patients with MS have a family history of the disease: it is said that this figure is greater than would be expected by chance (Compston and Coles 2002). In twin studies it has been found that there is a higher rate of concordance of MS in monozygotic twins compared to dizygotic twins (~25% vs. 2-3%: Mumford *et al.*, 1994). In those who were adopted early in life and later developed MS, the new family did not incur any extra risk of MS, however the biological parents were found to be at increased risk (Ebers *et al.*, 1995). Equally children of parents, who both have MS, are at greater risk of developing MS, than if just one parent is affected (Robertson *et al.*, 1997). It has been also found that the risk of a relative developing MS increases with the degree with which they are related to them (Dyment *et al.*, 2006). Based on these and other observations in families with two or three affected individuals, no clear mode of inheritance is apparent in MS, however it is clear that genes play a definite role in its pathogenesis (Compston *et al.*, 2006).

Initial studies identified the link between MS and major histocompatibility complex (MHC) (Compston *et al.*, 1976). The genes for the Human Leukocyte Antigen (HLA) lie within the MHC, an area that contains extreme levels of polymorphism (Horton *et al.*, 2004). A number of HLA genes have been identified in association with MS including: DRB\*1501, DRB5\*0101, DQA180102 and

DQB2\*0602 (Olerup and Hilbert 1991). Since the association was proven with MHCs and MS a number of other potential candidate genes have been studied but with limited success.

Whole genome screens have been done for linkage to MS in the UK, US and Canada, however none of these studies found any significant linkages even when meta-analysis was used (Sawcer 2008). Later genomewide association studies (GWAS) were performed. The International Multiple Sclerosis Genetics Consortium studied 931 family trios, testing them for association by analysing single nucleotide polymorphisms (SNPs) in 2692 samples (IMSGC 2007). Two significant associations in SNPs were found in genes encoding IL2R $\alpha$  and IL7R $\alpha$  chains. These were deemed to be of importance as IL2R $\alpha$  gene has been implicated in a number of other autoimmune diseases (Vella *et al.*, 2005; Brand *et al.*, 2007) and IL7 has been shown to be important in the generation of autoreactive T cells in MS, particularly in the early stages of the disease (Bielekova *et al.*, 1999). The Wellcome Trust Case Control Consortium (WTCCC) performed the second GWAS analysing potential associations with MS (Burton *et al.*, 2007). This study analysed 12 374 SNPs, however no significant associations were found with MS.

Other GWAS studies have been performed, which have been followed by replication studies to assess the more frequently identified abnormalities. The Gene Associations in Multiple Sclerosis in 2009 identified a number of potential candidate loci, each of which had a modest effect, including: glypican proteoglycan 5 (GPC5) genes, which may be involved in sequestering pro-inflammatory cytokines. PARK2 or Parkin, already identified as playing a role in

autosomal recessive Parkinson's due to proteasomal degradation. Its role in MS is believed to be due to mitochondrial dysfunction and apoptosis of neuronal cells. Reelin (RELN) was also found to be associated with age of onset of MS (Baranzini *et al.*, 2009).

In the same year a GWAS study was published by the Australia and New Zealand Multiple Sclerosis Genetics Consortium (ANZgene 2009). Two previously unidentified MS susceptibility loci were identified on chromosome 12 and 20. Methyltransferase-like protein 1 (METTL1) and cyclin-dependent kinase 4 (CDK4), which is down regulated in T cells in Japanese MS cases. Both loci are associated with other autoimmune diseases.

A meta-analysis of MS susceptibility loci was performed in the same year as the ANZgene study (De Jager *et al.*, 2009). Three previously unreported associations were identified: tumour necrosis factor receptor superfamily member 1A (TNFRSF1A), interferon response factor 8 (IRF8) and CD6 loci. TNFRSF1A had previously been implicated in disorders of tumour necrosis factor (TNF) and IRF8 is implicated in the response to type I interferons and is involved in macrophage cell function. CD6 is believed to be involved in T-cell stimulation and differentiation and may have a role in inflammatory conditions where T cells are implicated in pathogenesis.

The two GWAS studies identified STAT3 gene, a risk allele for Crohn's disease (Jakkula *et al.*, 2010) and CBLB gene that regulates B and T cell activity and mice deficient in this gene are more susceptible to experimental autoimmune encephalomyelitis (EAE) (Sanna *et al.*, 2010). A more recent genetic study in MS has identified 48 new susceptibility variants (IMSG 2013), including associations

with SNPs encoding proteins related to inflammatory B and T cell activity, contiguous with the inflammatory hypothesis of the disease.

However there are a number of limitations to genetic analysis in MS. Firstly MS is not a common disease in the whole population, so huge population based studies are required to estimate epidemiological parameters (Sawcer 2008). Secondly MS is a heterogeneous disorder with a wide spectrum of phenotypes making genetic analysis a greater challenge (Compston *et al.*, 2006). Thirdly even the associations found to date such as variation in the allele for IL7 occur in up to 72% of white Europeans, the vast majority of who will never develop MS (Sawcer 2008). As with environmental factors in MS there is substantial evidence for a genetic component but its study remains challenging.

#### **1.2.4 Pathology**

The pathology of MS was first described by Carswell and Cruveilhier (Carswell 1838; Cruveilhier 1841) and later summarised by Frommann and Charcot (Frommann 1878; Charcot 1880). Since first described the sclerotic plaque has been appreciated to be one of the most important findings in MS. The plaque results from a complex process of inflammation, demyelination and repair accompanied by variable axonal loss (Compston and Coles 2008).

Oligodendrocytes in the CNS manufacture myelin and the development of these cells is regulated by growth factors (Barres 1992). The sections of the axon in between the myelin are known as nodes, containing sodium channels, which facilitate saltatory conduction along the axon (Compston *et al.*, 2006). In MS the oligodendrocytes are damaged by activated inflammatory T lymphocytes. It is

believed that these T lymphocytes are not regulated in MS, which allows the immune dysregulation to occur (Compston and Coles 2008).

During the stage of myelin destruction microglial cells are also activated immunologically (Ulvestad *et al.*, 1994). These activated microglial cells contribute to inflammation with myelin damage and also to repair by removal of myelin debris and promotion of remyelination. Due to a combination of a failure of remyelination and axonal loss, saltatory conduction is altered along the axon. This results in a redistribution of ion channels (Compston and Coles 2008).

As this process is hypothesised to be driven by T cells their role in the pathology of MS has been studied extensively. The evidence for T cells is based on the EAE model of MS and similar immune mediated molecules are seen in viral infections of the CNS (Lassman 1999). Interleukin 17, regulated by interleukin 23 is believed to be secreted by T lymphocytes (Langrish *et al.*, 2005). A combination of interleukin 17 and 22 disrupt the blood brain barrier, which allows migration of Th17 cells into the CNS (Kebir 2007). A combination of B and T lymphocytes and other immune cells activate the microglia, culminating in myelin loss through cell surface bound tumour necrosis factor  $\alpha$  (Zajicek *et al.*, 1992). The plaque itself is then surrounded by undifferentiated oligodendrocytes, macrophages and other cells and can be seen on gross specimens.

However demyelination alone does not seem to be responsible for disease progression in MS. Axonal loss in a neurodegenerative manner almost certainly results in disease progression (Compston *et al.*, 2006). It has been suggested that both inflammation and non-inflammatory processes may initiate axonal loss and

sometimes inflammation and axonal loss occur simultaneously. Axonal loss may be marked pathologically (Compston and Coles 2008).

The plaques in MS are readily seen in the white matter of the CNS; however, MS is not exclusively a disease of white matter and grey matter has long been recognised as being involved (Dawson 1916). Clinico-pathological correlation in MS with white matter lesions does not seem to account for all the potential deficits seen such as: cognitive impairment, memory impairment, attention deficits and reduced mental processing. However the process of axonal loss and demyelination in the CNS grey matter has not been clearly elucidated to date, although some have suggested it may be secondary to white matter inflammation (Geurts and Barkhof 2008). The pathology of grey matter does differ from white matter lesions, as inflammatory cells or disruption in blood brain barrier are not readily detected in grey matter lesions (Bö *et al.*, 2003). Grey matter lesions exhibit marked cellular loss and have been reported to be associated with progressive MS (Kutzelnigg *et al.*, 2005).

Pathological studies have given an insight into the disease mechanisms in MS and the wide range of symptoms experienced by the patient. Although pathology can provide a definitive diagnosis of MS, particularly in atypical presentations (Phadke and Best 1983), it is not a practical way to diagnose those suspected of having MS in life, therefore a number of different diagnostic criteria have been drawn up based on clinical and laboratory (especially magnetic resonance imaging [MRI]) findings.

### 1.2.5 Diagnosis

Since MS was first described the diagnosis was based solely on clinical findings. With the advent of clinical trials and disease modifying therapy, more stringent criteria have been developed to exclude other possibilities and confirm a diagnosis of MS. A number of different criteria have been published, incorporating laboratory data as well as magnetic resonance imaging (MRI); the more frequently cited criteria are summarised below.

One of the first proposed diagnostic criteria were written by Schumacher et al. on the basis that there were at that time no clear guidelines for enrolling patients into therapeutic trials (Schumacher *et al.*, 1965). A number of difficulties with clinical trials, some of which still exist today, are highlighted by the authors including: difficulty with diagnosis, unpredictable course of MS and lack of biological markers. At the time of writing the guidelines were based on the concept of dissemination in time and space with objective abnormalities on neurological examination. Each attack was defined as lasting for more than 24 hours and by definition had to be more than a month from the preceding event.

The authors recommended routine laboratory tests, in an effort to exclude alternate conditions and a lumbar puncture was also included, to look for an increase in CSF gamma globulin and mononuclear cells. Schumacher and colleagues also recommended that progressive presentations over the course of six months or more should be excluded: this will be addressed again later. It was also suggested that 'no better explanation' is possible to account for the symptoms or signs, an observation that is also reflected in more recent criteria.

Following on from the Schumacher criteria, Poser et al (Poser *et al.*, 1983) incorporated the use of supportive laboratory data in making a definitive MS diagnosis, however accepting that the diagnosis does remain a clinical one. As in earlier criteria clinical definitions such as what constitutes an attack and remission are defined and again the basis is that of dissemination in time and space of lesions, with objective findings on neurological examination and CSF.

The main purpose of the lumbar puncture is to determine if unmatched oligoclonal bands (OCBs) are present in the CSF but not in the serum. These consist of intrathecal IgG bands detected on electrophoresis and are suggestive of an immunological process in the CNS. Their presence is supportive of MS diagnosis; however, they may be present in other CNS inflammatory conditions such as sarcoid, syphilis, subacute sclerosing panencephalitis (SSPE) and systemic lupus erythematosus (SLE).

There are restrictions given of ages between 10 and 59 years and again progressive onset of disease is excluded from making an MS diagnosis. With the aforementioned caveats, Poser et al. proposed the following categories: clinically definite MS, laboratory supported definite MS, clinically probable MS, laboratory supported probable MS.

With the advent of MRI and its widespread use in MS and other neurological diseases its contribution was reflected in diagnostic criteria for the disease. MRI findings in MS are a reflection of the pathology seen, e.g. with callosal involvement (Dawson 1916), and early post mortem studies showed that MRI T2 high signal lesions corresponded with plaques of demyelination (Ormerod *et al.*, 1987). Paty et al. wrote a set of criteria that included MRI as well as other

paraclinical parameters for a diagnosis of MS (Paty *et al.*, 1988). The use of MRI was based on the fact that previous studies had shown clear abnormalities using this modality of imaging in MS (Robertson *et al.*, 1985). The other parameters assessed were CT, OCBs, visual evoked potentials and somatosensory evoked potentials (SSEP).

Visual evoked potentials (VEPs) involve the use of a chequer board pattern of black and white flashing squares as a stimulus. The visual evoked potential response is then recorded from the occipital scalp region and can be compared to mean values. SSEP involves electrical stimulation of median or posterior tibial nerves; again the response is recorded over the scalp. Both of these assessments of evoked potentials (visual and somatosensory) may be delayed, although not exclusively, in demyelinating diseases such as MS.

The criteria developed by Paty *et al.* included abnormalities in the above named parameters as well as a history of dissemination in time and space. Whether the MRI was strongly suggestive of, possible or not MS was based on the number of lesions seen. The authors recommended the following: an MRI strongly suggestive of MS has four lesions or three one of which is periventricular; for possible MS two lesions must be present or one lesion in a periventricular location. If there is one lesion or none, then another diagnosis should be considered. The authors also introduced the concept that a single appropriate lesion could be used to demonstrate dissemination in space. However given the increase in non specific lesions seen with advancing age it is was also recommended that OCBs are a prerequisite for a diagnosis for those over 40.

The issue of MRI abnormalities with advancing age was then addressed by Fazekas *et al.* to improve specificity of MRI for MS (Fazekas *et al.*, 1988). As alluded to in previous criteria again the use of MRI lesions on T2-weighted images was incorporated as evidence of dissemination in space. The investigators compared T2-weighted lesions in healthy volunteers to those seen in MS patients and suggested at least two of the three following MRI criteria for a diagnosis of MS: lesion size greater than 6mm, lesions abutting the body of the lateral ventricle, infratentorial lesion. When these criteria were applied to elderly volunteers with non-specific high signal changes none of them were attributed with an incorrect MS diagnosis. It is also noted that MS remains a clinical diagnosis.

Several potential MRI features for supporting a diagnosis of MS were then applied to a cohort of subjects with a clinically isolated syndrome (CIS) suggestive of MS, and then development of clinically definite MS (i.e. further clinical relapse in a different CNS location) during follow up was used to evaluate their performance (Barkhof *et al.*, 1997). As new T2 lesions had previously been shown to be representative of dissemination in time (Paty *et al.*, 1988), the introduction of contrast in MRI led to the concept of enhancing lesions with non-enhancing lesions on MRI representing dissemination in time and space (Heun *et al.*, 1988). The presence of enhancing lesions was incorporated into the new diagnostic criteria following a logistic regression analysis of the previous criteria (Fazekas *et al.*, 1988; Paty *et al.*, 1988) in CIS patients. The recommendations from the study were as follows: presence of at least one enhancing lesion or nine T2 weighted lesions: one juxtacortical, one infratentorial and three

periventricular (Barkhof *et al.*, 1997). It was found that the diagnostic accuracy increased from 69 to 80% when the number of lesions was increased from four to nine.

Tintoré *et al.* later addressed the criteria recommended by Barkhof *et al.* (1997), in a further study on CIS patients (Tintoré *et al.*, 2000). This study was done on the basis that a diagnosis of MS cannot be made in those with CIS, as they do not fulfil the criteria of dissemination in time. Again it was found that the Barkhof criteria were superior to earlier proposed criteria; however, it was recommended that at least three out of the four criteria be fulfilled to optimise the accuracy in diagnosis.

A meeting of the NMSS-supported International Panel on MS Diagnosis then presented what later became known as the McDonald criteria (McDonald *et al.*, 2001). These criteria integrated MRI into the diagnosis as well as: evidence of dissemination in time (DIT) and space (DIS), objective clinical signs, CSF analysis, visual evoked potentials. Importantly for the first time the McDonald criteria made provisions for the subset of patients with progressive forms of MS and include this in the criteria.

The MRI criteria were based on those of Barkhof and Tintoré (Barkhof *et al.*, 1997; Tintoré *et al.*, 2000); three of the four of the following were required: one gadolinium enhancing lesion or nine T2 hyperintense lesions, at least one infratentorial lesion, at least one juxtacortical lesion, at least three periventricular lesions. These initial McDonald criteria also included, to a limited extent, the presence of spinal cord abnormalities on MRI. Dissemination of

lesions in time was satisfied by the presence of gadolinium (Gd) enhancing or a new T2 weighted lesion in an MRI at least three months from the initial event.

The McDonald Criteria were then revised in 2005 following a meeting of the International Panel on the Diagnosis of Multiple Sclerosis (Polman *et al.*, 2005).

The Panel reviewed all literature published on the original McDonald criteria and recognised the potential for misdiagnosis of MS in conditions that are not typical of adult onset MS in a Western adult population. The modified criteria again incorporate CSF analysis, VEPs and clinical findings as well as three of the MRI criteria as outlined in the 2001 criteria with some modifications. Any number of cord T2 lesions could substitute for a brain lesion (whereas only one could in 2001 criteria) and a cord lesion was recognised as having the same significance as an infratentorial lesion. The other modification was in the definition of DIT: the originally proposed time period of three months for DIT was altered to one month for a new T2 lesion to satisfy DIT or detection of Gd enhancement at least three months after the onset of the clinical event.

The European multicentre collaborative research network that studies MRI in MS (MAGNIMS) (Montalban *et al.* 2010) proposed criteria for MS based on a single scan. The proposed MRI criteria are as follows: (i) one or more lesion(s) in at least two of 4 locations considered characteristic for MS (juxtacortical, periventricular, infratentorial and spinal cord), as outlined before, to satisfy dissemination in space, and (ii) simultaneous presence of Gd enhancing and non enhancing lesions or a new enhancing lesion or T2 weighted lesion on any follow up scan to satisfy dissemination in time.

These MAGNIMS criteria were subsequently appraised and incorporated into the 2010 revisions to the McDonald criteria (Polman *et al.*, 2011). DIS again was defined as one or more T2 lesions in at least two of four characteristic areas of the CNS (Periventricular, juxtacortical, infratentorial, spinal cord). However, symptomatic lesions in the brainstem or spinal cord are excluded and Gd enhancement is not required to demonstrate DIS. DIT has been defined as a new T2 or Gd enhancing lesion on a follow up MRI scan, with reference to the original scan or presence of Gd enhancing and non Gd enhancing lesions. The criteria for a diagnosis of PPMS are also given whereby patients must have one year of progression with two of the following: Evidence of DIS in the brain ( $\geq 1$  T2 lesion in following locations: periventricular, juxtacortical or infratentorial), evidence of DIS in the spinal cord, based on  $\geq 2$  T2 lesions in the cord, positive unmatched OCBS. The issues of ethnic heterogeneity and differential diagnosis are discussed (discussed in detail below). Again, however it is emphasised that these criteria must be applied in an appropriate clinical context with objective signs on clinical examination. These updated criteria differ substantially from previous iterations of the McDonald criteria because it is now possible to confirm a diagnosis of MS at the first presentation suggestive of demyelination.

In presenting any new criteria, it is generally acknowledged that MS is highly heterogeneous condition with a large number of conditions that can mimic it clinically and/or on imaging (Charil *et al.*, 2006; Miller *et al.*, 2008); no criterion is entirely reliable on its own, and expert clinical evaluation by an experienced neurologist remains at the centre of an effective diagnostic process. It is also

essential that the specificity and sensitivity of each proposed new set of criteria are rigorously scrutinised to reduce the chance of a misdiagnosis of MS.

### **1.2.6 Differential diagnosis**

MS has a number of 'typical' presentations such as optic neuritis, partial myelitis or brain stem syndromes, however these presentation may have numerous other causes to consider in the differential diagnosis, and furthermore, a number of atypical or unusual presentations of MS are possible such as: psychosis (Felgenhauer 1990), behavioural or intellectual changes (Young *et al.*, 1976), aphasia (Lacour *et al.*, 2004) hemianopia or seizures (Striano *et al.*, 2003). Given the diverse range of symptoms and signs possible MS often enters the differential diagnosis of unexplained neurological symptoms and equally a number of other varied conditions can mimic MS, which may result in misdiagnosis.

The differential diagnosis of MS is highlighted in the McDonald criteria (McDonald *et al.*, 2001), listing a number of different potential mimics. The clinical presentation and the characteristic imaging findings in MS can be caused by ischaemic changes due to conditions such as antiphospholipid antibody syndrome, CADASIL, and systemic lupus erythematosus (SLE) (Compston *et al.*, 2006). A number of genetic disorders such as leukodystrophies can produce white matter changes on MRI.

Given the relapsing nature of MS a number of CNS infections can present in a similar fashion, such as CNS Lyme disease and neurosyphilis. Possible infective

aetiologies can often be elucidated by CSF analysis, which is alluded to in early diagnostic criteria for MS (Schumacher *et al.*, 1965).

Other disorders such as acute disseminated encephalomyelitis (ADEM) or neuromyelitis optica (NMO) are more closely related to MS and can pose diagnostic dilemmas. However with recently discovered antibody for NMO (Lennon *et al.*, 2004), the distinction between MS and NMO is possible in suspected cases.

Miller *et al.* addressed the issue of differential diagnosis and 'red flags' in the diagnosis of MS (Miller *et al.*, 2008). There were 79 red flags identified, which were classified as: major, intermediate or minor. The authors provided a diagnostic algorithm to eliminate alternative diagnoses and to confirm a diagnosis of CIS or MS. CIS is further defined as being monofocal or multifocal based on clinical or radiological features.

The issue of differentiation between NMO and MS is also addressed based on: differences in response to immunomodulatory therapy, predilection in NMO for severe optic neuritis and myelitis with T2 weighted spinal cord lesions on MRI extending over three or more spinal segments, expression of aquaporin 4 antibodies (seen in ~70% with NMO) and OCBs are less likely to be present (10-20% of NMO cases vs. 70-90% MS). NMO can be excluded with biopsy evidence of sarcoidosis or vasculitis although seropositivity for antinuclear antibodies (ANA) or Sjögren's (SSA/SSB) does not exclude an NMO diagnosis.

The diagnosis of ADEM and its differential diagnosis are also outlined. ADEM typically presents as a subacute encephalopathy over one week to three months

and may have improvement or recovery; it may follow an infectious illness. MRI brain in ADEM typically shows symmetrical or large multifocal brain lesions (Kesselring *et al.*, 1990), however it has been proposed that no clinical or MRI criteria reliably distinguishes fulminant episodes of MS from ADEM (Banwell *et al.*, 2007) and the diagnosis of ADEM is often revised to that of MS after continued surveillance (de Seze *et al.*, 2007).

Following a meeting of the MAGNIMS (Magnetic Resonance Network in Multiple Sclerosis) a list of imaging red flags for MRI were compiled for images atypical for MS where another diagnosis is more likely (Charil *et al.*, 2006). The imaging characteristics of NMO, with minimal cerebral lesions, ADEM, with symmetrically defined lesions and poorly defined lesion margins are discussed as well as the findings in a number of other conditions such as CADASIL, abscesses and progressive multifocal leucoencephalopathy (PML).

In summary, it is clear that a wide spectrum of disorders can mimic MS highlighting the importance of investigations and imaging when suspicious of an MS mimic. MRI clearly plays a key role in the diagnosis of MS as outlined above; an introduction to MRI is given in chapter two.

## **Chapter 2 - Magnetic resonance imaging**

### **2.1 Magnetic resonance imaging principles**

The human body is composed of a number of different tissue types, each with varying amounts of water present. Each water molecule is composed of hydrogen and oxygen atoms, which contain: protons, neutrons and electrons. It is the nucleus of the hydrogen atom that is of particular interest in MRI as this contains a proton, which has a net charge and spin on its own axis. These protons have a magnetic moment and can align with an external magnetic field.

When an external magnetic field ( $B_0$ ) is applied to a hydrogen nucleus the magnetic moment of the nucleus will align in either the same direction (parallel), or in the opposite direction (anti-parallel). The net moment of the hydrogen nuclei is known as the net magnetisation vector (NMV), which is initially longitudinal i.e. along the z-axis. When the  $B_0$  is applied, an additional rotatory movement occurs around the applied field, this movement is known as precession. The frequency of precession is called the Larmor frequency and is governed by the magnetic field strength and gyromagnetic ratio.

Resonance occurs when an applied force matches the natural frequency of an object, giving rise to an increase in the amplitude oscillations that occur. The same principle of resonance applies to protons, when an external force matches the precessional frequency of the nucleus. If a radio frequency (RF) pulse is applied with a frequency equal to the Larmor frequency that causes resonance to occur, this resulting process is known as excitation.

The application of the RF pulse flips the NMV towards the transverse plane i.e. along x-y axis from the original z-axis. In the special case of a 90° the NMV is entirely orientated in the transverse plane. The phase and magnitude of the NMV in plane is measured by the receiver coil.

## 2.2 T1 - longitudinal relaxation

Immediately after excitation, the NMV returns to the original longitudinal vector, which is known as the longitudinal or T1 relaxation (shown in Figure 2.1).

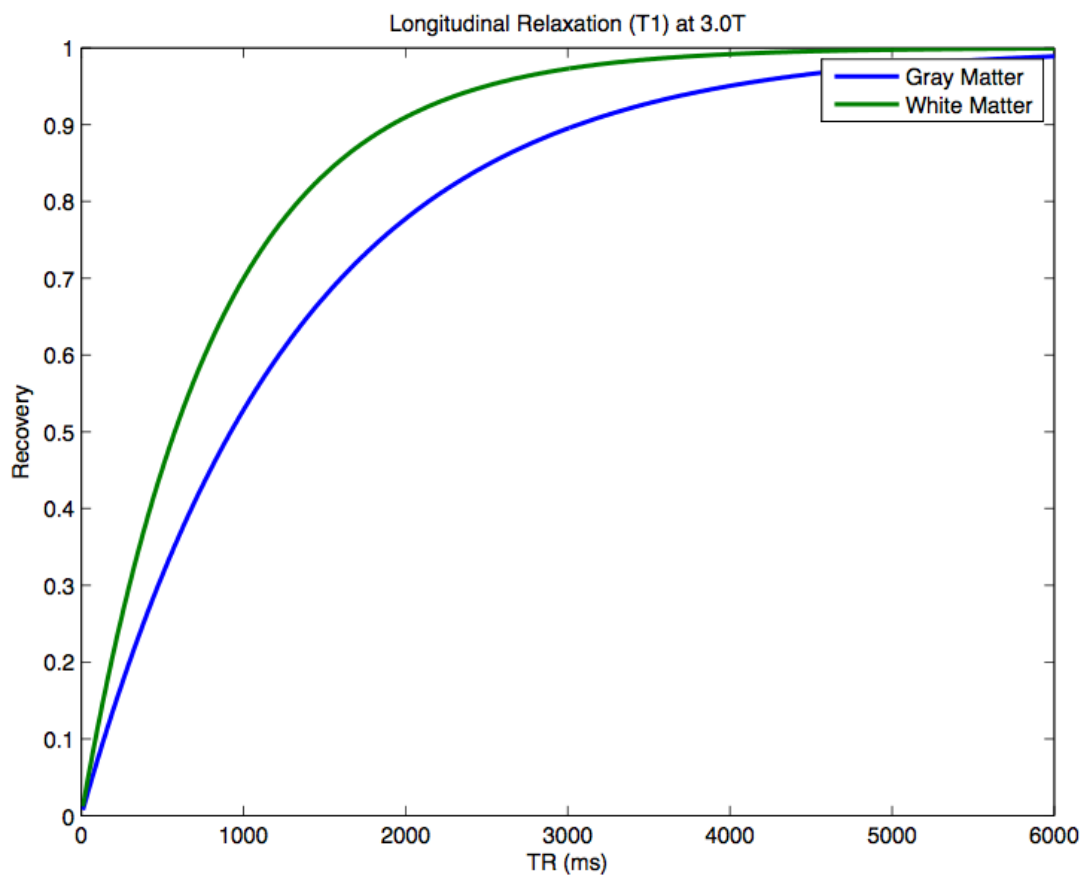


**Figure 2.1** T1 relaxation of brain grey and white matter (image from [www.mcauslander.sc.edu](http://www.mcauslander.sc.edu))

The removal of the RF pulse causes the NMV magnitude of the protons to spiral back to their original precessional position around the static magnetic field from

the transverse plane during the application of the RF pulse. T1 is defined as the time required for longitudinal magnetisation to restore to 63% of its final value.

### 2.3 T2 – transverse relaxation

During the application of the RF pulse, a large number of protons precess with the same phase in the transverse plane. Due to spin-spin interactions (T2 relaxation) and field inhomogeneities (T2\* relaxation), less and less protons precess in phase, which combined result in transverse relaxation. T2 relaxation is shown in Figure 2.2.

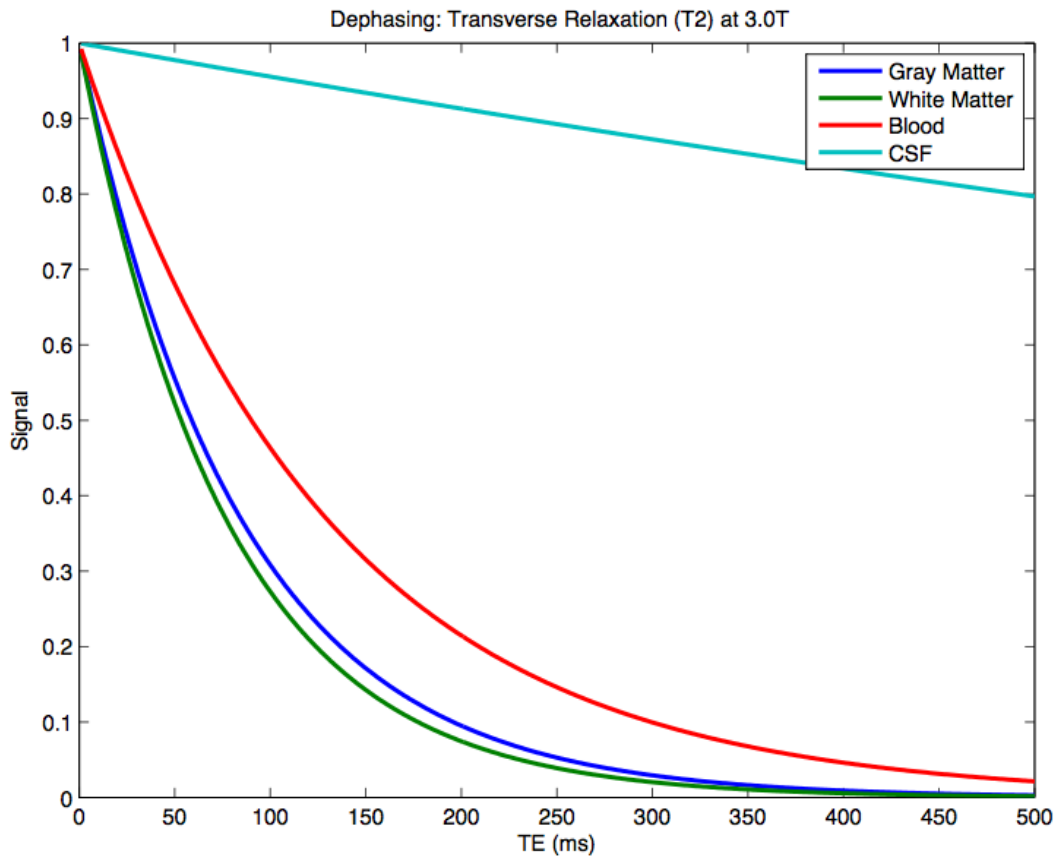


**Figure 2.2** T2 (transverse relaxation) of grey matter, white matter, blood and CSF (image from [www.mcauslander.sc.edu](http://www.mcauslander.sc.edu))

As a result of magnetic field inhomogeneities, the process of decay known as T2\* decay also occurs and represent the reduction in the induced signal.

T2 is defined as a time required for a decrement, from the transverse magnetisation value to decrease to a value of 37%.

## **2.4 Pulse sequences**

Pulse sequences are designed to take advantage of different relaxation times in tissues and are constructed through the use of different combinations of RF pulses and gradients. The main parameters of a pulse sequence are the echo time (TE) and the repetition time (TR). TR is the time between subsequent excitations. The time from the RF pulse to the acquisition is known as the TE.

## **2.5 Spin Echo sequences**

If a transverse magnetisation is produced by an RF pulse, a transient MR signal occurs at the Larmor frequency, which decays with a characteristic T1 and T2\*. This decay is known as the free induction decay. However, the re-appearance of the NMR signal can occur after this point, as a consequence of the effective reversal, or rephasing, of the dephasing spins by a specific 180° RF pulse in a spin echo (SE) sequence.

The fast spin echo sequence differs slightly from the conventional SE, as multiple 180° RF pulses are applied and this produces a series of echoes with a resultant reduction in total acquisition time. Fast spin echo sequences are usually T2 weighted and the use of this sequence in MS is discussed later in relation to its use in the spinal cord (Kidd *et al.*, 1993).

## **2.6 Gradient echo sequences**

Gradient echo sequences are an alternative means rephase the spins compared to SE sequences, as they are usually faster and allow shorter echo times. No  $180^\circ$  pulse is applied, in contrast to SE sequences and which facilitates the short TE and TR.

A commonly used gradient echo sequence in investigation of multiple sclerosis is the T1 weighted magnetically prepared rapid acquisition gradient echo sequence (MP-RAGE) (Mugler and Brookeman 1990). T1 MPRAGE sequences have also been used for evaluation of spinal cord atrophy (Lin *et al.*, 2003) and its use will be discussed further later.

## **2.7 Image contrast**

Contrast is of importance in MRI so that abnormalities in normal appearing tissue can be readily determined, such as demyelination in the CNS in MS.

Different tissues in the body have intrinsic contrast parameters that are fixed, however by altering parameters such as TR and TE, amongst others, extrinsic contrast can be changed. When viewing the image areas of high signal appear brighter and low signal are darker.

### **2.7.1 T1-weighted imaging**

T1 recovery is dependent on the intrinsic properties of the tissue type that is being examined. Fat has a short T1 time whereas water's T1 time is prolonged as a result of its molecular structure. Since fat has a short T1 it appears bright on a

T1-weighted image and water or CSF appears have a longer T1 and as a result appear dark. The amount of T1-weighting is determined by TR, which is short for a T1-weighted spin echo sequence to maximize the contrast between different tissues e.g. grey matter, white matter and CSF in the brain. Therefore a T1-weighted image is created by using a short TR and short TE.

In addition to the contrast produced by different MRI weighting, paramagnetic substances can be injected intravenously such as gadolinium (Gd) chelates, which act as enhancement agents in MRI. Gadolinium shortens the T1 of effected tissue by altering the local magnetic field. In imaging the brain in MS, Gd enhancement is thought to reflect areas of acute inflammation with disruption of the blood-brain barrier (Nesbit *et al.*, 1991).

T1-weighted images and in particular Gd enhanced T1 weighted images are of importance in MS. The onset of a relapse in MS is often accompanied by Gd enhancing lesions on MRI (Miller *et al.*, 1993). Equally, some hypo-intense lesions can be seen on T1-weighted images in MS and these are termed black holes, which, when persistent, have been shown to correlate with axonal loss on histopathology (Bruck *et al.*, 1997). When acute contrast enhancing lesions are analysed 80% appear hypointense (van Waesberghe JH *et al.*, 1998). In a four year follow up study, it was found that approximately 60% of these so-called 'acute' black holes evolve into permanent ones and that the persistence of black holes correlated with the duration of enhancement (Bagnato *et al.*, 2003).

### **2.7.2 T2-weighted imaging**

As with T1, T2 imaging decay varies according to the tissue being imaged as decay is determined by the result of magnetic fields of nuclei interacting with each other. Fat has a short T2 time and water has a long T2, due to slower dephasing of water molecules. Water therefore appears as high signal on T2-weighted imaging and fat appears dark. The degree of T2-weighting is varied by changing the TE; T2-weighted images typically have a long TR (to minimise T1 contrast) and long TE, to maximise the differences in T2 decay as seen in Figure 2.2.

T2-weighted images have also been evaluated in the context of MS as a measure of inflammatory disease burden and net changes in the brain T2 lesion volume have been used as endpoints in clinical trials (Paty *et al.*, 1993). The net change of T2 weighted lesion volume in a serial MRI study reflects the volume of new or enlarging and resolved or shrinking lesions (Willoughby *et al.*, 1989).

### **2.6.3 Proton density imaging**

The number of protons in the tissue being examined determines the proton density. The signal is determined in proton density (PD) weighted image by the number of protons present, high signal is produced by greater number of protons by an increase in the transverse component of magnetisation. If the effects of T1 and T2 are decreased, this results in increased proton density weighting on an image. Typically this is achieved by using a long TR and short TE.

Proton density-weighted sequences may be of particular value in MS for imaging lesions in the posterior fossa. In one study assessing the MRI findings in patients with a known internuclear ophthalmoplegia, a common finding in MS, it was found that proton density-weighted imaging was superior to other sequences in detecting lesions in the medial longitudinal fasciculus (Frohman *et al.*, 2001).

## Chapter 3 - Spinal cord magnetic resonance imaging in multiple sclerosis

### 3.1 Introduction

In clinically definite MS, spinal cord lesions are detected in up to 85% of patients and if atrophic changes are included then up to 90% of patients will have an abnormal MRI of the spinal cord (Lycklama *et al.*, 1998). This degree of involvement of the cord, a clinically eloquent site, is likely to be a contributory factor to the physical disability experienced by MS patients.

As MS has been proven in post mortem studies to involve all of the central nervous system (CNS) it is desirable to image it in its entirety. However, MRI of the spinal cord poses a number of technical difficulties as the cord itself is a small, mobile structure (Mikulis *et al.*, 1994), which is also susceptible to motion artefacts from respiration, cardiac contraction and cerebrospinal fluid (CSF) flow artefact (Bronskill *et al.*, 1988; Curtin *et al.* 1989; Czervionke *et al.*, 1988; Hinks *et al.*, 1988; Levy *et al.*, 1988). These technical difficulties can be addressed by several approaches including cardiac gating, presaturation slabs and fast imaging techniques.

Due to these technical limitations earlier MR studies had difficulty detecting smaller and more chronic lesions, particularly in the thoracic cord whereas larger more acute lesions were more easily identified (Miller *et al.*, 1987; Turano *et al.*, 1991). Furthermore, the duration of image acquisition was prolonged in early studies in order to obtain diagnostic quality images for detection of lesions using conventional T2-weighted spin echo images. The issues of length of time and image quality were addressed using multi-array coils and T2-weighted fast

spin echo sequencing (Kidd *et al.*, 1993). This new imaging technique was also able to give an indication of cord atrophy, which correlated with the level of disability experienced by the patient.

Routine clinical assessment of the spinal cord in suspected or confirmed MS, typically involves both sagittal and axial T2-weighted images. Fluid attenuated inversion recovery (FLAIR), unlike in the brain, has not proven useful in the assessment of cord lesions (Keiper *et al.*, 1993), nor has T1-weighted imaging (Lycklama *et al.*, 2003). This may be due to the organisation of tissue in the cord. However, T1-weighted imaging can be used for the evaluation of cord atrophy (Lycklama *et al.*, 1998). Axial T2-weighted images are also of use in the detection of MS lesions (Stevenson *et al.*, 1998); they may confirm an equivocal abnormality seen on a sagittal image as well as localising the lesion more accurately within the cord.

MRI is an important marker of disease activity in MS as the administration of gadolinium (Gd) contrast can demonstrate activity despite absence of clinical manifestations of the disease (Bastianello *et al.*, 1990; Harris *et al.*, 1991; Miller *et al.*, 1998; Thompson *et al.*, 1991; Barkhof *et al.*, 1992; Capra *et al.*, 1992; McFarland *et al.*, 1992). In a study examining serial Gd enhanced MRI of the brain and spinal cord (Thorpe *et al.*, 1996); it was found that 10% of the enhancing lesions found were in the spinal cord. It was also found that 31% of the enhancing spinal cord lesions cause symptoms, in comparison with the much larger number of enhancing lesions in the brain with a very low number of corresponding relapses. New enhancing brain lesions are more likely to be found

than in the cord and simultaneous enhancement of brain and cord lesions is often found.

To assess the MRI abnormalities in the MS spinal cord, investigators have compared pathological findings directly with the post mortem images obtained from MRI. This allows complete imaging of the spinal cord without any flow or movement artefacts and permits a direct comparison. In one study, the spinal cords of 19 patients and three controls were examined histologically and radiologically using 1.0T MRI with 1mm pixel resolution (Lycklama *et al.*, 2001). In this study the sensitivity of MRI was found to be high when compared to histology and there was also a good correlation with the subtype of MS. It was found that high signal change on MRI corresponded with demyelination and changes extended into grey matter in some patients and the distribution of lesions were similar to previous studies (Oppenheimer 1978; Fog 1950). It was also noted when the MRI was reviewed concurrently with the histology that mild signal increase corresponded to partial demyelination. In the PPMS group more extensive abnormalities consisted of diffuse signal change on proton density weighted spin echo sequences.

In a separate study a comparison was made between 1.5T, 4.7T MRI and the histopathology in spinal cords of seven MS cases (Bergers *et al.*, 2002). The findings were similar however the authors point out that; sagittal views on MRI underestimate the number and extensiveness of spinal cord lesions, as well as diffuse abnormalities in the MS spinal cord.

### 3.1.1 Spinal cord imaging in clinically isolated syndrome

MRI has been used to assess the number of asymptomatic lesions in the spinal cord, in patients with a clinically isolated syndrome (CIS), a presumed inflammatory demyelinating event, which often heralds the onset of MS (O’Riordan *et al.*, 1998). It was found that there was a high frequency of asymptomatic cord lesions found, irrespective of the clinical syndrome. The lesions found were predominantly in the cervical and thoracic cord with no lumbar lesions found. These findings correlated with previous neurophysiologic studies on the cord in CIS (Hume *et al.*, 1988). O’Riordan *et al.* argue that spinal cord MRI may assist in the diagnosis of demyelination in patients over 50, where high signal changes in the brain are likely to be seen due to ischaemia, whereas abnormalities of the cord are less likely.

The role of spinal cord imaging in patients who presented with an optic neuritis has been assessed (Dalton *et al.*, 2003); it was found that 27% of patients with optic neuritis had spinal cord lesions at presentation. Using diagnostic criteria (McDonald *et al.*, 2001) for MS spinal cord imaging was felt to be of limited value in this study. Other studies however, have shown that the frequency of developing MS, has been found to be higher in patients with both brain and spinal cord lesions at baseline, than brain lesions alone (Brex *et al.*, 1999).

In a more recent study of 100 patients with optic neuritis, followed up for six years, it was found that asymptomatic cord lesions were seen in 26% of patients (Swanton *et al.*, 2009). It was found in those with cord lesions at presentation there was an increased odds of higher disability at six years and that this effect

was independent of brain lesion load. Swanton et al. argue that there may be a role for spinal cord imaging in patients with optic neuritis in assessing the risk for future disability.

In a multicentre retrospective study 282 patients with CIS were assessed to investigate the performance of the McDonald criteria in those who developed CDMS (Swanton *et al.*, 2007). T2-weighted spinal cord images were available for 130 patients, with abnormalities detected in 45 patients and five had normal brain imaging. It was found that spinal cord MRI increased the sensitivity and specificity of the McDonald criteria by up to 3%.

As not all those with a CIS will convert to clinically definite MS (CDMS), other studies have assessed spinal cord imaging in recently diagnosed MS (Bot *et al.*, 2004). The presenting feature often determines whether the spinal cord is imaged or not in CIS. In this study of 104 patients with early MS 82.7% had an abnormal MRI of the spinal cord. The fact that not all patients with CIS convert to MS may account for the disparity in the percentage of abnormal spinal cord images obtained in CIS patients compared to recently diagnosed MS patients in this study. The spinal cord MRI obtained in this cohort allowed a diagnosis of MS in three patients who did not fulfil the Paty criteria and in 28 patients who did not fulfil the Barkhof/Tintoré criteria. It was also found that with substitution of a spinal cord lesion for a brain lesion to determine dissemination in space the sensitivity of the McDonald criteria reached 84.6%.

### **3.2 Utility of spinal cord MRI in diagnosis**

The diagnosis of multiple sclerosis is based on diagnostic criteria; following a meeting of an International Panel on the diagnosis of MS the McDonald criteria were established (McDonald *et al.*, 2001 Tables 3.1 and 3.2). The original criteria were to be applied to patients in whom there was a clinical suspicion of demyelinating disease and no other explanation could account for the symptoms. The criteria were based largely on brain MRI that contained: one Gd enhancing lesion or nine T2 enhancing lesions if there is no Gd enhancing lesion, at least one infratentorial lesion, at least one juxtacortical lesion, or at least three periventricular lesions. However it was recommended that one spinal cord lesion could be substituted for one brain lesion.

**Table 3.1** McDonald MRI criteria to demonstrate dissemination of lesions in time:

<b>Original McDonald Criterion</b>	<b>2005 Revisions</b>
<p>1. If a first scan occurs 3 months or more after the onset of the clinical event, the presence of a Gd-enhancing lesion is sufficient to demonstrate dissemination in time, provided that it is not at the site implicated in the original clinical event. If there is no enhancing lesion at this time, a follow up scan is required. The timing of this follow up scan is not crucial, but 3 months is recommended. A new T2- or Gd-enhancing lesion at this time fulfils the criterion for dissemination in time</p>	<p>1. There are two ways to show dissemination in time using imaging:</p> <ul style="list-style-type: none"> <li>a. Detection of Gd enhancement at least 3 months after the onset of the initial clinical event, if not at the site corresponding to the initial event</li> <li>b. Detection of a <i>new</i> T2 lesion if it appears at any time compared with a reference scan at least 30 days after the onset of the initial clinical event</li> </ul>
<p>2. If the first scan is performed less than 3 months after the onset of the clinical event, a second scan done 3 months or longer after the clinical event showing a new Gd-enhancing lesion provides sufficient evidence for dissemination in time. However, if no enhancing lesion is seen at this second scan, a further scan not less than 3 months after the first scan that shows a new T2 lesion or an enhancing lesion will suffice.</p>	

**Table 3.2** McDonald MRI Criteria to demonstrate brain abnormalities and demonstration of dissemination in space:

<b>Original McDonald Criteria</b>	<b>2005 Revisions</b>
<p>Three of the following:</p> <ol style="list-style-type: none"> <li>1. At least one Gd Enhancing lesion or nine T2 hypertintense lesions if there is no Gd-enhancing lesion</li> <li>2. At least one infratentorial lesion</li> <li>3. At least one juxtacortical lesion</li> <li>4. At least three periventricular lesions</li> </ol>	<p>Three of the following:</p> <ol style="list-style-type: none"> <li>1. At least one Gd-enhancing lesion or nine T2 hyperintense lesion if there is no Gd-enhancing lesion</li> <li>2. At least one infratentorial lesion</li> <li>3. At least one juxtacortical lesion</li> <li>4. At least three periventricular lesions</li> </ol>
<p>NOTE: One spinal cord lesion can substitute for one brain lesion</p>	<p>NOTE: A spinal cord lesion can be considered equivalent to a brain infratentorial lesion: an enhancing spinal cord lesion is considered to be equivalent to an enhancing brain lesion and individual spinal cord lesions can contribute together with individual brain lesions to reach the required number of T2 lesions</p>

Criteria reproduced from Polman *et al.* 2005

Following a further meeting of the International Panel a number of conclusions were reached regarding spinal cord MRI in suspected MS, which are reflected in the 2005 revisions to the McDonald Criteria (Polman *et al.*, 2005, Table 3.1 and 3.2). The Panel recognised the use of spinal cord imaging in excluding an alternative diagnosis, such as a compressive lesion (e.g. tumour or intervertebral disc), and also that intrinsic cord lesions are unlikely to occur in a healthy person with aging as brain white matter lesions do (Kidd *et al.*, 1993; Lycklama *et al.*, 2003). Thus cord lesions provide more specificity, especially in older adults, when brain imaging is less specific. It was also recommended that spinal cord imaging could be used to determine dissemination in space, if this is not found on brain imaging in suspected MS. The cord lesion can substitute for an infratentorial lesion but not for a periventricular or juxtacortical lesion. It was recommended that spinal cord lesions should be focal and clearly delineated on T2-weighted imaging.

The presence of spinal cord lesions are also included in the 2010 revisions to the McDonald criteria and may provide evidence of DIS in MS or in the context of PPMS if there are more than two spinal cord lesions this may serve as evidence of DIS in the spinal cord (Table 3.3).

**Table 3.3** The 2010 McDonald criteria for diagnosis of multiple sclerosis

<b>Clinical Presentation</b>	<b>Additional Data Needed for MS Diagnosis</b>
≥2 attacks; objective clinical evidence of ≥2 lesions or objective clinical evidence of 1 lesion with reasonable historical evidence of a prior attack	None
≥2 attacks; objective clinical evidence of 1 lesion	DIS, demonstrated by: ≥1 T2 lesion in at least 2 of 4 MS-typical regions of the CNS (periventricular, juxtacortical, infratentorial, or spinal cord); or await a further clinical attack implicating a different CNS site
1 attack; objective clinical evidence of ≥2 lesions	DIT, demonstrated by: Simultaneous presence of asymptomatic Gd-enhancing and non enhancing lesions at any time; or a new T2 and/or Gd-enhancing lesion(s) on follow-up MRI, irrespective of its timing with reference to a baseline scan; or await a second clinical attack
1 attack; objective clinical evidence of 1 lesion (clinically isolated syndrome)	DIS and DIT, demonstrated by: For DIS: ≥1 T2 lesions in at least 2 of 4 MS-typical regions of the CNS (periventricular, juxtacortical, infratentorial, or spinal cord); or await a second clinical attack implicating a different CNS site; and for DIT: Simultaneous presence of asymptomatic Gd-enhancing and non enhancing lesions at any time; or a new T2 and/or Gd-enhancing lesion(s) on follow-up MRI, irrespective of its timing with reference to a baseline scan; or await a second clinical attack
Insidious neurological progression suggestive of MS (PPMS)	1 year of disease progression (retrospectively or prospectively determined) plus 2 of 3 of the following criteria: 1.Evidence for DIS in the brain based on ≥1 T2 lesions in the MS-characteristic (periventricular, juxtacortical or infratentorial) regions 2.Evidence for DIS in the spinal cord based on ≥2 T2 lesions in the cord 3.Positive CSF (isoelectric focusing evidence of oligoclonal bands and/or elevated IgG index)

In two long-term follow-up studies (Beck *et al.*, 2003; Fisniku *et al.*, 2008), it was found that MS developed in up to 86% of those with an abnormal brain MRI with a CIS. In order to provide an early diagnosis of MS the European multicentre collaborative research network that studies MRI in MS (MAGNIMS) drew up diagnostic criteria (Montalban *et al.*, 2010), which can provide an MS diagnosis in the earliest stage of the disease. These criteria also reflect the importance of spinal cord imaging as in the McDonald criteria.

Spinal cord MRI has been recommended both for early diagnosis and may also be useful in determining clinical subtypes (Lycklama *et al.*, 1998). It has also been recommended in differentiating MS from other inflammatory disorders affecting the spinal cord. Autoimmune conditions, such as systemic lupus erythematosus, Sjögren disease, sarcoidosis and small vessel ischaemic changes can mimic the T2-weighted signal changes of MS in an MRI of the brain. Thus the sensitivity of brain MRI in MS is higher than its specificity (Ormerod *et al.*, 1987). The result is that patients with neurological symptoms and an abnormal MRI brain could be potentially inappropriately diagnosed as having MS. As spinal cord abnormalities in MS have been well defined radiologically as either focal lesions or atrophic changes these findings rarely are found in the spinal cord in a healthy population. Inflammatory conditions can cause changes in the spinal cord but these often differ from MS (Provenzale *et al.*, 1994; Junger *et al.*, 1993). In one study of patients with various autoimmune neurological conditions, who had a brain MRI mimicking MS, no cervical cord lesions were seen (Rovaris *et al.*, 2000). It has been suggested that MS can be confirmed with a positive predictive value of 85%

when the spinal cord MRI is abnormal and when the spinal cord is normal; the exclusion of MS has a negative predictive value of 97% (Bot *et al.*, 2002).

Typically spinal cord lesions in MS are detected in the sagittal plane using T2 or PD-weighted images and are then confirmed on axial images. The lesions are usually less than one vertebral segment in length, most commonly in the cervical cord, however diffuse involvement of the spinal cord can also be seen (Lycklama *et al.*, 2003). The lesions involve the lateral and posterior white matter and also involve the grey matter with a wedge shaped appearance on axial images (Tartaglino *et al.*, 1995). Acutely, MS plaques can cause swelling of the cord and can enhance with Gd contrast, longstanding lesions can merge to form diffuse areas of signal change. Focal or generalised atrophy may also occur. In some instances only diffuse changes are seen without the appearance of demarcated focal lesions and are associated with progressive forms of the disease (Lycklama *et al.*, 1997).

Although spinal cord MRI is useful when MS is a differential diagnosis based on brain imaging, it is also useful when there is a high clinical suspicion of MS but the patient has a normal MRI brain, as is the case in a minority of patients with MS (Allen *et al.*, 1981). MRI excludes an alternate diagnosis for the symptoms attributed to the cord, such as a compressive cause, and increases the sensitivity and specificity of imaging for an MS diagnosis (Thorpe *et al.*, 1996). In the same study it was commented that cord imaging is particularly helpful in progressive forms of MS where there may be a limited number of lesions on the brain and a high proportion of cord lesions.



**Figure 3.1** Sagittal T2-weighted T2 MRI of cervical cord with MS lesion indicated by the yellow arrow

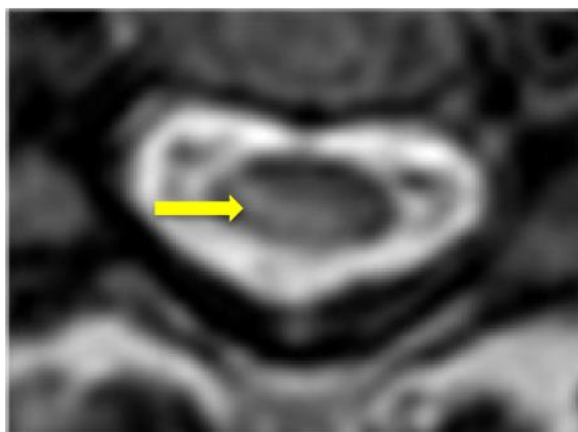


**Figure 3.2** Axial T2-weighted MRI of the cervical spinal cord with MS lesion, indicated by the yellow arrow as a hyper-intense abnormality

### 3.3 Spinal cord atrophy on MRI

The abnormalities found in spinal cord imaging have been evaluated to determine if they correlate with the subtype of MS: RR or progressive forms of the disease (Lycklama *et al.*, 1998). There was a correlation found between the number of brain T1 lesions and number of focal spinal T2 lesions. There was also found to be a correlation between spinal cord atrophy and expanded disability status scores (EDSS) (Kurtzke 1983) in all groups. However, a difference in the degree of atrophy of the cord was noted between RRMS and progressive forms of the disease (PPMS, SPMS). This study was of importance as earlier studies (Filippi *et al.*, 1995) evaluating the correlation between brain MRI abnormalities and disability were disappointing. These findings were emphasised in a further study evaluating dimensions of the cervical spinal cord in benign MS and SPMS compared to controls (Filippi *et al.*, 1996). There was found to be an inverse association between cord atrophy and disability and cord dimensions in benign MS were similar to healthy controls. However a comparison of the T2-weighted lesions on brain MRI did not correlate with disease subtype or degree of disability.

As earlier studies had shown a variable relationship between cord atrophy and disability (Kidd *et al.*, 1993; Filippi *et al.*, 1995), a new reproducible method of measuring cord atrophy was developed by Losseff *et al.* (1996). In this study a 1.5T MRI was performed on sixty patients with various forms of MS. From this scan five axial 3mm slices were used at the level of C2/C3 intervertebral disc. This level was chosen for three reasons: the CSF space is wide so that the cord lies centrally (maximising cord/CSF contrast); there is little variability of cross

sectional area at this level; and it is an uncommon site for disc protrusion. A semi-automated technique was used, the accuracy of which was determined by calculating the area of resin rods in fluid to simulate spinal cord measurement. From these images a region of interest was drawn around the cord in the top slice and then around the cord and CSF space. The technique provided a measure of cord cross-sectional area with a coefficient of variation of 0.8%, indicating its reproducibility. A strong correlation was found between EDSS score and cord area and a correlation between reductions in cord area compared to controls with increasing levels of disability. The functional system scores of the EDSS were also found to correlate with cord area using this technique.

Cord atrophy has been found to occur independently of focal lesions (Bergers *et al.*, 2002) and these findings have correlated with pathological studies (Ganter *et al.*, 1999). The axonal loss and increase in axonal diameter noted pathologically was confirmed to occur in normal appearing spinal cord as well as totally and partially demyelinated areas. This study provided further evidence for the lack of correlation between T2-weighted lesions and physical disability as measured by the EDSS. As pathological studies indicated axonal loss from early in the course of the disease, radiological studies have also examined possible axonal loss in patients with a CIS using atrophy as a surrogate marker of this pathology (Brex *et al.*, 2001). Those patients with an abnormal brain MRI were found to have a more atrophic spinal cord than those with a normal brain MRI compared to controls. Spinal cord syndromes accounted for 12% of those studied, suggesting that axonal loss occurs in the spinal cord irrespective of clinical presentation.

The investigators also reported atrophic changes found in the brain in the early stages of MS following CIS (Brex *et al.*, 2000).

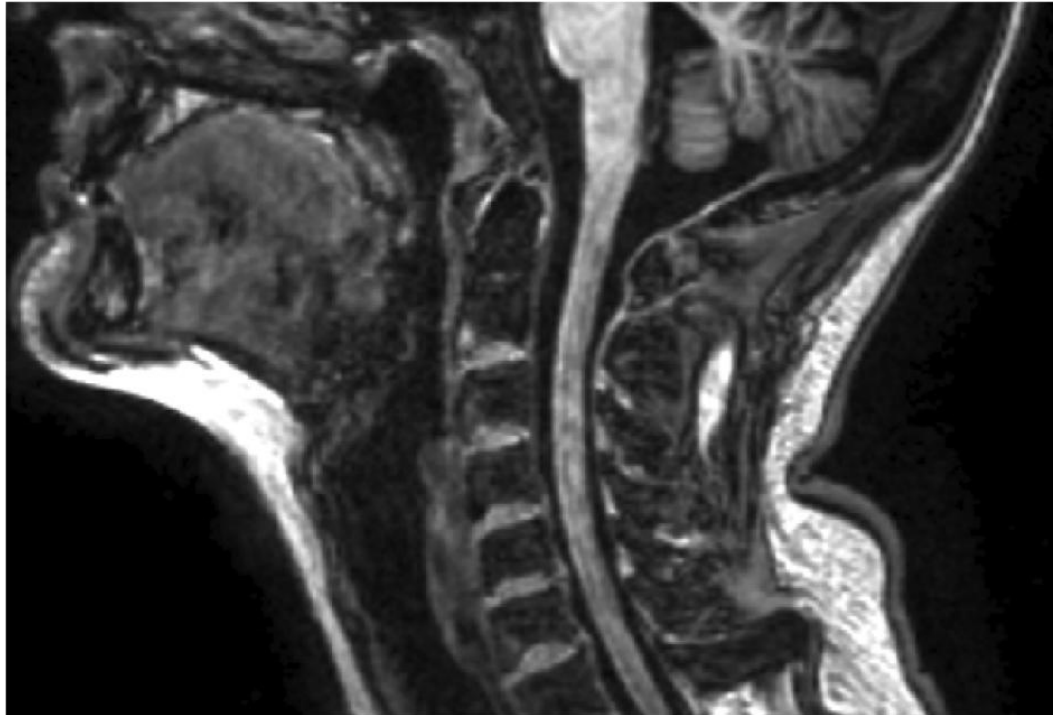


**Figure 3.3** Sagittal 3D T1-weighted cervical spine MRI: used in calculating spinal cord area in MS.

### **3.4 Association between spinal cord MRI abnormalities and disability**

The EDSS, developed by Kurtzke (1983), remains one of the most frequently used measures of disability in MS in clinical trials and studies of MS. A number of criticisms have been made of the EDSS since it was developed: insensitivity to small changes, poor intra-rater and inter-rater variability and its focus on ambulatory function without all measures of disability being taken into account (Hobart *et al.*, 2000). Spinal cord cross sectional area on MRI, however, has been shown to correlate with EDSS and functional system scores (FSS) (Losseff *et al.*, 1996) and given the lack of correlation between T2-weighted lesions on brain MRI and disability, a number of investigators have assessed the use of spinal cord MRI parameters as an objective and reproducible measure of disability.

The abnormalities found on spinal cord MRI appear to correlate with the subtype of MS (Lycklama *et al.*, 1997). As there had been no correlation found between the number of focal lesions and disability (Bergers *et al.*, 2002) Lycklama *et al.* investigated whether diffuse changes seen on proton density-weighted images, rather than focal T2 hyperintense lesions could account for disability in the subgroups of MS assessed. Sixty patients with RRMS, SPMS and PPMS were imaged and examined using the EDSS (Kurtzke 1983) and also the Functional Systems Score (Kurtzke 1961). It was found that the presence of diffuse abnormalities was associated with progressive forms of MS and higher scores on the EDSS and Functional Systems Score.

As there has been an established link between cord atrophy and disability (Losseff *et al.*, 1996), studies have determined whether this is a reliable MRI

parameter for assessment of physical disability in long-term follow up studies (Stevenson *et al.*, 1998; Losseff *et al.*, 1996).

By using a volume acquired inversion-prepared fast spoiled gradient echo (FSPGR) acquisition the problem of reproducibility was addressed by Stevenson *et al.* (Stevenson *et al.*, 1998). The cord area was measured at C2/C3 in 28 patients with MS. Intra-rater reproducibility was improved at 0.51% compared to 0.73% in the assessment by Losseff *et al.* (Losseff *et al.*, 1996). Again there was a strong correlation between EDSS scores, however the MRI parameters were found to be reproducible in this long-term follow up study.

MRI of the brain in PPMS often shows limited abnormalities (Thompson *et al.*, 1991); with the result that prediction of disability was limited in this progressive form of the disease based on this modality of imaging alone. In a long term follow up study of PPMS (Sastre-Garriga *et al.*, 2005), it was found that cord atrophy over two years predicted clinical outcome on long-term follow up.

In a ten-year follow up study of 101 patients with PPMS, patients were assessed using 10m metre timed walking test (TWT), nine hole peg test (9-HPT), EDSS and T1 and T2-weighted MRI of the brain and spinal cord at baseline one and two years (Khaleeli *et al.*, 2008). Cervical cord cross sectional area was calculated using the technique described by Losseff *et al.* (Losseff *et al.*, 1996). Changes in the EDSS score as well as other parameters were recorded. Although spinal cord cross sectional area predicted disability at five years it did not do so at ten years. The strongest predictor of long term disability in PPMS was TWT at baseline.

Earlier studies (Stevenson *et al.*, 1998; Losseff *et al.*, 1998; Losseff *et al.*, 1995) focused on cord atrophy as a marker of disability however this has not been the only MRI parameter assessed in relation to disability, more recent studies have used quantitative MRI measures as a means of assessing the cord and correlation with disability.

### **3.5 Inversion recovery MRI in the spinal cord**

Inversion recovery MRI techniques invert the magnetisation in a T1 sequence by applying a pulse, resulting in a strong contrast between tissues with different T1 relaxation times and can also suppress signal from fluid or fat. Inversion recovery sequences can also provide greater sensitivity for Gd enhancement (Lee *et al.*, 2000). A number of different inversion recovery techniques have been employed imaging multiple sclerosis: short T1 inversion recovery (STIR), phase sensitive inversion recovery (PSIR) and double inversion recovery (DIR).

#### **3.5.1 Short T1 inversion recovery**

Imaging the cord in the sagittal plane in MS is useful as it can give anatomical level of lesions seen along the length of the cord, this can be done using a number of different sequences including short T1 inversion recovery (STIR). Enhanced T1 and T2 contrast are obtained by shortening the inversion time (Bydder *et al.*, 1985). The signal change due to increase in T1 and T2 is of importance as this is commonly seen in spinal cord lesions, such as in MS; the sequence also has less susceptibility to motion artefacts and enhanced fat suppression (Mascalchi *et al.*,

1992). This technique was first employed in the spinal cord in 48 patients with varied spinal cord syndromes, not exclusively demyelinating. The STIR sequence was found to be superior to cardiac gated spin echo images; however, there was a lower signal to noise ratio (SNR) with STIR (Mascalchi *et al.*, 1992).

This technique was then employed to evaluate exclusively patients with MS who had symptoms or signs suggestive of spinal cord pathology (Thorpe *et al.*, 1994). The STIR sequences obtained on the spinal cord were compared to FSE sequences. More lesions were seen on the STIR sequence; however, there was poorer anatomic definition and again a lower SNR. Using a combination of STIR and FSE the overall number of lesions detected increased by 25% and the authors recommend using a combination of both sequences.

Rocca *et al.* compared the use of STIR with gradient echo (GE) and T2-weighted FSE in a study of 56 patients with MS (Rocca *et al.*, 1999). Both GE and STIR sequences increased the number of lesions detected when compared to FSE, with STIR having the best sensitivity of the three sequences and also the greatest number of lesions was detected with STIR. In a separate study the STIR sequence was compared to conventional spin echo sequence (CSE) in a cohort of patients with secondary progressive MS (Bot *et al.*, 2000). The STIR sequence showed 33% more lesions, including smaller focal lesions, and with a higher contrast to noise ratio (CNR). STIR was recommended as an adjunct in detecting abnormalities in the spinal cord in MS.

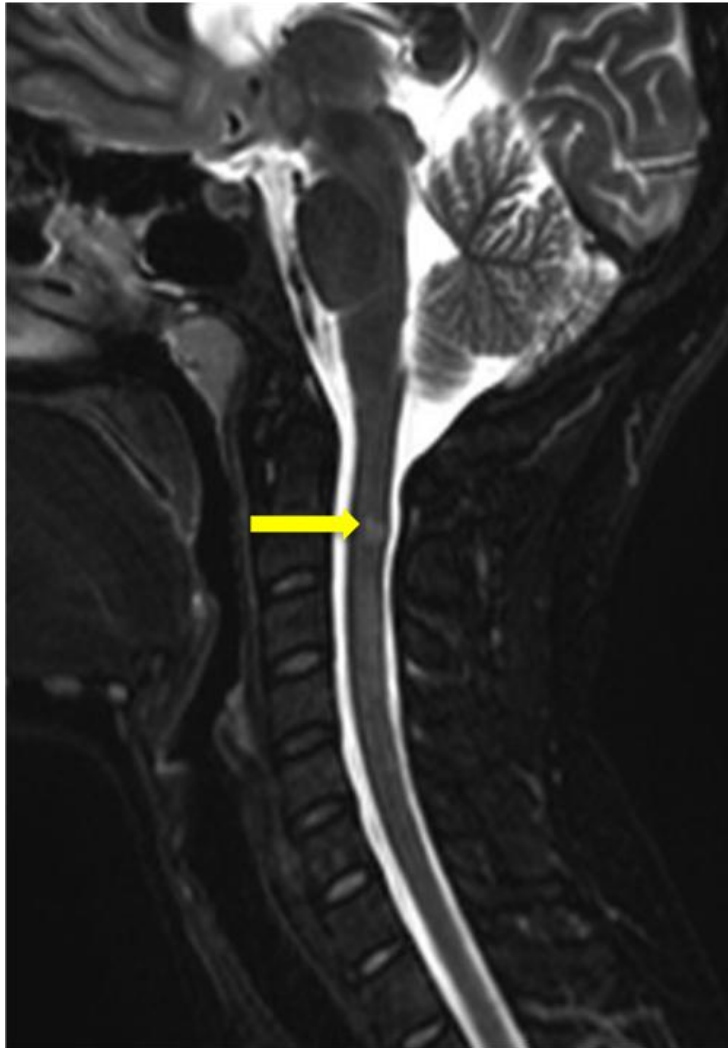


**Figure 3.4** Sagittal STIR image of cervical spine showing MS lesion in the cervical cord

### **3.5.2 Phase sensitive inversion recovery imaging**

As with other inversion recovery techniques, phase sensitive inversion recovery (PSIR) can provide strong contrast between tissues with different T1 relaxation times by estimating and removing background phase and retrieving correct polarity information. PSIR has shown to be effective in cortical grey matter lesion detection with clear lesion delineation (Hou *et al.*, 2005; Nelson *et al.*, 2007, Sethi *et al.*, 2012; Sethi *et al.*, 2013). PSIR has been prospectively compared with FSE and STIR imaging in the spinal cord in MS (Poonawalla *et al.*, 2008). Contrast between lesions was compared using the different sequences with FSE as the reference. The highest lesion to cord contrast was seen with the PSIR sequences and both this sequence and the STIR improved lesion detection compared to FSE. The authors recommend that STIR alone is not sufficient for lesion detection.

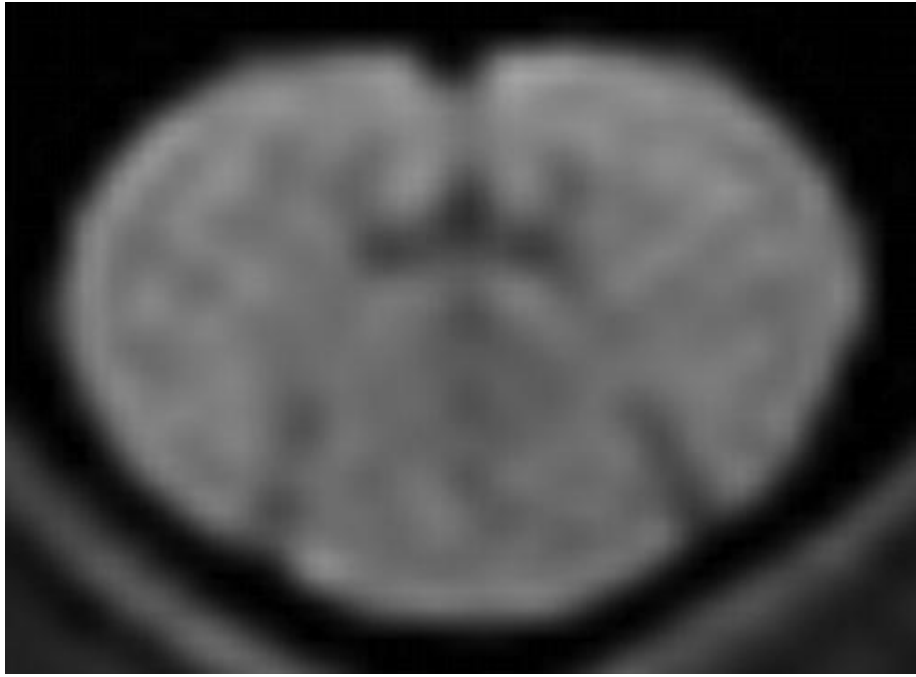


**Figure 3.5** Axial PSIR of healthy cervical spinal cord at the level of C2/C3

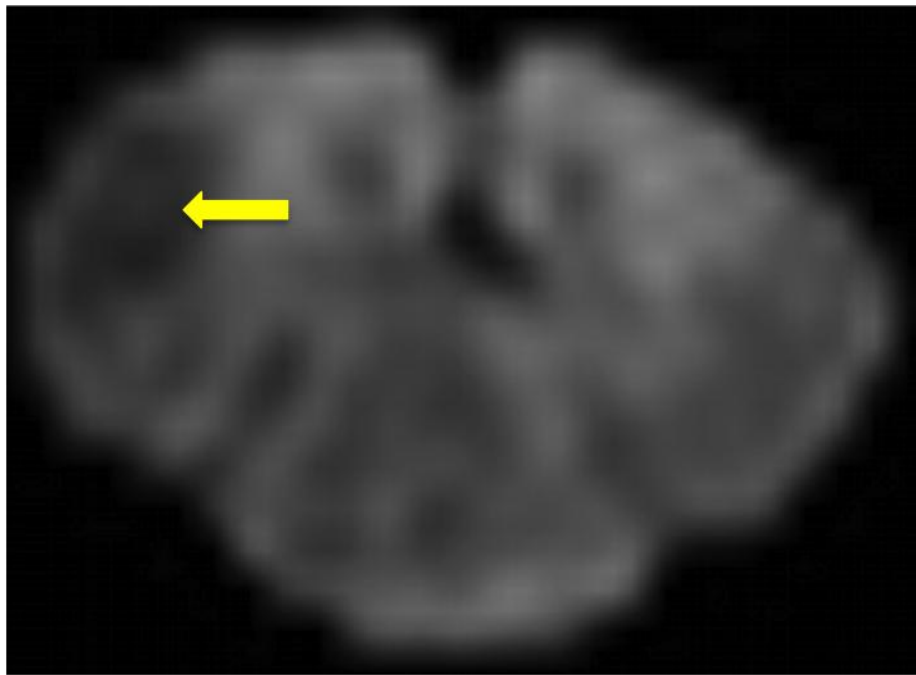


**Figure 3.6** Axial PSIR of MS cervical spinal cord with lesion visible (highlighted by yellow arrow) in the lateral column of the white matter

### **3.5.3 Double inversion recovery imaging**

Double inversion recovery imaging (DIR) suppresses signal from white matter and CSF, which allows easier identification of lesions (Bedell *et al.*, 1998). DIR has been utilised for detection of cortical lesions in MS that may not be visible on conventional MRI (Geurts *et al.*, 2005). This sequence has its limitations however as it is susceptible to flow artefacts, it also has a low SNR and has poor definition of lesion borders. However, use of DIR in combination with PSIR may improve the identification of cortical lesions in MS (Nelson *et al.*, 2007). DIR imaging has been used for identification of cortical lesions in MS by several investigators (Calabrese *et al.*, 2007; Geurts *et al.*, 2005; Nelson *et al.*, 2007; Wattjes *et al.*, 2007); however there is limited information as yet on using this technique in the spinal cord in MS.

### **3.6 Quantitative spinal cord MRI**

The importance of MRI in the diagnosis of MS has been reflected by its inclusion in all of the most recent diagnostic guidelines for this disease (McDonald *et al.*, 2001; Polman *et al.*, 2005; Montalban *et al.*, 2010). It has also been used as an objective marker of disease activity in a number of clinical trials for treatments in MS (Rovaris *et al.*, 1999). However conventional MRI has its limitations in detecting the nature and extent of damage in T2-weighted lesions (Kappos *et al.*, 1999; Molyneux *et al.*, 2001). A number of quantitative measures have been developed to elucidate the pathology of MS, which include: Magnetisation-

transfer MRI, diffusion-weighted MRI, functional MRI and magnetic-resonance spectroscopy.

### **3.6.1 Magnetic resonance spectroscopy**

In normal brain tissue four main metabolites are detected from in vivo proton magnetic resonance spectroscopy using long TEs: choline containing compounds, creatine/phosphocreatine, N-acetylaspartate (NAA) and lactate. Spectroscopy of acute MS lesions reveals a change in the normal values with increases in choline and lactate in the acute phase and a decrease in NAA (Davie *et al.*, 1994; DeStefano *et al.*, 1995). NAA is located in neurones and axons only and reduced NAA levels are thought to reflect axonal damage. NAA is synthesised in the mitochondria together with adenosine triphosphate and oxygen consumption (Bates *et al.*, 1996) and although its exact function is unclear it is known to be the second most abundant amino acid in the CNS (Simmons *et al.*, 1991).

NAA is of particular importance in assessing spectra as its level is a reflection of axonal integrity, it can be permanently decreased reflecting axonal loss or there can be a reversible component suggesting axonal dysfunction in an acute lesion (Davie *et al.*, 1994). Decreases in NAA can precede visible abnormalities on MRI by several months (Pan *et al.*, 2001) and levels are correlated with disability and cognitive dysfunction (Bjartmar *et al.*, 2000; Kendi *et al.*, 2004).

In a study by Bjartmar *et al.* (2007) the NAA levels in the post-mortem spinal cords of five disabled patients with MS were measured. Spinal cord area, axonal loss and NAA levels were measured on the pathological specimens. It was shown

that axonal loss was correlated with decreased NAA in both myelinated and demyelinated axons. These data support the use of decreased NAA levels in MR spectroscopy (MRS) as a marker of axonal loss and consequently disability in MS.

Studies initially focused on MRS in the brain of patients with MS, however more recently a number of studies involving the spinal cord have been done. The first such study was carried out by Kendi *et al* (2004), comparing MRS in the cervical cord of nine patients with MS and twelve healthy controls. In keeping with histopathological findings (Bjartmar *et al*, 2000) there was a prominent decrease in NAA levels in the spinal cord of MS patients, with all other metabolites unchanged from controls. The same technique was investigated in a separate study with 11 patients with MS and 11 controls (Blamire *et al*, 2007). Again it was found that NAA levels were substantially reduced in the spinal cord compared to controls and there was significant cord atrophy on conventional MRI sequences in MS cases. However, no significant correlation was found between NAA levels and EDSS scores, the authors point out that this may be due to the small sample size or the heterogeneity of cases used. The decrease in NAA was also found to be greater than compared to normal appearing white matter in the brain it is hypothesised that this disparity may be due to axonal damage, Wallerian degeneration or transection of the cord but not in the brain.

MRS has also been employed as a method of understanding the mechanism of spinal cord repair following an acute relapse (Ciccarelli *et al*, 2010). Fourteen patients with a diagnosis of MS and a spinal cord syndrome localised to the cervical cord clinically and radiologically were recruited and imaged at three monthly intervals following their initial presentation. It was found that the

patients who did not improve had an overall decrease in NAA over time across the three time points (1, 3 and 6 months). In comparison with those who recovered, where there was an increase in NAA from one month to six months, and those with a better recovery had a corresponding greater increase. It was found that a longer disease duration was associated with a smaller increase in NAA after one month and both those who recovered and those who didn't had an overall decrease in cord area over time. It is hypothesised that the increase in NAA may reflect enhanced mitochondrial activity, which is a proposed mechanism for recovery following demyelination.

In a similar study by the same group (Ciccarelli *et al.*, 2007) acute disability was assessed, following a cervical cord relapse, in 14 patients with MS, using spinal cord spectroscopy and diffusion based tractography. Radiological parameters were compared with the EDSS, 9-hole peg test (9-HPT) (Goodkin *et al.*, 1988) and 25-foot walk test (TWT) (Cutter *et al.*, 1999). It was found that NAA, although significantly lower than controls, did not correlate with EDSS or TWT but there was a correlation with 9-HPT.

Myo-inositol, is a further metabolite that may be analysed from MRS and is a potential marker of glial cell function (Brand *et al.*, 1993) and also may be increased in the normal appearing white matter in the MS brain (Fernando *et al.*, 2004). The authors found that myo-inositol correlated with the EDSS and creatine levels correlated with 9-HPT.

More recently, myo-inositol in the cervical cord has been reported to be useful in distinguishing neuromyelitis optica (NMO) spectrum disorders from MS (Ciccarelli *et al.*, 2013). The lower myo-inositol levels seen in this study in NMO

are thought to reflect astrocytic necrosis, which is a prominent feature pathologically in this disorder. This may have implications for future studies that aim to investigate biomarkers capable of distinguishing NMO from MS.

### **3.6.2 Magnetisation-transfer imaging**

Magnetisation transfer involves transfer of magnetisation from the hydrogen nuclei of protons (including macromolecular protons e.g. in myelin and membranes) that have restricted movement to those that are unrestricted or free. The hydrogen nuclei in the water molecules are usually referred to as protons. Proton movement differs depending on their location whether they are in fluid, with free movement, or in tissue, where movement is more restricted (Woff *et al.*, 1989). The free protons have fewer interactions with the environment and a longer T2 time compared to the protons that interact with the local structures and have a shorter T2. Magnetisation transfer is a measurement of the interaction between these two pools of protons and from this the magnetisation transfer ratio (MTR) can be calculated. It is of significance in MS because a low MTR indicates damage to macromolecular structures including myelin and other neuronal structures. A substantial reduction of MTR indicates severe tissue damage (van Wasenberghe *et al.*, 1999).

As with other modalities of quantitative MRI, initial studies were done on the brain, with subsequent work done on the spinal cord, including a comparison of magnetisation transfer imaging to histopathology in the spinal cord (Bot *et al.*, 2004). In this study the cervical cords from 11 patients with MS and two controls were imaged using 4.7T MRI and examined histologically. Conventional MRI sequences were performed as well as quantitative measures; axonal number,

diameter and myelin content were then established from the histology. Quantitative MR findings were compared with conventional MRI and it was found that total cord area measurement showed a prolonged T1 relaxation time, which was increased in MS cases. This finding was replicated with T2 measurements and a reduced MTR compared to controls. There was a strong correlation found between MTR and demyelination but not axonal features. However the authors indicate that a number of factors may have influenced this lack of correlation: length of disease, varying degrees of gliosis of the cord, formalin fixation and high field strength.

In a similar *post mortem* study on the spinal cord, using 7T MRI, Mottershead et al. evaluated a number of different MRI parameters, including MTR, with pathological samples (Mottershead *et al.*, 2003). It was found that there was a strong correlation between MTR and axonal density as well as myelin content. The change in MTR values were felt to be due to a reduction in bound protons, due to axonal loss, with a corresponding increase in free protons. This study supports the use of MTR to quantify both myelin and axonal loss.

*In vivo* studies have also examined the use of quantitative MRI measures, including the examination of sensorimotor dysfunction and its correlation with spinal column damage in MS (Zackowski *et al.*, 2009). Images were obtained on a 3T MRI using cerebrospinal-fluid-normalised magnetisation transfer (MTCSF), which allowed evaluation of spinal columns or grey matter. MTCSF uses CSF as an internal intensity standard, allowing inter-individual comparison of MT data without the need for a reference scan. It allows for quantitative measures of specific spinal columns. MTCSF was calculated in lateral columns and dorsal

columns and grey matter volume were assessed from C2/C3. Measures of impairment, reflecting damage in these structures were calculated using vibratory sense, postural sway, ankle dorsiflexion and walking velocity. It was found that EDSS scores correlated with MTCSF results there were significant correlations between vibration and dorsal columns and dorsiflexion and walking velocity with lateral columns. This study demonstrated that MTCSF could be used as a measure of disability in the spinal cord column being assessed. It was also noted that grey matter volume MTCSF was significantly correlated with disability. The fact that MT imaging is specific for demyelination, as seen in post-mortem studies (Bot *et al.*, 2004), could indicate that demyelination plays an important role in disability, as evidenced by this study.

Other studies have focused more on the correlation between grey matter and disability using MTR (Agosta *et al.*, 2007). MS lesions are found on pathological studies on the grey matter of the spinal cord, however, the position of lesions with respect to grey and white matter is not easily determined on conventional MRI (Lycklama *et al.*, 2001; Gilmore *et al.*, 2006). The cervical cord grey matter of 18 patients with RRMS was assessed by MTR and findings were correlated with EDSS scores (Agosta *et al.*, 2007). Findings were compared to healthy controls. RRMS patients were found to have significantly lower MTR in the cervical cord grey matter. MTR was also found to correlate with the EDSS score.

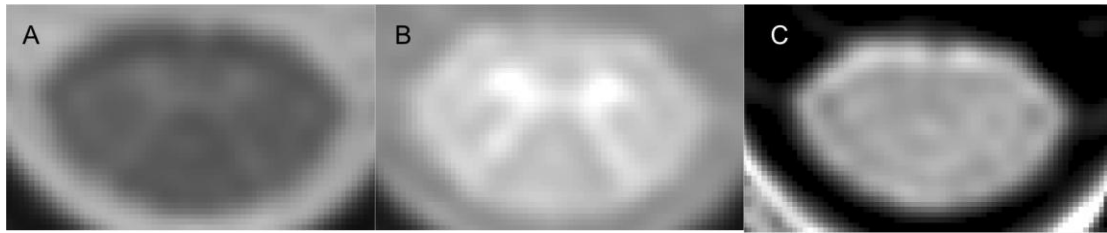


**Figure 3.7** MTR imaging in healthy cervical spinal cord. A) MT 'on' B) MT 'off' C) MTR map

### 3.6.3 Diffusion weighted imaging

Diffusion MRI is an alternate means of assessing the motion of water molecules, as an apparent diffusion coefficient (ADC). The structure that contains the water molecules alters the direction of movement, such as myelin in the brain. During a diffusion weighted MRI scan, diffusion sensitising gradients encode the diffusion properties of the tissue being investigated; this facilitates the sensitivity of the MR signal to the diffusion behaviour spins of the protons in the tissue. By measuring the ADC diffusion MRI is thereby able to give information about the microstructure of tissue along a diffusion-sensitised direction (Filippi *et al.*, 2003). The water molecules in the structure are defined as having anisotropy, which is the property of being directionally dependent. Anisotropy results in variation of diffusivity with direction of measurement (Le Bihan *et al.*, 1991). By acquiring a number of different diffusion directions a diffusion tensor (DT) can be reconstructed as an ellipsoid construct. The full direction of a molecule's diffusion can be plotted along one of the three orthogonal axes (x, y, z), which are known as eigenvectors. The measure of length of each eigenvector provides an eigenvalue, from which quantitative measures can be calculated, including the

mean diffusivity (average of ADCs in three orthogonal directions). These values can be characterised using a 3 x 3 matrix known as tensor (Piperpaoli *et al.*, 1996), from which fractional anisotropy (which is a scalar value between zero and one that describes the degree of anisotropy of a diffusion process) and radial diffusivity (index of diffusivity perpendicular to the main axis of DT i.e. perpendicular to the main fibre direction) can be evaluated (Basser *et al.*, 1996). Studies have shown abnormal values of ADC, mean diffusivity ([MD] i.e. the average magnitude of molecular displacement by diffusion) and FA in T2 lesions in MS, with more abnormal values when the lesion is hypointense on T1 (Rovaris *et al.*, 2005).

Diffusion tensor imaging (DTI) has been possible in the spinal cord and has been shown to be possible in healthy volunteers including tractography (Smith *et al.*, 2010). The technique involves advanced protocols and had been applied to study MS in the spinal cord.

A technique known as zonally oblique multislice (ZOOM) technique had previously been developed (Wheeler-Kingshott *et al.*, 2002); the same technique was extended to establish DTI in the spinal cord. However, this technique was limited by the fact that a slice gap was required, which precluded the acquisition of contiguous slices. A method of obtaining contiguous slices was then developed (CO-ZOOM) which was used in both the optic nerve and spinal cord (Agosta *et al.*, 2007). The technique used was later employed for spinal cord tractography in MS (Ciccarelli *et al.*, 2007), as it had been shown to reduce distortions due to susceptibility variations and allows for study of axonal damage where nerve fibre tracking is performed.

Clark *et al.* (2000) have examined the use of diffusion imaging in multiple sclerosis in three patients with significant locomotor impairment (mean EDSS score of 6) compared to four healthy controls. MD was significantly higher in MS cord lesions than in controls, with a correspondingly reduced anisotropy although this was not found to be statistically significant. Both values were found to have a high standard deviation, which may represent the heterogeneity of the lesions. The abnormal values were attributed to demyelination and axonal loss and in acute lesions to vasogenic oedema. These findings were based on the assumption that the spinal cord has cylindrical symmetry.

DT MRI has been shown in cross sectional studies to correlate with the level of disability associated to demyelinating and degenerative conditions in the spinal cord (Valsasina *et al.*, 2005; Valsasina *et al.*, 2007). Following these studies a longitudinal study was performed on 42 patients with varied MS subtypes (Agosta *et al.*, 2007). FA and MD values were calculated in the cervical cord as well as routine MRI studies, which allowed calculation of cross sectional area. The decrease in FA over time was found to be associated with patients' age and clinical phenotype, higher in PPMS than other groups. However no significant correlation was found with longitudinal change in cord atrophy, or T2-weighted lesions with changes in FA or MD. This study demonstrated that not just cord atrophy changes over time but also the intrinsic tissues of the cord as reflected by DTI changes. It was also shown that the intrinsic abnormalities precede the development of atrophy reflected on MRI imaging. Furthermore, the changes in FA of the cervical cord were associated with EDSS scores at baseline and with the accrual of disability over time.

It has been shown that axonal damage in the spinal cord occurs independent of T2-weighted lesions in the spinal cord (Bergers *et al.*, 2002) and that T2-weighted lesions in the brain do not correlate with disability (Filippi *et al.*, 1995). Applying the same principles to DTI imaging, Van Hecke *et al.* assessed the spinal cord diffusion properties in MS patients with and without T2 weighted lesions in the spinal cord (Van Hecke *et al.*, 2009). In each patient the following parameters were calculated: FA, MD, axial (longitudinal) diffusivity ( $\lambda_{||}$ ), radial (transverse) diffusivity ( $\lambda_{\perp}$ ) and the ratio of axial to radial diffusivity ( $\lambda_{||}/\lambda_{\perp}$ ). Regions of interest (ROI) were manually placed on axial images to avoid volume averaging by inclusion of CSF. Diffusion tractography was also performed on the spinal cord. It was found that FA and the ratio of longitudinal and transverse diffusivity ( $\lambda_{||}/\lambda_{\perp}$ ) were both significantly reduced in the spinal cord of patients with and without any lesions and no statistical difference between the subgroups of patients. MD values were found to be increased, but not found to be statistically significant. Other authors have suggested that normalisation of the MD value can occur due to astrocytic proliferation, cell debris, fibrillary gliosis and inflammatory infiltrates (Agosta *et al.*, 2005). Such findings suggest that FA and  $\lambda_{||}/\lambda_{\perp}$  are more sensitive to the micro structural changes in the spinal cord in MS and may imply that pathology in the spinal cord is present even when lesions are only seen in the brain.

Using diffusion weighted imaging, a three dimensional modelling technique can be used to visually represent neural tracts. Although tractography is typically done in the brain, it may also be performed in the spinal cord. However, there have been limitations with tractography algorithms that inhibit their application

in clinical practice or trials: the process of generating tract measures may be laborious and with high variability, which can limit sensitivity to detect longitudinal change and may be further compounded in destructive processes (Wheeler-Kingshott *et al.*, 2009). To overcome these difficulties two novel techniques have been developed: (i) *tract based spatial statistics*, allowing comparison of different tracts by simplifying the structure (Smith *et al.*, 2006); (ii) *tract probability maps* from DTI data, based on probability of a voxel belonging to a known tract (Hua *et al.*, 2008). Reich *et al.* compared these techniques in a recent study (Reich *et al.*, 2010). MRI scans were performed on healthy volunteers to generate tract probability maps and patients with MS were studied and results from the two methods were compared. It was found that there was a correlation found in the optic radiation and corpus callosum but less so in the optic tract. It was also found that the tract probability map method correlated well with Paced Auditory Serial-Addition Test (PASAT – a component of the MSFC [Cutter *et al.*, 1999]) scores for the corpus callosum.

DTI has also been used to elucidate the mechanism whereby some people with MS do not accrue increasing levels of disability over a prolonged period of time, in a variant of the disease known as benign MS (BMS) (Benedetti *et al.*, 2010). In this study BMS patients were compared with SPMS, who had a higher EDSS. Parameters recorded included: cervical cord MD and FA, with histograms produced for each, cross sectional area of the cord and brain T2 lesion volume. It was found that both BMS and SPMS patients had significant increases in cord MD compared to healthy controls, SPMS patients were also found to have a significant decrease in average FA compared with BMS and healthy controls. The

authors suggest that the discrepancy between FA and MD in BMS may be due to a preservation of white matter bundles in the cervical cord. Thus DTI can potentially give a further insight into the mechanism of disability in MS and why some individuals are relatively spared.

In a recent study by Oh et al. (2012) spinal cord FA and MD were found to be independently associated with hip flexion, vibration sense and EDSS.

Associations with a number of similar measures of physical disability, used in the study by Oh et al., have also been shown to be associated with spinal cord RD and FA (Naismith *et al.*, 2013). Furthermore, spinal cord DTI metrics (FA and MD) were shown to be able to discriminate between disability levels in MS, whereas T2-weighted lesions were unable to do so (Oh *et al.*, 2013). These important associations with disability and discriminatory capacity of DTI may reflect the microstructural abnormalities (such as axonal loss and demyelination) being detected in the spinal cord, that may not be detected using conventional T2-weighted images (Bergers *et al.*, 2002).

## Chapter 4 - Spinal cord atrophy in long disease duration multiple sclerosis

### 4.1 Introduction

Understanding the causes of long-term disability in MS is a key goal of current research; it is directly relevant to how we monitor and treat the disease. Histopathology studies have shown that MS affects brain grey (GM) and white matter (WM) (Brownwell and Hughes 1962), and the spinal cord (Fog 1950). However, from such work (Bø *et al.*, 2003; Kutzelnigg *et al.*, 2005; Gilmore *et al.*, 2006) it is difficult to determine which is most clinically relevant, and which is most likely to serve as a useful marker of disease progression and treatment effectiveness. MRI, while being less pathologically specific, facilitates assessment of tissue abnormalities *in vivo* and approximate histopathological changes. Previous work measuring brain lesion load, brain and spinal cord atrophy, has demonstrated correlations between changes in all these regions and clinical outcomes, albeit of varying strengths in different cohorts and with no single measure found to fully explain variability in disability scores. Given this, there has been increasing interest in the use of combinations of MRI measures in parallel to more fully characterise clinically relevant pathology in life.

Of the conventional MRI techniques available, WM lesions determined using T2-weighted imaging have been studied more extensively, and have a clear role in the diagnosis of MS (Polman *et al.*, 2011) and in monitoring response in treatment trials (Barkhof *et al.*, 2011). Following a clinically isolated syndrome (CIS) the load and location of brain and spinal cord lesions seen on T2 weighted

scans, and appearance of new lesions on serial scans, has been shown to predict the conversion from CIS to MS. The accrual of brain WM lesions also, in part, predicts disability and conversion to secondary progressive MS (Brex *et al.*, 2002; Rudick *et al.*, 2006; Fisniku *et al.*, 2008). Furthermore, a combination of lesions and relapses has been proposed as a marker of progression in MS (Sormani *et al.*, 2011). However, despite the frequent use of brain T2-lesion volume (T2LV) as an endpoint in clinical trials (Polman *et al.*, 2006; Coles *et al.*, 2012; Radue *et al.*, 2012) its contribution to disability in the long term has yet to be fully elucidated (Barkhof *et al.*, 2009), although some evidence suggests T2LV early in the course of the disease may be predictive of mortality (Goodin *et al.*, 2012).

Neuro-axonal loss has been shown on histopathological examination of brain GM and WM (Trapp *et al.*, 1998; Ganter *et al.*, 1999; Wegner *et al.*, 2006) and MRI parameters that are affected by this, such as GM volumes, have been found to correlate with disability (Fisniku *et al.*, 2008; Roosendaal *et al.*, 2011). In particular, GM atrophy has been shown to have a role in predicting conversion from CIS to MS (Calabrese *et al.*, 2011), as well as reflecting disease subtype (Fisniku *et al.*, 2008; Fisher *et al.*, 2008). Atrophy has also been observed in WM but appears to progress less rapidly than in GM (Ge *et al.*, 2001; Chard *et al.*, 2002) albeit with the caveat that there have been few very long-term studies, and correlations with disability have not been consistently found. Measures of brain atrophy are being used as outcome measures in clinical trials in both relapsing remitting (Miller *et al.*, 2007, Kappos *et al.*, 2010) and progressive MS (Leary *et al.*, 2003; Kapoor *et al.*, 2010; Connick *et al.*, 2012).

Spinal cord involvement by MS is a major cause of locomotor disability. Axonal loss has been demonstrated in the spinal cord, and is a contributory factor for spinal cord atrophy in pathological studies (Ganter *et al.*, 1999; Bergers *et al.*, 2002; Bot *et al.*, 2004). Several MRI studies have found correlations of disability with upper cervical spinal cord atrophy (Losseff *et al.*, 1996; Stevenson *et al.*, 1998; Horsfield *et al.*, 2010; Rocca *et al.*, 2011).

Two studies have investigated brain and spinal cord atrophy in combination. A single site study of 70 people followed up for 20 years after a CIS suggestive of MS, 43 of whom had clinically definite MS when scanned (median expanded disability status scale [EDSS] in the whole group 2.5, in the clinically definite MS group 3.5), found that brain grey matter and spinal cord atrophy both independently associated with disability (Bonati *et al.*, 2011); and another smaller single site study (21 patients) in patients with a shorter disease duration (mean 8 years) and lower levels of disability (mean EDSS 1.6) found that measures of spinal cord atrophy correlated with disability, while brain lesion load and atrophy did not (Cohen *et al.*, 2012).

In this multicentre cross-sectional study, the relationship between spinal cord and brain atrophy and brain lesion load with long term disability in MS is explored. The aim of this study is to investigate whether spinal cord atrophy is associated with higher levels of physical disability, independently from brain pathology, in people with at least twenty years disease duration.

## **4.2 Methods**

### **4.2.1 Patients**

Seven centres participated in this study, and patients with relapse-onset (relapsing remitting [RR] or secondary progressive [SP]) MS with first symptom onset 20 or more years prior to their clinical and MRI examinations were included. MS subgroups were classified by Lublin-Reingold criteria (Lublin and Reingold 1996). Previous or on-going disease modifying drugs (DMD) were noted.

All patients had EDSS determined (Kurtzke 1983). RRMS patients who had an EDSS score of  $\leq 3$  were defined as having benign MS (Filippi *et al.*, 1994).

Data from patients who had been treated with steroids in the month prior to MRI acquisition were excluded. The ethics committee from each of the participating centres approved this work, and written informed consent was obtained from each subject.

### **4.2.2 MRI acquisition**

MRI scans were acquired using 1.5T (n=5) or 3T (n=2) scanners and included 3D T1-weighted gradient echo sequences of the brain and cervical cord, and dual-echo 2D spin-echo sequences of the brain. The acquisition parameters are summarised in Table 4.1.

**Table 4.1** MRI parameters in each participating centre

	<b>Centre</b>	<b>London</b>	<b>Barcelona</b>	<b>Basel</b>	<b>Milan Don Gnocchi</b>	<b>Milan San-Raffaele</b>	<b>Rome</b>	<b>Amsterdam</b>
	<b>Scanner manufacturer</b>	<b>Phillips (3T)</b>	<b>Siemens (1.5T)</b>	<b>Siemens (1.5T)</b>	<b>Siemens (1.5T)</b>	<b>Siemens (1.5T)</b>	<b>GE (1.5T)</b>	<b>GE (3T)</b>
<b>T2 brain scan</b>	Slice (mm)	3	3	3	3	5	4	3
	TR (ms)	3500	2500	3980	3310	3800	2620	2300
	TE (ms)	85	91	112	11	112	116	114.1
	Matrix (mm <sup>2</sup> )	240x240	240x320	250x256	256x256	256x256	512x512	512x512
	Resolution (mm <sup>2</sup> )	1x1	0.78x0.78	0.98x0.98	0.98x0.98	0.98x0.98	0.63x0.63	0.49x0.49
<b>3D T1 brain scan</b>	Slice (mm)	1	1.2	1	1	1.5	1	1
	TR (ms)	6.8	2300	2080	1900	2000	21	7.8
	TE (ms)	3.1	3	2.93	3.4	2.9	6	3
	Matrix (mm <sup>2</sup> )	256x256	240x256	250x256	192x256	256x256	256x256	256x256
	Resolution (mm <sup>2</sup> )	1x1	1x1	0.98x0.98	1x1	0.82x0.82	0.98x0.98	0.94x0.94
<b>3D T1 cervical spine scan</b>	Slice (mm)	1	1.2	1	0.9	1	1	1
	TR (ms)	8.1	2300	2700	1160	1160	21	7.2
	TE (ms)	3.7	3	4.2	4.2	4.2	6	3
	Matrix (mm <sup>2</sup> )	256x256	240x256	256x256	256x512	256x256	256x256	512x512
	Resolution (mm <sup>2</sup> )	1x1	1x1	1x1	0.45x0.45	1x1	0.98x0.98	0.5x0.5

### 4.2.3 *Image analysis*

#### *T2 lesion volume*

Lesions on T2-weighted scans were outlined using a semi-automated edge finding tool (JIM v. 6.0, Xinapse systems, Aldwinckle, UK, <http://www.xinapse.com>). Total lesion volume was recorded in mLs for each subject.

#### *Brain tissue volumes*

To avoid segmentation errors due to WM lesions, an automated lesion-filling technique was employed (Chard *et al.*, 2010). Lesion masks were created based on 3D-T1 weighted sequences only (i.e. without reference to previously created masks on T2-weighted images). The lesion-filled images were segmented into WM, GM and cerebrospinal fluid (CSF) using the ‘new segment’ option on SPM8 (statistical parametric mapping; Wellcome Trust centre for NeuroImaging, UCL Institute of Neurology, London). All segmentations were reviewed to exclude errors. WM and GM fractional (WMF and GMF) volumes relative to total intracranial volume (the sum of GM, WM and CSF volumes) were calculated.

#### *Spinal cord atrophy*

Sagittal spinal cord images were reformatted axially into five 3mm thick slices perpendicular to the long axis of the spinal cord centred at C2/C3. Upper cervical cord cross-sectional area (UCCA) was then evaluated using an active surface model (Horsfield *et al.*, 2010), which has been used in a multi-centre study (Rocca *et al.*, 2011). Mean cord area of the five slices was determined for each subject (Healy *et al.*, 2012).

#### 4.2.4 Statistical analysis

Univariable associations between EDSS and the four MRI predictors (WMF, GMF, T2LV, and UCCA) and between MRI variables were assessed using Spearman correlation.

For the binary EDSS models (dividing into groups by EDSS scores  $<6/\geq 6$ , as an EDSS score of 6 marks the requirement of a walking aid) univariable logistic regression followed by multiple logistic regression were performed with the four MRI predictors and centre, age at scan, age at onset, disease duration, disease modifying drugs and gender initially included as potentially confounding covariates: only centre and age at scan, contributed significantly (at  $p < 0.05$ ) or materially affected coefficients, and these were subsequently retained in all models. Along with centre and age at scan, the four MRI predictors were entered together and then individually removed from the final multivariable model if they did not significantly contribute (at  $p < 0.05$ ). The C-statistic was calculated to assess the predictive performance of the logistic model; this statistic can range from 0.5 (no better than chance) to 1 (perfect prediction).

With four-category EDSS ( $\leq 1.5 / > 1.5, < 3 / \geq 3, < 6 / \geq 6$ , categories chosen for even frequency distribution) a similar procedure to the above was carried out using instead proportional odds multiple ordered logistic regression; again centre and age at scan were the only covariates to either be significant (at  $p < 0.05$ ) or materially affect MRI coefficients, and were retained in models. The four part model enabled more complete analysis across the spectrum of disability, as per previously published work (Fisniku *et al.*, 2008).

Differences in means between patient groups were assessed by t-test or ANOVA (for comparison of RR and SP and subgroups of RR with SP). In the same way patients with an EDSS  $\leq 3$  were compared to those with an EDSS  $\geq 6$ , irrespective of disease subtype.

Analyses were carried out in Stata 12 (Stata Corporation, College Station, TX, USA) and SPSS 20 (IBM, USA).

### 4.3 Results

Demographics of patients in each participating centre and disability category are summarised in Tables 4.2 and 4.3. For the whole group, patients had a mean age of 52 years (SD 8.8) with a mean age of disease onset 25.8 years (SD 7.7), 111 females and 48 males, of whom 92 had RRMS and 67 SPMS, with a mean disease duration of 26.2 years (SD 6.7) and a median EDSS of 4 (range 0-8). For the four-category EDSS model patient numbers were as follows:  $\leq 1.5$ : 28,  $>1.5, <3$ : 33,  $\geq 3, <6$ : 44,  $\geq 6$ : 54.

Brain segmentation failed for four people (155 volumetric brain scans were used), two patients did not have a T2W scan (157 patients were included in T2LV analysis) and in three patients spinal cord scan was distorted so could not be analysed.

**Table 4.2** patient demographics by centre

Centre	Age (years) Mean $\pm$ SD	Gender (female, male)	Age at disease onset (years) Mean $\pm$ SD	Disease duration (years) Mean $\pm$ SD	Number of RRMS, patients	Number of SPMS patients	EDSS Median, range
1. London, n=20	55.3 $\pm$ 7.9	13, 7	27.8 $\pm$ 6.7	27.0 $\pm$ 6.3	9	11	6, 1-8
2. Barcelona, n=20	53.6 $\pm$ 8.9	14, 6	25.2 $\pm$ 6.9	28.4 $\pm$ 9.1	7	13	4, 2-8
3. Basel, n=12	56.0 $\pm$ 9.9	7, 5	24.0 $\pm$ 8.4	32.0 $\pm$ 7.8	8	4	4, 2-6
4. Milan Don Gnocchi, n=23	53.0 $\pm$ 8.0	17, 6	28.0 $\pm$ 9.0	25.0 $\pm$ 6.0	8	15	6, 2-7.5
5. Milan San-Raffaele, n=64	50.0 $\pm$ 8.9	43, 21	25.0 $\pm$ 8.0	25.0 $\pm$ 6.0	45	19	2.5, 0-6.5
6. Rome, n=11	47.4 $\pm$ 5.9	11, 0	25.9 $\pm$ 6.2	25.0 $\pm$ 5	9	2	2, 0-6.5
7. Amsterdam, n=9	52.2 $\pm$ 9.0	6, 3	29.1 $\pm$ 7.5	22.7 $\pm$ 4.0	6	3	4, 1.5-7
All centres n=159	52.0 $\pm$ 8.8	111, 48	25.8 $\pm$ 7.7	26.2 $\pm$ 6.7	92	67	4, 0-8

**Table 4.3** patient demographics by EDSS category

	RRMS (EDSS $\leq$ 3)	RRMS (EDSS $\geq$ 3.5)	SPMS
n	70	22	67
Age (years) mean $\pm$ SD	49.5 $\pm$ 8.1	49.7 $\pm$ 7.5	55.4 $\pm$ 8.7
Gender (female, male)	49, 21	20, 2	42, 25
Disease duration mean $\pm$ SD	25.2 $\pm$ 0.5	26.1 $\pm$ 4.1	27.3 $\pm$ 7.8

#### **4.3.1 Correlations between MRI features**

WMF was significantly correlated with T2LV ( $r=-0.21$ ,  $p=0.01$ ) and UCCA ( $r=0.28$ ,  $p<0.01$ ). GMF did not correlate significantly with either T2LV or UCCA but was inversely correlated with WMF ( $r=-0.26$ ,  $p<0.01$ ).

#### **4.3.2 MRI features and clinical subgroups** (Table 4.4 and 4.5)

WMF, T2LV and UCCA were found to differ significantly in ANOVA analysis between the RRMS and SPMS groups, but no significant difference was found for GMF.

T2LV was significantly higher in SPMS than in benign RRMS ( $EDSS\leq 3$ ) (mean  $\pm$  SD  $21.3 \pm 14.7$  vs.  $15.7 \pm 11.7$ ,  $p=0.02$ ), and showed a non-significant trend to be higher in SPMS than in the non-benign RRMS group (mean  $\pm$  SD  $21.3 \pm 14.7$  vs.  $16.1 \pm 14.5$ ,  $p=0.16$ ). On the other hand T2LV were almost identical in the benign and non-benign RRMS groups (mean  $\pm$  SD  $15.7 \pm 11.7$  vs.  $16.1 \pm 14.5$ ,  $p=0.94$ ). T2LV was also found to differ significantly between all subjects with  $EDSS \geq 6$  and those with  $EDSS \leq 3$  (mean  $24.3 \pm$  SD  $14.4$  vs.  $15.7 \pm 11.7$ ,  $p<0.01$ ).

UCCA was significantly higher in benign RRMS when compared with both non-benign RRMS (mean  $\pm$  SD  $69.7 \pm 8.1$  vs.  $64.8 \pm 8.7$ ,  $p=0.02$ ) and SPMS (mean  $\pm$  SD  $69.7 \pm 8.1$  vs.  $64.2 \pm 9.7$ ,  $p<0.01$ ). On the other hand, UCCA values were almost identical in non-benign RRMS and SPMS subgroups (mean  $\pm$  SD  $64.8 \pm 8.7$  vs.  $64.2 \pm 9.7$ ,  $p=0.80$ ). UCCA was also found to differ significantly between all subjects with  $EDSS \geq 6$  and those with  $EDSS \leq 3$  (mean  $63.3 \pm$  SD  $10.3$  vs.  $69.7 \pm 8.1$ ,  $p<0.01$ ).

**Table 4.4** MRI parameters in benign and 'non-benign' RRMS and SPMS

		All RRMS	Benign RRMS	Non-Benign RRMS	SPMS
T2LV (mLs)	Mean	16.0	15.7	16.1	21.3
	SD	12.3	11.7	14.5	14.7
UCCA (mm <sup>2</sup> )	Mean	68.6	69.7	64.8	64.2
	SD	8.4	8.1	8.7	9.7
WMF	Mean	0.332	0.335	0.324	0.324
	SD	0.019	0.018	0.021	0.017
GMF	Mean	0.460	0.462	0.457	0.460
	SD	0.014	0.014	0.012	0.014

**Table 4.5** Comparison of MRI parameters between benign and ‘non-benign’ RRMS and SPMS using ANOVA

	MS subtypes being compared	p value
T2LV (mLs)	Benign RRMS/Non-Benign RRMS	0.94
	Benign RRMS/SPMS	0.02
	Non-Benign RRMS/SPMS	0.16
	All RRMS/SPMS	0.02
UCCA (mm <sup>2</sup> )	Benign RRMS/Non-Benign RRMS	0.02
	Benign RRMS/SPMS	<0.01
	Non-Benign RRMS/SPMS	0.80
	All RRMS/SPMS	<0.01
WMF	Benign RRMS/Non-Benign RRMS	0.02
	Benign RRMS/SPMS	<0.01
	Non-Benign RRMS/SPMS	0.98
	All RRMS/SPMS	0.01
GMF	Benign RRMS/Non-Benign RRMS	0.24
	Benign RRMS/SPMS	0.55
	Non-Benign RRMS/SPMS	0.47
	All RRMS/SPMS	0.81

#### 4.3.3 *MRI features and physical disability (EDSS)*

EDSS was significantly correlated with T2LV (Spearman’s  $r=0.19$ ,  $p=0.02$ ), WMF ( $r=-0.32$ ,  $p<0.01$ ) and UCCA ( $r=-0.31$ ,  $p<0.01$ ), whereas the correlation between EDSS and GMF was not significant ( $r=-0.07$ ,  $p=0.36$ ). Scatter plots of MRI variables against EDSS are shown in Figure 4.1.

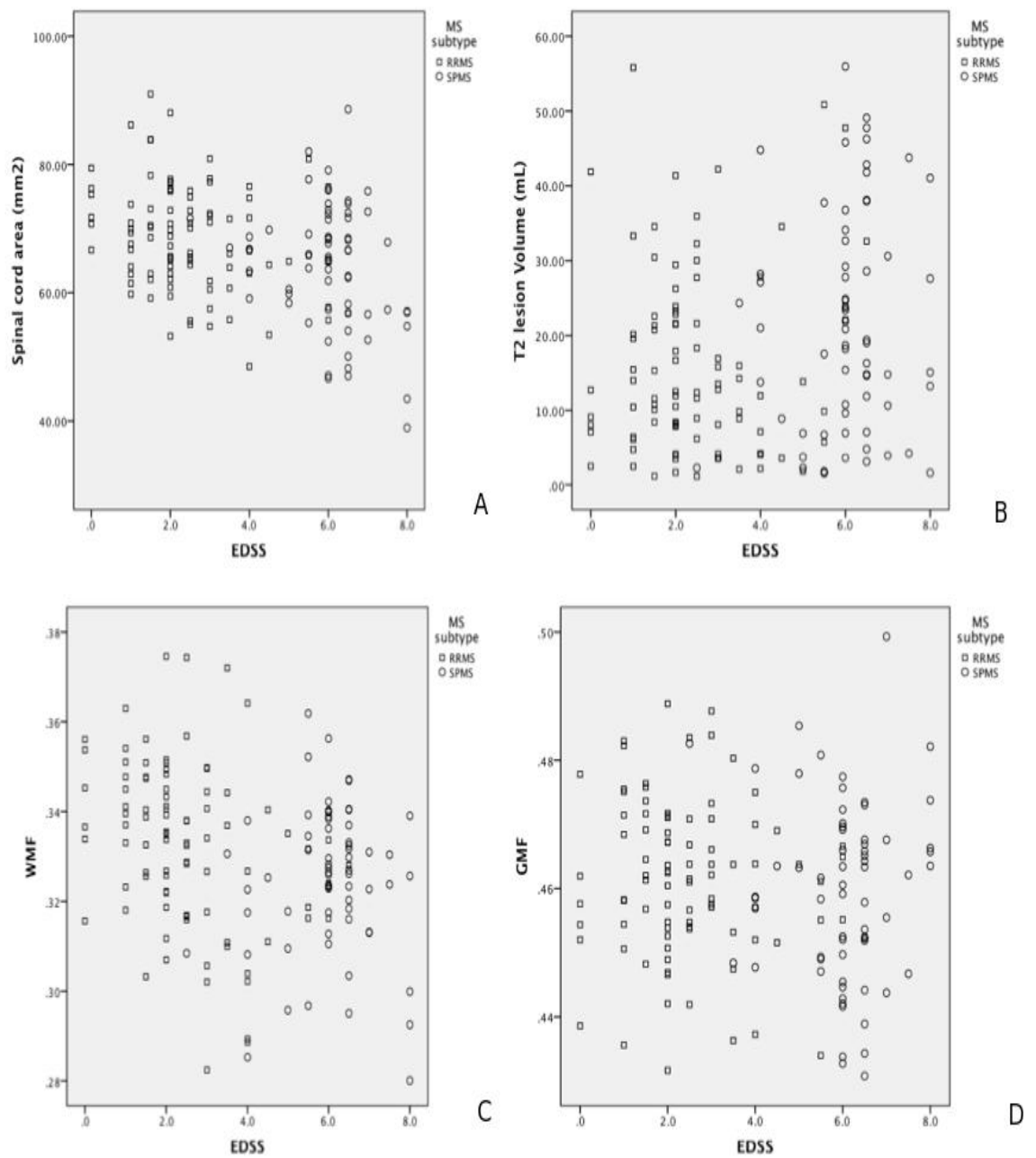


**Figure 4.1** Graphs of spinal cord area (A), T2 lesion volume (B), white matter fraction (C) and grey matter fraction (D) against EDSS.

In a univariable logistic regression analysis for binary EDSS groups, both T2LV (odds ratio=1.98 per 1 SD larger T2LV, 95% CI 1.39, 2.82,  $p < 0.01$ ) and UCCA

(odds ratio=0.55 per 1 SD higher cord area, 95% CI 0.38, 0.79,  $p<0.01$ ) were found to be associated with EDSS  $\geq 6$ . In a univariable ordered logistic regression for four-category EDSS the following were found to be associated with EDSS: T2LV (odds ratio=1.56 per 1 SD larger T2LV, 95% CI 1.16, 2.10,  $p<0.01$ ), UCCA (odds ratio=0.53 per 1 SD higher cord area, 95% CI 0.39, 0.72,  $p<0.01$ ) and WMF (odds ratio=0.62 per 1 SD WMF, 95% CI 0.47, 0.82,  $p<0.01$ ).

Subsequently in a multivariable analysis was performed, again using a binary and then four-part model of EDSS. Both T2LV (odds ratio=1.67 per 1 SD larger T2LV, 95% CI 1.09, 2.56,  $p=0.02$ ) and UCCA (odds ratio=0.57 per 1 SD higher cord area, 95% CI 0.37, 0.86,  $p=0.01$ ) were found to be associated independently with the requirement of a walking aid (i.e. EDSS  $\geq 6$ ). The C-statistic for this model was 0.8, with 81% sensitivity and 75% specificity and 77% correctly classified.

In a multivariable ordered logistic regression model with a four-part model of EDSS, the following were found to be associated with EDSS: UCCA (odds ratio=0.55 per 1 SD higher cord area, 95% CI 0.40, 0.77,  $p<0.01$ ), T2LV (odds ratio=1.56 per 1 SD larger T2LV, 95% CI 1.08, 2.25,  $p=0.02$ ) and GMF (odds ratio=0.67 per 1 SD GMF, 95% CI 0.46, 0.98,  $p=0.04$ ).

#### 4.4 Discussion

In this chapter a large group of MS patients, two to three decades after first symptom onset, were studied. The results demonstrate a strong association between spinal cord atrophy and EDSS. In the same model T2LV and to a lesser extent GM atrophy were also found to be independently associated with physical disability.

When considering the results, it should be noted that this cohort differs from previous studies looking simultaneously at spinal cord and brain measures in MS (Bonati *et al.*, 2011; Cohen *et al.*, 2012). Firstly, the present cohort is larger, with 159 patients, compared with 70 studied by Bonati *et al.* and 21 by Cohen *et al.* Secondly, it includes patients with longer disease durations (mean of 26 years compared to 20 years and 8 respectively). Thirdly, it includes more people with higher levels of disability (median EDSS 4, Bonati *et al.* median EDSS 2.5, Cohen *et al.* mean EDSS 1.6), and more SPMS patients (current study n=67, Bonati *et al.* n=11, Cohen *et al.* n=1). However, (unlike the previous two studies), this is a multicentre study and so differences in scanners can introduce inter-site variability (Reig *et al.*, 2009). The statistical analyses employed in this study adjusted for centre effects, thereby minimising this effect on the results.

Overall, these findings are in agreement with previous studies (Bonati *et al.*, 2011; Cohen *et al.*, 2012) demonstrating spinal cord atrophy to be independently related to disability. With regard to changes in the brain, Cohen *et al.* found no additional association with disability in a group of mostly RRMS patients with low EDSS scores, while in a mixed CIS, RRMS and SPMS cohort with long disease duration Bonati *et al.* observed that GMF independently associated with EDSS in

all cases, and T2LV in those with clinically definite MS. In the present cohort, T2LV and – in the four-part EDSS model only - GMF were found to contribute to variability in EDSS. The consistent independent relationship of spinal cord atrophy with disability in all three studies of cohorts with RRMS and SPMS and disease durations ranging from a mean of 8-26 years is noteworthy. An association of disability with T2LV and GM atrophy *independent of spinal cord atrophy* was only evident in the 20 and 26 year disease duration cohorts, suggesting that the effects of brain GM pathology in MS may become more relevant with longer disease duration.

Given that it can be difficult to determine the onset of progressive MS, and a natural history study suggested SPMS tends to occur at a similar rate when a disability threshold is reached rather than being determined by prior relapses (Confavereux *et al.*, 2000), it is of interest to see if there are MRI differences between benign and non-benign RRMS, and non-benign RRMS and SPMS. In order to do this the RRMS cohort was split into 'benign' (i.e. EDSS  $\leq 3$ ) and those with an EDSS of  $\geq 3.5$ . In doing so it is important to be aware that this division is defined by physical disability, and that cognitive deficits may be considerable in people with physically 'benign' MS (Rovaris *et al.*, 2008). No significant differences emerged between T2LV brain or cord atrophy between non-benign RRMS and SPMS. This suggests that, the division between these groups on the basis of clinical progression may be arbitrary and not strongly supported by differences in MRI characteristics.

Lower cord areas were evident in both SPMS and non-benign RRMS when compared with benign MS, thus spinal cord atrophy seems to relate to

concurrent physical disability. In this study EDSS was used as a measure of disability, although it does not fully reflect the clinical impact of MS. Above 3.5, the EDSS is heavily weighted towards mobility, and so corticospinal tract integrity. In turn, those MRI measures that are more directly linked with the corticospinal tracts are more likely to correlate with EDSS, hence the association between spinal cord atrophy and disability emerges consistently in all models. This study builds on previous work, demonstrating that spinal cord atrophy is relevant to physical disability in MS, and that this relationship remains significant in the long-term, in people with higher EDSS.

A question arising from our observation that the highest T2LV was seen in SPMS is whether a high T2LV in earlier years might predict future secondary progression? Although our cross-sectional study could not directly investigate this, evidence from two other studies supports a long term prognostic role of T2LV in relapse-onset MS. First, a 20-year follow up of a CIS cohort found that the rate of increase of T2LV was three times higher in those that develop SPMS compared to those patients who remained RRMS, and the higher T2LV was already evident after 5 years in those who later developed SPMS (Fisniku *et al.*, 2008). Secondly, in a recent 21-year follow up study that reported mortality outcomes of RRMS patients who had participated in a clinical trial of beta interferon, Goodin *et al.* found that the baseline T2LV was an independent predictor of death (Goodin *et al.*, 2012); although no information on neurological status was provided in that study, it is plausible that the higher mortality reflects a greater likelihood of patients with high lesion loads having developed secondary progression with severe disability.

In the current study, in univariable analyses WMF was associated with EDSS, but not in multivariable analysis where GMF was independently associated. This can be explained by inter-relationships between MRI measures. For an MRI measure to be retained in a regression model, it must correlate with the outcome of interest and do so at least partly independently of other measures. WMF was significantly correlated with both T2LV and UCCA, whereas GMF was not, and when both T2LV and UCCA were included in the statistical multivariable model, WMF did not add to the predictive power of the model above that of T2LV and UCCA alone. In contrast, while GMF alone did not correlate with clinical measures in univariate analysis, once variability due to T2LV and UCCA had been accounted for, it did contribute independently to disability in the four-part model of EDSS, albeit with modest significance ( $p=0.04$ ). Although a negative correlation was found between GMF and WMF, this is very likely to represent a mathematical interaction between the two fractional volumes that have a common denominator, rather than an error in segmentation - when the actual GM and WM volumes were compared without normalisation, a strong positive correlation was seen, as expected (data not shown).

As a conceptual limitation of this chapter, it cannot be assumed the same associations would be observed if different outcome measures were used. Cognitive impairment is common in MS, particularly in SPMS (Rao *et al.*, 1991; Comi *et al.*, 1995), and if cognitive scores were used instead, the imaging associations may differ. A previous longitudinal study in SPMS demonstrated a significant correlation of reductions in GM volume, but not UCCA or T2LV, with paced auditory serial addition test (PASAT) scores (Furby *et al.*, 2010). However

in this current study physical disability is the main outcome measure of interest in order to determine the contribution of spinal cord atrophy to disability in long disease duration MS.

Although GMF was associated independently with EDSS in the four-part model, no significant differences were established between GMF in RRMS and SPMS cohorts, although a weak trend was observed between lower GMF values with higher EDSS scores. A stronger correlation between EDSS and GMF was observed in a previous study of a MS cohort with 20-year disease duration (Fisniku *et al.*, 2008). Several factors may have limited the association observed in the present study. First, many subjects had large lesion loads, which could have had subtle effects on brain segmentation in spite of using lesion filling to correct tissue volumes (Chard *et al.*, 2010). Secondly, lesions partly involving the deep GM may still sometimes have been classified as WM leading to slight inaccuracies of WMF and GMF computation. Thirdly, there was often substantial atrophy. The GM and WM segmentation algorithm used (SPM) has been developed from a normal (non-atrophic) brain template and its performance may differ in the presence of marked brain atrophy. Finally, the cohort studied had a disease duration that considerably exceeds that of other cohorts in whom associations were observed between GM atrophy and disability (Fisher *et al.*, 2008; Fisniku *et al.*, 2008) and it is possible that GM atrophy may reach a nadir at a later point in the natural history of the disease, beyond which it has a lesser independent contribution to disability.

Two other study limitations are noted. First this study was cross-sectional, and although T2LV, spinal cord atrophy, and to a lesser extent GMF, were found to be

independently associated with *concurrent* disability, the rate of change of these measures over time was not examined. Longitudinal observations would be required to clarify their temporal dynamics, and relationship to changes in disability measures.

Secondly, this study was multi-centre. This allowed a larger cohort to be studied, but will have introduced some variability in MRI measures, and while these were accounted for in the statistical models, they may still have influenced the apparent strength of associations between MRI measures and clinical scores.

This chapter demonstrates that spinal cord and brain pathology are both relevant, and contribute independently to long-term physical disability in relapse-onset MS.

## **Chapter 5 - Evaluation of methodologies for improved quantification of spinal cord atrophy**

### **5.1 Introduction**

Spinal cord involvement in MS often results in clinically manifest progressive locomotor disability (Mc Donald and Compston 2006) and is relevant in determining physical disability in long disease duration as demonstrated in the preceding chapter. Although the presence of demyelinating plaques is a characteristic feature of MS in the spinal cord (Fog 1950; Oppenheimer 1978), it is axonal loss rather than lesions that represent the main pathological substrate of irreversible physical disability, as demonstrated by spinal cord neuropathological studies (Ganter *et al.*, 1999; Lovas *et al.*, 2000; DeLuca *et al.*, 2006).

*In vivo* measurement of the spinal cord cross-sectional area (CSA) is possible using MRI (Kidd *et al.*, 1993). A reduction in CSA of the spinal cord can be expected to occur when there is significant axonal loss (Losseff *et al.*, 1996; Bot *et al.*, 2004), and a robust correlation has been established between CSA and the expanded disability status scale (EDSS), which mainly reflects impairment in ambulatory function (Kurtzke 1983). Considering that a decrease in CSA may reflect pathological processes that underlie progressive disability, it is a biologically plausible surrogate endpoint to clinical trials, to evaluate the effect of treatments that aim to prevent neuroaxonal loss and irreversible disability in MS.

Perhaps because of the challenges in developing a sensitive and reproducible method of measuring cord atrophy in MS, only a small number of clinical trials (one relapsing remitting MS (Lin *et al.*, 2003) and three in PPMS (Kalkers *et al.*, 2002; Leary *et al.*, 2003; Montalban *et al.*, 2009) have used CSA as an exploratory endpoint. CSA may be a particularly pertinent outcome measure in progressive forms of the disease, where there is currently no effective disease modifying treatment, and where trials with clinical disability endpoints require large numbers of subjects and long term (2-3 years) follow up, in order to achieve sufficient power to observe a useful treatment effect on disability. Therefore, a sensitive surrogate imaging marker that reflects the pathology causing irreversible physical disability could serve as an endpoint in proof-of-concept phase one and two clinical trials in patients with progressive disease.

The average rate of atrophy of the spinal cord in MS subjects is estimated to be approximately 1% per year, although with substantial inter-subject variation (Rashid *et al.*, 2006). In order to detect these small changes longitudinally, a highly reproducible method is required. Such a method has proven difficult to establish due to several factors, above and beyond the challenges posed by conventional clinical MRI scanning of the spinal cord (Dietrich *et al.*, 2008).

Early efforts to measure CSA involved manual outlining of axial images (Kidd *et al.*, 1993). Subsequently, Losseff *et al.* reported a semi-automated edge-detection (SAED) method. This involves manually drawing two regions of interest (ROIs), one around the spinal cord and the other around the outer boundary of the surrounding cerebrospinal fluid (CSF) and then calculating the mean signal intensity of the cord and surrounding CSF and using a signal intensity threshold

halfway between the two to define the edge of the spinal cord, from which CSA can be measured (Losseff *et al.*, 1996). Following on from this, a method was developed that used an automated edge detection technique (which reduced operator input) (Lin *et al.*, 2003; Vaithinanthar *et al.*, 2003).

A new method known as the active surface model (ASM) has been developed, which allows rapid measurement of the spinal cord size (Horsfield *et al.*, 2010). This involves the placement of cord markers on some representative axial slices and subsequently an outline of the spinal cord is created automatically and allows detection of atrophy over a larger portion of the cervical cord. Following development of the ASM, it has been used in a large multicentre study (Rocca *et al.*, 2011).

The reproducibility of these methods is variable with published intra-rater coefficients of variation (COV) ranging from 0.73% to 2.15% for the SAED technique (Losseff *et al.*, 1996; Horsfield *et al.*, 2010); using different techniques to the SAED (such as the automated edge finding and ASM), lower intra-rater COVs (0.42% and 0.44%) have been reported (Lin *et al.*, 2003; Horsfield *et al.*, 2010). For inter-rater reproducibility COV, values have been reported ranging from 0.83% to 7.95% for SAED method and 1.07% for ASM. Data on scan re-scan reproducibility is reported as 0.79% using SAED method.

In order to determine the most reproducible combination of sequence and estimate the number of patients required for clinical trials, in this chapter the SAED and ASM methods are tested with two different sequences: 3D magnetization prepared rapid acquisition T1-weighted gradient echo (3D-TFE) and 3D-phase sensitive inversion recovery imaging (3D-PSIR).

T1-weighted 3D-TFE is the most frequently used sequence for the calculation of CSA in MS (Losseff *et al.*, 1996; Lin *et al.*, 2003; Leary *et al.*, 2003; Horsfield *et al.*, 2010). This sequence can be used with isotropic voxel dimensions, thereby allowing axial reconstruction (without in-plane resolution being affected). High-resolution imaging also reduces partial volume averaging, as it has been shown that approximately half of voxels in the spinal cord edge form the cord-cerebrospinal fluid (CSF) interface and are subject to partial volume averaging (Tench *et al.*, 2003). In a T1-weighted image there is a strong signal intensity gradient between the cord and CSF, which facilitates identification of the edge of the cord (Losseff *et al.*, 1996).

PSIR sequence was chosen for comparison as it is a T1 weighted sequence with phase reconstruction. The inversion recovery pulse and phase sensitive reconstruction confer a number of advantages. Firstly this sequence applies an inversion radio-frequency (RF) pulse; therefore the magnetisation can be positive or negative depending on the tissue relaxation times (Hou *et al.*, 2005). In this case the mean signal intensity of the cord is positive, while the mean signal intensity of the CSF is negative. This feature of PSIR sequence was expected to further reduce partial volume averaging between the cord and CSF. Secondly, PSIR has been shown to improve signal to noise ratio (Bernstein *et al.*, 1989), which could further enhance detection of the cord outline. Lastly, this sequence can be acquired at higher in-plane resolution within a clinically acceptable scan time (Hou *et al.*, 2005).

The aim of this chapter is to investigate whether a combination of high resolution axial PSIR images, with an active surface model, provides a more

reproducible measure of upper cervical cord cross-sectional area in MS; compared to a semi-automated edge finding method combined with both axially acquired or axially reconstructed images of the upper cervical cord.

## **5.2 Methods**

### **5.2.1 *Subjects***

15 healthy controls (6 female, mean age 37 years, SD 9.5) and 15 patients with a diagnosis of MS (Polman *et al.*, 2011) (10 female, 7 with relapsing-remitting MS (RRMS) were included in this study, 8 with secondary-progressive MS (SPMS), mean age 44.9 years, SD 12.3). Patients' level of disability was evaluated using the EDSS prior to MRI (median EDSS score at baseline 4, range 0-6.5). None of the subjects had experienced a relapse or received a course of corticosteroids within a month prior to imaging. Six patients were being treated with interferon- $\beta$  at the time of recruitment.

Nine patients (5 female, mean age 42, SD 10.6, 5 SPMS, 4 RRMS) and nine healthy controls (3 female, mean age 34, SD 6.4) returned for follow up at six month time point, MR imaging and clinical assessment was repeated. In patients, the median EDSS score at 6-months was 4. At this time point, the scan was performed twice with the subject being removed from the scanner coil then repositioned within it between the scans. This enabled an evaluation of scan-rescan reproducibility.

Informed written consent was obtained from all subjects.

### **5.2.2 *MRI Protocol***

Subjects were scanned at 3T using a Philips Achieva MRI system with RF multi-transmit technology (Philips Healthcare, Best, the Netherlands) and a 16-channel neurovascular coil (which permitted coverage of the entire cervical spine), with care taken to position the patient comfortably to minimize motion artefact and allowed consistent re-positioning of subjects for follow up scans.

Firstly a 3D-TFE sequence was acquired in the sagittal plane with FoV=256x256mm<sup>2</sup>, matrix=256x256, TR=8ms, TE=3.7ms, TI=860ms, SENSE factor 2 in the anterior-posterior direction, TFE factor 205 (using a linear k-space profile order). The voxel size was 1x1x1mm<sup>3</sup> (Figure 5.1). Secondly, a 3D-PSIR sequence was acquired in the axial plane with a voxel size of 0.5 x 0.5 x 3 mm<sup>3</sup>, TR = 8 ms; TE = 3.7 ms; flip angle  $\alpha = 5^\circ$ ; FOV = 256 x 256 mm; NEX = 1. The scanning time was 14:22 min for PSIR sequence and 6:31 min for 3D-TFE (Figure 5.2).

3D-TFE imaging covered the entire cervical spine, while PSIR imaging was centred at C2/C3 intervertebral disc. This anatomical location was chosen as post-mortem work has demonstrated that with flexion and extension of the head the spinal cord can move up to 1.8cm, however this effect is least evident in the high cervical cord (Reid 1960). Secondly, in previous work this level yields the most reproducible-cross sectional area values (Losseff *et al.*, 1996). Therefore, to minimise cord displacement due to movement and optimise reproducibility, C2/C3 was chosen for this study.

### **5.2.3 *Image Analysis***

From the 3D-TFE images five contiguous 3mm axial slices were reformatted using the centre of C2/C3 intervertebral disc as a caudal landmark, with the slices perpendicular to the spinal cord (Figure 5.1). Five contiguous 3mm axial slices were also extracted from the 3D PSIR images in a similar way (i.e. ensuring by visual inspection that the central slice was through the centre of C2/C3 intervertebral disc).

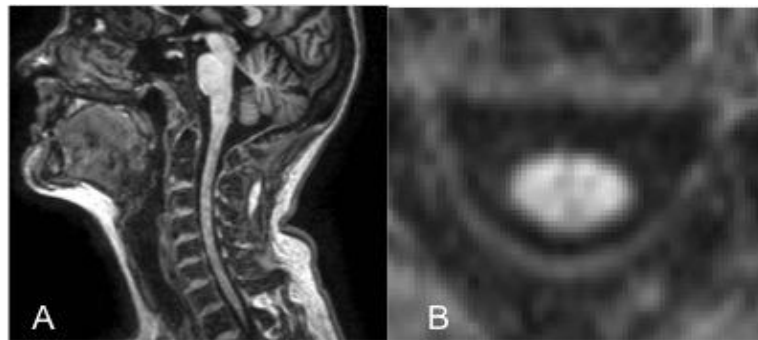


**Figure 5.1** 3D-TFE 1x1x1mm<sup>3</sup> voxels 6min 30secs 16 channel NV coil. A: sagittal view. B: Axial 3D-TFE reconstruction at C2/C3

The five axial slices for the two sequences were then analyzed in two ways: (i) using SAED technique (Losseff *et al.*, 1996), the mean area of the slices were calculated using Dispunc display software package (D.L. Plummer, University College, London, UK). (ii) ASM using Jim6 software (Xinapse systems, [www.xinapse.com](http://www.xinapse.com)).

The SAED method (i) is based on the principle that if the signal intensities (SI) of the cord and CSF are uniform then an outline drawn at the point where the SI is midway between the two, would represent the position of the cord outline. This method involves manually drawing a region of interest (ROI) around the spinal cord, and then a ROI is manually drawn around the outer edge of the CSF space.

From these two manually drawn ROIs, the mean signal intensities of cord and CSF are calculated. The cord/CSF boundary is indicated by calculating the halfway SI between the two and an automated border is constructed around the spinal cord, from which CSA is measured for each of the five slices and the mean CSA is obtained.

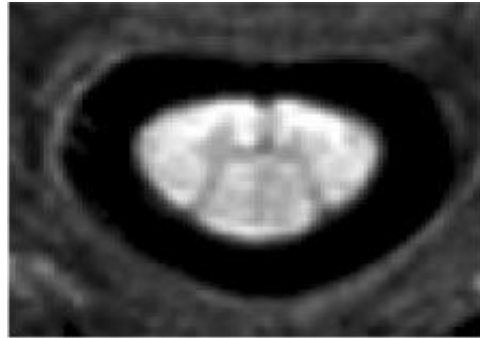


**Figure 5.2** PSIR  $0.5 \times 0.5 \times 3 \text{mm}^3$  acquired with 16 channel NV coil.

The ASM (Figure 5.3) (ii) involves placing a pre-determined size and shape ROI in the centre of the cord on each slice. The programme then uses intensity gradient information to calculate the radius of each slice and the centre of each slice. The centre line is refined from the initial user estimate and segmentation then involves a multistage approach allowing greater complexity of the cord radius to be calculated (Horsfield *et al.*, 2010). This enhances the cord outline where it has been distorted due to atrophic changes. The outline of the cord is then automatically generated for each slice. Similarly to the SAED method, the CSA is measured for each of the five slices and the mean area is calculated.

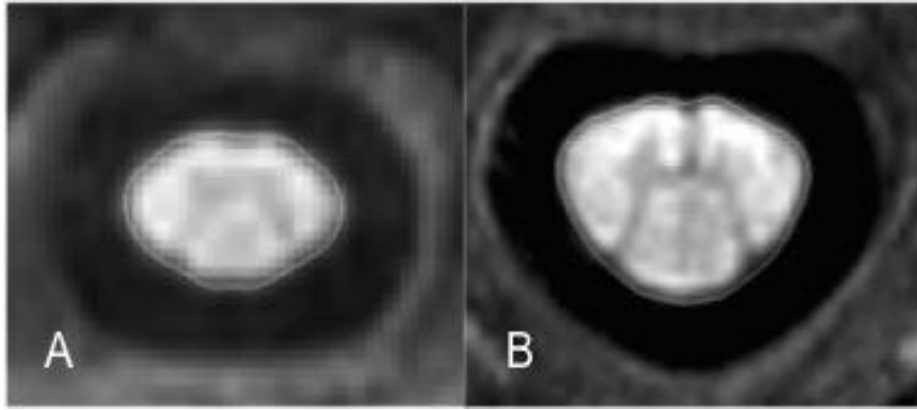


**Figure 5.3** Spinal cord outlined using ASM. A: axially reformatted 3D-TFE B: PSIR

Spinal cord scans are sometimes normalised by brain volume or other measures of body size. The purpose of this process is to remove differences between patients that are unrelated to pathology. A recent study investigated the effects of eight different methods of normalisation including: number of slices, intracranial volume, body mass index, body surface area, no normalisation and combinations of these parameters (Healy *et al.*, 2012). Of these, only the number of slices had a notable effect on reproducibility or discrimination between an atrophic and healthy cord. Therefore, the spinal cord area was normalised by the number of slices.

### 5.2.3.1 Calculation of relative contrast

The relative contrast was calculated for all scans (Lavdas *et al.*, 2010). The mean signal intensity was estimated in the CSF and spinal cord by placing an identical ROI in each structure (Figure 5.4). Relative contrast was calculated by using the formula:  $((S_1 - S_2) / (S_1 + S_2)) \times 100$ , where  $S_1$ =signal in the spinal cord and  $S_2$ =signal in the CSF.

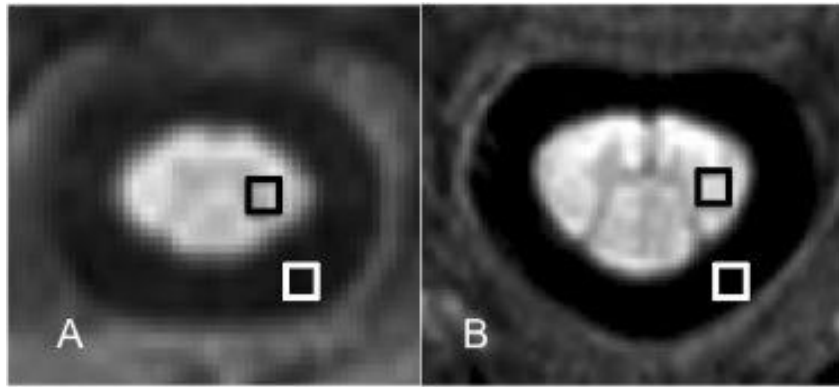


**Figure 5.4** Calculation of CNR with ROI placed in CSF and on spinal cord. A: 3D-TFE B: 3D-PSIR

### 5.2.3.2 *Reproducibility*

After an interval of one week all the reformatted images were re-analysed using both methods by one reader to evaluate intra-rater reproducibility. The same reformatted images were analysed by two other readers to evaluate inter-rater reproducibility. At six month follow up the images were analysed by the same reader to evaluate scan re-scan reproducibility. In addition, the first of the two scans at six month time point was used for comparison with baseline to evaluate longitudinal change in CSA over time.

### 5.2.4 *Statistics*

SPSS software package (version 20, SPSS Inc.) for Macintosh was used for statistical analysis.

Average CSA was calculated for each combination of sequence and method used. Firstly, an independent samples t-test was employed to determine differences

between mean, CSA and age in patients and controls; significance was established as  $p \leq 0.05$  with 95% confidence intervals.

#### **5.2.4.1 Reproducibility**

Reproducibility was evaluated in all subjects together as follows.

Firstly intra-rater reproducibility was measured by calculating COV expressed as a percentage of the mean area ( $COV = 100 \times (SD \text{ of the two measurements} / \text{Mean of the two measurements})$ ) (Kirkwood and Sterne 2003). Intra-rater reproducibility was further examined by calculating the intra-class correlation coefficient (ICC) and subsequently 1-ICC (Bland and Altman 1986). In this context 1-ICC represents the proportion of variability, which is due to measurement error (within-subject) rather than biological variation (between-subject). Thus, whereas the COV assesses within-subject variability as a proportion of the mean, the ICC assesses within-subject variability as a proportion of the total variability (within plus between).

Inter-rater reproducibility was examined by recording the COV between the three raters and both ICC and 1-ICC for each combination of sequence and processing technique.

Similarly, scan-rescan reproducibility was calculated using COV, ICC and 1-ICC.

#### **5.2.4.2 Change in CSA over six month follow up and correlation with disability at baseline**

To examine differences in mean CSA over time, a paired t-test was used in both the patient and healthy control groups. In each group, this test was repeated for each combination of sequence and analysis technique.

Spearman correlation coefficients were calculated to determine the correlation between CSA and EDSS scores for all combinations of sequences and analysis methods at baseline.

#### **5.2.4.3 *Sample size calculations for clinical trials***

Sample sizes were calculated for each combination of sequence and analysis method. These calculations were based on the between-subject SD of the mean CSA of 15 patients at baseline. An estimate of the Pearson correlation coefficient is given between CSA at baseline and six months.

Estimate of treatment effects were calculated by measuring the change in cord area (in 9 patients and 9 controls) after six months. The difference between these mean changes, control-patient, was obtained and considered to be the MS disease-specific change in CSA. A decrease of this full amount of CSA change while on an experimental treatment was then considered to be a 100% treatment effect for a six-month duration trial. From this, the amount of decrease in CSA change constituting a 30% and 50% treatment effect, and the corresponding sample sizes for a placebo-controlled trial, were calculated. The reduction in CSA change for a 100% treatment effect over six months were doubled to allow an estimation of sample sizes for a 12-month trial (assuming linearity in the changes over time in both groups).

### **5.3 Results**

### 5.3.1 Comparison of relative contrast between PSIR and 3D-TFE

Relative contrast was found to be 1811.11% for PSIR, and 74.45% for the 3D-TFE. The relative contrast for PSIR was found to be higher than the 3D-TFE by a factor of 24.

### 5.3.2 Differences between groups at baseline

A significant difference between patients and controls was found for CSA ( $p < 0.001$ ) for all combinations of sequence and method of analysis. No significant difference was found in the ages of patients and controls.

### 5.3.3 Reproducibility

The combination of ASM with PSIR was more reproducible than the other methods (intra-rater COV for PSIR/ASM 0.002%, inter-rater COV for PSIR/ASM 0.03%); in terms of both lower COV and higher ICC, for all subjects. Again the combination of ASM technique with PSIR proved to have greater reproducibility for scan-rescan (scan-rescan reproducibility COV for PSIR/ASM 0.1%). Results of intra-observer and inter-observer reproducibility are summarised in tables 5.1 and 5.2. Results of scan-rescan reproducibility are summarised in table 5.3.

Analysis method/MRI sequence	Mean CSA (mm <sup>2</sup> )	COV (%)	ICC	1-ICC
<b>SAED/3D-TFE</b>	70.94	3.86	0.108	0.892
<b>SAED/PSIR</b>	72.49	0.3	0.946	0.054
<b>ASM/3D-TFE</b>	72.98	0.04	0.990	0.01
<b>ASM/PSIR</b>	76.52	0.002	0.999	0.001

**Table 5.1** Intra-observer reproducibility in all subjects (COV: coefficient of variation)

Analysis method/MRI sequence	Observer 1 mean CSA (mm <sup>2</sup> )	Observer 2 mean CSA (mm <sup>2</sup> )	Observer 3 mean CSA (mm <sup>2</sup> )	COV (%)	ICC	1-ICC
<b>SAED/3D-TFE</b>	70.94	69.72	70.49	0.88	0.782	0.218
<b>SAED/PSIR</b>	72.49	72.82	73.12	0.43	0.919	0.081
<b>ASM/3D-TFE</b>	72.98	72.95	73.23	0.21	0.993	0.007
<b>ASM/PSIR</b>	76.52	76.48	76.47	0.03	0.999	0.001

**Table 5.2** Inter-observer reproducibility in all subjects

Analysis method/MRI sequence	Scan 1 mean CSA (mm <sup>2</sup> )	Scan 2 mean CSA (mm <sup>2</sup> )	COV (%)	ICC	1-ICC
<b>SAED/3D-TFE</b>	69.76	69.37	0.41	0.755	0.245
<b>SAED/PSIR</b>	70.43	69.99	0.45	0.911	0.089
<b>ASM/3D-TFE</b>	72.64	73.14	0.48	0.978	0.022
<b>ASM/PSIR</b>	75.11	75.00	0.10	0.981	0.019

**Table 5.3** Scan-rescan reproducibility in all subjects

#### 5.3.4 *Change in cord area over six month follow up and correlation with disability at baseline*

At six month follow up none of the patients had a change in EDSS. The control scans did not show any significant change. The least change in control CSA was seen with ASM/3D-TFE (absolute change of 0.06mm<sup>2</sup>). In patients all methods demonstrated a decrease in CSA, apart from the combination of ASM and 3D-TFE which demonstrated a 0.18% increase in CSA. None of the changes detected in

patients reached significance with a paired t-test. Results of patients and controls longitudinal data are shown in tables 5.4 and 5.5 respectively.

Analysis method/MRI sequence	Mean CSA at baseline $\pm$ SD (mm <sup>2</sup> )	Mean CSA at 6 month follow up $\pm$ SD (mm <sup>2</sup> )	Absolute change in mean CSA (mm <sup>2</sup> )	Change in mean CSA (%)	p value from t-test comparing baseline to follow up
<b>SAED/3D-TFE</b>	64.93 $\pm$ 11.79	62.98 $\pm$ 10.10	-1.96	-3.01	0.410
<b>SAED/PSIR</b>	64.11 $\pm$ 10.76	62.07 $\pm$ 8.57	-2.04	-3.19	0.102
<b>ASM/3D-TFE</b>	63.85 $\pm$ 11.01	63.96 $\pm$ 9.82	+0.11	+0.18	0.512
<b>ASM/PSIR</b>	67.92 $\pm$ 10.57	66.48 $\pm$ 10.34	-1.44	-2.11	0.061

**Table 5.4** Longitudinal cord area measures in patients

Analysis method/MRI sequence	Mean CSA at baseline $\pm$ SD (mm <sup>2</sup> )	Mean CSA at 6 month follow up $\pm$ SD (mm <sup>2</sup> )	Absolute change in mean CSA (mm <sup>2</sup> )	% change in mean CSA	p value from t-test comparing baseline to follow up
<b>SAED/3D-TFE</b>	77.76 $\pm$ 6.28	76.53 $\pm$ 8.79	-1.22	-1.57	0.277
<b>SAED/PSIR</b>	80.16 $\pm$ 8.27	78.81 $\pm$ 9.88	-1.35	-1.68	0.186
<b>ASM/3D-TFE</b>	81.17 $\pm$ 7.27	81.12 $\pm$ 7.31	-0.06	-0.07	0.224
<b>ASM/PSIR</b>	84.50 $\pm$ 7.99	83.93 $\pm$ 9.12	-0.57	-0.68	0.119

**Table 5.5** Longitudinal cord area measures in controls

Using each combination of sequence and method a significant negative correlation was seen between CSA and EDSS. The strongest correlation was seen with SAED and PSIR ( $r=-0.75$ ,  $p=0.001$ ) (Table 5.6).

Analysis method/MRI sequence	Spearman's R	p value
<b>SAED/3D-TFE</b>	-0.525	0.045
<b>SAED/PSIR</b>	-0.745	0.001
<b>ASM/3D-TFE</b>	-0.693	0.004
<b>ASM/PSIR</b>	-0.725	0.002

**Table 5.6** Correlation with EDSS at baseline (15 patients)

### 5.3.5 Sample size calculations

The calculations of differences between longitudinal CSA changes in patients and controls - that were used to estimate treatment effects and perform sample size calculations for a placebo-controlled trial in which an active treatment reduces CSA loss over time - are provided in Table 5.7. Estimated sample sizes are given per arm for six month and 12 month trials in Table 5.8. For a 12 month treatment trial with 50% treatment effect and 80% power the lowest number of subjects required was found using PSIR/ASM combination (n=89), which was substantially lower than the number required with SAED/3D-TFE (n=1172).

	<b>ASM/PSIR</b>	<b>ASM/3D-TFE</b>	<b>SAED/PSIR</b>	<b>SAED/3D-TFE</b>
<b>SD</b>	11.27	11.13	10.83	11.25
<b>Correlation</b>	0.98	0.99	0.97	0.83
<b>Mean change in controls</b>	-0.57	0.12	-1.35	-1.22
<b>Mean change in patients</b>	-1.44	-0.34	-2.04	-1.96
<b>Difference in mean changes<sup>1</sup> (100% treatment effect)</b>	0.87	0.47	0.70	0.73

<sup>1</sup> Discrepancies on subtraction due to rounding

**Table 5.7** Calculation of differences between longitudinal changes in patients and controls to estimate treatment effect

	ASM/PSIR		ASM/3D-TFE		SAED/PSIR		SAED/3D-TFE	
<b>Treatment effect; power</b>	<b>6 m</b>	<b>12 m</b>	<b>6 m</b>	<b>12 m</b>	<b>6 m</b>	<b>12 m</b>	<b>6 m</b>	<b>12 m</b>
30% 90%	1323	331	1454	364	3279	820	17427	4357
30% 80%	988	247	1086	272	2449	613	13018	3255
50% 90%	476	119	524	131	1181	296	6274	1569
50% 80%	356	89	391	98	882	221	4687	1172

**Table 5.8** Estimated sample sizes per arm for six month (m) and 12 month placebo-controlled treatment trials

## 5.4 Discussion

Spinal cord atrophy has already been used as an exploratory endpoint in clinical trials in MS (Kalkers *et al.*, 2002; Leary *et al.*, 2003; Lin *et al.*, 2003; Montalban *et al.*, 2009). Improving reproducibility of cord area measurement should be beneficial for clinical trials by increasing sensitivity to detect neuroprotective therapies and reducing the sample sizes needed to show such a treatment effect. Spinal cord atrophy could then be especially useful as an outcome measure in phase 1 and 2 proof-of-concept trials.

In this chapter the cross sectional area of the spinal cord is measured, as this has been measured in previous MS clinical trials (Kalkers *et al.*, 2002; Leary *et al.*, 2003; Lin *et al.*, 2003; Montalban *et al.*, 2009) and the image analysis software used in this study enabled area to be measured with both SAED and ASM techniques. However, other studies have measured spinal cord volume as an assessment of atrophy in MS (Hickman *et al.*, 2003; Zivadinov *et al.*, 2008) and a future study comparing the COVs of area (using the methodology in this study) and volume measurements would be of interest.

Two methods of analysis were evaluated in this study at baseline and at six month follow up. The combination of PSIR and ASM in all subjects yielded the highest intra-rater reproducibility for cord area reported so far in MS (COV=0.002%). This combination also had the lowest value of COV for inter-observer (0.03%) and scan-rescan reproducibility (COV 0.1%). The lowest value of 1-ICC was seen with PSIR/ASM, demonstrating that there is a low proportion of variability due to measurement errors. Intra-rater reproducibility was substantially lower with the combination of 3D-TFE and SAED method. This was

likely to have been due to the manual input required by the rater combined with the lower in-plane scan resolution.

The relative contrast was higher in both 3D-PSIR than 3D-TFE by a factor of 24. This provides a higher contrast between cord and CSF, thereby improving the detection of the cord outline. PSIR also had a higher in-plane resolution than 3D-TFE (0.5x0.5mm vs. 1x1mm) which reduced partial volume effects at the boundary between cord tissue and CSF. PSIR scans did not require reconstruction in a different plane, unlike 3D-TFE. Owing to the fact that the PSIR sequence is a 3D acquisition, three views can be reviewed simultaneously allowing accurate choice of the central slice for analysis from the sagittal view. A combination of these factors is likely to have contributed to the improved reproducibility with PSIR sequence.

Though not significant the rate of change in patients' cord area was higher than expected for 3 of the 4 analysis methods over the course of six months. The small cohort size with different subtypes of MS may have been a contributory factor to this finding. A larger decrease in both patients and controls was seen with the SAED method. As this method was shown to have inferior reproducibility compared to ASM, measurement error may account for the larger changes seen.

Cord atrophy measurements are of particular interest as they correlate with EDSS (Losseff *et al.*, 1996). In the present study, the Spearman correlations were in a similar range to previously reported values in larger MS patient cohorts (Losseff *et al.*, 1996; Lin *et al.*, 2003; Horsfield *et al.*, 2010). A strong negative correlation was seen with PSIR and active surface model ( $r=-0.725$ ,  $p=0.002$ ).

The correlation seen in this study strengthens the case for the use of spinal cord

atrophy as an objective marker of physical disability in studies. Although strong correlations were seen with EDSS it was not possible to comment on whether change in CSA using PSIR/ASM can reflect significant changes in EDSS as none of the patients followed up developed a change in disability status.

Given the need for sensitive biomarkers in treatment trials sample sizes from the data in this study were estimated to demonstrate that it would be feasible to use the cord area as an endpoint to a clinical trial. These calculations are based on the cohort of nine patients followed up at six months and more accurate figures could be established from larger cohorts with longer duration of follow up.

Nevertheless, based on the estimates in this study it would be possible to detect a 50% treatment effect (decrease in cord area loss) in a twelve month trial in less than 100 patients per arm, suggesting this would be a feasible endpoint for a proof-of-concept trial involving relatively few centres. The results of the sample size calculations also reveal that there are minimal differences between PSIR and 3D-TFE, in the number of patients required in each treatment arm, provided the ASM is used to analyse the images. If the SAED method is used sample sizes required would be significantly larger.

#### **5.4.1** *Limitations and future directions*

Although the reproducibility of the measures in this study was greater than that of previously published methods, a few limitations must be taken into account. First, it was not possible in our study to blind raters to the differences between 3D-TFE and PSIR. Secondly, raters were not blinded to the two time points (baseline or six months) or whether scan one or two was being analysed at six month time point; however, the raters were blinded to subject status (control or

MS) and we are confident that the differences in CSA change between controls and MS (Table 5.7) - that formed the basis of the sample size calculations - are robust. As already noted the sample size at follow up was small which influenced the accuracy of sample size calculations.

Thirdly, the scan time of PSIR was considerably longer than the 3D-TFE scan, this may potentially limit this scans usefulness (as part of a multimodal imaging protocol) due to motion artefacts.

Fourthly, the 3D-TFE scan was acquired in this study with a larger voxel size than PSIR. Although this allowed direct comparison with previously published results, it may have been a contributory factor to the reduction in reproducibility. In order to improve reproducibility with 3D-TFE, this sequence could be acquired with a smaller voxel size (0.5x0.5mm in plane) equivalent to the PSIR sequence. Fifthly, rather than sagittal acquisition (which potentially introduces operator error into the measurement) an axial acquisition of the 3D-TFE sequence may improve its reproducibility. Finally, although the PSIR-ASM method was the most reproducible, the PSIR sequence may not be routinely available with all scanners manufacturers, potentially limiting its use in some multicentre trials; in such circumstances, the 3D-TFE-ASM approach may be more suitable and in our study it yielded only slightly higher sample sizes.

This chapter has demonstrated a new methodology for measuring spinal cord atrophy in MS that has greater reproducibility than previously reported methods. Furthermore it has also demonstrated that it would be feasible to use this method as an endpoint in a clinical trial of neuroprotection in MS.

## Chapter 6 - (i) A Pilot study to evaluate two high resolution axial sequences for spinal cord lesion detection in multiple sclerosis

### 6.1 Introduction

Spinal cord pathology is a major cause of disability in multiple sclerosis (MS). Pathological studies of the spinal cord in MS have detailed the morphology and distribution of lesions demonstrating wedge-shaped lesions predominantly in the posterior and lateral white matter (WM) columns (Fog, 1950). More recent *post mortem* magnetic resonance imaging (MRI) and histopathologic studies have identified additional involvement of central grey matter (GM) by spinal cord lesions, with both GM-only and mixed WM-GM lesions being detected (Gilmore *et al.*, 2006, Lycklama à Nijeholt *et al.*, 2001, Gilmore *et al.*, 2009, Mottershead *et al.*, 2003, Bot *et al.*, 2004).

Conventional *in vivo* T2-weighted MRI sequences detect focal spinal cord lesions and sometimes more diffuse abnormalities in the spinal cord in MS (Kidd *et al.*, 1993). The presence of focal cord lesions is valuable in the diagnosis of MS, as reflected by their inclusion in new diagnostic criteria (Polman *et al.*, 2011).

However, the number or load of T2-weighted lesions seen on sagittal scans of the spinal cord has little correlation with measures of disability in MS (Bergers *et al.*, 2002).

The clinical effects of spinal cord WM lesions will depend on their locations, e.g., motor deficits from lateral column lesions and sensory symptoms from posterior or anterior column lesions. The effect of GM lesions is uncertain. Better *in vivo* MRI localisation of focal cord lesions should help understand their functional effects. Conventional axial T2-weighted MRI sequences have provided limited

information on the WM column or GM involvement by MS lesions, because of relatively low spatial resolution (typically 1x1mm in plane voxel size), insufficient contrast between WM and GM, motion and other types of artefacts (Dietrich *et al.*, 2008).

The hypothesis being investigated in this pilot study is that a combination of two high resolution axial images will be able to consistently visualise the spinal cord grey matter; the purpose of which is to identify the individual spinal cord white matter columns and thereby identify the anatomical location of focal spinal cord lesions in MS.

## **6.2 Methods**

### **6.2.1 *Subjects***

15 patients with a diagnosis of MS were recruited (Polman *et al.*, 2011) (10 female, 8 with relapsing-remitting MS (RRMS), 7 with secondary-progressive MS (SPMS), mean age 44.8, SD 10.53, range 28-64) (Lublin and Reingold, 1996) and one patient with a clinically isolated syndrome (CIS). The patient with CIS presented with optic neuritis and fulfilled the MS criteria for dissemination in space (DIS) but not dissemination in time (DIT) on brain MRI (Polman *et al.*, 2011). Subject inclusion was based solely on clinical diagnosis supported by brain MRI findings. Previous spinal cord MRI findings were not considered in order to avoid the potential to bias the study cohort based on prior descriptions of spinal cord lesions.

None of the subjects had experienced a relapse or received a course of corticosteroids within a month prior to imaging. All patients on disease modifying treatment were on the treatment for at least six months at the time of the study MRI. Informed written consent was obtained from all subjects.

### 6.2.2 *MRI Protocol*

Scanning was performed using a 3T Philips Achieva MRI system with RF multi-transmit technology (Philips Healthcare, Best, the Netherlands) and a 16-channel neurovascular (NV) coil. Coverage of the two sequences acquired is outlined in Figure 6.1.

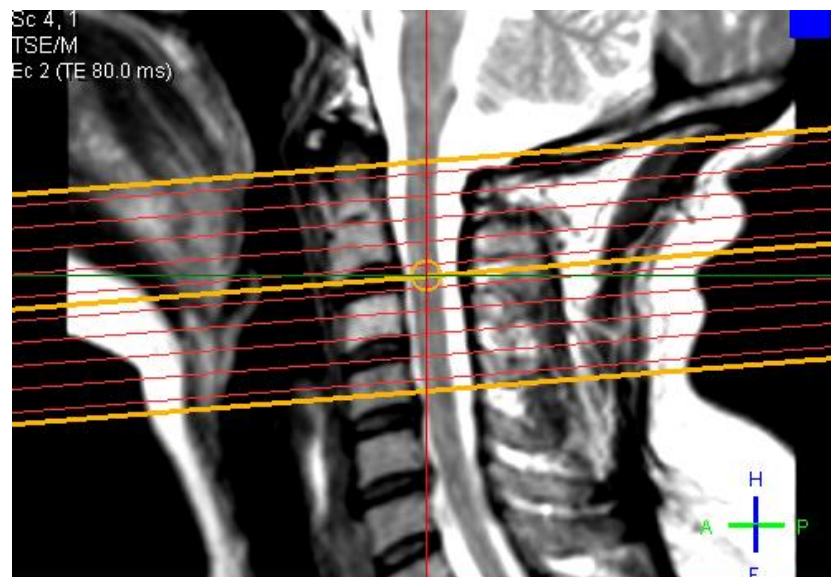


**Figure 6.1** Survey image demonstrating coverage of axial images acquired in this study

Two 3D gradient-echo sequences – one with predominantly proton density weighting, the other with T1 weighting – were selected for this study of MS patients by an experienced neuroradiologist (KM), as they provided good

depiction of central grey matter (GM) and white matter (WM) columns of the cord (Figure 6.2), and because it was anticipated that they would detect MS lesions that are typically associated with an increase in proton density and T1-relaxation time. Both of these scans were optimised in healthy controls and provided a clear outline of the cord anatomy without distortion by artefacts, through 3D averaging.

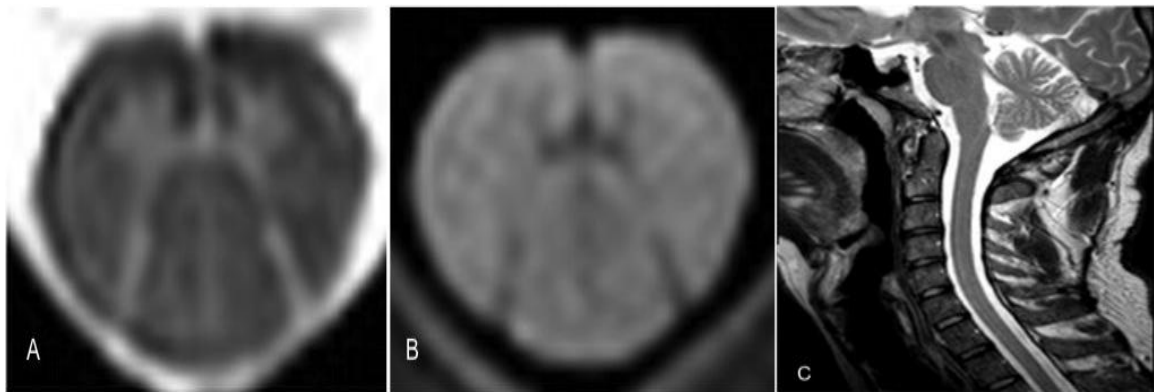


**Figure 6.2** Axial cervical cord MRI (A) FFE and (B) PSIR in a healthy control showing central grey matter and white matter columns. (C) Sagittal T2 weighted image used for orientation of slices

The proton density-weighted sequence was a 3D gradient echo (fast field echo [FFE]) sequence that showed central GM with higher signal than cord WM. The T1-weighted sequence was a phase sensitive inversion recovery (PSIR) sequence, i.e. an inversion prepared 3D gradient echo (turbo field echo [TFE]) sequence with phase sensitive reconstruction, as has been previously described (Hou et al., 2005) that provides a greater range of signal intensity because it additively combines the effects of negative and positive longitudinal magnetization in the image. PSIR also provides better GM-WM tissue contrast than other T1-weighted sequences and was previously shown to improve detection of cortical GM lesions

and spinal cord lesions when combined with other MR sequences (Nelson et al., 2007, Poonawalla et al., 2008; Sethi *et al.*, 2012).

The two scans were acquired in the same position through the upper cervical cord, by geometrically linking the two volumes during prescription, with the middle of the volume through the C2/C intervertebral disc. The copied geometry of the two volumes allowed corresponding slices to be reviewed simultaneously. High in plane resolution (0.5 x 0.5mm voxel size) and relatively small voxel sizes (1.25mm<sup>3</sup>) were chosen to achieve good anatomical definition. Care was given to immobilizing the patient using polystyrene filled bags to reduce motion artefact.

The sequence details were:

1. 3D PSIR was acquired in the axial plane without parallel imaging containing 10 contiguous slices, FOV=256x128mm<sup>2</sup>, matrix=512x256, TR=12ms, TE=6.1ms, dual RF transmit, TI=843.6ms and number of averaged signals=3. The voxel dimensions were 0.5x0.5x5mm<sup>3</sup> and the acquisition time was 14:22 minutes.
2. 3D FFE image was acquired in the axial plane containing 10 contiguous slices, FOV 240x180mm<sup>2</sup>, TR 23ms, TE 5ms, flip angle  $\alpha=7^\circ$ , and number of averaged signals=8. The voxel dimensions were 0.5x0.5x5mm<sup>3</sup> and the acquisition time was 13:34 minutes.

### 6.2.3 *Image Analysis*

#### 6.2.3.1 *Lesion identification and location*

Two readers (HK and KM) reviewed both axial images simultaneously (i.e. on a slice-by-slice basis). Lesions were identified first on 3D-FFE images then confirmed on the 3D-PSIR images. Lesions were identified as sharply delineated areas of increased signal intensity on 3D-FFE imaging and hypo-intensity on 3D-PSIR images (Figure 6.3 and 6.4).

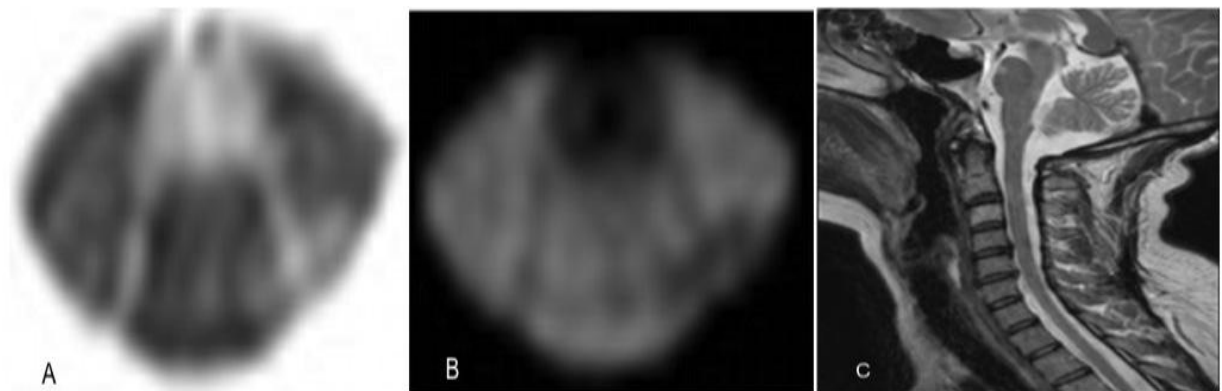


**Figure 6.3** Axial cervical cord MRI (A) FFE and (B) PSIR in a MS patient showing (i) a WM-GM lesion involving the anterior column lesion and ventral horn of GM and (ii) a GM-WM lesion in the left lateral column and extending to adjacent dorsal horn and posterior column. (C) Sagittal T2 weighted image used for slice orientation showing a hyper-intense lesion at C2/C3 level

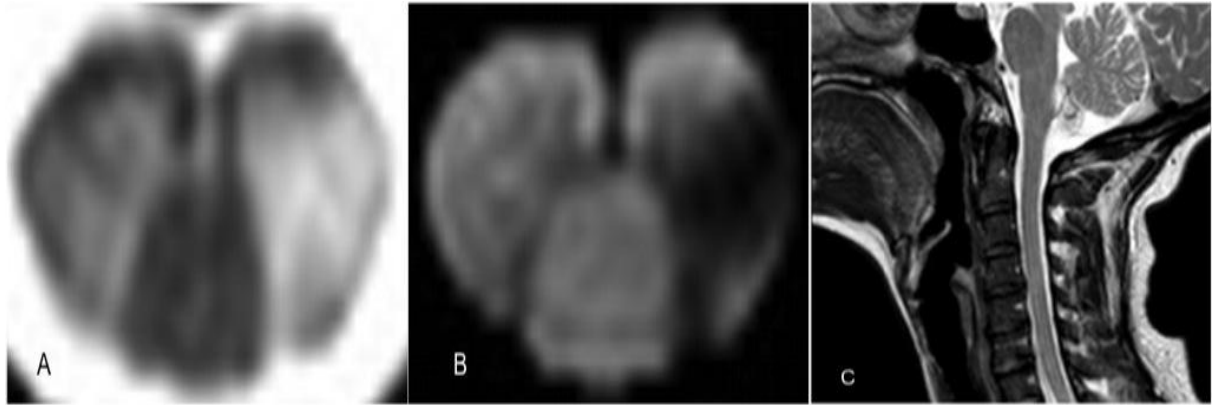


**Figure 6.4** Axial cervical cord MRI (A) FFE and (B) PSIR in a MS patient showing a WM-GM lesion involving the left lateral column and adjacent dorsal horn GM. (C) Sagittal T2 weighted image with no visible lesions

Following lesion identification on 3D-FFE, GM involvement was defined using PSIR. As lesions were hyper-intense on 3D-FFE, they have similar signal intensity to GM; this problem was not encountered on PSIR. Thus PSIR helped to clarify GM involvement by a lesion. Areas of diffuse abnormality were sometimes visible, mainly on the FFE sequence (Figure 6.5), in both subtypes of MS; however, only focal lesions were recorded in this study. Both images were used to define lesion location as fully as possible. Lesions were differentiated from motion artefact as any lesion included had to be identifiable on both sequences in the same location, as the two sequences were acquired separately this reduced the possibility of motion artefacts being misclassified as lesions.

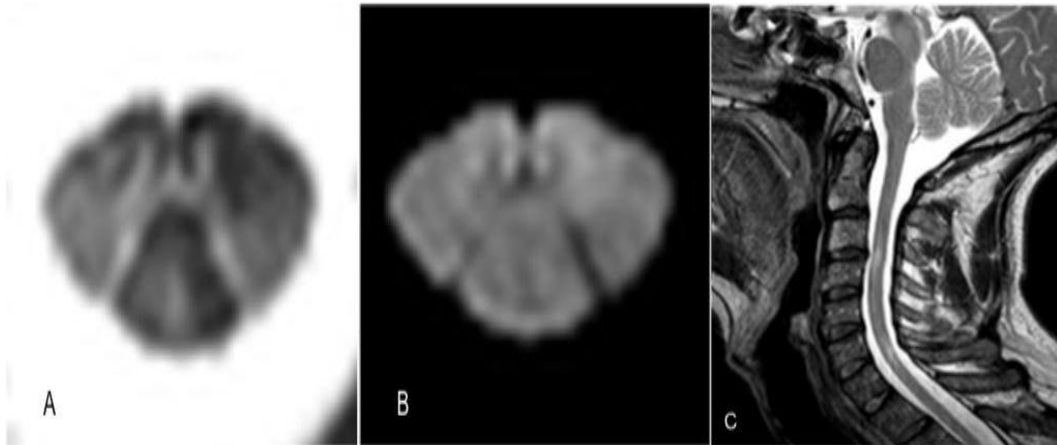


**Figure 6.5** Axial cervical cord MRI (A) FFE and (B) PSIR demonstrating diffuse changes seen in both lateral columns and posterior column on the FFE sequence. These were seen on 3 consecutive FFE slices at the C2/C3 level in the absence of focal lesions at the same level. (C) Sagittal T2 weighted image shows a focal lesion at C3-4 only

Lesions were classified as WM-only (Figures 6.6 and 6.8), mixed WM-GM (Figures 6.4 and 6.7) or GM-only. Location within WM columns was also recorded: posterior column (PC), lateral column (LC), anterior column (AC). If a lesion involved more than one column, it was recorded as involving the column where it was predominantly located. When lesions extended over more than one slice, involvement of both WM and GM on any slice was sufficient to classify it as a mixed WM-GM lesion (Figure 6.4). Lesions were classified as WM-only when no GM involvement was seen on any slice over the entire lesion length (Figure 6.6 and 6.8). GM-only lesions were categorised as not involving WM on any slices.

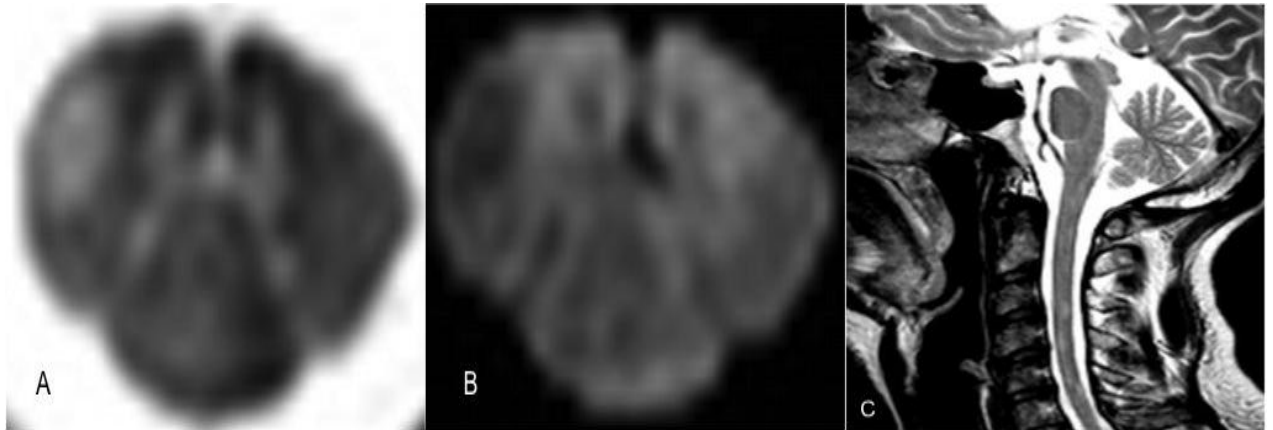


**Figure 6.6** Axial cervical cord MRI (A) FFE and (B) PSIR in a MS patient showing a WM-only lesion in the right lateral column. (C) Sagittal T2 weighted image with multiple focal lesions

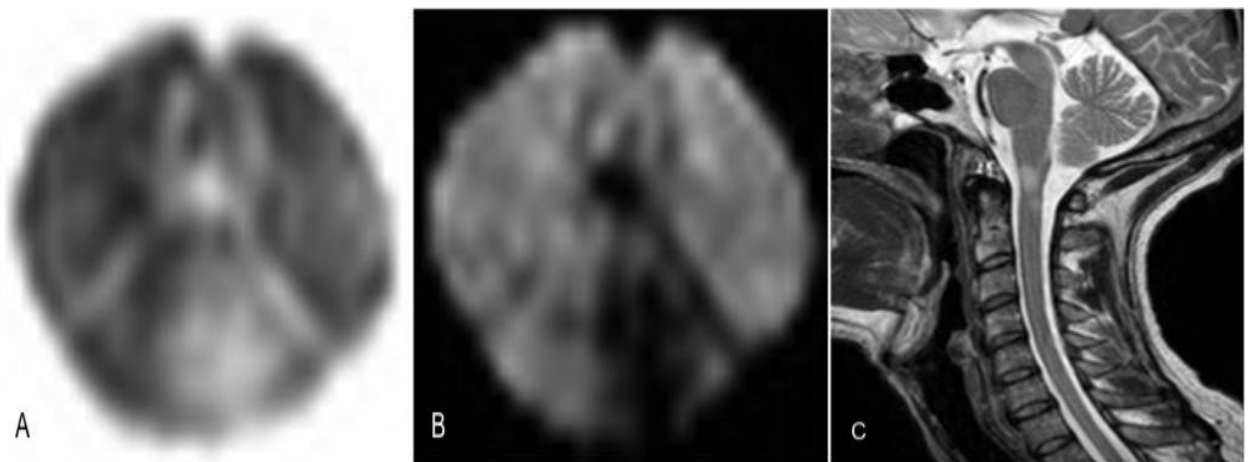


**Figure 6.7** Axial cervical cord MRI (A) FFE and (B) PSIR in a MS patient showing a WM-GM lesion involving posterior column and adjacent left dorsal horn GM; the GM involvement is more clearly evident on PSIR. (C) Sagittal T2 weighted image with large focal lesion at the level of the foramen magnum

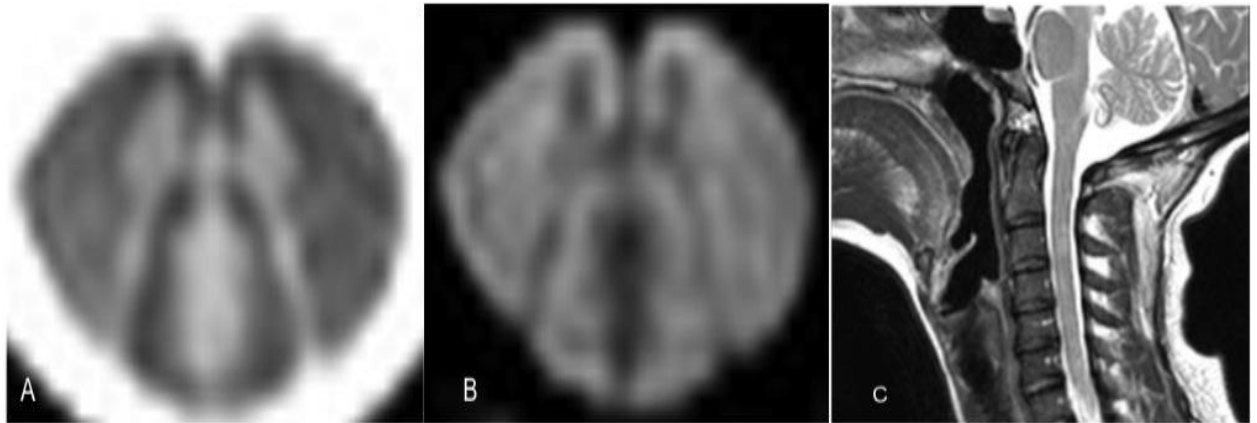


**Figure 6.8** Axial cervical cord MRI (A) FFE and (B) PSIR in a MS patient showing a WM-only lesion in the posterior column. (C) Sagittal T2 weighted image with a focal lesion visible above the C3/4 intervertebral disc

### 6.2.3.2 Lesion area and length

Cross-sectional cervical cord area of each subject was calculated on 3D-PSIR images using an active surface model on JIM software (Horsfield *et al.*, 2010) (version 6, Xinapse Systems, Northants, UK), and mean cord area for each slice was calculated. The 3D-PSIR sequence was chosen for this purpose as it has a high contrast to noise ratio between cord and CSF (Hou *et al.*, 2005). Lesions within each WM tract were outlined on the same 3D-PSIR image using a semi-automated tool on JIM software package. The area of each lesion was recorded on each slice. The proportion of the whole cross-sectional cord area affected by lesions was calculated as:  $(\text{lesion area}/\text{whole cord area}) \times 100\%$ . The number of axial slices that each lesion involved was also recorded to document lesion length.

### 6.3 Results (Tables 6.1 and 6.2)

51 lesions were identified in total, 24 in RRMS cohort, 22 in SPMS cohort, and 5 in the case of CIS. Three lesions were seen in the AC (one in CIS, one in RRMS group and one in SPMS), 30 in LC (three in CIS, 16 in RRMS and 11 in SPMS) and 18 in PC (one in CIS, seven in RRMS, ten in SPMS). The highest number of lesions was seen in the LC (n=30, 59%) and PC (n=18, 35%) with the lowest number seen in AC (n=3, 6%).

In total 19 (37%) WM-only lesions were seen and 32 (63%) mixed GM/WM lesions were seen. Lesions typically involved only a part of a WM column and it was possible to detect lesions with a wide range of areas (range 1.9-20.6mm<sup>2</sup>). An occasional WM lesion was seen to extend from one column across central GM and in to another WM column (Figure 6.2). No GM-only lesions were identified.

In the CIS case two of the five lesions were mixed GM/WM lesions and three were WM only. In RRMS cohort, 8 (33%) WM-only and 16 (67%) mixed GM/WM lesions were seen. In the SPMS cohort, 8 WM-only (36%) and 14 mixed GM/WM (64%) lesions were seen.

Mean lesion area was 4.3mm<sup>2</sup> in AC (SD 0.97), 8.5mm<sup>2</sup> in the LC (SD 3.72) and 11.3mm<sup>2</sup> in the PC (SD 4.61), which corresponded with 6.1%, 12% and 16.1% of mean cord area respectively. Mean lesion length in AC was 18.3mm, in the LC was 17.6mm and in the PC was 24.8mm.

	All Subjects			CIS			RRMS			SPMS		
	WM only	Mixed WM /GM	All	WM only	Mixed WM/GM	All	WM only	Mixed WM/GM	All	WM only	Mixed WM/GM	All
Anterior Column	1	2	3	0	1	1	0	1	1	1	0	1
Posterior Column	7	11	18	1	0	1	3	5	8	3	6	9
Lateral Column	11	19	30	2	1	3	5	10	15	4	8	12
All regions	19	32	51	3	2	5	8	16	24	8	14	22

**Table 6.1** Spinal cord lesion number and location in all MS patients and clinical subgroups (WM: white mater, GM: Grey matter)

		<b>Total</b>	<b>CIS</b>	<b>RRMS</b>	<b>SPMS</b>
<b>Mean Lesion Area (mm<sup>2</sup>)</b>	Anterior Column	4.3 ± 0.9	4.8 ± 1.1	4.5 ± 0.5	3.6 ± 0.4
	Lateral Column	8.5 ± 3.7	4.8 ± 1.9	9.5 ± 3.7	7.8 ± 3.3
	Posterior Column	11.3 ± 4.6	6.3 ± 3.2	11.9 ± 4.7	10.5 ± 4.3
<b>Mean lesion length (mm)</b>	Anterior Column	18.3 ± 7.6	20	10	25
	Lateral Column	17.6 ± 12.8	11.7 ± 7.1	20.6 ± 12.5	20.5 ± 14.8
	Posterior Column	24.8 ± 12.8	15	30.6 ± 10.2	28.9 ± 14.5
<b>% of cord area covered by lesion</b>	Anterior Column	6.1	6.8	6.4	5.1
	Lateral Column	12	6.8	13.4	11.1
	Posterior Column	16.1	8.9	16.9	14.9

**Table 6.2** Mean (±SD) Lesion area and length in white matter columns

## 6.4 Discussion

In this pilot study a 3T MR system and 3D-FFE and 3D-PSIR sequences were used, as an alternative to 2D conventional acquisitions. It was possible to visualise lesions affecting the central GM and WM columns in the spinal cord of patients with MS. Many WM-only and mixed WM-GM MS lesions were detected, whilst no GM-only lesions were detected.

The imaging appearances of the WM column lesions correspond well with several pathological studies (Fog, 1950, Gilmore *et al.*, 2006, Lycklama à Nijeholt *et al.*, 2001) as does their predominant location in the posterior and lateral columns.

The relative proportion of lesions classified as WM-only or as mixed WM-GM lesions (37% versus 63% respectively) is similar to the proportions that were reported in a previous detailed histopathological study (33% versus 45% respectively) (Gilmore *et al.*, 2006), suggesting that the sensitivity of these two sequences for detecting such lesions is good. However, although it was possible to comment on the involvement of GM it was not possible to accurately determine the border between the lesion and the normal appearing GM, especially on the 3D-FFE sequence where central GM had a signal intensity that was often similar to the WM lesions. The 3D-PSIR sequence improves detection of MS lesions in the cerebral cortex (Nelson *et al.*, 2007), and it was helpful in depicting GM involvement in the spinal cord.

The absence of GM-only lesions seen in our study differs from a previous histopathological study that reported 22% of cord lesions being confined to central GM (Gilmore *et al.*, 2006). The pathology study noted that GM-only lesions seen on a single slice were sometimes seen to expand into the WM in subsequent slices, suggesting that they were in fact mixed WM-GM lesions. However, it is likely that the MR parameters used with each sequence in this study may have been suboptimal for detecting GM-only lesions.

Difficulties with conventional T2-weighted fast spin echo (FSE) imaging in the spinal cord have been well documented and other sequences have proved superior in lesion detection in the cervical spinal cord (Rocca *et al.*, 1999). Recently, conventional FSE imaging has been compared to multi-echo recombined gradient echo (MERGE) sequence (similar to FFE sequence in this study) (White *et al.*, 2011, Martin *et al.*, 2012). In both studies MERGE appears superior in detection of spinal cord lesions with the rationale given that improved contrast between GM and WM aids lesion detection. In a similar manner PSIR has been compared to short time inversion recovery (STIR) and FSE and also was found to improve lesion detection with GM visible on axial images (Poonawalla *et al.*, 2008). However none of these studies comment on the frequency of involvement of GM by spinal cord lesions.

Better detection of central GM involvement *in vivo* might be possible with higher resolution images, providing that adequate SNR can be achieved within a feasible imaging time. This should be facilitated by acquiring the present sequences with thinner slices, e.g., 3mm thickness. Alternative ways to improve resolution and SNR would involve the use of improved multi-channel coil designs, or higher

magnetic field 7 Tesla scanners (where improved cerebral cortical MS lesion detection has already been shown [Mainero *et al.*, 2009, Schmierer *et al.*, 2010]) and higher resolution spinal cord images may be acquired in clinically acceptable time frames in the spinal cord (Zhao *et al.*, 2013). There may also be other sequences (e.g. double inversion recovery) and contrast mechanisms with potential to improve GM lesion detection in the spinal cord.

The imaging sequences used in this pilot study are not likely to be useful in routine diagnosis, mainly because of their long acquisition time and limited coverage of spinal cord. However, they may be helpful in research directed at understanding the structure-function relationship of MS spinal cord pathology. Therefore, in the latter half of this chapter these two sequences are employed in a significantly larger cohort of people with CIS and MS to accurately characterise spinal cord lesion morphology on axial imaging.

## **(ii) Classification of spinal cord lesions in different phenotypes of multiple sclerosis using high resolution axial MRI**

### **6.5 Introduction**

Spinal cord abnormalities may be detected in up to 90% of cases of MS on MRI (Bot *et al.*, 2002; Bot *et al.*, 2004) and are typically seen as abnormal regions of hyper-intense signal, less than two vertebral segments in length, on T2-weighted images (Kidd *et al.*, 1993).

Although spinal cord lesions may be visualised on sagittal imaging, it has been suggested that this approach underestimates their number (Bergers *et al.*, 2002) and axial acquisitions may improve detection (Weier *et al.*, 2012). A further advantage of axial imaging is that the spinal cord grey matter (GM) and columns may be visualised (Poonawalla *et al.*, 2008; White *et al.*, 2011; Martin *et al.*, 2012). However, to our knowledge, there are no reports to date investigating the association between spinal cord lesions' GM involvement *in vivo* and MS.

In the pilot study, in the former part of this chapter, the utility of a combination of axial (0.5 x 0.5 mm<sup>2</sup> in plane) 3D-fast field echo (FFE) and 3D-phase sensitive inversion recovery (PSIR) scans was evaluated, using a 3T MRI system, to record the anatomical location and grey matter involvement of cervical cord lesions.

In this latter part of the chapter, spinal cord lesion morphology is studied in a larger cohort of people with MS, in order to investigate whether diffuse abnormalities and more extensive focal lesions, that traverse two or more spinal cord columns and involve the grey matter, are associated with progressive MS.

## 6.6 Methods

### 6.6.1 *Subjects*

People with clinically isolated syndrome (CIS) or MS (Polman *et al.*, 2011) were recruited. Subtypes of MS were classified using published criteria (Lublin and Reingold 1996). Recruitment was performed without reference to earlier spinal cord imaging findings. None of the subjects had a relapse or received corticosteroids within a month prior to participation. Disability was recorded using the expanded disability status scale (EDSS [Kurtzke 1983]). Informed written consent was obtained from all participants.

### 6.6.2 *MRI protocol*

MRI scans were performed using a 3T Philips Achieva MRI system with radiofrequency (RF) multi-transmit technology (Philips Healthcare, Best, the Netherlands). To minimise motion artefacts during scanning a polystyrene filled vacuum bag was placed behind the neck of each participant and subsequently the air was removed to immobilise the neck. The axial spinal cord images acquired in the upper cervical cord contained ten slices of 5mm thickness and were centred at C2/C3:

#### 6.6.2.1 *Spinal cord acquisitions*

- (i) Sagittal PD/T2 cervical spine: TR=4000ms, TE=15/80ms (dual echo), NEX=2, FOV=256 X 160 mm<sup>2</sup>, 12 slices, voxel size=1 x 1 x 3mm<sup>3</sup>, TSE=12.
- (ii) Axial 3D-PSIR: was acquired in the axial plane in the cervical cord centred at C2/C3 intervertebral disc, with a voxel size of 0.5 x 0.5 x 5 mm<sup>3</sup>, TR

= 8 ms; TE = 3.7 ms;  $\alpha = 5^\circ$ ; FOV = 256 x 256 mm<sup>2</sup>; NEX = 1.

- (iii) Axial 3D-FFE sequence using identical slice prescription geometry as in  
(ii) with TR = 23ms; TE = 5ms;  $\alpha = 7^\circ$ ; FOV 240 x 180mm<sup>2</sup>; voxel size  
0.5 x 0.5 x 5mm<sup>3</sup>

### **6.6.2.2 Brain acquisition**

- (i) Axial PD/T2 images using a 2D turbo spin echo sequence (TSE) with 3mm slice thickness; the following parameters were employed: TR=3500 ms; TE=19/85 ms; matrix 240 x 240 mm<sup>2</sup>; in plane voxel size = 1 x 1 mm.

### **6.6.3 Image analysis**

Using the sagittal image for orientation of axial slices, lesions were recorded on the slice-matched 3D-FFE and 3D-PSIR images by one reader (HK) under the supervision of an experienced neuroradiologist (KM). Lesions were analysed on all ten 5mm thick slices of the axial images. Both readers were blinded to the clinical status of the cases being reviewed.

#### **6.6.3.1 Focal lesions**

Focal lesions were defined as abnormal areas of clearly increased signal intensity on the 3D-FFE image and decreased signal intensity on 3D-PSIR and a clearly demarcated border from the surrounding tissue. Focal lesions were only recorded when they were clearly visible simultaneously as a hyper-intense abnormality on the 3D-FFE scan and hypo-intense abnormality on 3D-PSIR scan.

Focal lesions were then categorised based on the number of spinal cord columns involved. For this, either unilateral or bilateral involvement of the anterior and posterior columns was counted as a single column and involvement of the right and left lateral columns was counted separately. Thus anywhere between one and four columns could be involved (Table 6.3). The spinal cord column predominantly involved by the lesion was recorded and if extension into one or more additional columns was seen (e.g. a lateral column lesion extending into the posterior column) this was also noted.

Type I	Spinal cord lesion involving a single column and confined to the white matter
Type II	Spinal cord lesion involving a single column and grey matter
Type III	Spinal cord lesion involving two columns and grey matter
Type IV	Spinal cord lesion involving three or four spinal cord columns and grey matter

**Table 6.3** Classification system used for focal spinal cord lesions identified on axial scans

Lesions involving a single column were either confined to white matter only (Type I – demonstrated in Figure 6.9), or extended to involve GM (Type II – Figure 6.10). When focal lesions involved two (Type III – Figure 6.11) or more (Type IV – Figure 6.12) columns, the GM adjacent to the affected columns was also invariably involved, i.e., no lesions involved two or more columns without

including GM. For lesions that covered multiple slices of the image, their extent was classified from the slice with maximal involvement.

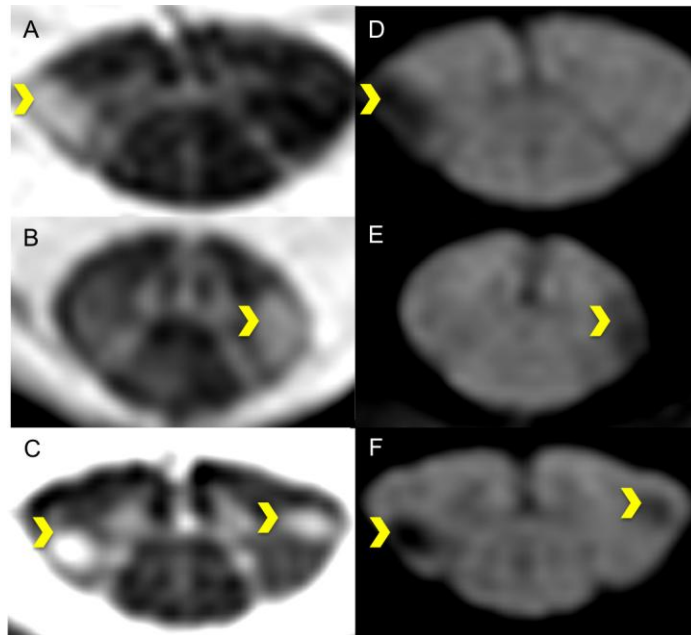


**Figure 6.9** Three cases of lesions involving a single spinal cord column restricted to the white matter (Type I lesions). 1A-C: 3D-FFE  $0.5 \times 0.5 \text{ mm}^2$  in plane voxel size, 1D-F: 3D-PSIR  $0.5 \times 0.5 \text{ mm}^2$  in plane voxel size. Focal lesions are marked by a yellow single chevron and are located in the left lateral column (Figures A/D and C/F) and in the right lateral column (Figures B/E and C/F)

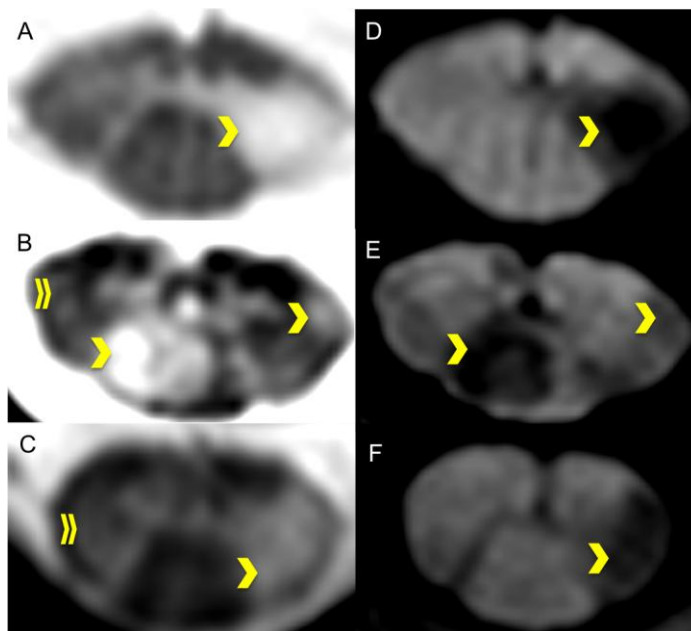


**Figure 6.10** Three cases of lesions involving a single spinal cord column also involving the grey matter (Type II lesions). 2A-C: 3D-FFE  $0.5 \times 0.5 \text{ mm}^2$  in plane

voxel size, 2D-F: 3D-PSIR  $0.5 \times 0.5 \text{ mm}^2$  in plane voxel size. Diffuse abnormalities are demonstrated on the 3D-FFE images 2B and 2C in the right lateral column indicated by a double chevron. Focal lesions involving the grey matter are demonstrated in the left lateral column by a single chevron in all images and a separate focal lesion is demonstrated in the posterior column (Figure B and E).

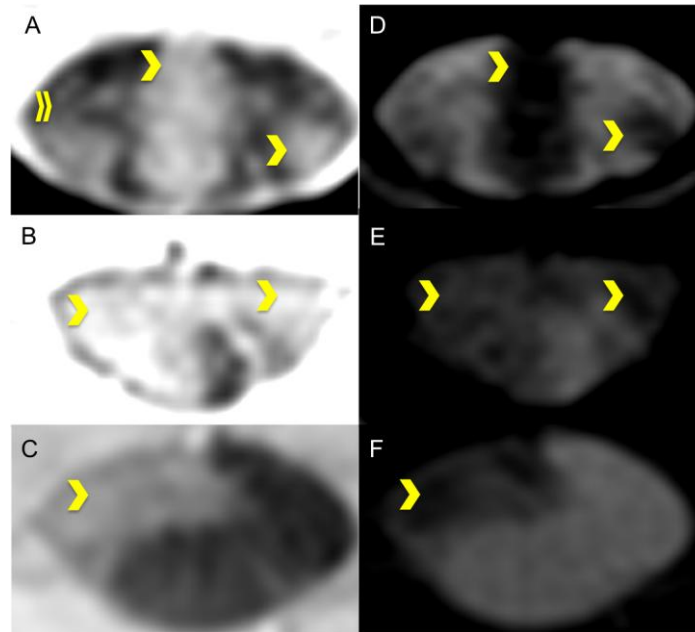


**Figure 6.11** Three cases of focal lesions (indicated by single chevrons) involving two spinal cord columns and the grey matter (Type III lesions). 3A-C: 3D-FFE  $0.5 \times 0.5 \text{ mm}^2$  in plane voxel size, 3D-F: 3D-PSIR  $0.5 \times 0.5 \text{ mm}^2$  in plane voxel size. A focal lesion crossing from the anterior to posterior column is demonstrated in Figures A and D. Figure B and E demonstrate lesions crossing from the lateral to the posterior column and a separate focal lesion in the left lateral column. Figure A also shows diffuse abnormalities in the right lateral column (indicated by double chevron). A focal lesion crossing from the lateral to the anterior column is demonstrated in Figure C and F.

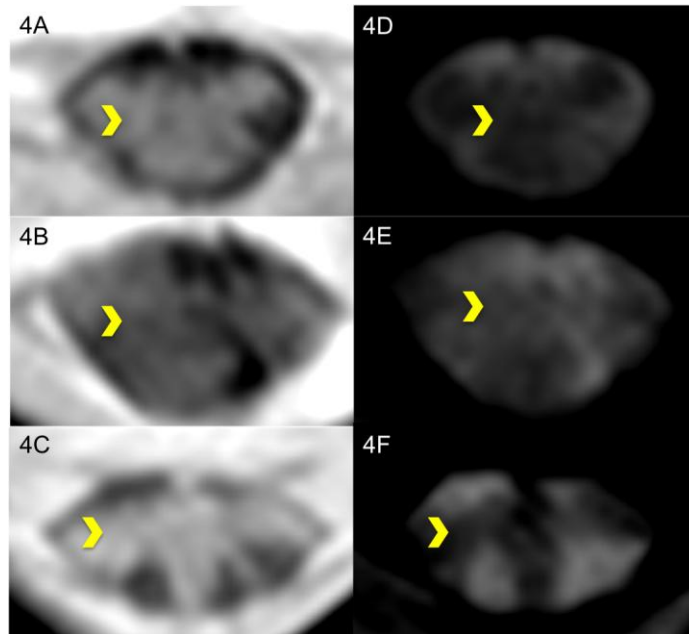


**Figure 6.12** Three cases of lesions involving three spinal cord columns and the grey matter (Type IV lesions). 4A-C: 3D-FFE 0.5 x 0.5 mm<sup>2</sup> in plane voxel size, 4D-F: 3D-PSIR 0.5 x 0.5 mm<sup>2</sup> in plane voxel size. Focal lesions are shown in all images by a single chevron.

### 6.6.3.2 Diffuse abnormalities

These were defined as abnormal areas of intermediate signal intensity, between that of focal plaques and normal appearing spinal cord tissue (Figure 6.13).

Diffuse abnormalities also lacked a well demarcated border from adjacent normal appearing spinal cord tissue. These were recorded on the 3D-FFE scan, where they were visible as an intermediate hyper-intense abnormality relative to the normal appearing spinal cord. Diffuse abnormalities were often not seen on the PSIR scan, or if they were, they were less well defined areas of subtle hypo-intensity relative to normal appearing cord.

Diffuse abnormalities were recorded, when seen, as present or absent. An anatomical classification system based on spinal cord columnar involvement – as

undertaken for focal lesions - could not be implemented for diffuse abnormalities, due to the absence of a clearly defined border demarcating their termination.

Images degraded by artefacts on visual inspection were excluded from analysis.

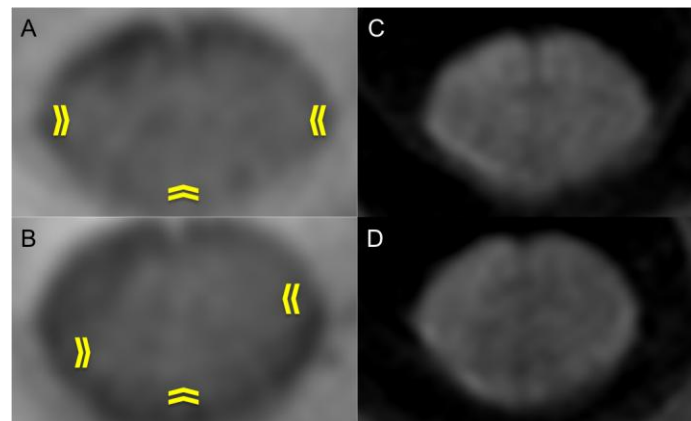


**Figure 6.13** Images demonstrating diffuse abnormalities on 3D-FFE images (A and B) shown by double chevrons. Corresponding slices of 3D-PSIR image shown in images C and D.

#### **6.6.4** *Statistical analysis*

Stata 13 (Stata Corporation, College Station, Texas, USA) was used for statistical analysis.

##### **6.6.4.1** *Comparison of focal lesion characteristics, GM involvement and diffuse abnormalities between CIS and MS subtypes*

Firstly, to investigate significant differences in the number of focal spinal cord lesions between CIS and MS and between each MS subtype, a single test for 'linear trend' (Altman *et al.*, 1991) by regressing the lesion variable (i.e. number

of focal lesions) on a group variable coded numerically in the order: 0=CIS, 1=RRMS, 2=PPMS, 3=SPMS.

Secondly, to test the hypotheses that more extensive focal lesions, GM involvement and diffuse abnormalities would be seen more frequently in progressive MS, these lesion characteristics were compared between CIS and MS subtypes using logistic regression.

In each regression model constructed, the lesional element being compared (lesion extent, GM involvement and diffuse abnormalities) was entered in a binary fashion as the dependent variable. Disease subtype (CIS or MS) was entered as a predictor in each model and adjustment was made for age, gender and disease duration (where appropriate). Separate adjustment was performed so that age and duration were not in the model simultaneously, since across subject groups duration will necessarily vary substantially in patients of the same age. Where patients did not have a particular lesion characteristic (e.g. diffuse abnormalities) an exact chi-square test was used and this is indicated in the Results. Comparisons performed were as follows: CIS vs. RRMS, SPMS vs. RRMS and PPMS vs. RRMS/SPMS.

Due to the exploratory nature of the study, no adjustment for multiple comparisons was performed (Bender and Lange 2001). However, to limit the number of statistical tests being performed, comparisons were restricted solely to the hypotheses being investigated.

#### **6.6.4.2** *Investigation of independent associations between spinal cord lesion characteristics and physical disability*

In order to investigate independent associations between lesion variables and physical disability, a multiple linear regression model was constructed with EDSS as response variable on the lesion predictors listed in the Table 6.4. A standard manual forward stepwise procedure was used as follows: (i) age, gender and disease duration were retained in the model throughout; the first MRI variable entered was the subject classification according to their most extensive lesion (ii) each MRI variable entered was retained if  $P < 0.05$ , while any MRI variables with  $P > 0.05$  were removed; with each new variable combination thus constructed, the procedure was repeated, until all MRI variables in the model were  $P < 0.05$  and no other variable improved the model at  $P < 0.05$ . There was no marked deviation from normality or homoscedascity of regression residuals, but the regression estimates for the final model were confirmed using the non-parametric bias-corrected and accelerated bootstrap (Carpenter and Bithall 2000).

Lesion number	The total number of lesions per patient
Lesion characteristics	The most extensive lesion seen in each patient (Type I – IV)
Diffuse abnormalities	The presence of diffuse abnormalities
Spinal cord columnar involvement by focal lesions	The mean number of columns involved per lesion
	The largest number of columns involved in any one lesion
	The number of lesions involving the anterior, lateral or posterior columns
Spinal cord grey matter involvement by focal lesions	The number of lesions involving the grey matter
	The number of lesions involving the anterior, lateral or posterior columns and the grey matter
	Diffuse abnormalities and spinal cord grey matter involvement by a focal lesion

**Table 6.4** A list of all MRI variables that were tested prior to construction of the final regression model investigating independent associations between spinal cord lesion variables with EDSS

## 6.7 Results

### 6.7.1 *Demographics of CIS and MS groups*

In this study 120 people were recruited: 25 CIS, 35 RRMS, 30 SPMS and 30 PPMS.

Demographic details of the subjects recruited are summarised in Table 6.5.

Three scans were excluded due to motion artefacts: CIS (1), RRMS (1) and SPMS (1).

	CIS n = 25	RRMS n = 35	PPMS n = 30	SPMS n = 30
Age (years)	36.5 ± 9.0	38.7 ± 9.7	50.6 ± 9.9	51.1 ± 9.2
Gender Female: Male	14:11	23:12	13:17	18:12
Disease duration (years)	0.4 ± 0.4	6.5 ± 5.2	10.4 ± 7.5	19.9 ± 11.5
Median EDSS (range)	1 (0 - 3.5)	2.5 (0 - 6)	6 (2 - 7.5)	6.5 (4 - 8)
Disease modifying drugs (%)	0 (0)	19 (54)	0 (0)	5 (17)

**Table 6.5** Demographics of all CIS and MS patients recruited for this study. Data represents mean ± standard deviation (SD).

The CIS cohort had the following presentations: optic neuritis (21), partial myelitis (2), multifocal CIS (1, optic neuritis with a brainstem syndrome) and hemispheric presentation (1, unilateral hand weakness due to a motor cortex lesion). Criteria for dissemination in space was fulfilled in 15 cases, however,

dissemination in time could not be determined as gadolinium was not used (Polman *et al.*, 2011).

In the MS cohort 19 of the 35 RRMS patients were taking disease modifying drugs:  $\beta$ -interferon (13), natalizumab (5), and glatiramer acetate (1). In the SPMS cohort, five of the 30 patients were taking  $\beta$ -interferon.

### **6.7.2** *Number of spinal cord lesions recorded (Tables 6.6a and 6.6b)*

Lesion numbers in each category (Type I-IV) are summarised in Table 6.6a in total 354 focal spinal cord lesions were identified. A higher number of Type IV lesions were identified in progressive MS: SPMS (8), PPMS (5) than RRMS (1) and CIS (0).

Total number of lesions	Type I	Type II	Type III	Type IV
CIS n = 18	8 (44.5%)	8 (44.5%)	2 (11%)	0 (0%)
RRMS n = 94	36 (38%)	41 (44%)	16 (17%)	1 (1%)
PPMS n = 106	36 (34%)	55 (52%)	10 (9%)	5 (5%)
SPMS n = 136	37 (27%)	69 (51%)	22 (16%)	8 (6%)
All subjects n = 354	117 (33%)	173 (49%)	50 (14%)	14 (4%)

**Table 6.6a** Number (percentage) of lesion types I-IV recorded in each clinical subgroup.

In line with pathological reports of the MS spinal cord, lesions involved the lateral and posterior columns more frequently (75% and 38% of lesions respectively) than the anterior column (6%). The GM was involved by 67% of the lesions seen. Lesion numbers recorded in each anatomical location are summarised in Table 6.6b.

Total number of lesions	Grey matter involvement	Anterior column	Posterior column	Lateral column
CIS n = 18	10 (56%)	2 (11%)	5 (28%)	13 (72%)
RRMS n = 94	58 (62%)	5 (5%)	38 (40%)	67 (71%)
PPMS n = 106	70 (66%)	7 (7%)	37 (35%)	79 (75%)
SPMS n = 136	99 (73%)	6 (4%)	54 (40%)	107 (79%)
All subjects n = 354	237 (67%)	20 (6%)	134 (38%)	266 (75%)

**Table 6.6b** The number (percentage) of lesions involving the spinal cord grey matter and each column of the spinal cord in each clinical subgroup. Note: the numbers in this table do not add to the total number of lesions, since some lesions seen involved more than one column e.g. extension into the lateral and posterior column by the same lesion.

### 6.7.3 *Lesion characteristics by MS subtype (Tables 6.7a, 6.7b)*

The proportion of people with focal spinal cord lesions increased in the order: CIS (42%), RRMS (85%), PPMS (97%) and SPMS (100%) - Table 6.7a.

Total number of people	Number of people with focal spinal cord lesions	Number of people with Type I lesions	Number of people with Type II lesions	Number of people with Type III lesions	Number of people with Type IV lesions	Number of people with lesions involving the grey matter	Number of people with diffuse abnormalities
CIS n = 24	10 (42%)	8 (33%)	5 (21%)	2 (8%)	0 (0%)	6 (25%)	0 (0%)
RRMS n = 34	29 (85%)	20 (59%)	21 (62%)	12 (35%)	1 (3%)	25 (74%)	6 (18%)
PPMS n = 30	29 (97%)	22 (73%)	25 (83%)	9 (30%)	5 (17%)	27 (90%)	17 (57%)
SPMS n = 29	29 (100%)	20 (69%)	27 (93%)	17 (59%)	7 (24%)	28 (97%)	16 (55%)

**Table 6.7a** Number (percentage) of people with CIS or MS with spinal cord lesions, each lesion type, spinal cord grey matter involvement and diffuse abnormalities. Note: Three peoples' scans were excluded from analysis due to motion artifacts on images: CIS (1), RRMS (1) and SPMS (1).

Table 6.7b shows mean number and type of lesions per person. The mean of the total number of lesions per patient increases also in the order CIS (mean 0.8), RRMS (2.8), PPMS (3.5), and SPMS (4.7). This increase is approximately linear with a significant increase of 1.2 (95% CI 0.9, 1.6; P<0.001) lesions per MS subtype. Adjustment for age and gender did not affect the results.

Number of people	Type I	Type II	Type III	Type IV	Grey matter involvement
CIS n = 24	0.33, 0 (0-1)	0.33, 0 (0-2)	0.08, 0 (0-1)	0, 0 (0)	0.42, 0 (0-3)
RRMS n = 34	1.06, 1 (0-5)	1.21, 1 (0-4)	0.47, 0 (0-3)	0.03, 0 (0-1)	1.71, 1 (0-5)
PPMS n = 30	1.20, 1 (0-4)	1.83, 1.5 (0-6)	0.33, 0 (0-2)	0.17, 0 (0-1)	2.33, 2 (0-6)
SPMS n = 29	1.27, 1 (0-5)	2.37, 2 (0-6)	0.75, 1 (0-3)	0.28, 0 (0-2)	3.41, 3 (0-8)

**Table 6.7b** Mean, median (range) of the number of spinal cord lesions in each category and involving the grey matter seen in each person with CIS and MS.

In line with the hypothesis being explored, the proportion of subjects with more extensive lesions (defined as Type III or IV), was significantly higher in RRMS vs. CIS (OR 6.8, 95% CI 1.4, 33.9; P=0.019), SPMS vs. RRMS (3.1, 95% CI 1.1, 8.7; P=0.033) and in SPMS vs. PPMS (OR 3.8, 95% CI 1.3, 11.2; P=0.015). These

comparisons were not materially affected by adjustment for age, gender or disease duration.

The proportion of subjects with lesions involving the GM (Type II, III and IV lesions) was also greater in RRMS vs. CIS (OR 8.3, 95% CI 2.5,27.6; P=0.001) and SPMS vs. RRMS (10.1, 95% CI 1.2, 85.3; P=0.034) but not significantly greater in SPMS vs. PPMS (OR 3.1, 95% CI 0.3, 31.8; P=0.338).

As anticipated, diffuse abnormalities were present in over half of PPMS (57%) and SPMS (55%) patients but only in 18% of RRMS and none of CIS (P=0.037 for RRMS vs. CIS, exact chi-square test). The odds ratio for having diffuse abnormalities in PPMS vs. RRMS was 6.1 (CI 2.0, 19.1; P=0.002) and for SPMS vs. RRMS, 5.7 (95% CI 1.8, 18.1; P=0.003). Adjustment for age, gender or disease duration did not materially alter these results.

#### **6.7.4 Independent associations between EDSS and spinal cord lesion characteristics**

The best independent predictor of EDSS was found to be the number of a subject's lesions which involved both a lateral column and GM. Compared to subjects with no such lesions, having 1, 2 and 3+ lateral column lesions with GM involvement, predicted respectively 0.8 (95% CI -0.26,1.77; P=0.143), 0.7 (-0.46, 1.81; P=0.239) and 2.1 (0.94, 3.32; P=0.001) higher mean EDSS (with P=0.0007 for the overall contribution of the categorical variable).

None of the other MRI variables entered additionally into this model (see Table 6.4) was significant, but in particular neither (i) the total number of lesions, nor (ii) the number of lesions involving a lateral column, nor (iii) the number of

lesions with GM involvement, contributed significantly to the above model, confirming the importance of the more specific predictor.

EDSS was also predicted with borderline significance to be higher by 0.4 (95% CI 0.01, 0.78; P=0.046) per category (Type I-IV) of the subject's most extensive lesion.

Age at scan (predicted 0.06 increase in mean EDSS per year of age, P<0.001), gender (predicted 0.60 higher mean EDSS in men compared to women, P=0.032) and disease duration (predicted 0.07 increase in mean EDSS per year duration, P=0.001) were also associated with EDSS.

The proportion of explained variance ( $R^2$ ) in this regression model was 66%, compared to 46% for a model with only age, gender and duration, and with 44% for a model with just the two lesion variables (though this rose to 50% when subject's most extensive lesion was entered as categorical).

## 6.8 Discussion

In this study two novel associations between spinal cord lesion characteristics and progressive MS have been demonstrated. Firstly, lesions involving two or more spinal cord columns and the grey matter, as well as diffuse abnormalities, are more frequent in progressive MS. Secondly, lateral column lesions with grey matter involvement, are independently associated with physical disability.

### 6.8.1 Association of more extensive focal lesions and diffuse abnormalities with progressive MS

*Post mortem* spinal cord studies have demonstrated extensive 'fan shaped' focal lesions traversing several white matter columns and grey matter (Fog 1950; Oppenheimer 1978), as well as diffuse abnormalities in progressive MS (Bergers *et al.*, 2002). However, due to the inherent limitations of axial spinal cord imaging (Stroman *et al.*, 2014), there are limited data on the morphology of focal lesions seen in progressive MS *in vivo*; compared directly to earlier stages of the disease.

This present study is in agreement with previous studies demonstrating a greater number of focal lesions in progressive MS (Lycklama *et al.*, 1997; Nijeholt *et al.*, 1998; White *et al.*, 2011; Weier *et al.*, 2012; Lukas *et al.*, 2013). However, this study extends these findings in two ways. Firstly, a greater number of spinal cord columns covered by individual focal lesions in progressive MS was noted (as seen in pathology studies [Fog 1950; Oppenheimer 1979]). This observation was in comparison to RRMS and CIS, where focal lesions seen were more

frequently restricted to a single column. Through the inclusion of people with earlier phases of the disease, an association has been demonstrated between these larger lesions, covering two or three columns, and progressive MS. Secondly the grey matter involvement of the extensive focal lesions seen was recorded. These results suggest that spinal cord grey matter involvement is extensive in progressive MS, in line with pathology reports (Gilmore *et al.*, 2006; Gilmore *et al.*, 2009).

A question arising from this observation is how lesions restricted to a single column of the cord, evolve to encompass multiple columns. Pathology reports of the spinal cord in progressive MS have demonstrated extensive inflammation and demyelination (Lovas *et al.*, 2000; DeLuca *et al.*, 2004). This may provide a milieu in the spinal cord conducive to the formation of new extensive lesions, or facilitate the extension and/or coalescence of existing lesions. However, longitudinal studies are required to elucidate the exact mechanisms involved.

Consistent with previous spinal cord studies we have also observed frequent diffuse abnormalities in progressive MS (Lycklama *et al.*, 1997; Nijeholt *et al.*, 1998; Weier *et al.*, 2012; Lukas *et al.*, 2013). An *ex vivo* study has suggested the histopathological correlate of this imaging abnormality is demyelination (Bergers *et al.*, 2002). Therefore, the more frequent identification of diffuse abnormalities in progressive MS in this study is in agreement with the extensive demyelination seen in *post mortem* spinal cord studies (Fog 1950; Oppenheimer 1979; Lovas *et al.*, 2000; DeLuca *et al.*, 2004; Gilmore *et al.*, 2009).

In this present study patients with progressive MS were almost six times more likely to have diffuse abnormalities, compared to RRMS. The significance of

diffuse abnormalities in progressive MS is discussed in the 2005 revisions to the McDonald diagnostic criteria (Polman *et al.*, 2005). However, diffuse abnormalities were not included due to a lack of reliability. The spinal cord imaging studies referenced in the 2005 revisions contained sagittal views only, unlike the present axial study. The detection of diffuse abnormalities in progressive MS may be improved upon (as seen with focal lesions [Weier *et al.*, 2012]), through the use of high resolution axial views in future studies.

### **6.8.2 Lesions involving lateral columns and grey matter are independently associated with disability**

In the subsequent chapter (seven) of this thesis, spinal cord lesion load measured quantitatively is shown to be independently associated with disability. In line with this, the current chapter also demonstrates an independent association between spinal cord lesions and disability. However, this present study characterised the anatomical location of lesions, in order to identify their functional effects in individual spinal cord columns.

The independent association between lateral column lesions with grey matter involvement and EDSS, may be due to corticospinal tract abnormalities and/or de-afferentation between sensory and motor tracts, as a consequence of grey matter inter-neuronal loss (Gilmore *et al.*, 2009). The EDSS is heavily weighted towards ambulatory function (Hobart *et al.*, 2000), which may explain the association between lateral column abnormalities and physical disability.

The most extensive lesion seen in patients (defined by the number of columns involved), not recorded in previous studies, was also associated with EDSS, albeit

with borderline significance. Such extensive lesions may contribute to axonal pathology by acute transection (Trapp *et al.*, 1998) or Wallerian degeneration (DeLuca *et al.*, 2004). However, the strength of the association seen may have been weakened by the effect of lesions outside of the field of view of the scans acquired.

### **6.8.3 *Limitations and future directions***

A number of limitations should be considered in the interpretation of the results of this study. Firstly, the images acquired were restricted to the upper cervical cord. Although limited, this approach minimised physiological motion and likely provided the greatest yield of lesions for analysis (Fog 1950; Oppenheimer 1979).

Secondly, with multiple statistical tests there may be an increased chance of obtaining false positive results: caution is especially needed interpreting results when the P-values obtained were significant at the 0.05 but not 0.01 level; such results should be regarded as hypothesis-generating only and need to be confirmed in future studies.

Finally, small focal lesions and subpial or peripheral lesions of the spinal cord, extending over two columns without GM involvement, may not have been visualised with the in-plane resolution used in the present study. Furthermore, lesions' extent within the spinal cord GM could not be quantified. Spinal cord lesion detection and classification may be improved upon in future studies

performed at 7T, with higher resolution acquisitions within clinically acceptable timeframes (Zhao *et al.*, 2013).

#### **6.8.4 Conclusions**

Through the use of high resolution, axial cervical spinal cord MR imaging on a 3T scanner, significant associations have been demonstrated in this chapter between the extent of focal spinal cord lesions, grey matter involvement and diffuse abnormalities with progressive MS and disability. The techniques used improve the detection and quantification of cord lesions in MS, and warrant further investigation for their potential to assist diagnosis and provide new outcome measures in clinical trials.

## **Chapter 7 - Investigation of associations between spinal cord lesion load, magnetisation transfer ratio and physical disability**

### **7.1 Introduction**

The progressive phase of MS often includes a prominent spinal cord syndrome (Kremenutzky *et al.*, 2006) and *post mortem* studies have demonstrated multiple and sometimes extensive 'wedge-like' or 'fan-shaped' lesions (Fog 1950; Oppenheimer 1978). However, the relationship of spinal cord lesion-load with clinical course is uncertain and direct pathological comparison of lesion-load in progressive forms of MS versus the relapsing-remitting (RR) phase of the disease is impeded by the rarity with which MS tissue becomes available in early disease.

MRI provides a technique to detect spinal cord lesions *in vivo* and can compare their frequency and extent at all stages of the disease. Perhaps surprisingly, MRI studies have generally shown no or only limited correlations between measures of spinal cord lesion-load and physical disability (Kidd *et al.*, 1993; Nijeholt *et al.*, 1998). However, almost all MRI studies of spinal cord lesions have been based on images acquired only in a sagittal plane, and therefore provide no indication of the extent to which the spinal cord is involved in its transverse dimensions. These studies have also used qualitative or only semi-quantitative methods to measure lesion-load, such as counts of lesion number (Kidd *et al.*, 1993; Nijeholt *et al.*, 1998) or the number of segments involved by lesions (Lukas *et al.*, 2013). Only one study has reported on lesions detected with axial (transverse) MRI scans, and in this study lesions were counted but their size was not reported (Weier *et al.*, 2012).

No study has previously attempted to quantify the extent of lesions involvement of the spinal cord by measuring the total lesion area in images acquired in the axial (transverse plane). Newer T2- and T1-weighted sequences have been developed that acquire high in-plane axial images through the upper cervical cord (Chapter 6), a level at which lesions are often seen pathologically and on conventional T2-weighted MRI. Lesions are clearly depicted on these sequences and demonstrate morphological appearances similar to those described on transverse histopathological slices (Fog 1950; Oppenheimer 1978).

In the present study, high in-plane resolution axial upper cervical cord images were acquired in a large cohort of patients with both RR and progressive forms of MS and with widely varying disease duration and disability. The hypotheses being explored were that firstly; carefully quantified cross-sectional spinal cord lesion area – measured on high-resolution axial slices - would be higher in progressive forms of MS than in RR disease and secondly, that lesion load would be significantly correlated with disability. Thirdly, magnetisation transfer ratio (MTR) values were measured in both intrinsic lesional and non-lesional spinal cord tissue, to investigate whether greater MTR abnormalities, reflecting more extensive demyelination, would be identified in progressive MS, compared to earlier stages of the disease (Dousset *et al.*, 1992; Bot *et al.*, 2004; Schmierer *et al.*, 2004; Chen *et al.*, 2013).

## **7.2 Methods**

### **7.2.1 Subjects**

In this study people with MS (Polman *et al.*, 2011) were recruited. MS subtype was classified using published criteria (Lublin and Reingold) and physical disability was recorded prior to the MRI scan using the expanded disability status scale (EDSS) (Kurtzke 1983) and multiple sclerosis functional composite (MSFC) (Fischer *et al.*, 1999). The nine hole peg test (9-HPT) and paced auditory serial addition tests (PASAT) were analysed in standard z-score form. The timed walk test (TWT) was analysed as a z-score formed from the inverse of walk times (i.e. walk speed), as walk times are highly positively skewed. None of the subjects had experienced a relapse within a month prior to participation. This study was approved by our local ethics committee and informed written consent was obtained from all participants.

### **7.2.2 MRI protocol**

MRI scans were acquired using a 3T Philips Achieva MRI system with radiofrequency (RF) multi-transmit technology. To minimise motion during scans a polystyrene filled bag surrounding the neck was used. The spinal cord sequences were performed in the upper cervical cord centred at the C2/C3 level and covering C2-C4.

*SC Imaging:*

- (i) 3D phase sensitive inversion recovery (PSIR): voxel size of  $0.5 \times 0.5 \times 3$  mm<sup>3</sup>, TR = 8 ms; TE = 3.7 ms; flip angle  $\alpha = 5^\circ$ ; FOV = 256 x 256 mm; NEX = 1
- (ii) MTR data were obtained by acquiring a 3D slab selective spoiled gradient echo sequence with two echoes using TR = 36ms, TE1/TE2 = 3.5/5.9ms, flip angle ( $\alpha$ )=9°, with and without Sinc-Gaussian shaped MT saturating pulses of nominal  $\alpha=360^\circ$ , offset frequency 1kHz, duration 16ms applied prior to the excitation pulse. Twenty-two 5mm slices were acquired in an axial orientation, with FOV = 180 x 240 mm<sup>2</sup> and acquisition matrix = 240 x 320 (voxel size 0.75 x 0.75mm<sup>2</sup>, reconstructed to 0.5 x 0.5mm<sup>2</sup>), with SENSE factor 2 in the foot/head direction, and 2 signal averages (NEX).
- (iii) 3D fat-suppressed fast field echo (3D-FFE) was acquired in the axial plane containing 10 contiguous slices, FOV 240x180mm<sup>2</sup>, TR 23ms, TE 5ms, flip angle  $\alpha=7^\circ$ , and number of averaged signals=8

*Brain imaging:*

- (i) 3D magnetisation-prepared turbo field echo (3D-TFE) sequence was used with slice thickness= 1mm; TR=6.8 ms; TE=3.1 ms; matrix = 256 x 256 mm<sup>2</sup>; in plane voxel size 1 x 1mm<sup>2</sup>
- (ii) Axial PD/T2 images using a 2D turbo spin echo sequence (TSE) with 3mm slice thickness, and the following acquisition parameters: TR=3500 ms; TE1/TE2=19/85 ms; matrix 240 x 240 mm<sup>2</sup>; in plane voxel size = 1 x 1 mm<sup>2</sup>

**7.2.3 Image analysis**

### 7.2.3.1 Upper cervical cord lesion-load and cross-sectional area

An inclusion criterion for each scan was the absence of motion artefacts. Focal spinal cord lesions were defined as abnormal areas of decreased signal change, with a clearly visible hypo-intense abnormality suggestive of a demyelinating plaque that had clearly defined margins and could be demarcated from the surrounding tissue on 3D-PSIR images. Lesions were outlined using a semi-automated edge-finding tool in JIM 6.0 (Xinapse systems, <http://www.xinapse.com>) on the 3D-PSIR image (Figure 7.1). Poorly demarcated areas of equivocal decrease in signal intensity were not outlined. The area of individual SC lesions and calculated the upper cervical cord lesion load for each subject (as described in Chapter six). Reproducibility of cord lesion-load measurement was evaluated by re-analyzing ten MS subjects' scans after a period of one week. The mean upper cervical cord cross-sectional area was also recorded (Chapter five) and then the cord lesion load was expressed as a percentage of cord area.

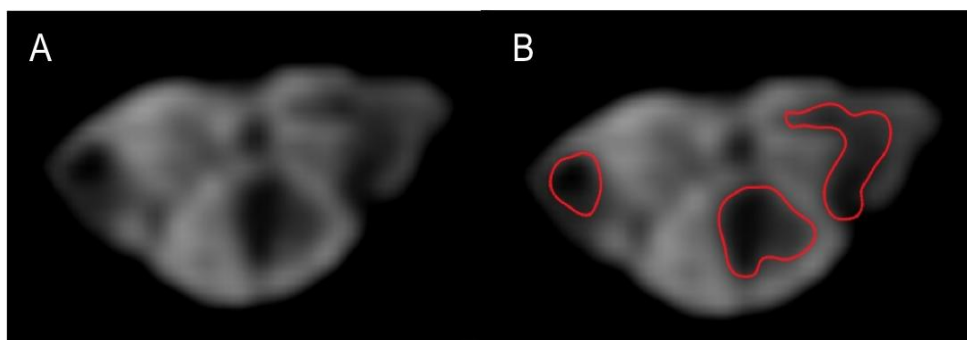


**Figure 7.1** 3D-Phase sensitive inversion recovery image (PSIR); 0.5 x 0.5 mm<sup>2</sup> in plane voxel size, centred at C2/C3 intervertebral disc acquired using 16-channel neurovascular coil. Image (A) demonstrating lesions seen as hypo-intense areas in both lateral columns and posterior column in the spinal cord of a patient with

SPMS (EDSS 6.5). The central canal can also be seen as a hypo-intensity above the central grey matter. Image (B) shows lesions circumscribed to calculate cervical cord lesion-load. The cord lesion load in this case was 12.59 mm<sup>2</sup> the ratio between cord lesion load/area was 18.62%.

### 7.2.3.2 MTR analysis

The central ten slices of the MT volume were extracted and then the MT-on and MT-off images were registered using the linear registration tool in FSL (<http://www.fmrib.ox.ac.uk/fsl/>). An MTR map was created in the MT-off space regions of interest (ROIs) were marked on the MT-off image to avoid bias. All focal lesions seen were marked using a semi-automated edge-finding tool. As the MT-off image was geometrically linked to the 3D-FFE during prescription, this enabled its use as a reference for marking lesions (Figure 7.2). The perimeter of the spinal cord on the MT-off image was outlined using the active surface model (Horsfield *et al.*, 2010) (Figure 7.3) to create a whole-cord mask. In the cases where focal lesions were identified, a lesion masks was created by applying the respective ROIs independently to the MTR mask. Both masks were converted to binary format using FSL and the lesion mask was then subtracted from the whole-cord mask, resulting in a mask of normal appearing spinal cord (NASC) tissue. Mean MTR values were obtained for: whole-cord, lesions and NASC. In healthy controls (i.e. without lesions) whole-cord measurements only were obtained.

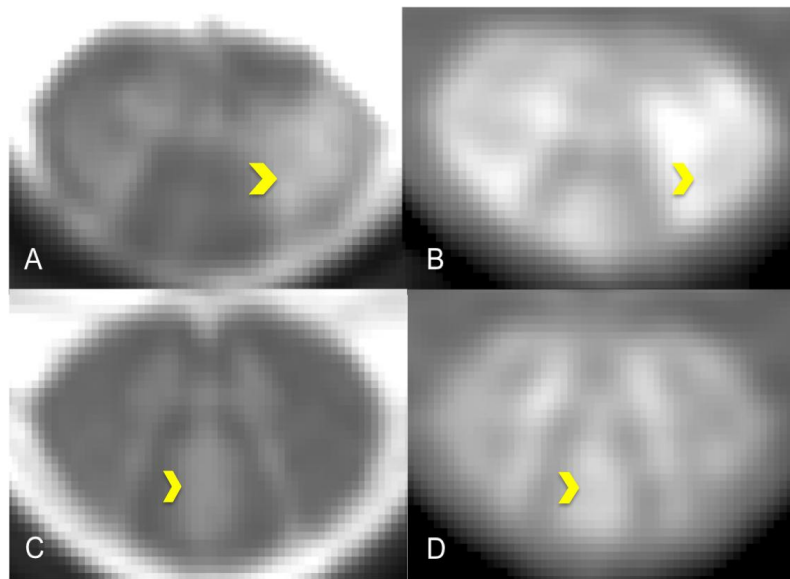


**Figure 7.2** Images (A) and (C) demonstrate representative images of the 3D-FFE sequence;  $0.5 \times 0.5 \text{ mm}^2$  in plane voxel size, centred at C2/C3 intervertebral disc acquired using 16-channel neurovascular coil. Images (B) and (D) demonstrate the corresponding MT-off images;  $0.5 \times 0.5 \text{ mm}^2$  in plane voxel size, centred at C2/C3 intervertebral disc acquired using 16-channel neurovascular coil. Images (A) and (B) demonstrate a focal lateral column lesion (indicated by yellow chevron) with extension into the dorsal horn of the grey matter. Images (C) and (D) show a posterior column lesion restricted to the white matter (indicated by yellow chevron).

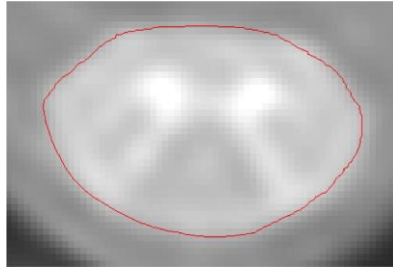


**Figure 7.3** MT-off images; 0.5 x 0.5 mm<sup>2</sup> in plane voxel size, centred at C2/C3 intervertebral disc acquired using 16-channel neurovascular coil demonstrating the cord outline region of interest acquired using the active surface model.

#### **7.2.3.3** *Brain image analysis*

Brain T2 lesion volume (T2LV) and brain parenchymal fraction (BPF) (the sum of white and grey matter relative to total intracranial volume) were measured as described in Chapter four.

#### **7.2.4** Statistical analysis

Reproducibility of cord lesion-load measurement was analyzed using the coefficient of variation (expressed as a percentage [COV]) and intra-class correlation coefficient (ICC) between the two measures.

To compare MRI variables, multiple linear regression was used on the whole sample (including controls except for lesion-MTR) with MRI as response variable and subject group indicators as predictors with the following potential

confounders as covariates: age, gender, BPF and cord area (except when cord area was the response variable being compared across groups).

P-values and confidence intervals for the multiple comparisons between groups were inflated, to account for the six between-group differences, using Šidák's method (Šidák 1967), though this is quite conservative since the comparisons are not all independent. The control versus MS group comparisons were adjusted for the covariates above and adjustment for two other covariates – disease duration and EDSS - is also reported for comparisons between MS subtypes.

There was no indication that regression residuals deviated materially from normality; some comparisons showed signs of heteroskedasticity, and in these cases the regression was repeated using robust Huber-White standard errors (Huber 1967), and this result is reported if materially different.

To identify independent predictors of disability, multiple regression models were constructed for the disability scores: all MRI and socio-demographic predictors (Tables 7.1 and 7.2) were entered, and manual stepwise backwards elimination removed singly predictors with highest P-value, until all model predictors were significant at  $P < 0.05$  (or borderline). Regression residuals did not materially deviate from normality but, as a precaution, for EDSS inference was confirmed using the bias-corrected and accelerated non-parametric bootstrap.

Analyses were implemented in Stata 13.1 (Stata Corporation, College Station, Texas, USA). All p-values are two-tailed and statistical significance is reported at  $P < 0.05$  (including any Šidák inflation).

### 7.3 Results

#### 7.3.1 *Subjects and MRI measures*

120 people were recruited: 28 controls, 34 RRMS, 29 SPMS and 29 PPMS patients. Lesions in the SC were visible in 80% (27/34) of cases with RRMS, 96% (28/29) with SPMS and 90% (26/29) in PPMS. Group demographics are summarised in Table 7.1.

	<b>Gender</b>	<b>Age (years)</b>	<b>Median EDSS (range)</b>	<b>Disease duration (years)</b>
Controls n=28	19 F, 9 M	41.43 ± 10.33		
RRMS n=34	22 F, 12 M	38.59 ± 9.82	2.5 (0 – 6)	6.53 ± 5.23
SPMS n=29	17 F, 12 M	51.34 ± 9.25	6.5 (4 – 8.5)	19.86 ± 11.74
PPMS n=29	12 F, 17M	50.66 ± 10.05	6.0 (2 – 7.5)	10.50 ± 7.66

**Table 7.1** Demographics of cohort studied presented as mean ± standard deviation.

#### 7.3.2 *Reproducibility analysis*

Cord lesion load measurement was found to be reproducible with a COV of 1.95% and ICC 0.995.

### 7.3.3 Comparison of MRI measures between MS and controls

	<b>Controls n=28</b>	<b>RRMS n=34</b>	<b>SPMS n=29</b>	<b>PPMS n=29</b>
Upper cervical cord lesion-load (mm <sup>2</sup> )		8.10 (9.26)	16.68 (7.41)	13.2 (10.85)
Upper cervical cord cross-sectional area (mm <sup>2</sup> )	79.59 (8.24)	76.79 (7.50)	63.64 (9.66)	69.33 (9.54)
% Spinal cord area covered by lesions		11.1 (12.1)	28.4 (14.5)	19.3 (15.9)
Whole cord MTR	49.70 (1.04)	47.75 (2.29)	45.49 (2.53)	46.48 (2.89)
Normal appearing spinal cord MTR	49.70 (1.04)	48.31 (2.06)	46.56 (2.49)	47.51 (2.51)
Spinal cord lesion MTR		43.37 (3.49)	40.54 (2.04)	41.26 (2.28)
Brain parenchymal fraction (BPF)	0.823 (0.015)	0.811 (0.018)	0.788 (0.022)	0.799 (0.014)
Brain T2 lesion volume (mLs)		13.00 (13.51)	23.34 (16.71)	16.57 (19.72)

**Table 7.2** Mean (standard deviation) of MRI parameters analyzed in controls and each subtype of MS

In keeping with the first hypothesis being tested, spinal cord lesion-load was significantly higher in progressive MS compared to RRMS. Mean differences: SPMS vs. RRMS 8.06mm<sup>2</sup>, P=0.008 (95% CI 1.69, 14.44) and PPMS vs. RRMS:

6.38mm<sup>2</sup>, P=0.021 (95% CI 0.74, 12.02). However, the difference between PPMS and SPMS was not significant: 1.69mm<sup>2</sup>, P=0.817 (95% CI -3.53, 6.80).

When the regression was repeated accounting for some heteroscedasticity of residuals, the SPMS vs. RRMS comparison remained significant (P=0.005) but the PPMS vs. RRMS comparison lost significance (P=0.09). When Including EDSS as a covariate, these differences were greatly reduced and non-significant: SPMS vs. RRMS: 11.56mm<sup>2</sup>, P=0.980 and PPMS vs. RRMS: 4.73 mm<sup>2</sup>, P=0.997.

As anticipated, both SPMS and PPMS groups had significantly lower cord areas compared to controls: mean adjusted differences were SPMS vs. controls: -15.08mm<sup>2</sup>, P<0.001 (95% CI -22.83, -7.33), PPMS vs. controls: -10.45mm<sup>2</sup>, P=0.001 (95% CI -17.40, -3.50). No differences in cord area were seen between RRMS and controls -2.40mm<sup>2</sup>, P=0.893 (95% CI -8.71, 3.91).

Significantly smaller cord areas were recorded in SPMS vs. RRMS (-12.68mm<sup>2</sup>, P<0.001, 95% CI -19.65, -5.71) and PPMS vs. RRMS (-8.05mm<sup>2</sup>, P=0.009, -14.65, -1.46). However, no significant difference in cord area was seen between the two progressive cohorts: (-4.63mm<sup>2</sup>, P=0.302, 95% CI -11.10, 1.85).

Both progressive MS subtypes had significantly lower whole-cord-MTR than controls. Mean adjusted differences were SPMS vs. controls: -2.46, P=0.011(95% CI -4.52, -0.40), PPMS vs. controls: -2.32, P=0.004 (95% CI -4.10, -0.55), RRMS vs. controls -1.09, P=0.288 (95% CI -2.61, 0.42). However, there were no significant adjusted differences in whole-cord-MTR between the MS groups. There were no significant adjusted differences in NASC-MTR between MS subgroups and

controls and between MS subgroups. There were no significant differences in lesion MTR between MS subgroups.

#### ***7.3.4 Associations between MRI measures and disability***

In line with the second hypothesis EDSS was independently associated with cord lesion-load ( $P < 0.001$ ), along with cord area ( $P = 0.003$ ), age ( $P < 0.001$ ) and gender ( $P = 0.001$ ,  $R^2 = 0.58$  for this model).

Cord lesion-load increase by  $1\text{mm}^2$  predicts an increase in EDSS by 0.008 (95% CI 0.004, 0.012), which translates to a predicted EDSS increase of 0.37 SDs per 1 SD increase in lesion-load. A decrease of  $1\text{mm}^2$  in cord area predicts an increase in EDSS by 0.05 (95% CI 0.02, 0.09), translating to a 0.27 SD EDSS increase per SD decrease in cord area.

Further support for our hypothesis that cord lesion-load would be associated with disability, was seen in the independent association with the 9-HPT ( $P = 0.003$ ) in addition to cord area ( $P = 0.034$ ), BPF ( $P = 0.007$ ) and, with borderline significance, gender ( $P = 0.085$ ) ( $R^2 = 0.42$ ).

A  $1\text{mm}^2$  increase in lesion-load predicts a 9-HPT z-score decrease by 0.003 SD (95% CI 0.001, 0.005). A  $1\text{mm}^2$  smaller cord area predicts a z-score decrease by 0.02 SD (95% CI 0.002, 0.04) and a 0.1 increase in BPF predicts a higher z-score by 1.33 SD (95% CI 0.37, 2.29).

Independent associations with the TWT were seen with: cord area ( $P < 0.001$ ), disease duration ( $P < 0.001$ ) and gender ( $P = 0.007$ ), ( $R^2 = 0.38$ ). A  $1\text{mm}^2$  higher cord area predicts 0.035 SD (95% CI 0.02, 0.05) higher walk speed.

As expected none of the spinal cord MRI measures were associated with PASAT. However, brain T2LV ( $P=0.035$ ) and, with borderline significance, BPF ( $P=0.05$ ) were associated with PASAT ( $R^2=0.14$ ).

### ***7.3.5 Associations with disability in MS patients with EDSS $\leq 6$***

To determine if the independent associations seen in this study maintained significance in populations with lower levels of physical disability - such as those commonly seen in clinical trials in RRMS - the analysis was repeated in this subset of the study population.

The independent associations between spinal cord lesion-load and age coefficients with EDSS were not materially altered and retained significance ( $P=0.001$  and  $P<0.001$  respectively), while gender also remained significant at  $P=0.02$ . However, the association with cord area lost significance, ( $P=0.868$ , cord area coefficient over 90% smaller).

The association between cord lesion load and 9-HPT also remained significant at  $P=0.01$ . In contrast, the cord area coefficient lost significance ( $P=0.876$ ) and BPF maintains borderline significance ( $P=0.048$ ).

The associations between cord area ( $P=0.632$ ), gender ( $P=0.116$ ) and TWT also lost significance and the coefficients are reduced, though disease duration remains significant at  $P=0.014$ .

No significant associations with the PASAT test were seen in patients with an EDSS  $\leq 6$ .

## 7.4 Discussion

The main study finding is that a quantitative measure of upper cervical cord lesion-load – measured from axial, high-resolution images - is significantly greater in progressive forms of MS than in RRMS and is associated with physical disability in MS, independent of an effect of cord atrophy.

### 7.4.1 Association of cord lesion-load with progressive MS and disability

In this present study cord lesion-load was calculated, for the first time, by circumscribing individual lesions on axial scans and measuring their mean area across all axial slices in mm<sup>2</sup>, in an effort to replicate the methodology in *post mortem* studies (Evangelou et al., 2005; DeLuca et al., 2006). The cord lesion-load was significantly higher in progressive than RRMS in spite of the smaller cord area in the progressive groups. Indeed, the proportion of the transverse section of the upper cervical cord involved by lesions was about 30% in SPMS and 20% in PPMS whereas it was around only 10% in RRMS.

The associations of physical disability with cord lesion-load (EDSS and 9-HPT) were independent of the associations observed with cord atrophy. Only one previous study of MS, with axial cord imaging has investigated lesion counts and atrophy qualitatively (Weier et al., 2012). However, in this present study, lesion area was quantified electronically (in mm<sup>2</sup>) with higher in-plane resolution (0.5 x 0.5 mm<sup>2</sup> vs. 1.1 x 0.5 mm<sup>2</sup> voxel size) and acquired at higher field strength (3T vs. 1.5T) than in the previous study. The PSIR sequence was chosen for lesion-load measurement, as it has previously been shown to improve both lesion localization, and boundary definition with normal appearing spinal cord tissue

(Poonawalla et al., 2008). A combination of these factors should have led to more sensitive and accurate quantitation of lesion-load, and thereby facilitated detection of a robust independent association with disability.

Although the cord lesion-load and area differences between progressive and RRMS lost significance when including EDSS as a covariate, this is likely to reflect the strong association between these MRI measures and EDSS. Therefore, people with the same EDSS score will tend to have very similar lesion-load irrespective of the MS subtype. However, in the analysis of MS patients with an EDSS  $\leq 6$ , the association between cord lesion-load and disability is maintained. In contrast, the association between cord atrophy and disability loses significance. These results, combined with its reproducibility, support the use of cord lesion-load as a potential endpoint for clinical trials involving MS subjects with an EDSS  $\leq 6$ , which is the case in virtually all trials in RRMS.

Previous regression analyses have investigated the contributions of brain MRI measures of lesion-load and/or atrophy along with cord atrophy to EDSS, and have identified independent associations with both (Chapter four, Bonati et al., 2011). Our present regression analyses have identified independent contributions to EDSS variability by cord measures alone, and this probably reflects the sensitive measures of cord pathology used, especially cord lesion-load. Our study emphasizes the predominant role of cord pathology in causing locomotor disability and thereby contributing to higher EDSS scores seen in progressive MS.

#### 7.4.2 Associations between other MRI measures and disability

In confirmation of previous studies, this present study has also shown that both progressive cohorts had more marked cord atrophy than RRMS and that cord atrophy was also associated with physical disability (Losseff et al., 1996; Horsfield et al., 2010; Rocca et al., 2011; Furby et al., 2010). The greater extent of atrophy is consistent with more severe axonal loss in the cord in both progressive MS groups compared with RRMS (Ganter et al., 1999; Lovas et al., 2000), thereby resulting in locomotor-disability. Given the limited region of cord investigated, it is also possible that atrophy is contributed to by Wallerian degeneration from distant lesions.

Although abnormalities in the whole-cord MTR were evident in progressive MS groups, the measure was not independently associated with disability. The MT ratio may reflect demyelination and/or inflammation in the spinal cord (Dousset et al., 1992). However, it is thought that axonal loss, rather than demyelination, represents the pathological substrate for disability in the spinal cord (Ganter et al., 1999; Lovas et al., 2000; Tallantyre et al., 2010). The lack of evidence of abnormal whole cord MTR in RRMS may reflect limited sensitivity to detect effects of Wallerian degeneration.

Brain atrophy (BPF) had a significant and independent association with the 9-HPT. The association between brain atrophy and 9-HPT might reflect cerebellar pathology resulting in impaired co-ordination. The lack of an association between the spinal cord MRI parameters used and PASAT test emphasizes their specificity, as cord measures were exclusively associated with physical disability.

#### 7.4.3 Association of demographic features with disability

Not surprisingly older age and longer disease duration were more likely associated with higher disability and progressive MS (Confavreux and Vukusic 2006; Leray *et al.*, 2010; Scalfari *et al.*, 2014). Male gender also associated with higher disability and there was a higher male-female ratio in PPMS versus other MS subtypes, consistent with previous studies (Thompson *et al.*, 1997; McDonnell *et al.*, 1998; Kremenchutzky *et al.*, 2006).

#### 7.4.4 Spinal cord MRI findings in primary and secondary progressive MS

Both spinal cord atrophy and lesion-load measurements did not significantly differ between SPMS and PPMS. These results are coherent with the similar levels of disability recorded in both subtypes. As cord atrophy and lesion-load are independently associated with disability, it is plausible that they each contribute to disability in both progressive MS groups.

No difference was found in lesion-MTR when comparing the progressive and RRMS groups. However, MTR is sensitive to demyelination *per se* (Dousset *et al.*, 1992; Bot *et al.*, 2004; Schmierer *et al.*, 2004; Chen *et al.*, 2013) and it is conceivable that a reduction in lesion-MTR reflects an effect of demyelination alone, while not excluding a difference in axonal density. More specific *in vivo* assessment of axonal density within lesions may be possible using measures based on diffusion tensor (Xu *et al.*, 2013) and/or diffusion-weighted (Zhang *et al.*, 2012) imaging sequences, and analysis of lesions in PPMS and SPMS using such techniques would be of interest in a future study.

#### **7.4.5 Study limitations**

The study has several limitations. First, the imaging acquisitions were confined to the upper cervical cord, in order to minimize physiological motion and enable high resolution multi-sequence imaging within an acceptable time frame. Although lesions in the upper cervical cord are common in MS (Fog 1950; Oppenheimer 1978) further studies should investigate cord lesions at other levels and their relationship to clinical function.

Secondly, although cord lesion load and atrophy were independently associated with disability, the variability in these imaging measures (and additional clinical parameters) only explained about a half of the variability in disability measures. Probably multiple factors impact on the strength of such associations, including limitations in coverage of the spinal cord, and the pathophysiological specificity of the imaging metrics themselves.

Thirdly, although the sample size was sufficient to investigate our *a priori* hypotheses that cord lesion load is greater in progressive MS groups than in RRMS and is associated with disability, it may not have been sufficient to detect a smaller difference in lesion load between the PPMS and SPMS groups. A study comparing quantitative spinal cord MRI measures in larger cohorts with PPMS and SPMS would be of interest.

#### **7.4.6 Conclusion**

The results presented in this chapter show that both cord lesion-load and atrophy are independently associated with physical disability in MS.

Longitudinal studies are required to understand the evolution of cord lesion-load in MS, and to consider its potential as an outcome measure in clinical trials.

## **Chapter 8 - Investigation of magnetisation transfer ratio-derived pial and subpial abnormalities in the multiple sclerosis spinal cord**

### **8.1 Introduction**

Although the exact causative mechanisms of multiple sclerosis are unclear, it has been suggested from the findings in neuropathological studies that meningeal inflammation may play a role in the development of earlier disability in progressive forms of the disease (Magliozzi *et al.*, 2007; Howell *et al.*, 2011; Choi *et al.*, 2012). It has also been reported that B cell follicles (as well as T cells) are present in the meninges of post-mortem brain specimens (Serafini *et al.*, 2004; Lovato *et al.*, 2011). However, Frischer *et al.* (2009) reported that B cells may only be found in the progressive forms of the disease. Neuropathology studies have also suggested that cortical demyelination may be a characteristic finding in multiple sclerosis (Dawson 1916; Brownwell and Hughes 1962). Another *post-mortem* study has suggested that cortical demyelination is more commonly found in progressive multiple sclerosis and inflammation is more diffuse, when compared directly to the relapsing-remitting form of the disease (Kutzelnigg *et al.*, 2005).

Taking in to account the above observations, an hypothesis has arisen that the pathological processes of meningeal inflammation and cortical demyelination may be interconnected and in turn play a role in the development of a progressive disease course. A paper by Magliozzi *et al.* (2010) has demonstrated the co-localisation of areas of meningeal inflammation (composed of B cells and

dendritic cells) and cortical demyelination. Furthermore, extensive subpial demyelination has been recorded in the cortex in multiple sclerosis (Bø *et al.*, 2003; Bö *et al.*, 2007). It has been proposed that cortical demyelination (especially subpial) may occur in the presence of meningeal inflammation due to the release of inflammatory cytokines in the subarachnoid space (Brown *et al.*, 2007; Ransohoff 2009). In progressive forms of multiple sclerosis, where there appears to be long standing inflammation, this may create a milieu, which favours further retention of inflammatory cells (Krumbholz *et al.*, 2005; Meinl *et al.*, 2008). This retention of inflammatory cells in multiple sclerosis may result in the activation of microglia and subsequently demyelination (Magliozzi *et al.*, 2010).

It has been reported that in relapsing-remitting multiple sclerosis meningeal inflammation may be present, with inflammation involving T cells rather than B cells (Frischer *et al.*, 2009). As neuropathology studies are predominantly composed of cases of progressive multiple sclerosis, an important insight was gained into the process of meningeal inflammation in a study examining biopsies of patients with early relapsing-remitting multiple sclerosis or a clinically isolated syndrome (Lucchinetti *et al.*, 2011). In this paper it was found that subpial cortical demyelination may be associated with meningeal inflammation.

Imaging studies have also provided a means of studying patients when they present with a clinically isolated syndrome suggestive of multiple sclerosis, which is the earliest clinical manifestation of the condition in most cases. The use of a double inversion recovery sequence has demonstrated the presence of

cortical lesions in clinically isolated syndrome patients (Calabrese *et al.*, 2007). Furthermore, a decrease in magnetisation transfer ratio (MTR) of the cortex, which might reflect demyelination (Chen *et al.*, 2013), - has also been observed in clinically isolated syndrome subjects (Audoin *et al.*, 2005; Fernando *et al.*, 2005). These imaging observations also suggest that cortical demyelination occurs early in the disease course.

The meninges of the spinal cord have also been reported to be inflamed in multiple sclerosis (Androdias *et al.*, 2010; DeLuca *et al.*, 2013), with the inflammatory cells predominantly composed of T cells in one study (Androdias *et al.*, 2010). Meningeal inflammation in the spinal cord has been related to axonal loss (Androdias *et al.*, 2010; DeLuca *et al.*, 2013). As axonal loss has been hypothesised to be the pathological substrate for disability (Ganter *et al.*, 1999; Evangelou *et al.*, 2000; Lovas *et al.*, 2000; Schirmer *et al.*, 2011), and because much of the physical disability from multiple sclerosis arises from spinal cord involvement, a greater understanding of meningeal abnormalities in the spinal cord, and their relationship to disease course, would seem to be relevant.

However, to date the effect of multiple sclerosis on the spinal cord meninges has not been investigated *in vivo*, due to image resolution constraints and other technical challenges associated with magnetic resonance imaging (MRI) protocol optimisation in the spinal cord (Dietrich *et al.*, 2008; Stroman *et al.*, 2013). Magnetisation transfer ratio (MTR) imaging in the spinal cord has been employed for some time (Mezzapesa *et al.*, 2004; Charil *et al.*, 2006). The MTR of a tissue is related to its macromolecular structure and an important contribution

in central nervous system tissue comes from myelin (Dousset *et al.*, 1992). Recent MTR imaging studies in the spinal cord have provided insights into the mechanisms of disability in multiple sclerosis (Zackowski *et al.*, 2009; Oh *et al.*, 2013). With the implementation of higher resolution structural and MTR acquisitions in the spinal cord than those previously acquired (Yiannakas *et al.*, 2012), the potential to investigate the effects of multiple sclerosis on the outer region of the spinal cord, that would be expected to include the pia mater of the meninges, could provide further insights into the pathophysiology of multiple sclerosis.

The aims of this chapter are threefold:

1. To characterise the outermost region of the spinal cord which is expected to include contributions from the pia mater and subpial region of the spinal cord, using high in-plane resolution, magnetisation transfer-weighted images to measure MT ratio (MTR) in healthy controls and in people with multiple sclerosis or a clinically isolated syndrome.
2. To compare the outer spinal cord MTR measures of people with a clinically isolated syndrome or multiple sclerosis with those of healthy controls
3. To compare outer spinal cord MTR findings seen in different clinical subgroups – clinically isolated syndrome, relapsing remitting, primary and secondary progressive multiple sclerosis – and explore the relationship of outer cord MTR with measures of both spinal cord atrophy and physical disability.

## 8.2 Methods

### 8.2.1 *Subjects*

People with no prior neurological diseases (n = 26) and those with either clinically isolated syndrome (n = 22) or multiple sclerosis: relapsing remitting (n = 29), secondary progressive (n = 28) and primary progressive (n = 28), were recruited. Multiple sclerosis (MS) was diagnosed using the 2010 McDonald criteria (Polman *et al.*, 2011). The clinically isolated syndrome (CIS) cohort was recruited following a single clinical episode consistent with demyelination and at least one lesion on a T2-weighted axial brain scan. The MS subgroups were classified using the Lublin-Reingold criteria (Lublin and Reingold 1996). Informed written consent was obtained from each participant prior to inclusion in the study.

All people with CIS or MS had expanded disability status scale (EDSS [Kurtzke 1983]) determined as well as multiple sclerosis functional composite (MSFC) (Fischer *et al.*, 1999). Subsequently Z-scores were calculated from normative values displayed in the National Multiple Sclerosis Society Task Force Database (Fischer *et al.*, 1999) for the 25-foot timed walk test (TWT), 9-hole peg test (HPT) and 3 s paced auditory serial addition test B (PASAT). American Spinal Injury Association (ASIA) motor (m) and sensory (s) scores (Maynard *et al.*, 1997) were also recorded for all people with MS and CIS. Assessment of physical function was performed immediately before the magnetic resonance imaging (MRI).

None of the subjects had experienced a relapse or received a course of corticosteroids within a month prior to imaging.

### **8.2.2 *MRI protocol***

Subjects were scanned at 3T using a Philips Achieva MRI system with radiofrequency (rf) multi-transmit technology (Philips Healthcare, Best, the Netherlands). A 16-channel receive-only neurovascular coil was used for spinal cord scanning and brain scanning was performed using the product 32-channel receive-only coil. A polystyrene filled vacuum fixation bag was placed behind the neck of all participants to provide a head rest and neck restraint and to minimise motion artefacts. The following sequences were acquired:

(iv) 3D fat-suppressed fast field echo (3D-FFE) was acquired in the axial plane containing 10 contiguous slices, FOV 240x180mm<sup>2</sup>, TR 23ms, TE 5ms, flip angle  $\alpha=7^\circ$ , and number of averaged signals=8

(v) MTR data were obtained by acquiring a 3D slab selective spoiled gradient echo sequence with two echoes using TR = 36ms, TE1/TE2 = 3.5/5.9ms, flip angle ( $\alpha$ )=9°, with and without Sinc-Gaussian shaped MT saturating pulses of nominal  $\alpha=360^\circ$ , offset frequency 1kHz, duration 16ms applied prior to the excitation pulse. Twenty-two 5mm slices were acquired in an axial orientation, with FOV = 180 x 240 mm<sup>2</sup> and acquisition matrix = 240 x 320 (voxel size 0.75 x 0.75mm<sup>2</sup>,

reconstructed to  $0.5 \times 0.5 \text{mm}^2$ ), with SENSE factor 2 in the foot/head direction, and 2 signal averages (NEX).

- (vi) 3D-phase sensitive inversion recovery (PSIR): voxel size of  $0.5 \times 0.5 \times 3 \text{mm}^3$ , TR = 8 ms; TE = 3.7 ms; flip angle  $\alpha = 5^\circ$ ; FOV =  $256 \times 256 \text{mm}$ ; NEX = 1
  
- (vii) Axial PD/T2 images using a 2D turbo spin echo sequence (TSE) with 3mm slice thickness, and the following acquisition parameters: TR=3500 ms; TE1/TE2=19/85 ms; matrix  $240 \times 240 \text{mm}^2$ ; in plane voxel size=  $1 \times 1 \text{mm}^2$
  
- (viii) 3D magnetisation-prepared turbo field echo (3D-TFE) sequence was used with slice thickness= 1mm; TR=6.8 ms; TE=3.1 ms; matrix =  $256 \times 256 \text{mm}^2$ ; in plane voxel size  $1 \times 1 \text{mm}^2$

### 8.2.3 *Image Analysis*

#### 8.2.3.1 *MTR values*

An inclusion criterion for all MRI images was the absence of motion artefacts. Using JIM 6.0 (Xinapse systems, <http://www.xinapse.com>) the central 10 slices of the MTR volume were extracted and the MT-off and MT-on images were registered independently to the volumetric 3D-FFE using linear registration in FSL (<http://www.fmrib.ox.ac.uk/fsl/>). Subsequently an MTR-map was created in the 3D-FFE space (Figure 8.1) (Yiannakas *et al.*, 2012). All MTR-maps were reviewed to confirm that no artefacts were introduced during the registration step.

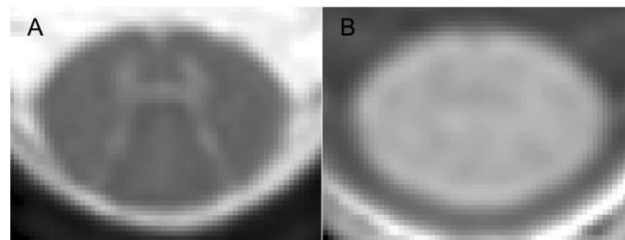


**Figure 8.1** (A) Axial 3D-FFE image (voxel size  $0.5 \times 0.5 \times 5\text{mm}^3$ ) through the C2/C3 intervertebral disc (B) Following independent linear registration of the MT-on and MT-off to the FFE the MTR-map is created in this space (voxel size  $0.5 \times 0.5 \times 5\text{mm}^3$ )

Three slices centred at the C2/C3 intervertebral disc were extracted from the volumetric 3D-FFE image and then created two regions of interest (ROIs): (i) spinal cord outline using an active surface model (Horsfield *et al.* 2010) (ii)

spinal cord GM using a semi-automated fuzzy connector method (Udupa and Samarasekera 1996) (Figure 8.2). Using these two ROIs a mask of the cord outline and GM were created from the MTR-map and then converted to binary format using FSL tools (<http://www.fmrib.ox.ac.uk/fsl/>). This process enabled the subtraction of the binary GM mask from the binary cord outline resulting in two masks: (i) spinal cord WM MTR-mask and (ii) spinal cord GM MTR-mask. The mean value of the spinal cord GM MTR-mask was recorded for each participant.

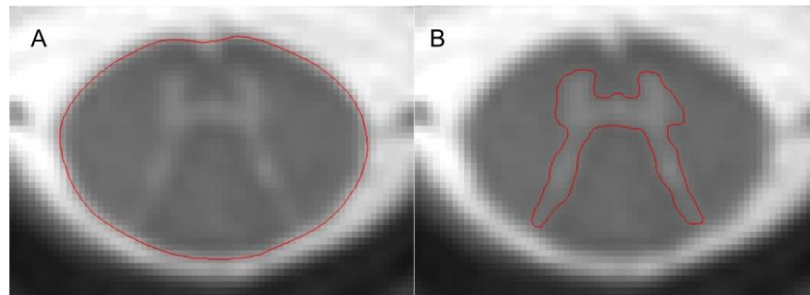


**Figure 8.2** (A) Axial 3D-FFE image (voxel size  $0.5 \times 0.5 \times 5\text{mm}^3$ ) demonstrating the spinal cord outline created using the active surface model (B) Axial 3D-FFE (voxel size  $0.5 \times 0.5 \times 5\text{mm}^3$ ) demonstrating grey matter region of interest outlined using the fuzzy connector.

The WM MTR-mask was then further analysed by eroding the image using iterations based on 4-connected neighbours written in Matlab 2012a (the Mathworks, Natick USA). The outermost row of pixel of the image was discarded to avoid contamination by cerebrospinal fluid (CSF). As the image was acquired at  $0.75 \times 0.75 \text{mm}^2$  voxel size and subsequently reconstructed to  $0.5 \times 0.5 \text{mm}^2$ , the next voxel layer was also considered to be also

contaminated by CSF due to the voxels' interpolation and consequently this voxel was also discarded. Therefore, the next voxel layer was designated as being the outermost voxel layer of the spinal cord and the mean MTR values of the voxels in this layer were recorded across the three selected slices for each subject. The classification of peripheral voxels in the image is illustrated in Figure 8.3 and on MRI in Figure 8.4; this layer was considered likely to include both pia mater and subpial spinal cord tissue. Following removal of the three outermost voxels the mean value from the spinal cord WM-MTR mask was recorded for each subject and this was designated as the WM-MTR value. Finally, the mean GM MTR value was recorded across the three slices.

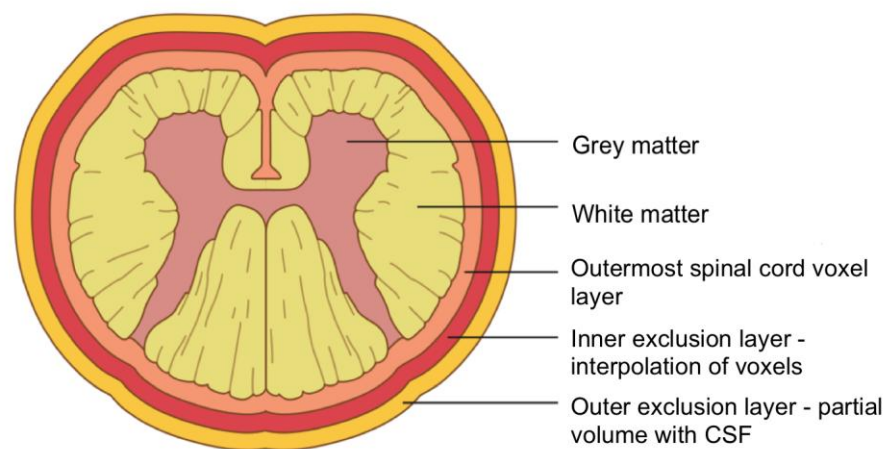


**Figure 8.3** Graphical representation of voxel layers analysed in the outermost region of the spinal cord.

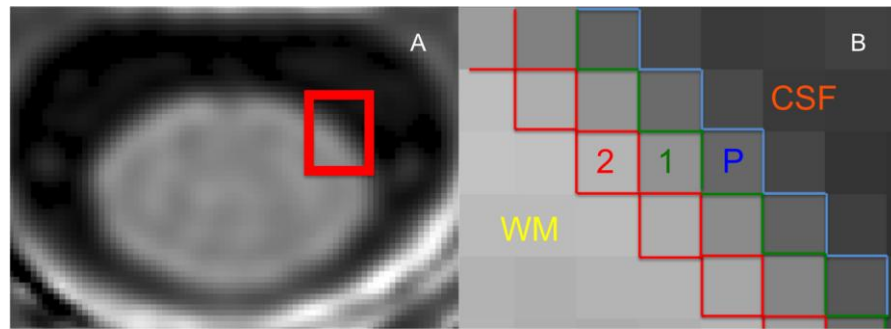


**Figure 8.4** (A) MTR-map (voxel size  $0.5 \times 0.5 \times 5\text{mm}^3$ ) demonstrating a square shaped region of interest from which (B) was obtained in the periphery of the spinal cord (B) Zoomed image of the periphery of the spinal cord demonstrating from right to left: Cerebrospinal fluid (CSF), (P) Outer exclusion voxel layer - partial volume with CSF (1) inner exclusion layer - interpolation of voxels (2) Outermost spinal cord voxel layer, (WM) spinal cord white matter

### 8.2.3.2 Spinal cord area

Spinal cord mean cross-sectional area was measured from the 3D-PSIR image using the active surface model (Horsfield *et al.* 2010). In order to do this five 3mm thick slices centred at C2/C3 were extracted and then the area of each of the five slices was recorded (c.f. Chapter Five). Spinal cord area was normalised by the number of slices used i.e. the mean area of the five slices for each participant was calculated. This method of normalisation was chosen as a previously published report has demonstrated that normalisation of spinal cord volume by slice number is superior to the use of brain volume or other measures of body habitus (Healy *et al.*, 2012). The spinal cord measurements are presented as area normalised by slice number rather than as volume, as cord area is more commonly reported in clinical trials of

multiple sclerosis (Kalkers *et al.*, 2002; Leary *et al.*, 2003; Lin *et al.*, 2003; Montalban *et al.*, 2009).

#### **8.2.3.3 *Brain scan analysis***

The brain parenchymal fraction (BPF) was then recorded for each subject using the methodology described in chapter four. The volume of T2-weighted lesions (T2LV) was also recorded for each subject in mLs (chapter four).

#### **8.2.4 Statistical Analysis**

SPSS 21 (IBM) was used for statistical analysis.

#### *Comparisons of MRI measures in controls and patient subgroups*

In healthy controls the differences in mean MTR values were evaluated between (i) Outer spinal cord and spinal cord white matter (ii) Outer spinal cord and spinal cord grey matter (iii) spinal cord white matter with grey matter, using a paired samples t-test. Subsequently the same tests were employed in clinically isolated syndrome patients and each subgroup of multiple sclerosis separately. Differences in cord area and brain parenchymal fraction were also tested between MS and CIS patients and controls using an independent samples t-test.

To explore the hypothesis that MTR abnormalities in each tissue component of the spinal cord (outer spinal cord, white matter and grey matter) may differ between clinically isolated syndrome or each subtype of MS patients and

controls, a linear regression model was constructed, with the case (i.e. multiple sclerosis subgroup, clinically isolated syndrome and control) set as the dependent variable and MTR added as an independent variable. To compare each patient group (clinically isolated syndrome or multiple sclerosis subgroups) with controls, or with each other, a separate regression model was constructed for each comparison of MTR values (outer spinal cord, white matter and grey matter) being performed. To investigate whether differences seen in MTR values between subject groups (dependent variable) were affected by cord atrophy in the multiple sclerosis subgroups, spinal cord area was included as an independent variable in every model and the comparison was corrected for age and gender by adding these as independent variables. Adjustments for multiple comparisons were not performed due to the exploratory nature of this study (Bender and Lange 2001).

#### *Relationship between cord MTR measures and cord area*

To investigate the relationship between spinal cord MTR and cord area univariate Pearson's correlation coefficients were calculated with the MTR of the grey matter, white matter and outer spinal cord versus cord area in all multiple sclerosis patients combined. In order to identify the components of the spinal cord MTR (i.e. outer spinal cord, grey and white matter) which were associated with atrophy, independently from the others and from age and gender, a multivariate linear regression model was constructed. In this model cord area was set as the dependent variable, and MTR values from each region of the spinal cord that had a significant univariate correlation with cord area were added as independent variables, in a forward stepwise manner, to determine those with

independent associations with cord area. Independent variables retained in the final model with a p-value of  $< 0.05$  were considered to be independently associated with cord area (dependent variable).

#### *Relationship between MRI and disability measures*

To explore the relationship of each MRI measure analysed (spinal cord area, spinal cord MTR [outer cord, white matter and grey matter], brain parenchymal fraction and brain lesion load) with disability, univariate correlations were calculated firstly between these variables, in all multiple sclerosis patients combined. We used Spearman's rank correlation coefficient for the EDSS, as this scale is logarithmic. For all other disability scales (multiple sclerosis functional composite Z-scores, ASIAs and ASIAm) univariate correlations were calculated with the MRI parameters using Pearson's correlation coefficient. For univariate associations,  $p < 0.01$  was considered significant.

In order to further investigate the relationship between the MRI parameters analysed and physical disability, independent associations between these two variables were sought. To achieve this, a multivariate linear regression model was constructed with the disability measure of interest set as the dependent variable. A separate model was constructed for each disability measure used i.e. multiple comparisons were not performed. To refine the choice of independent variables added to the model, only MRI parameters which had a significant univariate correlation with the dependent variable (i.e. the disability measure of interest), were included in the regression analysis. In each model constructed, age and gender were also added as independent variables, to correct for any

influence these may have on the association being tested. The MRI parameters were added to the model, as independent variables, in a forward stepwise manner and those variables retained in the final model, with a p-value of  $< 0.05$ , were deemed to be independently associated with the disability scale (dependent variable).

## 8.3 Results

### 8.3.1 *Subjects and their clinical and conventional MRI characteristics*

In total 133 subjects were studied; 26 healthy controls, 22 people with CIS, 29 relapsing remitting (RR) MS, 28 secondary progressive (SP) MS and 28 primary progressive (PP) MS. Characteristics of the group are shown in Table 8.1. In the CIS cohort there were 18 cases of unilateral optic neuritis, one multifocal CIS (consisting of optic neuritis, facial numbness and diplopia), one hemispheric presentation (unilateral hand weakness due to a lesion in the right motor cortex) and two cases of partial myelitis (one cervical and one thoracic).

With regard to the conventional MRI scans, in the CIS cohort 15 cases fulfilled criteria for dissemination in space (DIS) (Polman *et al.*, 2011); the criteria for dissemination in time could not be evaluated on this single scan as a gadolinium-contrast agent was not administered. Asymptomatic T2-weighted brain lesions were seen in 18/22 cases and in one case the symptomatic lesion was seen (in the motor cortex). There were eight spinal cord lesions seen on cord PSIR and FFE scans, seven asymptomatic and one due to cervical cord partial myelitis.

	Controls n=26	CIS n=22	RRMS n=29	SPMS n=28	PPMS n=28
Gender F:M	18:8	12:10	20:9	17:11	12:16
Age in years	40.6 ± 10.2	36.2 ± 9.3	38.1 ± 9.5	51.3 ± 9.4	50.5 ± 9.9
Mean disease duration (years for MS groups; (months for CIS group)		5.8 ± 4.3	6.1 ± 4.0	20.11 ± 11.89	10.9 ± 7.6
Median EDSS (range)		1 (0-3)	2.5 (0-7)	6.5 (4- 8.5)	6.0 (2-8)
Brain parenchymal fraction	0.824 ± 0.015	0.822 ± 0.013	0.811 ± 0.017 §	0.788 ± 0.022 §	0.798 ± 0.014 §
T2 lesion volume (mLs)		2.9 ± 3.8	13.1 ± 14.3	23.4 ± 17.0	16.4 ± 20.2
Spinal cord cross- sectional area (mm <sup>2</sup> )	80.3 ± 7.7	82.6 ± 7.3	78.1 ± 9.0	63.6 ± 9.8 §	68.1 ± 9.7 §

**Table 8.1** Demographics and conventional magnetic resonance imaging parameters in healthy controls, CIS and MS. Significant differences between MRI parameters from controls (i.e.  $p < 0.01$ ) are denoted by § symbol.

### **8.3.2 Comparison of cord area and brain volume between groups**

There was no significant difference in the cord area of healthy controls with either the CIS ( $p = 0.06$ ) or RRMS ( $p = 0.18$ ) groups. The SPMS ( $63.5 \text{ mm}^2 \pm 10.0$  vs.  $80.2 \text{ mm}^2 \pm 6.8$ ,  $p < 0.01$ ) and PPMS ( $68.1 \text{ mm}^2 \pm 9.7$ ,  $p < 0.01$ ) groups both had lower cord areas than healthy controls. Results for all groups are presented in Table 8.1.

No significant difference was seen in BPF in the CIS group compared to controls but significant differences in BPF were seen between controls and all subgroups of MS ( $p < 0.01$ ), with smaller BPFs in the MS subgroups.

### **8.3.3 Comparison of outer spinal cord and spinal cord WM MTR values within each subject group (Table 8.2)**

In each subject group, MTR of the outer spinal cord was higher than MTR of spinal cord WM: controls ( $51.35 \pm 1.29$  vs.  $49.87 \pm 1.45$ ,  $p < 0.01$ ), CIS ( $50.46 \pm 1.39$  vs.  $49.13 \pm 1.19$ ,  $p < 0.01$ ), RRMS ( $48.86 \pm 2.89$  vs.  $47.44 \pm 2.70$ ,  $p < 0.01$ ), SPMS ( $46.33 \pm 2.84$  vs.  $44.75 \pm 3.10$ ,  $p < 0.01$ ), PPMS ( $46.99 \pm 3.78$  vs.  $45.62 \pm 3.40$ ,  $p < 0.01$ ).

	Controls	CIS	CIS (excluding two cases of myelitis)	RRMS	SPMS	PPMS
Outer spinal cord MTR	51.35 ± 1.29	50.46 ± 1.39	49.9 ± 1.40	48.86 ± 2.89	46.33 ± 2.84	46.99 ± 3.78
Comparison between outer spinal cord and white matter MTR values	p < 0.01	p < 0.01	p < 0.01	p < 0.01	p < 0.01	p < 0.01
MTR spinal cord white matter	49.87 ± 1.45	49.13 ± 1.19	49.21 ± 1.31	47.44 ± 2.70	44.75 ± 3.10	45.62 ± 3.4
Comparison between spinal cord white and grey matter MTR values	p < 0.01	p < 0.01	p < 0.01	p < 0.01	p = 0.02	p < 0.01
MTR spinal cord grey matter	48.23 ± 1.76	47.72 ± 1.23	47.8 ± 1.30	46.6 ± 2.43	43.88 ± 2.62	44.88 ± 3.09

**Table 8.2** Mean MTR values ( $\pm$  standard deviation) of spinal cord region subtypes (outer cord, white matter, grey matter) in the control group and in each patient group. The CIS cohort is presented with and without the two cases of myelitis included.

#### **8.3.4 Comparison of spinal cord WM and GM MTR values within each subject group**

(Table 8.2)

In each subject groups, the spinal cord WM had higher MTR values than spinal cord GM.

#### **8.3.5 Outer spinal cord MTR in controls versus patient subgroups (Table 8.3)**

The outer spinal cord MTR values were higher in controls than all patient groups: controls vs. CIS (coefficient = -0.32,  $p = 0.03$ , 95% CI -0.22, -0.01), controls vs. RRMS (coefficient = -0.48,  $p < 0.01$ , 95% CI -0.28, 0.09), controls vs. SPMS (coefficient = -0.51,  $p < 0.01$ , 95% CI -0.31, -0.15), controls vs. PPMS (coefficient = -0.38,  $p < 0.01$ , 95% CI -0.36, -0.06). Cord area was not a significant covariate in any of the models used.

#### **8.3.6 Spinal cord WM and GM MTR in controls versus patient subgroups (Table**

8.3)

MTR of spinal cord WM was higher in controls than in all patient groups. MTR of spinal cord GM was not different between controls and the CIS group but was significantly higher in controls than in all three MS subgroups.

#### **8.3.7 Outer spinal cord MTR: comparison between patient subgroups (Table 8.3)**

Outer spinal cord MTR was lower in RRMS than CIS (coefficient = -0.28,  $p = 0.02$ , 95% CI -0.10, -0.01). Both SPMS (coefficient -0.24,  $p = 0.02$ , 95% CI -0.07, -0.01) and PPMS (coefficient = -0.29,  $p = 0.02$ , 95% CI -0.16, -0.01) had lower outer

spinal cord MTR values compared to RRMS. No significant difference was found between SPMS and PPMS.

MTR value	Groups being compared	SE	Coefficient	Significance (p value)	95% CI (lower, upper)
Outer spinal cord MTR	CIS/control	0.05	-0.32	0.03	-0.22, -0.01
	RRMS/control	0.05	-0.48	< 0.01	-0.28, -0.09
	SPMS/control	0.04	-0.51	< 0.01	-0.31, -0.15
	PPMS/control	0.07	-0.38	< 0.01	-0.36, -0.06
	CIS/RRMS	0.02	-0.28	0.02	-0.10, -0.01
	RRMS/SPMS	0.02	-0.24	0.02	-0.07, -0.01
	RRMS/PPMS	0.04	-0.29	0.02	-0.16, -0.01
	SPMS/PPMS	0.02	-0.02	0.89	-0.05, 0.04
	MTR WM	CIS/control	0.39	-0.34	0.03
RRMS/control		0.30	-0.56	<0.01	-1.95, -0.76
SPMS/control		0.23	-0.98	<0.01	-2.74, -1.80
PPMS/control		0.22	-0.80	<0.01	-1.79, -0.92
MTR GM	CIS/control	0.42	-0.17	0.26	-1.3, 0.37
	RRMS/control	0.29	-0.36	<0.01	-1.38, -0.21
	SPMS/control	0.20	-0.74	<0.01	-1.84, -1.05
	PPMS/control	0.19	-0.75	<0.01	-1.50, -0.73

**Table 8.3** Comparison of MTR values between patient and control groups using a linear regression model adjusted for age, gender and cord area (SE=standard error, CI=confidence interval)

### **8.3.8** *Univariate correlations and associations between MTR measures and cord area in all MS patients combined*

The following MRI parameters were correlated with cord area: Outer spinal cord MTR ( $r = 0.39$ ,  $p < 0.01$ ), MTR WM ( $r = 0.36$ ,  $p < 0.01$ ), MTR GM ( $r = 0.36$ ,  $p < 0.01$ ) and BPF ( $r = 0.27$ ,  $p = 0.01$ ). However, only outer spinal cord MTR (coefficient = 0.40,  $p < 0.01$ , 95% CI 0.63, 1.88) was found to be independently associated with cord area.

### **8.3.9** *Univariate correlations between MRI parameters and disability in all MS patients combined (Table 8. 4)*

Significant univariate correlations between MRI parameters and disability are presented in Table 8.4. Although significant correlations were seen between outer spinal cord MTR and each disability measure used (apart from PASAT z-score), stronger correlations were seen between cord area and disability measures reflecting motor function. Brain T2LV was not found to be correlated with any disability measures except for PASAT z-score

MRI parameter	Disability measure						
	EDSS*	ASIAm	ASIAs	Z-score PASAT	Z-score 9-HPT	Z-score 25ft TWT	Z-score MSFC
Outer MTR	<b>r = -0.41</b>	<b>r = 0.38</b>	<b>r = 0.30</b>	r = 0.03	<b>r = 0.41</b>	<b>r = 0.36</b>	<b>r = 0.42</b>
MTR WM	<b>r = -0.32</b>	r = 0.23	<b>r = 0.30</b>	r = 0.01	<b>r = 0.42</b>	<b>r = 0.40</b>	<b>r = 0.43</b>
MTR GM	<b>r = -0.34</b>	r = 0.27	<b>r = 0.29</b>	r = 0.05	<b>r = 0.38</b>	<b>r = 0.37</b>	<b>r = 0.40</b>
Cord area	<b>r = -0.60</b>	<b>r = 0.49</b>	<b>r = 0.39</b>	r = 0.14	<b>r = 0.48</b>	<b>r = 0.38</b>	<b>r = 0.44</b>
BPF	<b>r = -0.40</b>	r = 0.22	r = 0.06	<b>r = 0.35</b>	<b>r = 0.48</b>	<b>r = 0.29</b>	<b>r = 0.40</b>
T2LV	r = 0.19	r = -0.04	r = 0.17	<b>r = -0.36</b>	r = -0.29	r = -0.08	r = -0.29

**Table 8.4** Significant ( $p < 0.01$ ) univariate correlations between MRI parameters and disability measure in all MS patients combined are indicated in bold font (\*Spearman's coefficient used for EDSS and Pearson's coefficient for all other disability measures).

**8.3.10** *Independent associations between MRI parameters and disability in all MS patients combined (Table 8.5)*

Significant independent associations between MRI variables and disability measures are summarised in Table 8.5. The 9-HPT z-score was associated with MTR in the outer spinal cord. Tests of motor function (EDSS and ASIAm) were associated with cord area. The TWT z-score was associated with spinal cord WM MTR in MS. The PASAT z-score was associated with both brain T2 lesion volume and BPF.

Disability Measure	MRI parameter associated with disability	SE	Coefficient	Significance (p value)	95% CI (lower, upper)
EDSS	Cord area	0.02	-0.48	< 0.01	-0.13, -0.06
	BPF	9.45	-0.29	< 0.01	-48.78, -11.17
ASIAm	Cord area	0.13	0.42	<0.01	0.32, 0.85
ASIAs	Cord area	0.08	0.26	0.03	0.02, 0.34
Z-score PASAT	BPF	8.42	0.25	0.02	2.82, 36.32
	T2LV	0.01	-0.26	0.02	-0.04, -0.004
Z-score 9-HPT	Outer spinal cord MTR	0.04	0.27	< 0.01	0.04, 0.19
	BPF	0.41	0.41	<0.01	16.44, 14.99
Z-score 25 ft. TWT	MTR WM	0.15	0.36	<0.01	0.30, 0.89
Z-score MSFC	MTR WM	0.07	0.30	<0.01	0.07, 0.36
	Cord area	0.023	0.22	0.04	0.001, 0.09

**Table 8.5** Summary of MRI parameters significantly associated with disability measures from linear regression models using disability as dependent variable (SE=standard error, CI=confidence interval)

## 8.4 Discussion

There are a number of novel findings in this chapter. First, a quantitative imaging metric (MTR) was measured *in vivo* in the outer spinal cord – a region likely to include the pia mater and subpial spinal cord. Secondly, in healthy controls, outer cord MTR was higher than cord white matter MTR. Thirdly, there was a reduction in outer cord MTR at an early stage of MS, and in the absence of significant cord atrophy, as reflected by the findings in CIS and RRMS subgroups. Fourthly, outer cord MTR abnormality was significantly and independently correlated with cord atrophy and was also greater in progressive MS subgroups when compared with RRMS. Finally, there were several independent associations between spinal cord MRI metrics and disability measures. These findings are discussed in turn.

### *The outer spinal cord MTR measure and what it reflects anatomically*

MTR was quantified in a voxel layer in the expected location of the pia mater and subpial region of the spinal cord. As the spinal cord is surrounded by cerebrospinal fluid the outer voxels of the cord are susceptible to partial volume effects (Tench *et al.*, 2005). However, by excluding the most peripheral voxel layers this influence was likely to be negligible as the outer cord MTR values were actually higher than the remaining (deeper) spinal cord tissues, which will not be affected by cerebrospinal fluid.

The pia mater is composed of two layers in the spinal cord; the intima pia and epipial layer, of which the epipial layer (not present over the cerebral hemispheres) is the thicker of the two due to its composition of connective tissue (Millen and Woollam 1961). The combined thickness of these layers was 0.2mm in a post-mortem study of the thoracic spinal cord with an increase in higher segments of the cord (Reina *et al.*, 2004). The cord samples in this study were fixed with formaldehyde, and a reduction in tissue size of up to 19% can occur using a 10% formalin solution (Mouritzen Dam 1979). It therefore seems likely that a significant proportion of the outer cord voxel layer of the upper cervical cord region studied (which has an in-plane voxel size of 0.5mm) will contain pial meningeal tissue, although it is also likely to include subpial spinal cord white matter.

#### *Higher outer than white matter spinal cord MTR in healthy controls*

A question arising is why the MTR in the outer cord region should be higher than that of normally myelinated cord white matter. One possible explanation is that there is a tissue component other than myelin in the outer cord that has a relatively high MTR. In this regard, both the pial and subpial tissues in the spinal cord contain collagenous fibres (Reina *et al.*, 2004) and *in vitro* data obtained in phantoms has shown that higher MTR is correlated with higher collagen concentration (Laurent *et al.*, 2001). It seems therefore possible that collagen contributes to the higher outer cord MTR.

#### *Outer spinal cord MTR abnormalities in clinically isolated syndrome and relapsing remitting multiple sclerosis in the absence of cord atrophy*

The finding of reduced outer cord MTR without atrophy in the CIS and RRMS groups supports the robustness of the outer cord measure: had partial volume effects of cerebrospinal fluid the cause of decreasing outer cord MTR, an abnormality would not be seen when there was no difference in cord area between patient and control groups.

In the CIS cohort 15 fulfilled the criteria for dissemination in space and 18 of the 22 participants had at least one asymptomatic T2-weighted brain lesion evident on their brain MRI scan and are therefore at higher risk of conversion to MS (Fisniku *et al.*, 2008). Seven of this group had asymptomatic spinal cord lesions, the presence of which also increases the risk for conversion to MS (Sombekke *et al.*, 2013). The abnormalities detected in the outermost spinal cord in CIS compared to controls indicate that changes occur at a very early stage in relapse-onset MS.

The RRMS cohort was also at a relatively early stage of disease had little disability and no cord atrophy. Since cord atrophy is related to axonal loss in neuropathology studies (McGavern *et al.*, 2000; DeLuca *et al.*, 2004; Evangelou *et al.*, 2005), the decrease in MTR in the outer spinal cord seen at this stage of MS may be occurring in the absence of – and by implication preceding – significant axonal loss.

The pathological basis of the reduced outer cord MTR warrants further consideration. In an inflammatory animal model of MS (experimental allergic

encephalomyelitis) areas of oedema, signifying inflammation, exhibited a mildly decreased MTR in the absence of demyelination (Dousset *et al.*, 1992). A decrease in MTR also occurs with inflammation in spinal cord experimental allergic encephalomyelitis (Cook *et al.*, 2004). A *post-mortem* study in MS has demonstrated reduced MTR corresponding with an increased number of inflammatory T cells (Moll *et al.*, 2009). Other post mortem studies in MS also report a reduction in MTR in regions of demyelination in the cerebral cortex (Schmierer *et al.*, 2010; Chen *et al.*, 2013), brain white matter (Schmierer *et al.* 2004) and spinal cord (Bot *et al.*, 2004). As the outer spinal cord voxel layer in this study is likely to contain both the pia mater and subpial white matter tissue, a combination of inflammation in the former and demyelination in the latter may be responsible for the decrease seen in MS.

Although the limits of image resolution prevent a more specific interpretation of the MTR decrease that we saw in outer spinal cord region, it may nevertheless reflect a distinct pathogenic process in so far as co-localised subpial demyelination may occur secondary to meningeal inflammation. These pathological changes have been previously associated in brain biopsies of patients with early MS, where meningeal inflammation was found to have a 90% probability to be topographically associated with subpial demyelination (Lucchinetti *et al.*, 2011). Further pathological studies will be needed to determine whether such changes are topographically related in the spinal cord.

*Association of outer spinal cord MTR with cord atrophy and progressive multiple sclerosis*

In this study, outer spinal cord MTR was independently associated with cord atrophy. In a previous study of inflammation in the spinal cord meninges there was an association seen between meningeal inflammation and diffuse axonal loss in the spinal cord parenchyma (Androdias *et al.*, 2010). In a similar study by DeLuca *et al.* (2013) it was found that small peripheral axons are preferentially lost. In these studies inflammatory cells and mediators were demonstrated to be present in the cord meninges. Thus, in both of these pathology studies, meningeal inflammation and axonal loss were evident. It is likely that axonal loss, which can be profound in the MS spinal cord (Ganter *et al.*, 1999; Lovas *et al.*, 2000), is the major substrate of spinal cord atrophy. Thus, the link observed between outer cord MTR and cord atrophy would appear concordant with pathological association of meningeal inflammation and axonal loss in the cord. In contrast, the lack of independent association between the inner spinal cord (grey and white matter) MTR (implying demyelination) and atrophy (consistent with neuroaxonal loss) is consistent with a dissociation between these pathological processes, in line with previous pathological reports in the spinal cord (DeLuca *et al.*, 2006) and brain (Wegner *et al.*, 2006).

Although at present it is not known how meningeal inflammation might be associated with cord pathology, including axonal loss, a possible anatomical connection may be via the epi-pial layer of the spinal cord, which contains branches of blood vessels that penetrate the spinal cord (Millen and Woollam 1961). Furthermore, spinal cord lesions tend to occur around small veins (Oppenheimer *et al.*, 1978), and therefore the small epi-pial vessels could

potentially provide a route of entry for inflammatory cells from the meninges into the cord parenchyma.

The comparison of clinical subgroups showed that greater outer cord MTR abnormality in both primary and secondary MS groups compared with RRMS (Tables 8.2 & 8.3). In the comparison of the two progressive subtypes of MS no significant differences were found. These results suggest that the outer spinal cord (and by implication pial and/or subpial) abnormalities are greater in the progressive stage of MS.

The findings are consistent with previous neuropathology studies in the brain that have linked both meningeal inflammation and subpial demyelination with the progressive stage of multiple sclerosis (Magliozzi *et al.*, 2007). There can be extensive cortical subpial demyelination in progressive multiple sclerosis (Peterson *et al.*, 2001; Bö *et al.*, 2003; Kutzelnigg *et al.*, 2005; Vercellino *et al.*, 2005; Wenger *et al.* 2006). Although cortical subpial lesions are rarely visible on MRI (Geurts *et al.*, 2005), post mortem study has identified that regions of cortical demyelination have a reduced MTR (Chen *et al.* 2013), and a recent *in vivo* study reported a reduced MTR of the outer cortex in multiple sclerosis that was most marked in those with a secondary progressive course (Samson *et al.*, 2014). These observations support use of MTR to reflect subpial demyelination in the cortex and suggest that subpial demyelination could contribute to the lower MTR we observed in the outermost region of the spinal cord.

*Associations between spinal cord MRI metrics and disability measures*

Although outer spinal cord MTR had a univariate correlation with each disability measure used in this study, in a regression analysis it was found only to be associated with nine hole peg test z-score. This limited independent association with function may reflect the small region of spinal cord included in the outer voxel layer; the purpose in studying outer cord MTR was to investigate for abnormalities that reflect a process of pathogenic importance (i.e., meningeal and subpial pathology) and not for an association with disability.

Spinal cord white matter-MTR was independently associated with 25 foot timed walk test and multiple sclerosis functional composite z-scores; this relationship plausibly reflects pathology in functionally important motor and sensory pathways of the spinal cord. These results also confirm an earlier finding of a univariate correlation between spinal cord grey matter MTR and EDSS (Agosta *et al.*, 2007), although grey matter MTR was not independently associated with EDSS in the subsequent regression analysis. Amongst the several MRI metrics studied, the measure of spinal cord cross-sectional area (atrophy) had a generally stronger univariate correlation with each of the disability measures used. Furthermore, cord area was found to be independently associated with a number of measures of disability. The strong relationship between cord atrophy and disability may be due to this measure reflecting axonal loss, thought to be the pathological substrate for disability (Evangelou *et al.*, 2000; Lovas *et al.*, 2000; Schirmer *et al.*, 2011). A biologically coherent finding was that the PASAT z-score (a measure of cognition) was associated only with the two brain MRI

metrics (brain parenchymal fraction and T2 lesion volume) and with none of the spinal cord measures.

#### *Limitations and future directions*

Limitations should be noted when considering the findings in this chapter. Firstly, only the upper cervical spinal cord was studied. However, at this level, a robust registration technique could be employed and segmentation of the cord into grey matter and white matter regions was possible. Furthermore, spinal cord involvement by multiple sclerosis is most common in the cervical cord (Oppenheimer *et al.*, 1978), and this approach is likely to have yielded the most reliable results within the technical constraints of spinal cord MRI.

Secondly, this study was cross-sectional in nature and future longitudinal studies will be needed to elucidate outer cortical MTR changes over time and its relationship with evolution of disability and cord atrophy.

Thirdly, the in plane resolution of the axial images was constrained by time limitations necessitated in a clinical study. Future studies of the spinal cord at 7 Tesla field strength (Zhao *et al.*, 2013) may provide higher resolution images within an acceptable time frame.

Finally, this *in vivo* imaging study does not include MTR findings for histopathologically confirmed pia mater and subpial cord. To date, no such findings have been published, either in *ex vivo* multiple sclerosis spinal cord or in

animal models of the disease. A *post mortem* MRI-histopathology correlation study is needed to consolidate the findings of this *in vivo* study.

In conclusion MTR abnormalities have been recorded in an area corresponding to the expected location of the pia mater and subpial region in the outer cervical spinal cord. These outer spinal cord abnormalities occur early in the course of multiple sclerosis prior to significant cord atrophy and that a greater reduction in MTR values is seen in progressive multiple sclerosis.

## **Chapter 9 - Spinal cord grey matter abnormalities are associated with secondary progression and physical disability in multiple sclerosis**

### **9.1 Introduction**

Relapse-onset multiple sclerosis (MS) presents as a clinically isolated syndrome (CIS), later evolving to relapsing-remitting (RR) MS and, in many cases, secondary progressive (SP) MS (Weinshenker *et al.*, 1989). Physical disability in SPMS is often due to a progressive spinal cord syndrome (Kremenutzky *et al.*, 2006). It is important therefore to understand and monitor spinal cord pathology leading to irreversible disability, as it may facilitate treatment development.

While pathology of spinal cord white matter (WM) should contribute to the motor and sensory impairments in MS, the functional effects of cord grey matter (GM) pathology are uncertain. Noting that spinal GM may be extensively involved (Gilmore *et al.*, 2006; Gilmore *et al.*, 2009), and that brain GM abnormalities are associated with SPMS (Fisher *et al.*, 2008; Fisniku *et al.*, 2008), further investigation of cord GM abnormalities would seem worthwhile.

Magnetic resonance imaging (MRI) offers a tool for investigating spinal cord abnormalities during life and their relationship with functional status. In particular, diffusion tensor imaging (DTI) (Le Bihan *et al.*, 1995) may provide quantitative measures, sensitive to microstructural abnormalities and can be employed in the spinal cord (Wilm *et al.*, 2007).

Two recent publications reported associations between cervical cord DTI abnormalities and physical disability in an MS cohort containing both RR and progressive patients (Oh *et al.*, 2013). However, these studies did not investigate whether functional effects observed were related to WM or GM involvement.

Several studies have investigated DTI in the main WM columns affected by MS (posterior and lateral columns); they were largely confined to subjects with RRMS and low disability (Hesseltine *et al.*, 2006; Freund *et al.*, 2010; Raz *et al.*, 2013). Two studies investigated cord GM but only in RRMS (Hesseltine *et al.*, 2006; Raz *et al.*, 2013). No previous study has reported DTI findings in cord GM or WM columns in SPMS.

In this study a DTI protocol was implemented to investigate microstructural integrity of spinal cord grey matter and the two main white matter columns affected by MS in cohorts of patients with SPMS and RRMS. A cohort of CIS patients was also included along with healthy controls to investigate whether microstructural abnormalities are already present at what is often the first presentation of relapse-onset MS. The imaging findings were correlated with clinical functional measures in order to test the hypotheses - based on known pathology findings - that: firstly, abnormalities in cord grey matter would be significantly associated with secondary progressive MS and secondly, that grey matter microstructural abnormalities would be associated with physical disability.

## 9.2 Methods

### 9.2.1 *Subjects*

Healthy controls and people with CIS and relapse-onset MS (Polman *et al.*, 2011) were recruited. The subtype of MS was classified as RR or SP (Lublin and Reingold 1996). Disability was assessed with the expanded disability status scale (EDSS) (Kurtzke 1983) and the two motor components of multiple sclerosis functional composite (9-hole peg test [9HPT] and timed walk test [TWT]) (Fischer *et al.*, 1999) with z-scores calculated using published normative values. With a focus on spinal cord function, American spinal injury association (ASIA) motor and sensory scores and the Kurtzke functional scores for the motor, sensory and sphincter systems were also investigated (Maynard *et al.*, 1997). Testing of physical function was performed immediately prior to the MRI scan.

No one had experienced a relapse or received a course of corticosteroids within a month prior to imaging. Informed written consent was obtained from all participants.

### 9.2.2 *MRI protocol*

The upper cervical spine and brain of all participants was imaged using a 3T Philips Achieva MRI system with radiofrequency (RF) multi-transmit technology (Philips Healthcare, Best, the Netherlands). For the spinal cord and brain imaging the product 16 and 32 channel coils were used. Subjects were immobilised by placing a polystyrene filled vacuum fixation bag behind the

cervical spine, to decrease motion artefacts. The spinal cord imaging was centred at C2/C3 and imaging volume for all sequences covered from C2-C4.

*Spinal cord imaging:*

(i) Diffusion weighted scan: TE = 52 ms, TR = 12 RRs (cardiac gated), reduced FOV of 64 x 48 mm<sup>2</sup>, SENSE factor = 1.5, acquisition matrix = 64 x 48 for a voxel size of 1 x 1 x 5 mm<sup>3</sup>. The DW imaging protocol consisted of 30  $b = 1000 \text{ s mm}^{-2}$  DWI volumes with gradient directions evenly distributed over the sphere<sup>16</sup> and 3 non-DWI ( $b = 0, b_0$ ) volumes

(ii) 3D phase sensitive inversion recovery (PSIR): voxel size of 0.5 x 0.5 x 3 mm<sup>3</sup>, TR = 8 ms; TE = 3.7 ms; flip angle  $\alpha = 5^\circ$ ; FOV = 256 x 256 mm; NEX = 1

*Brain imaging:*

(i) Axial PD/T2 images using a 2D turbo spin echo sequence (TSE) with 3mm slice thickness; the following parameters were employed: TR=3500 ms; TE=19/85 ms; matrix 240 x 240 mm<sup>2</sup>; in plane resolution= 1 x 1 mm.

(ii) 3D magnetisation-prepared turbo field echo (3D-TFE) sequence was used with slice thickness= 1mm; TR=6.8 ms; TE=3.1 ms; matrix = 256 x 256; in plane voxel size 1 x 1mm<sup>2</sup>

### 9.2.3 *Image analysis*

#### 9.2.3.1 *DTI Analysis*

*WM regions of interest (ROI):* Three circular regions of interest (ROI) were marked on all ten slices of the b0 image: one within each lateral column and one in the posterior columns, as previously described (Hesseltine *et al.*, 2006; Freund *et al.*, 2010); care was taken to place the ROI entirely within the WM column and thereby avoid partial volume effects (Figure 9.1A). A single average value for each DTI parameter was calculated from the two lateral column ROIs (Freund *et al.*, 2010).

*GM segmentation:* Average diffusion-weighted images (DWIs) were created based on the angular threshold of the diffusion gradient direction with respect to the longitudinal axis of the spinal cord. All DWIs with diffusion gradient direction between 0° (i.e. parallel to the cord axis) and a given cut-off angle were averaged and visually assessed for their GM/WM contrast. The cut-off angles were set at 5° intervals from 40° through to 80°. Each threshold involved a variable number of DWIs, i.e. 10 images for a cut off value of 40° and one image for 80°. After review, by visual inspection, a threshold of 50° was chosen as the GM was then clearly visible as a hyper-intense 'H' shaped structure on a hypo-intense background (Figure 9.1B). This allowed the use of a semi-automated tool in JIM 6.0 software (Xinapse systems, <http://www.xinapse.com>) to delineate the GM and construct a mask that was then applied to the DTI maps to obtain quantitative values from

each parameter (FA, MD, AD, RD). The GM ROI was marked carefully in each case around hyper-intense voxels only, to minimise potential partial volume effects from the surrounding WM.

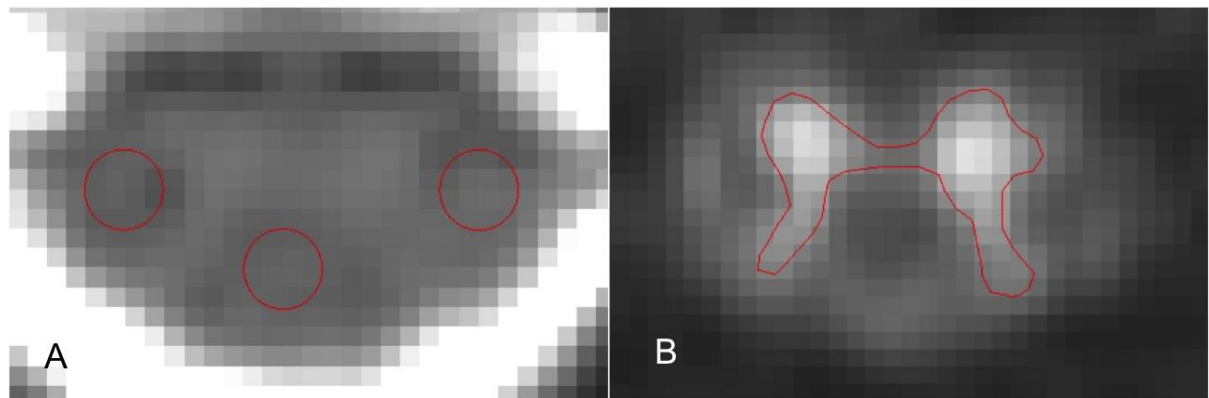


**Figure 9.1** A) b0 image with regions of interest displayed in lateral and posterior column B) Average transverse diffusion weighted image optimised displaying grey matter region of interest (see methods for details). Voxel size of images 1 x 1 x 5mm<sup>3</sup>

To determine the reproducibility of GM segmentation and WM ROI placement, ten control scans were analysed and then re-analysed by the same reader after a period of one month.

The DTI data were processed using the open-source Camino toolkit (Cook *et al.*, 2006) to create fractional anisotropy (FA), mean diffusivity (MD), radial diffusivity (RD) and axial diffusivity (AD) maps in the spinal cord.

### 9.2.3.2 *Conventional MRI analysis*

Upper cervical spinal cord cross-sectional area was measured from the PSIR image (previously described in chapter five). Spinal cord lesions were identified on the PSIR image (described in chapter six). Brain parenchymal fraction (BPF) and T2 lesion volume were measured as described in chapter four.

### 9.2.4 *Statistical analysis*

SPSS 21 (IBM) and Stata 13 (Stata Corporation, College Station, Texas, USA) were used for statistical analysis.

Reproducibility of GM segmentation and WM ROI placement was assessed using the coefficient of variation (COV [expressed as a percentage]) and the intra-class correlation coefficient (ICC).

Means of DTI metrics were compared between subject groups (each patient subgroup versus controls and comparisons between the 3 patient subgroups) using ANOVA with post hoc Bonferonni correction.

To further investigate for differences in DTI metrics between the 4 subject groups, a “linear trend test” analysis was performed (Altman 1991) across the groups by regressing the standardised DTI parameter on a group variables coded numerically in the following order: 0=control, 1=CIS, 2=RRMS, 3=SPMS (N.B.: the word “trend” in this context refers to a statistical analysis that investigates for *significant* linear differences from one disease subtype to the next; it does not

infer a result of borderline significance). Each DTI parameter was standardised (to units of 1 standard deviation [SD]) so that the “trend” coefficients are directly comparable, reflecting the increase in mean DTI parameter in SD units.

Univariable correlations with disability were calculated: Spearman’s rank correlation coefficient for EDSS and Pearson’s correlation coefficient for the MSFC. Significant univariable correlations were further investigated to identify independent DTI predictors with a multiple regression of the disability measure on the DTI parameters, adjusting for age, gender and UCCA.

Statistical significance was defined as  $p < 0.05$ .

## **9.3 Results**

### **9.3.1 *Demographics and conventional MRI scans*** (Table 9.1)

A total of 114 people were included; 30 controls, 21 CIS, 33 RRMS, 29 SPMS. Spinal cord lesions were identified and counted on 3D-PSIR sequence in 38% (8/21) of cases with CIS, 81% (27/33) with RRMS and 96% (28/29) in SPMS.

In the CIS cohort there were 18 cases of unilateral optic neuritis, one multifocal CIS (consisting of optic neuritis, facial numbness and diplopia), and two cases of partial myelitis (one cervical and one thoracic). Asymptomatic T2-weighted brain lesions were seen in all CIS cases and 15 fulfilled the criteria for dissemination in space, dissemination in time could not be assessed as gadolinium was not administered (Polman *et al.*, 2011).

None of the CIS patients were being treated with disease modifying drugs. In the RRMS cohort 19 were on treatment: interferon  $\beta$  (n = 13), glatiramer acetate (n = 1) and natalizumab (n = 5). Four of the 29 SPMS patients were being treated with interferon  $\beta$ .

### **9.3.2 Reproducibility of spinal cord GM segmentation**

Segmentation of the spinal cord GM on the diffusion weighted images was found to be reproducible: COV = 1.46%, ICC = 0.907. Placement of the ROIs in the lateral columns also reproducible, lateral column: COV = 1.05% ICC = 0.925 and posterior column: COV = 0.27% ICC = 0.949.

	Age (years)	Gender (F:M)	Disease duration (years)	Median EDSS (range)	T2 lesion volume (mLs)	Brain parenchymal fraction	Spinal cord area (mm <sup>2</sup> )
<b>Controls (n = 30)</b>	41.50 ± 10.34	19:11				0.823 ± 0.015	80.28 ± 7.29
<b>CIS (n = 21)</b>	35.14 ± 8.53	11:10	0.48 ± 0.36	1 (0 – 3)	2.98 ± 3.82	0.822 ± 0.013	83.55 ± 7.42
<b>RRMS (n = 33)</b>	39.58 ± 9.24	21:12	6.58 ± 5.21	2.5 (0 – 6)	12.90 ± 13.73	0.810 ± 0.018	76.31 ± 7.72
<b>SPMS (n = 29)</b>	51.14 ± 9.35	17:12	20.21 ± 11.62	6.5 (4 – 8.5)	23.41 ± 16.67	0.789 ± 0.017	62.50 ± 8.63

**Table 9.1** Demographic and conventional MRI features of all participants. Presented as mean ± standard deviation.

### 9.3.3 *DTI measures in controls versus patient subgroups* (Table 9.2)

In the CIS group, compared to healthy controls, significant abnormalities were seen in the lateral column FA ( $p = 0.02$ ) and RD ( $p = 0.04$ ).

No significant differences were seen between the CIS and RRMS cohorts.

In SPMS compared to RRMS, we observed higher MD ( $p < 0.01$ ) and RD ( $p < 0.01$ ) in the spinal cord GM, in line with the first hypothesis that the most significant GM abnormalities would be seen in SPMS. More extensive abnormalities were also seen in the posterior column MD ( $p < 0.01$ ) and RD ( $p < 0.01$ ) in SPMS, compared to RRMS. No differences were seen in AD between any of the groups compared.

Comparisons of CIS and MS subtypes with controls are shown in Table 9.2.

Spinal cord region analysed	DTI metric	Control	CIS	RRMS	SPMS
<b>Lateral column</b>	FA	0.76 ± 0.04	0.72 ± 0.05 *	0.71 ± 0.05 ***	0.69 ± 0.05 ***
	MD (x 10 <sup>-3</sup> mm <sup>2</sup> /s)	0.91 ± 0.06	0.95 ± 0.05	0.96 ± 0.07 *	0.98 ± 0.07 **
	RD (x 10 <sup>-3</sup> mm <sup>2</sup> /s)	0.39 ± 0.07	0.45 ± 0.06 *	0.49 ± 0.08 ***	0.50 ± 0.07 ***
	AD (x 10 <sup>-3</sup> mm <sup>2</sup> /s)	1.96 ± 0.11	1.95 ± 0.10	1.94 ± 0.10	1.93 ± 0.10
<b>Posterior column</b>	FA	0.79 ± 0.05	0.77 ± 0.05	0.73 ± 0.05 ***	0.71 ± 0.05 ***
	MD (x 10 <sup>-3</sup> mm <sup>2</sup> /s)	0.95 ± 0.06	0.93 ± 0.05	0.96 ± 0.06	1.03 ± 0.09 ***
	RD (x 10 <sup>-3</sup> mm <sup>2</sup> /s)	0.37 ± 0.07	0.39 ± 0.06	0.45 ± 0.08 **	0.51 ± 0.09 ***
	AD (x 10 <sup>-3</sup> mm <sup>2</sup> /s)	2.09 ± 0.17	2.01 ± 0.13	1.98 ± 0.10	2.05 ± 0.14
<b>Grey matter</b>	FA	0.56 ± 0.16	0.53 ± 0.04 *	0.51 ± 0.05 **	0.48 ± 0.05 ***
	MD (x 10 <sup>-3</sup> mm <sup>2</sup> /s)	0.82 ± 0.04	0.84 ± 0.04	0.86 ± 0.05 **	0.91 ± 0.06 ***
	RD (x 10 <sup>-3</sup> mm <sup>2</sup> /s)	0.53 ± 0.04	0.56 ± 0.04 **	0.59 ± 0.04 ***	0.64 ± 0.05 ***
	AD (x 10 <sup>-3</sup> mm <sup>2</sup> /s)	1.41 ± 0.11	1.41 ± 0.09	1.42 ± 0.10	1.45 ± 0.13

**Table 9.2** Mean ± standard deviation of DTI measures in patients and controls.

Significantly different from controls, ANOVA with post hoc Bonferroni

correction: \* p < 0.05; \*\* p < 0.01; \*\*\* p < 0.001

**9.3.4 “Linear trend test” analysis of standardised DTI measures across CIS, RRMS and SPMS subgroups (Figure 9.2)**

As trends in the data displayed in Table 9.2 seemed apparent, these were further investigated using a linear trend test analysis and significant changes were observed across the three subgroups (from least abnormal in CIS to most abnormal SPMS) in FA, RD and MD.

Mean FA decreased significantly by an estimated:

- (i) 0.43 SDs in the lateral column ( $p < 0.01$ , 95% CI -0.57, -0.28)
- (ii) 0.48 SDs in the posterior column ( $p < 0.01$ , 95% CI -0.62, -0.34)
- (iii) 0.46 SDs in the GM ( $p < 0.01$ , 95% CI -0.60, -0.32).

Mean RD increased significantly by an estimated:

- (i) 0.43 SDs in the lateral column ( $p < 0.01$ , 95% CI 0.29, 0.57)
- (ii) 0.50 SDs in the posterior column ( $p < 0.01$ , 95% CI 0.37, 0.64)
- (iii) 0.59 SDs in the GM ( $p < 0.01$ , 95% CI 0.47, 0.71).

Mean MD increased significantly by an estimated:

- (i) 0.32 SDs in the lateral column ( $p < 0.01$ , 95% CI 0.17, 0.48)
- (ii) 0.50 SDs in the posterior column ( $p < 0.01$ , 95% CI 0.18, 0.49)
- (iii) 0.49 SDs in the GM ( $p < 0.01$ , 95% CI 0.35, 0.63).

There were no significant changes across the subgroups in AD. Graphs with lines fitted across the mean of standardised DTI measures to demonstrate trends seen are shown in Figure 9.2.

Lateral column

Posterior Column

Grey Matter

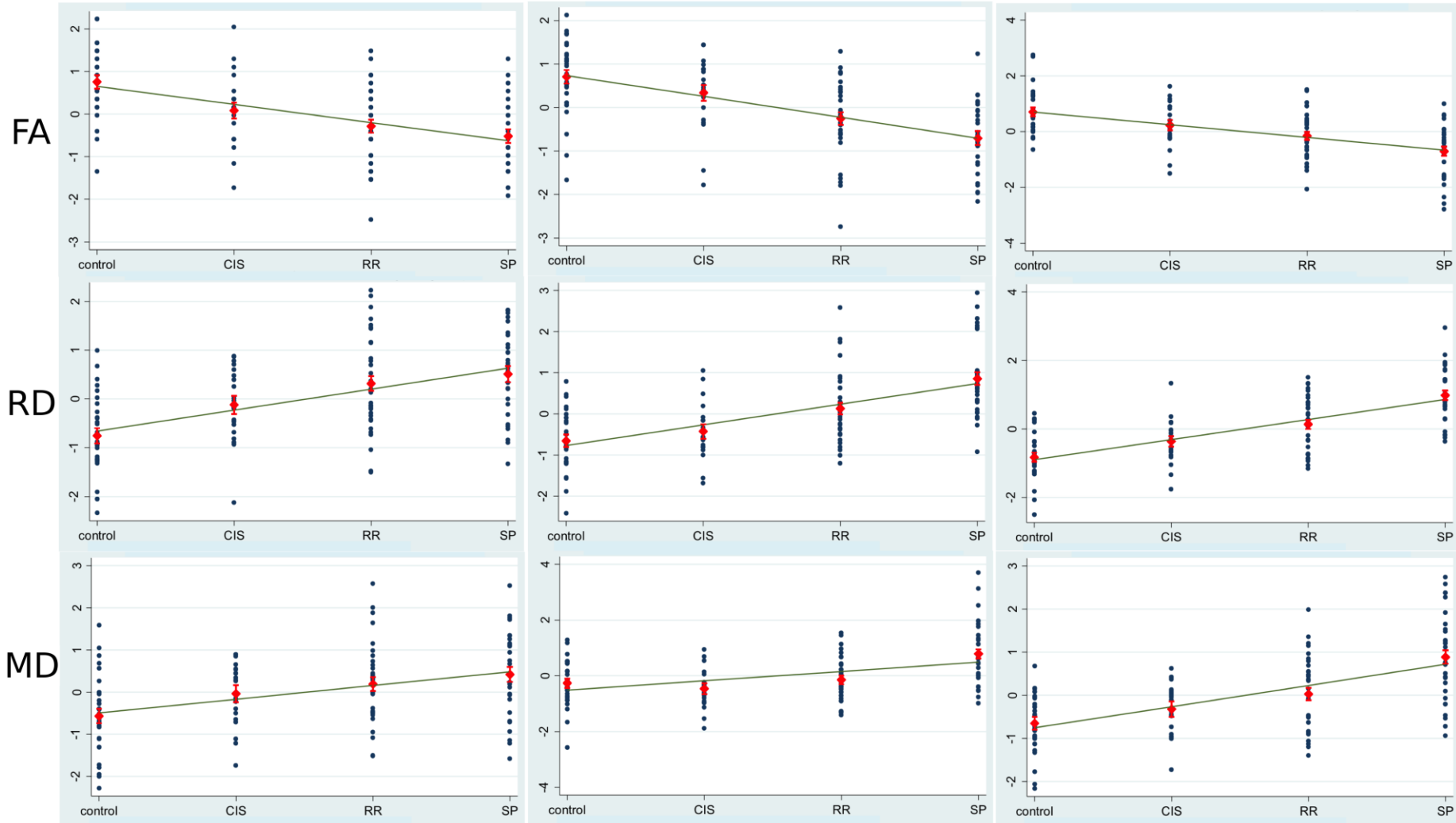


**Figure 9.2** Graphs of standardised DTI measures (FA, RD and MD): the trend lines demonstrated are fitted to the means in each group. Bars on either side of the mean represent the standard error of group means. CIS – clinically isolated syndrome, RR – Relapsing remitting MS, SP – Secondary progressive MS.

### **9.3.5 *Univariable correlations with disability*** (Table 9.3 and 9.4)

EDSS was significantly correlated with GM MD and RD; and posterior column FA, MD and RD.

The TWT z-score was significantly correlated with GM FA, MD and RD; and posterior column FA, MD and RD.

The 9-HPT z-score was significantly correlated with GM FA, MD, RD and AD; lateral column FA, MD and RD; and posterior column FA, MD and RD.

Univariable correlations with Kurtzke motor, sensory and sphincter functional systems and with ASIA motor and sensory scores are provided in a Table 9.4. The pattern of significant DTI correlations with motor and sphincter scores was similar to that seen for the EDSS, TWT and 9HPT, i.e., predominantly in GM and posterior columns, and including FA, RD, MD but not AD. Significant DTI correlations with sensory scales were mainly seen in the posterior column.

		<b>EDSS</b>	<b>25ft TWT</b>	<b>9-HPT</b>
<b>Lateral column</b>	<b>FA</b>	-0.22	0.15	<b>0.26 *</b>
	<b>MD</b>	0.14	-0.11	<b>-0.34 **</b>
	<b>RD</b>	0.22	-0.13	<b>-0.33 **</b>
	<b>AD</b>	-0.01	-0.02	-0.11
<b>Posterior column</b>	<b>FA</b>	<b>-0.47 ***</b>	<b>0.25 *</b>	<b>0.35 **</b>
	<b>MD</b>	<b>0.36 **</b>	<b>-0.24 *</b>	<b>-0.44 ***</b>
	<b>RD</b>	<b>0.51 ***</b>	<b>-0.27 *</b>	<b>-0.44 ***</b>
	<b>AD</b>	0.06	-0.03	-0.12
<b>Grey matter</b>	<b>FA</b>	-0.27	<b>0.25 *</b>	<b>0.25 *</b>
	<b>MD</b>	<b>0.37 **</b>	<b>-0.40 ***</b>	<b>-0.52 ***</b>
	<b>RD</b>	<b>0.46 ***</b>	<b>-0.42 ***</b>	<b>-0.52 ***</b>
	<b>AD</b>	0.16	-0.19	-0.19

**Table 9.3** Univariable correlations (r values presented) between DTI metrics and physical disability, significant correlations are highlighted in bold font: \* p < 0.05; \*\* p < 0.01; \*\*\* p < 0.001. (EDSS: expanded disability status scale, 25ft TWT: 25 foot timed walk test, 9-HPT: 9 hole peg test)

		Pyramidal functional system	Sensory functional system	Bowel and bladder functional system	ASIA motor	ASIA sensory
Lateral column	FA	-0.16	-0.21	<b>-0.34 **</b>	0.20	0.15
	MD	0.18	0.06	0.21	-0.19	0.01
	RD	0.20	0.17	<b>0.36 **</b>	<b>-0.23 *</b>	-0.10
	AD	0.05	0.01	0.04	-0.03	0.05
Posterior column	FA	<b>-0.39 ***</b>	<b>-0.34 **</b>	<b>-0.45 ***</b>	<b>0.31 **</b>	<b>0.22 *</b>
	MD	<b>0.34 **</b>	<b>0.26 *</b>	<b>0.39 ***</b>	<b>-0.28 *</b>	-0.16
	RD	<b>0.41 ***</b>	<b>0.34 **</b>	<b>0.48 ***</b>	<b>-0.34 **</b>	-0.21
	AD	0.02	-0.05	0.02	-0.02	0.02
Grey matter	FA	<b>-0.30 **</b>	<b>-0.26 *</b>	<b>-0.29 **</b>	<b>0.24 *</b>	0.21
	MD	<b>0.40 ***</b>	0.18	<b>0.34 **</b>	<b>-0.32 **</b>	-0.06
	RD	<b>0.45 ***</b>	<b>0.26 *</b>	<b>0.42 ***</b>	<b>-0.36 **</b>	-0.16
	AD	0.17	-0.01	0.14	-0.12	0.09

**Table 9.4** Significant univariable correlations between DTI metrics and physical disability. Significant correlations are highlighted in the table in bold font: \* p < 0.05; \*\* p < 0.01; \*\*\* p < 0.001. (ASIA: American spinal injury association)

### 9.3.6 *Independent associations with physical disability*

In confirmation of the second hypothesis being investigated, significant independent associations were seen with GM RD (coefficient = 0.33, p < 0.01, 95% CI 0.89, 1.92) and EDSS. Cord area (coefficient = -0.45, p < 0.01, 95% CI -0.13, -0.07) was also independently associated with EDSS ( $R^2 = 0.77$ ). No independent associations were seen with the brain MRI measures (i.e. T2LV and BPF) included in this model.

Further confirmation of our hypothesis that spinal cord GM would be associated with disability, was seen in the independent association with the 9-HPT and GM RD (coefficient = -0.33, p < 0.01, 95% CI; -1.14, -.36). UCCA (coefficient = 0.35, p <

0.01, 95% CI; 0.02, 0.06) and BPF (coefficient = 0.24,  $p = 0.02$ , 95% CI 2.15, 27.36) were also independently associated with the 9-HPT ( $R^2 = 0.57$ ).

Spinal cord GM RD (coefficient = -0.20,  $p = 0.04$ , 95% CI -0.32, -0.47) and UCCA (coefficient = 0.29,  $p < 0.01$ , 95% CI 0.04, 0.21) were both independently associated with the TWT ( $R^2 = 0.42$ ).

## 9.4 Discussion

This is the first MRI-DTI study to investigate the spinal cord in a cohort that included both CIS and relapse-onset MS patients. It investigated both cord GM and WM and found that a DTI measure of GM microstructural integrity (RD) was independently associated with disability.

### 9.4.1 *Spinal cord grey matter findings*

In a *post mortem* study in progressive MS more than 40% of the upper cervical cord GM exhibited demyelination, which was greater than the proportion of WM demyelination (Gilmore *et al.*, 2006). Reduced counts of neurons and interneurons also have been reported in areas of GM demyelination (Gilmore *et al.*, 2006), along with inter-neuronal atrophy in lesions and normal appearing GM.

The cord GM is a more anatomically complex structure than the WM and should be less anisotropic. Accordingly it should display a lower FA and AD and a higher RD, as was the case in our healthy controls.

Previous studies in WM tracts have shown associations between DTI and pathological abnormalities, the former exhibiting reduced FA and increased RD and MD and the latter displaying demyelination and neuroaxonal loss (Schmierer *et al.*, 2007; Zhang *et al.*, 2009; Klawiter *et al.*, 2011; Zollinger *et al.*, 2011). The same DTI abnormalities were observed in this *in vivo* study of cord GM and although such changes are not likely to be specific for any single pathological feature, it is plausible that they are a consequence of demyelination

and/or neuronal loss. In previous studies, AD abnormalities have been associated with acute axonal loss (Budde *et al.*, 2009) and following a spinal cord relapse (Freund *et al.*, 2010); the exclusion of subjects having a recent relapse may account for the absence of AD abnormalities in our study.

The clinical spectrum of our cohort is broad (from CIS to SPMS) and the findings in this present study indicate that pathological involvement of the cord GM is already present in early relapse-onset MS (CIS and RRMS) but is more severe, with abnormalities being greatest, in SPMS.

Pyramidal, sensory and sphincter deficits in MS are generally attributed to pathology in the spinal cord WM tracts and little consideration has been given to whether GM involvement may contribute. However, the descending motor tracts in the spinal cord terminate in the dorsal horn, where they synapse with interneurons and in turn with anterior horn cells (Williams and Warwick 1980). The spinal cord GM also contains interneurons between sensory and motor tracts. It would seem plausible that pathology in the cord GM could affect motor, sensory and sphincter function.

Only two studies have investigated DTI metrics in cord GM and these were confined to RRMS patients, most of whom had low disability (Hesseltine *et al.*, 2006; Raz *et al.*, 2013). These studies either sampled a small region in the anterior horn (Raz *et al.*, 2013) or a central cord region that included both GM and WM (Hesseltine *et al.*, 2006). This present study is the first to have segmented the whole cord, whilst also excluding WM as far as possible within the limits of image resolution. This approach, combined with the inclusion of both RRMS and SPMS patients, should have facilitated the detection of a

significant association of GM microstructural abnormalities with functional impairment.

The functional importance of cord GM pathology is suggested by a GM parameter (RD) being the only DTI measure to be independently associated with EDSS. Together, cord atrophy (which is already well-known to correlate with disability [Losseff *et al.*, 1996]) and abnormal GM RD findings accounted for 77% of the variance of EDSS in a regression analysis. GM RD was also independently associated with the 9-HPT and TWT. Pathological studies suggest that although RD is not specific, it is sensitive to myelin and/or neuroaxonal damage (Klawiter *et al.*, 2011; Zollinger *et al.*, 2011); this may explain why RD emerged as the sole DTI predictor of disability in the regression model. Interestingly, RD has previously been correlated with recovery of clinical function following relapses affecting the spinal cord (Freund *et al.*, 2010) and optic nerves (Naismith *et al.*, 2010).

Neuropathological studies of the brain in MS have identified extensive GM abnormalities (Peterson *et al.*, 2001; Bø *et al.*, 2003; Wegner *et al.*, 2006); however, there has been relatively little investigation of spinal cord GM involvement. Noting the significance of cortical GM abnormalities, the potential functional eloquence of the cord GM, and our new DTI findings that link cord GM abnormalities to disability and SPMS, further investigation of the nature of cord GM involvement in MS would seem worthwhile.

#### **9.4.2 Spinal cord white matter findings**

Similar to previous reports (Hesseltine *et al.*, 2006; Freund *et al.*, 2010; Raz *et al.*, 2013), abnormalities of FA, RD and MD were recorded in the posterior and lateral columns in RRMS. However, this study extends previous ones: showing abnormalities detectable in the lateral columns at presentation with a CIS, and increasing abnormalities across the three clinical subgroups. The increase was more evident in posterior columns, with significant differences seen between RRMS and SPMS.

Greater microstructural abnormality in the posterior columns in SPMS may help explain the stronger univariable correlations with disability than was seen for lateral column DTI measures (Table 9.3). Significant associations – albeit modest – were also seen between measures of sensory function and posterior column DTI measures only (Table 9.4). Posterior column pathology with deafferentation could affect balance and mobility thereby contributing to the associations observed.

The more limited associations of lateral column DTI measures with disability may have several explanations. First, although the pyramidal tract travels through the lateral columns, it may be affected by pathology at other levels in the cord, brain stem or cerebral hemispheres. Secondly, involvement of non-pyramidal motor tracts, such as cerebellar pathways, could contribute to impaired motor function.

Thirdly, while DTI investigates the microstructure of residual tissue, it does not account for tissue loss and we found that global spinal cord atrophy was independently associated with disability. A previous *post mortem* study reported that spinal cord atrophy in MS was due to loss of cord WM, with relative preservation of GM volume (Gilmore *et al.*, 2005). It would be of interest to investigate cord WM and GM tissue volumes in future work.

#### **9.4.3 *Study limitations***

A number of study limitations are recognised. First, it did not investigate longitudinal changes in spinal cord DTI abnormalities and future studies are needed to elucidate the evolution of imaging measures and their relationship to changes in clinical course and function.

Secondly, as lesions were not visible on DTI, it was not possible to investigate whether abnormalities arose from lesions and/or normal appearing cord. While it is nevertheless possible that lesions had a subtle influence on the segmentation of the spinal cord GM, in all cases it was possible to readily visualise the GM on the optimised average diffusion-weighted image. The image analysis performed on the lower resolution diffusion weighted images may be considered a somewhat circular approach and has the potential to include partial volume effects in the regions analysed. However, in the present study it was not possible to establish a satisfactory registration of the 3D-PSIR to the non-diffusion-weighted EPI-ZOOM images ( $b = 0$ ), due to a lack of anatomical details. In future, it may be possible to co-register high resolution anatomical images sensitive to lesions, with the DT images to investigate the effect of spinal cord lesions on DTI and further improve cord segmentation.

Thirdly, the study was limited to the upper cervical cord. This level is less susceptible to distortion or artefact related to physiological motion and has also been investigated in previous DTI studies in MS (Hesseltine *et al.*, 2006; Freund *et al.*, 2010; Raz *et al.*, 2013). Furthermore, the spinal cord is frequently affected by MS at this level (Oppenheimer *et al.*, 1978) and may therefore be representative of the cord in general.

Lastly, the EDSS may be affected by MS involving systems other than spinal cord, e.g., brain stem and cerebellum. However, it remains a 'gold standard' in MS, and the importance of spinal cord GM involvement is reinforced by correlations of GM DTI measures with specific measures of pyramidal, sensory and sphincter function (Table 9.3). Notwithstanding, future studies could include more quantitative and sensitive measures of sensory and motor function (Oh *et al.*, 2013).

#### **9.4.4 Conclusions**

In this DT imaging study, marked microstructural abnormalities were found in the spinal cord GM in SPMS compared to RRMS. A combination of abnormal cord GM tissue microstructure and global cord tissue loss explained 77% of the variation in the widely used EDSS disability scale. GM pathology in the spinal cord may contribute to developing SPMS and irreversible disability. Future studies in MS should investigate longitudinal changes in spinal cord GM DTI measures and the relationship with evolving clinical status.

## **Chapter 10 - Summary**

This thesis uses in vivo MR imaging on a 3 Tesla scanner to explore the pathology of MS in the spinal cord as well as the relationship between spinal cord abnormalities and physical disability. The results demonstrate that both macro and micro-structural abnormalities may be visualised using high field MRI and have significant independent contributions to physical disability. Specific findings of the thesis will now be discussed in turn.

### **10.1 Atrophy**

The relevance of spinal cord atrophy in long disease duration MS is explored in chapter four. Using a regression analysis spinal cord atrophy emerged as being significantly associated with the use of a walking aid ( $EDSS \geq 6$ ) and a higher EDSS score i.e. significantly higher levels of physical disability. These results emphasise the importance of using a combination of spinal cord and brain imaging in clinical trials, where MRI may be used as a primary or secondary endpoint.

However, as the spinal cord is a small mobile structure with minimal discernible anatomical landmarks, the inclusion of cord atrophy as a potential endpoint to clinical trials poses numerous technical challenges. In chapter five alternative combinations of sequences and methodologies were investigated to determine a more reproducible method of cord area measurement to those currently available. In this chapter the semi-automated edge finding technique (Losseff *et*

*al.*, 1996) was compared to the active surface model (ASM) (Horsfield *et al.*, 2010). The combination of the ASM with phase sensitive inversion recovery (PSIR) imaging proved to be the most reproducible method of cord area measurement (Reproducibility expressed as coefficient of variation [COV]: intra-rater COV 0.002%, inter-rater COV 0.03%, scan re-scan COV 0.1%).

To evaluate the possibility of using cord atrophy in a clinical trial in MS, sample sizes were calculated based on the between-subject mean standard deviation of the mean spinal cord cross-sectional area of 15 MS patients' baseline scan. The combination of PSIR and ASM required the smallest sample size for a trial, using cord atrophy as an endpoint. These data suggest that it may be feasible to include this MRI parameter in future trials of neuroprotection in MS.

## **10.2 Lesions**

As spinal cord lesions may also be visualised, as well as atrophy, on gross pathology (Opppenheimer 1979; Fog 1950), cord lesions were also investigated in this thesis. To identify high resolution axial sequences that could accurately identify the anatomical location of spinal cord lesions, a pilot study was performed firstly in a small group of people with MS. The results of this pilot study indicate that fast field echo (FFE) and phase sensitive inversion recovery (PSIR) images in combination may be useful in recording the presence and columnar involvement of spinal cord lesions.

Having established the utility of these two sequences in the pilot study, these sequences were then employed in the upper cervical cord of the whole cohort of CIS and MS patients studied in this thesis. In order to accurately record the

differences in lesion morphology between relapsing remitting and progressive MS, a classification system of spinal cord lesions detected on axial images, is proposed in this chapter six. Furthermore, the presence of diffuse abnormalities was also recorded (not previously done in the pilot study).

The results of this chapter suggest that larger, more extensive lesions, involving a greater number of WM columns, are more common in progressive MS compared to the relapsing remitting subtype. In agreement with the existing literature on spinal cord imaging (Lycklama à Nijeholt *et al.*, 1998), diffuse abnormalities were found more commonly in progressive MS. The spinal cord columnar involvement was also found to be in agreement with early *post mortem* studies of the spinal cord (Opppenheimer 1979; Fog 1950) indicating that the lateral and posterior columns are frequently involved by spinal cord lesions.

The results of this chapter suggest that spinal cord lesion morphology may be accurately characterised using high resolution axial imaging. However, it is important to emphasise the *caveat* that the scanning protocol implemented in this study would be too long to use in clinical practise. Therefore, a number of technical modifications would be required to reduce the scanning time (alternative sequences, higher field strength or different acquisition protocols) before this approach could be used more routinely.

---

Spinal cord pathology in MS results in a number of histopathological abnormalities including inflammation, gliosis, demyelination and axonal loss (Oppenheimer 1979; DeLuca *et al.*, 2006; Tallantyre *et al.*, 2009). Through the use of quantitative MRI, histopathological abnormalities were investigated in this thesis.

### **10.3 Lesion load**

In part two of chapter six, spinal cord lesion morphology and location are investigated; however, this approach did not investigate the volume of the lesions seen. Therefore, the subsequent chapter seven, utilised a quantitative approach to measure spinal cord lesion load, analogous to that used in *post mortem* studies (Evangelou *et al.*, 2005; DeLuca *et al.*, 2006), by individually circumscribing all the lesions detected on the PSIR scan. In addition the magnetisation transfer ratio (MTR) was measured in both normal appearing and lesional spinal cord.

The main result of this chapter is that spinal cord lesion load in the upper cervical cord was associated with physical disability independently from spinal cord atrophy. These two MRI parameters in combination explained 56% of the variance in EDSS in this cohort. These data also demonstrated modest associations between tissue integrity, measured by MTR and physical disability.

#### **10.4 Meningeal and subpial abnormality (MTR)**

Chapter eight also used MTR imaging of the spinal cord. However, in this instance it was used to investigate a concept that has arisen in brain studies suggesting that meningeal inflammation is associated with subpial demyelination and progressive MS (Magliozzi *et al.*, 2010; Lucchinetti *et al.*, 2011). Meningeal inflammation in the spinal cord has also been reported to be of importance in the pathophysiology of MS through its association with axonal loss (Androdias *et al.*, 2010; DeLuca *et al.*, 2013). However, these *post mortem* findings have not been previously investigated *in vivo*.

High resolution axial imaging was acquired in the upper cervical cord and the outermost region of the cord (thought to contain the pia mater and subpial white matter) was extracted to compare MTR values in this and the deeper white and grey matter. Significant higher MTR was measured in the outer spinal cord compared with deeper white matter in healthy controls, suggesting that the outermost region of the cord may be composed of different tissue types to the white matter, possibly reflecting collagen in pia mater. The MTR values in the outermost region were significantly lower in all patient subtypes (including clinically isolated syndrome [CIS] and MS) compared to controls. As MTR values were lower in CIS, these data suggest that early inflammation/demyelination may occur in the outermost region of the spinal cord.

The association between outer spinal cord inflammation and axonal loss was then explored via a regression analysis. A significant independent association

was seen between outer cord MTR (putative marker of meningeal inflammation and subpial demyelination) and cord atrophy (used as a marker of axonal loss), in agreement with previous pathology studies of the spinal cord (Androdias *et al.*, 2010; DeLuca *et al.*, 2013).

### **10.5 Grey matter (DTI)**

Pathological studies in progressive MS have also reported extensive grey matter pathology in the spinal cord (Gilmore *et al.*, 2006; Gilmore *et al.*, 2009). However, the functional effects of spinal cord grey matter involvement have not been fully elucidated. In chapter 9, diffusion tensor imaging (DTI) was used to investigate spinal cord grey matter abnormalities and their association with disability and secondary progressive MS.

The DTI metrics investigated in the spinal cord grey matter (fractional anisotropy, mean diffusivity and radial diffusivity) displayed significantly more abnormalities in secondary progressive MS compared to relapsing remitting MS and CIS. Furthermore, radial diffusivity (RD) of the spinal cord grey matter was independently associated with a number of measures of physical disability. A combination of cord atrophy and grey matter RD explained 77% of the variation in EDSS. These results indicate the spinal cord grey matter pathology may be of importance in the development of secondary progressive MS and irreversible physical disability.

## 10.6 Future questions

This thesis explores a number of facets of spinal cord involvement in MS.

However, it also raises questions that would be of interest to address in future studies of the spinal cord. The cross-sectional nature of this study precluded observation of the temporal dynamics of the MRI abnormalities accrued in the spinal cord. A longitudinal study could potentially address the relationship between an increasing number of spinal cord abnormalities detected on MRI (such as an increase in lesion load) and an increase in fixed disability. It will be especially relevant to investigate whether abnormal outer cord MTR (suggesting meningeal inflammation) predicts subsequent atrophy (implying axonal loss).

This thesis also implemented multi-modal imaging of the spinal cord with an overall scan time that would preclude implementation in its entirety in clinical practise to manage individual patients. Technological alterations, such as higher field strength or alterations in the scan acquisition could potentially shorten the scanning protocol or parts thereof, thereby facilitating its future implementation. The methods developed in this thesis could, however, already be applied in the setting of a clinical trial with a standardised and quality-controlled protocol, where they could provide outcome measures for investigating therapies aimed at preventing spinal pathology.

The coverage of the spinal cord was restricted to the upper cervical spinal cord in this thesis, therefore, the functional effects of spinal cord abnormalities in lower segments of the cord were not investigated and it may be of interest to do

so e.g. a quantitative MRI study of the thoraco-lumbar spinal cord in order to investigate the relationship between bladder dysfunction and cord pathology.

The measures of physical disability used were largely confined to the expanded disability status scale (EDSS) and MS functional composite (MSFC). Although the EDSS and MSFC scales confer the advantage of being familiar, from their implementation in clinical trials, neither scale is specific for spinal cord function. Previous quantitative MRI studies have implemented disability measures that were specific for spinal cord function, such as vibration sense and hip or foot flexion strength (Zackowski *et al.*, 2009; Oh *et al.*, 2013). Sensitive measures of spinal cord function, such as these, may provide additional valuable information in future studies.

Lastly, this thesis was confined to *in vivo* imaging of the spinal cord and did not address the pathological correlates of the abnormalities identified. An *ex vivo* study could directly investigate the relationship between the MRI abnormalities detected and spinal cord pathology.

## 10.7 Conclusions

The use of multi-modal imaging in the spinal cord in this thesis has provided insights into the pathology of MS in this clinically eloquent structure, as well as demonstrating the contribution of spinal cord abnormalities (both macro and micro) to physical disability. Through the use of different regression analyses, independent contributions of spinal cord abnormalities to commonly used measures of physical disability (such as EDSS) were identified. Overall, these results suggest an emerging and important potential role for *in vivo* spinal cord MRI in future clinical trials in MS where physical disability is used as a primary outcome measure.

## **REFERENCE LIST**

- Agosta F, Absinta M, Sormani MP, Ghezzi A, *et al.* *In vivo* assessment of cervical cord damage in MS patients: a longitudinal diffusion tensor MRI study. *Brain* 2007; 130:2211-2219
- Agosta F, Benedetti B, Rocca MA, *et al.* Quantification of cervical cord pathology in primary progressive MS using diffusion tensor MRI. *Neurology* 2005; 64:631-635
- Agosta F, Pagani E, Caputo D, Filippi M. Associations Between Cervical Cord Gray Matter Damage and Disability in Patients with Multiple Sclerosis. *Arch Neurol* 2007; 64:1302-1305
- Allen IV, Glover G, Anderson R. Abnormalities in the macroscopically normal white matter in cases of mild or spinal multiple sclerosis. *Acta Neuropathol (Berl)* 1981; suppl 7:176-8
- Altman DG. *Practical Statistics for Medical Research*, 1<sup>st</sup> ed. New York: CRC Press; 1991 p212-p213
- Androdias G, Reynolds R, Chanal M, Ritleng C, Confavreux C, Nataf S. Meningeal T cells associate with diffuse axonal loss in multiple sclerosis spinal cords. *Ann Neurol* 2010;68:465-76
- Ascherio A, Munger K. Environmental Risk Factors for Multiple Sclerosis. Part I: The Role of Infection. *Ann Neurol* 2007; 61:288-299
- Audoin B, Au Duong MV, Ranjeva JP, Ibarrola D, Malikova I, Confort-Gouny S, *et al.* Magnetic resonance study of the influence of tissue damage and cortical reorganization on PASAT performance at the earliest stage of multiple sclerosis. *Hum Brain Mapp.* 2005;24:216-28
- Australia and New Zealand Multiple Sclerosis Genetics Consortium (ANZgene). Genome-wide association study identifies new multiple sclerosis susceptibility loci on chromosomes 12 and 20. *Nat Genet* 2009; 41:824-828
- Bagnato F, Jeffries N, Richert ND, Stone RD, *et al.* Evolution of T1 black holes in patients with multiple sclerosis imaged monthly for 4 years. *Brain* 2003; 126:1782-1789
- Banwell B, Shroff M, Ness JM, *et al.* MRI features of pediatric multiple sclerosis. *Neurology* 2007; 68(Suppl. 2):S46-S53
- Baranzini SE, Wang J, Gibson RA, Galwey N, *et al.* Genome-wide association analysis of susceptibility and clinical phenotype in multiple sclerosis. *Hum Mol Genet* 2009; 18:767-778

- Barcellos LF, Sawcer S, Ramsay PP, *et al.* Heterogeneity at the HLA-DRB1 locus and risk for multiple sclerosis. *Hum Mol Genet.* 2006; 15:2813-2824
- Barkhof F, Filippi M, Miller DH, Scheltens P, *et al.* Comparison of MRI criteria at first presentation to predict conversion to clinically definite multiple sclerosis. *Brain* 1997; 120:2059-2069
- Barkhof F, Scheltens P, Frequin STFM, *et al.* Relapsing remitting multiple sclerosis: sequential enhanced MR imaging versus clinical findings in determining disease activity. *AJR* 1992; 159:1041-1047
- Barkhof F, Simon JH, Fazekas F, Rovaris M, Kappos L, de Stefano N, *et al.* MRI monitoring of immunomodulation in relapse-onset multiple sclerosis trials. *Nat Rev Neurol* 2011;8(1):13-21
- Barres BA, Hart IK, Coles HS, *et al.* Cell death and control of cell survival in the oligodendrocyte lineage. *Cell* 1992; 70:31-46
- Barson Jit I, Charnalia J. The vertebral level of the termination of the spinal cord. *J Anat Soc Ind* 1959; 8:93-101
- Basser PJ, Pierpaoli C. Microstructural and physiological features of tissues elucidated by quantitative diffusion tensor MRI. *J Magn Reson* 1996; 111:209-219
- Bastianello JA, Pozzilli C, Bernardi S, *et al.* Serial study of gadolinium-DTPA MRI enhancement in multiple sclerosis. *Neurology* 1990; 40:591-595
- Bates SE, Strangward M, Keelan J, Davey GP, Munro PM, Clark JB. Inhibition of N-acetylaspartate production: implications for 1H MRS studies in vivo. *Neuroreport* 1996; 7:1397-1400
- Beck RW, Trobe JD, Moke PS, *et al.* High- and low-risk profiles for the development of multiple sclerosis within 10 years after optic neuritis: experience of the optic neuritis treatment trial. *Arch Ophthalmol* 2003; 121:944-949
- Bedell BJ, Narayana PA. Implementation and evaluation of a new pulse sequence for rapid acquisition of double inversion recovery images for simultaneous suppression of white matter and CSF. *J Magn Reson Imaging* 1998; 8:544-47
- Bender R and Lange S. Adjusting for multiple testing: When and how? *J Clin Epidemiol* 2001;54:343-349
- Benedetti B, Rocca MA, Rovaris M, Caputo D, *et al.* A diffusion tensor MRI study of cervical cord damage in benign and secondary progressive multiple sclerosis patients. *J Neurol Neurosurg Psychiatry* 2010; 81:26-30
- Bergers E, Bot JCJ, De Groot CJA, Polman Ch *et al.* Axonal damage in the spinal cord of MS patients occurs largely independent of T2 MRI lesions. *Neurology* 2002; 59:1766-1771

- Bergers E, Bot CJ, van der Valk P, Castelijns JA, *et al.* Diffuse Signal Abnormalities in the Spinal Cord in Multiple Sclerosis: Direct Postmortem In Situ Magnetic Resonance Imaging Correlated with In Vitro High-Resolution Magnetic Resonance Imaging and Histopathology. *Ann Neurol* 2002; 51:652-656
- Bernstein MA, Thomasson DM, Perman WH. Improved detectability in low signal-to-noise ratio magnetic resonance images by means of a phase-corrected real reconstruction. *Med Phys* 1989;16:813-817
- Beutler E, Sipe JC, Romine JS, Koziol JA, *et al.* The treatment of chronic progressive multiple sclerosis with cladribine. *Proc Natl Acad Sci USA* 1996; 93:1716-20
- Bielekova B, Muraro PA, Golestaneh L, Pascal J, *et al.* Preferential expansion of autoreactive T lymphocytes from the memory T-cell pool by Il-7. *J Neuroimmunol* 1999; 100:115-123
- Bjartmar C, Kidd G, Mörk S, Rudick R, Trapp BD. Neurological Disability Correlates with Spinal Cord Axonal Loss and Reduced N-Acetyl Aspartate in Chronic Multiple Sclerosis Patients. *Ann Neurol* 2000; 48:893-901
- Blamire AM, Cader S, Lee M, Palace J, Matthews PM. Axonal Damage in the Spinal Cord of Multiple Sclerosis Patients Detected by Magnetic Resonance Spectroscopy. *Magn Reson Med* 2007; 58:880-885
- Bland JM, Altman DG. Statistical methods for assessing agreement between two methods of clinical measurement. *Lancet* 1986;1 (8476): 307-310
- Bö L, Geurts JJ, van der Valk P, Polman C, Barkhof F. Lack of correlation between cortical demyelination and white matter pathologic changes in multiple sclerosis. *Arch Neurol.* 2007;64:76-80
- Bö L, Vedeler CA, Nyland H, Trapp BD, Mörk SJ. Intracortical multiple sclerosis lesions are not associated with increased lymphocyte infiltration. *Mult Scler* 2003; 9:323-331
- Bø L, Vedeler CA, Nyland HI, Trapp BD, Mø SJ. Subpial demyelination in the cerebral cortex of multiple sclerosis patients. *J Neuropathol Exp Neurol.* 2003;62:723-32
- Bonati U, Fisniku LK, Altmann DR, Yiannakas MC, Furby J, Thompson AJ, *et al.* Cervical cord and brain grey matter atrophy independently associates with long-term MS disability. *J Neurol Neurosurg Psychiatry* 2011;82:471-472
- Bot JCJ, Barkhof F, Lycklama à Nijeholt G, *et al.* Comparison of a conventional cardiac-triggered dual spin-echo and a fast STIR sequence in detection of spinal cord lesions in multiple sclerosis. *Eur Radiol* 2000; 10:753-758
- Bot JCJ, Barkhof F, Lycklama à Nijeholt G, *et al.* Differentiation of Multiple Sclerosis from other Inflammatory disorders and Cerebrovascular Disease: Value of Spinal MR Imaging. *Radiology* 2002; 223:46-56

- Bot JCJ, Barkhof F, Polman CH, Lycklama à Nijeholt GJ, *et al.* Spinal cord abnormalities in recently diagnosed MS patients. Added value of spinal MRI examination. *Neurology* 2004; 62:226-233
- Bot JCJ, Blezer EL, Kamphorst W, Lycklama à Nijeholt GJ, *et al.* The Spinal Cord in Multiple Sclerosis: Relationship of High-spatial-Resolution Quantitative MR Imaging Findings to Histopathologic Results. *Radiology* 2004; 233:531-40
- Brand OJ, Lowe CE, Heward JM, *et al.* Association of the interleukin-2 receptor alpha (IL-2Ralpha)/CD25 gene region with Graves' disease using a multilocus test and tag SNPs. *Clin Endocrinol* 2007; 66:508-12
- Brand A, Richter-Landsberg C, Leibfritz D. Multinuclear NMR studies on the energy metabolism of glial and neuronal cells. *Dev Neurosci* 1993; 15:289-298
- Brex PA, Ciccarelli O, O'Riordan JI, Sailer M, Thompson AJ, Miller DH. A longitudinal study of abnormalities on MRI and disability from multiple sclerosis. *N Eng J Med* 2002;346:158-164
- Brex PA, Jenkins R, Fox NC *et al.* Detection of ventricular enlargement in patients at the earliest clinical stage of multiple sclerosis. *Neurology* 2000; 54:1689-91
- Brex PA, Leary SM, O'Riordan JI, Miszkiel KA *et al.* Measurement of spinal cord area in clinically isolated syndromes suggestive of multiple sclerosis. *J Neurol Neurosurg Psychiatry* 2001; 70:544-547
- Brex PA, O'Riordan JI, Miszkiel KA, Moseley IF, *et al.* Multisequence MRI in clinically isolated syndromes and the early development of MS. *Neurology* 1999; 53:1184-1190
- Bronskill MJ, McVeigh ER, Kucharczyk W, Henkelman RM. Syrinx-like artefacts on MR images of the spinal cord. *Radiology* 1988; 166:485-88
- Brown DA, Sawchenko PE. Time course and distribution of inflammatory and neurodegenerative events suggest structural bases for the pathogenesis of experimental autoimmune encephalomyelitis. *J Comp Neurol* 2007;502:236-60
- Brownell B and Hughes JT. The distribution of plaques in the cerebrum in multiple sclerosis. *J Neurol Neurosug Psychiatry* 1962;25:315-320
- Bruck W, Bitsch A, Kolenda A, Bruck Y, *et al.* Inflammatory central nervous system demyelination: correlation of magnetic resonance imaging findings with lesion pathology. *Ann Neurol* 1997; 42:783-793
- Bruck W, Porada P, Poser S *et al.* Monocyte/macrophage differentiation in early multiple sclerosis lesions. *Ann Neurol* 1994; 35:65-73
- Burton PR, Clayton DG, Cardon LR, Craddock N, *et al.* Association scan of 14,500 nonsynonymous SNPs in four diseases identifies autoimmune variants. *Nat Genet* 2007; 39:1329-1337
- Bydder GM, Young IR. MR imaging: Clinical use of the inversion recovery sequence. *J Comput Assit Tomogr* 1985; 9:659-675

- Cajal SR. Structure et connexions des neurons. Les Prix Nobel en 1906 pp 1-25, Norstedt and Söner:Stockholm
- Calabrese M, De Stefano N, Atzori M, Bernardi V, *et al.* Detection of Cortical Inflammatory lesion by Double Inversion Recovery Magnetic Resonance Imaging in Patients with Multiple Sclerosis. *Arch Neurol* 2007; 64:1416-1422
- Calabrese M, Rinaldi F, Mattisi I, Bernardi V, Favaretto A, Perini P, *et al.* The predictive value of gray matter atrophy in clinically isolated syndromes. *Neurology* 2011;77:257-263
- Cantorna MT, Hayes CE, DeLuca HF. 1,25-Dihydroxyvitamin D3 reversibly blocks the progression of relapsing encephalomyelitis, a mouse model of multiple sclerosis. *Proc Natl Acad Sci USA* 1996; 93:7861-7864
- Capra R, Marciano N, Vignolo LA, Chiesa A, Gasparotti R. Gadolinium-pentetic acid magnetic resonance imaging in patients with relapsing remitting multiple sclerosis. *Arch Neurol* 1992; 49:687-689
- Carpenter JR, Bithall JF. Bootstrap confidence intervals: when, which, what? A practical guide for medical statisticians. *Statistics in Medicine* 2000; 19:1141-1164
- Carswell J. Pathological anatomy: illustrations on elementary forms of disease. 1838 London: Longman
- Charcot JM. Histologie de le sclerose en plaques. *Gaz Hop (Paris)* 1868; 41: 554-566
- Charcot JM. Lecons sur les maladies du systeme nerveux faites a la salpetriere 1880 pp. 189-220 Paris: Cerf et fils
- Chard DT, Griffin CM, Parker GJ, Kapoor R, Thompson AJ, Miller DH. Brain Atrophy in clinically early relapsing-remitting multiple sclerosis. *Brain* 2002;125:327-37
- Chard DT, Jackson JS, Miller DH, *et al.* Reducing the impact of white matter lesions on automated measures of brain gray and white matter volumes. *J Magn Reson Imaging* 2010;32:223-228
- Charil A, Caputo D, Cavarretta R, Sormani MP, Ferrante P, Filippi M. Cervical cord magnetization transfer ratio and clinical changes over 18 months in patients with relapsing-remitting multiple sclerosis: a preliminary study. *Mult Scler.* 2006;12:662-5
- Charil A, Yousry TA, Rovaris M, Barkhof F, *et al.* MRI and the diagnosis of multiple sclerosis: expanding the concept of 'no better explanation'. *Lancet Neurol* 2006; 5(10):841-52
- Chen JT, Easley K, Schneider C, *et al.* Clinically feasible MTR is sensitive to cortical demyelination in MS. *Neurology.* 2013;80:246-52

Choi SR, Howell OW, Carassiti D, Magliozzi R, Gveric D, Muraro PA, et al. Meningeal inflammation plays a role in the pathology of primary progressive multiple sclerosis. *Brain* 2012;135:2925-37

Ciccarelli O, Altmann DR, McLean MA, Wheeler-Kingshott CA, *et al.* Spinal cord repair in MS. Does mitochondrial metabolism play a role? *Neurology* 2010; 74:721-727

Ciccarelli O, Thomas DL, De Vita E, Wheeler-Kingshott CA, et al. Low Myo-inositol indicating astrocytic damage in case series of neuromyelitis optica. *Ann Neurol* 2013doi: 10.1102/ana.23909. [Epub ahead of print]

Ciccarelli O, Wheeler-Kingshott CA, McLean MA, Cercignani M, *et al.* Spinal cord spectroscopy and diffusion-based tractography to assess acute disability in multiple sclerosis. *Brain* 2007; 130:2220-2231

Clark CA, Werring DJ, Miller DH. Diffusion imaging of the spinal cord in vivo: Estimation of the principal diffusivities and application to multiple sclerosis. *Magn Res Med* 2000; 43:133-138

Cohen AB, Neema M, Arora A, Dell'oglio E, Benedict RH, Tauhid S, et al. The relationships among MRI-defined spinal cord involvement, brain involvement, and disability in multiple sclerosis. *J Neuroimaging* 2012;22:122-8

Coles AJ, Fox E, Vladic A, Gazda SK, Brinar V, Selmaj KW, et al. Alemtuzumab more effective than interferon  $\beta$ -1a at 5-year follow-up of CAMMS223 clinical trial. *Neurology* 2012;78:1069-78

Coles AJ, Wing MG, Molyneux P, Paolilo A, *et al.* Monoclonal antibody treatment exposes three mechanisms underlying the clinical course of multiple sclerosis. *Ann Neurol* 1999; 46:296-304

Comi G, Filippi M, Martinelli V, et al. Brain MRI correlates of cognitive impairment in primary and secondary progressive multiple sclerosis. *J Neurol Sci* 1995;132:222-227

Compston A, Coles A. Multiple Sclerosis. *Lancet* 2002; 359:1221-31

Compston A, Coles A. Multiple Sclerosis. *Lancet* 2008; 372:1502-17

Compston A, Confavreaux C, Lassmann H, McDonald I, *et al.* *Mc Alpine's Multiple Sclerosis*. Fourth Edition Churchill Livingstone 2006

Compston DA, Batchelor JR, McDonald WI. B-lymphocyte alloantigens associated with multiple sclerosis. *Lancet* 1976; 308:1261-65

Confavreaux C, Aimard G, Devic M. Course and prognosis of multiple sclerosis assessed by the computerised data processing of 349 patients. *Brain* 1980; 103:281-300

Confavreaux C, Hutchinson M, Hours MM, Cortinovis-Tourniaire P, Moreau T and the pregnancy in Multiple Sclerosis Group. Rate of pregnancy related relapse in multiple sclerosis. *NEJM* 1998; 339(5):285-291

- Confavreux C, Vukusic S, Moreau T, Adeleine P. Relapses and progression of disability in multiple sclerosis. *N Eng J Med* 2000 16;343:1430-1438
- Confavreux C, Suissa S, Saddier P, Bourdès V, Vukusic S for the vaccines in multiple sclerosis study group. Vaccinations and the risk of relapse in multiple sclerosis. *NEJM* 2001; 344(5):319-326
- Confavreux C, Vukusic S. Natural history of multiple sclerosis: a unifying concept. *Brain* 2006;129:606-16
- Confavreux C, Vukusic S. Accumulation of irreversible disability in multiple sclerosis: from epidemiology to treatment. *Clin Neurol Neurosurg* 2006;108:327-32
- Connick P, Kolappan M, Crawley C, Webber DJ, Patani R, Michell AW, et al. Autologous mesenchymal stem cells for the treatment of secondary progressive multiple sclerosis: an open-label phase 2a proof-of-concept study. *Lancet Neurol* 2012;11:150-156
- Cook PA, Bai Y, Nedjati-Gilani S, et al. Camino: Open-Source Diffusion-MRI Reconstruction and Processing, 14th Scientific Meeting of the International Society for Magnetic Resonance in Medicine, Seattle, WA, USA, p. 2759, May 2006
- Cook LL, Foster PJ, Mitchell JR, Karlik SJ. In vivo 4.0-T magnetic resonance investigation of spinal cord inflammation, demyelination, and axonal damage in chronic-progressive experimental allergic encephalomyelitis. *J Magn Reson Imaging*. 2004;20:563-71
- Crawford DH. Biology and disease associations of Epstein-Barr Virus. *Philos Trans R Soc Lond B Biol Sci* 2001; 356:461-473
- Cruveilhier J. Anatomie pathologique du corps humaine. 1841 Paris: Balilliere
- Curtin AJ, Chakeres DW, Bulas R, Boesel CP, Finneran M, Flint E. MR imaging artefacts of the axial internal anatomy of the cervical spinal cord. *AJR Am J Roentgenol* 1989; 152:835-42
- Cutter GR, Baier ML, Rudick RA, et al. Development of a multiple sclerosis functional composite as a clinical trial outcome measure. *Brain* 1999; 122:871-82
- Czervionke LF, Czervionke JM, Daniels DL, Haughton VM. Characteristic features of MR truncation artefacts. *AJR Am J Roentgenol* 1988; 151:1219-28
- Dalton C, Brex P, Miszkiel K, Fernando K, et al. Spinal cord MRI in clinically isolated optic neuritis. *J Neurol Neurosurg Psychiatry* 2003; 74:1577-1580
- Davie CA, Hawkins CP, Barker GJ, et al. Serial proton magnetic resonance spectroscopy in acute multiple sclerosis lesions. *Brain* 1994; 117:49-58
- Dawson JW. The histology of multiple sclerosis. *Trans R Soc (Edinb)* 1916; 50:517-740

Dean G. Annual incidence, prevalence and mortality of multiple sclerosis in white South-African born and in white immigrants to South Africa. *BMJ* 1967; 2:724-730

Dean G, McLoughlin H, Brady R, *et al.* Multiple Sclerosis among immigrants to Greater London *BMJ* 1976; 1:861-864

Deen S, Bachetti P, High A, *et al.* Predictors of the location of multiple sclerosis relapse. *J Neurol Neurosurg Psychiatry* 2008; 79:1190-3

De Jager PL, Jia X, Wang J, de Bakker PIW, *et al.* Meta-analysis of genome scans and replication identify CD6, IRF8 and TNFRSF1A as new multiple sclerosis susceptibility loci. *Nat Genet* 2009; 41:776-782

DeLuca GC, Alterman R, Martin JL, Mittal A, Blundell S, Bird S, *et al.* Casting a light on multiple sclerosis heterogeneity: the role of HLA-DRB1 on spinal cord pathology. *Brain* 2013;136;1025-34

DeLuca GC, Ebers GC, Esiri MM. Axonal loss in multiple sclerosis: a pathological survey of the corticospinal and sensory tracts. *Brain* 2004; 127:1009-18

DeLuca GC, Williams K, Evangelou N, *et al.* The contribution of demyelination to axonal loss in multiple sclerosis. *Brain* 2006;129:1507-16.

De Seze J, Debouverie M, Zephir H, *et al.* Acute fulminant demyelinating disease: a descriptive study of 60 patients. *Arch Neurol* 2007; 64:1426-1432

De Stefano N, Matthews PM, Antel JP, Preul M, Francis G, Arnold DL. Chemical pathology of acute demyelinating lesions and its correlation with disability. *Ann Neurol* 1995; 38:901-09

De Stefano N, Matthews PM, Fu L, *et al.* Axonal damage correlates with disability in patients with relapsing remitting multiple sclerosis. Results of a longitudinal magnetic resonance spectroscopy study. *Brain* 1998; 121:1469-77

Dietrich O, Reiser MF, Schoenberg SO. Artifacts in 3-Tesla MRI: Physical background and reduction strategies. *Eur J Radiol* 2008;65(1);29-35

Dousset V, Grossman RI, Ramer KN, *et al.* Experimental allergic encephalomyelitis and multiple sclerosis: lesion characterization with magnetization transfer imaging. *Radiology*. 1992;182:483-91

Dowell NG, Jenkins TM, Ciccarelli O, Miller DH, Wheeler-Kingshott CA. Contiguous-slice Zonally Oblique Multislice (CO-ZOOM) Diffusion Tensor Imaging: Examples of in Vivo Spinal Cord and Optic Nerve Applications. *J Magn Res Med* 2009; 29:454-460

Dyment DA, Yee IM, Ebers GC, Sadovnick AD. Multiple sclerosis in stepsiblings: recurrence risk and ascertainment. *J Neurol Neurosurg Psychiatry* 2006; 77:258-9

Ebers GC, Sadovnick AD, Risch NJ. A genetic basis for familial aggregation in multiple sclerosis. Canadian Collaborative Study Group. *Nature* 1995; 377: 150-1

Emre M, de Decker C. Effects of cigarette smoking on motor functions in patients with multiple sclerosis. *Arch Neurol* 1992; 49:1243-1247

Evangelou N, DeLuca GC, Owens T, Esiri MM. Pathological study of spinal cord atrophy in multiple sclerosis suggests limited role of local lesions. *Brain*. 2005;128:29-34

Farrell RA, Antony D, Wall GR, Clark DA, *et al*. Humoral immune response to EBV in multiple sclerosis is associated with disease activity on MRI. *Neurology* 2009; 73:32-38

Fazekas F, Offenbacher, Fuchs S, Schmidt R, *et al*. Criteria for an increased specificity of MRI interpretation in elderly subjects with suspected multiple sclerosis. *Neurology* 1988; 38:1822-1825

Felgenhauer K. Psychiatric disorders in the encephalitic form of multiple sclerosis. *J Neurol* 1990; 237:11-18

Fernando KTM, McLean MA, Chard DT, MacManus DG, *et al*. Elevated white matter myo-inositol in clinically isolated syndromes suggestive of multiple sclerosis. *Brain* 2004; 127:1361-1369

Fernando KT, Tozer DJ, Miszkief KA, Gordon RM, Swanton JK, Dalton CM, Barker GJ, Plant GT, Thompson AJ, Miller DH. Magnetization transfer histograms in clinically isolated syndromes suggestive of multiple sclerosis. *Brain*. 2005;128:2911-25

Filippi M, Barker GJ, Horsfield MA, *et al*. Benign and secondary progressive multiple sclerosis: a preliminary quantitative MRI study. *J Neurol* 1994;241:246-251

Filippi M, Campi A, Colombo B, Pereira C, Martinelli V, *et al*. A spinal cord MRI study of benign and secondary progressive multiple sclerosis. *J Neurol* 1996; 243:502-505

Filippi M, Paty DW, Kappos L, Barkhof F, Compston DA, Thompson AJ, *et al*. Correlations between changes in disability and T2 weighted brain MRI activity in multiple sclerosis: a follow up study. *Neurology* 1995; 45:255-60

Filippi M, Preziosa P, Copetti M, *et al*. Gray matter damage predicts the accumulation of disability 13 years later in MS. *Neurology*. 2013;81:1759-67

Filippi M, Roccas MA, Comi G. The use of quantitative magnetic-resonance-based techniques to monitor the evolution of multiple sclerosis. *Lancet Neurology* 2003; 2:337-46

Fischer J, Rudick RA, Cutter G, Reingold S. The Multiple Sclerosis Functional Composite Measure (MSFC): an integrated approach to MS clinical outcome assessment. National MS society clinical outcomes assessment task force. *Mult Scler*. 1999;5:244-50

Fisher E, Lee JC, Nakamura K, Rudick RA. Gray matter atrophy in multiple sclerosis: a longitudinal study. *Ann Neurol* 2008;64:255-65

- Fisniku LK, Brex PA, Altmann DR, *et al.* Disability and T2 MRI lesions: a 20-year follow-up of patients with relapse onset multiple sclerosis. *Brain* 2008; 131:808-817
- Fisniku LK, Chard DT, Jackson JS, *et al.* Gray matter atrophy is related to long-term disability in multiple sclerosis. *Ann Neurol* 2008;64:247-254
- Fog T. Topographical distribution of plaques in the spinal cord of multiple sclerosis. *Archives of Neurology and psychiatry.* 1950; 63:382-414
- Freund P, Wheeler-Kingshott C, Jackson J, *et al.* Recovery after spinal cord relapse in multiple sclerosis is predicted by radial diffusivity. *Mult Scler.* 2010;16:1193-202
- Frischer JM, Bramow S, Dal-Bianco A, Lucchinetti CF, Rauschka H, Schmidbauer M, *et al.* The relation between inflammation and neurodegeneration in multiple sclerosis brains. *Brain* 2009;132;1175-89
- Frohman EM, Zhang H, Kramer PD, Fleckenstein J, *et al.* MRI characteristics of the MLF in MS patients with chronic internuclear ophthalmoparesis. *Neurology* 2001; 57:762-768
- Frommann C. Untersuchungen über die Gewebsveränderungen bei der Multiplen Sklerose des Gehirns und Rückenmarks 1878 pp. 1-123 Jena: Gustav Fischer
- Furby J, Hayton T, Altmann D, Brenner R, Chataway J, Smith KJ, *et al.* A longitudinal study of MRI-detected atrophy in secondary progressive multiple sclerosis. *J Neurol.* 2010;257:1508-16
- Ganter P, Prince C, Esiri MM. Spinal cord axonal loss in multiple sclerosis: a post-mortem study. *Neuropath and Appl Neurobiol* 1999; 25:459-467
- Gay FW, Drye TJ, Dick GW, Esiri MM. The application of multifactorial cluster analysis in the staging of plaques in early multiple sclerosis: identification and characterisation of primary demyelinating lesion. *Brain* 1997; 114:557-572
- Ge Y, Grossman RI, Udupa JK, Babb JS, Nyúl LG, Kolson DL. Brain atrophy in relapsing-remitting multiple sclerosis: fractional volumetric analysis of gray and white matter. *Radiology* 2001;220:606-610
- Geurts JJ, Barkhof F. Grey matter pathology in multiple sclerosis. *Lancet Neurol* 2008; 7:841-851
- Geurts JJ, Bö L, Pouwels PJ, Castelijns JA, Polman CH, Barkhof F. Cortical lesions in multiple sclerosis: combined postmortem MR imaging and histopathology. *AJNR Am J Neuroradiol.* 2005;26:572-7
- Geurts JJ, Pouwels PJ, Uitdehaag BM, Polman C, *et al.* Intracortical Lesions in Multiple Sclerosis: Improved Detection with 3D Double Inversion-Recovery MR Imaging. *Radiology* 2005; 236:254-260

Ghadirian P, Dadgostar B, Azani R, Maisonneuve P. A case-control study of the association between socio-demographic, lifestyle and medical history factors and multiple sclerosis. *Can J Public Health* 2001; 92:281-285

Gilmore CP, Bo L, Owens T, Lowe J, *et al.* Spinal cord gray matter demyelination in multiple sclerosis: a novel pattern of residual plaque morphology. *Brain Pathol* 2006; 16:202-208

Gilmore CP, DeLuca GC, Bö L, *et al.* Spinal cord atrophy in multiple sclerosis caused by white matter volume loss. *Arch Neurol.* 2005;62:1859-62

Gilmore CP, DeLuca GC, Bö L, *et al.* Spinal cord neuronal pathology in multiple sclerosis. *Brain Pathol* 2009;19:642-9

Gilmore CP, Donaldson I, Bö L, *et al.* Regional variations in the extent and pattern of grey matter demyelination in multiple sclerosis: a comparison between the cerebral cortex, cerebellar cortex, deep grey matter nuclei and the spinal cord. *J Neurol Neurosurg Psychiatry.* 2009;80:182-7

Gilmore CP, Geurts JJ, Evangelou N, Bot JC, van Schijndel RA, Pouwels PJ, *et al.* Spinal cord grey matter lesions in multiple sclerosis detected by post-mortem high field MR imaging. *Mult Scler.* 2009;15:180-8

Goldberg P. Multiple Sclerosis: vitamin D and calcium as environmental determinants of prevalence (a viewpoint). Part I: sunlight, dietary factors and epidemiology. *Int J Environ Stud* 1974; 6:19-27

Goodin DS. The causal cascade to multiple sclerosis: a model for pathogenesis. *PLoS One* 2009;4:e4565

Goodin DS, Reder AT, Ebers GC, Cutter G, Kremenchutzky M, Oger J, *et al.* Survival in MS: a randomized cohort study 21 years after the start of the pivotal IFN $\beta$ -1b trial. *Neurology* 2012;78:1315-22

Goodkin DE, Hertsgaard D, Seminary J. Upper extremity function in multiple sclerosis: improving assessment sensitivity with box-and-block and nine-hole peg test. *Arch Phys Med Rehabil* 1988; 69:850-4

Graham NM. The epidemiology of acute respiratory infections in children and adults: a global perspective. *Epidemiol Rev* 1990; 12:149-178

Hafler DA, Compston A, Sawcer S, *et al*; International Multiple Sclerosis Genetics Consortium. Risk alleles for multiple sclerosis identified by a genomewide study. *N Engl J Med.* 2007; 357(9):851-862

Haines JL, Ter-Minassian M, Bazyk A *et al.* Multiple Sclerosis Genetics Group. A complete genomic screen for multiple sclerosis underscores a role for the major histocompatibility complex. *Nat Genet.* 1996; 13(4):469-471

Harris JO, Frank JA, Patronas NJ, McFarlin DF, McFarland HF. Serial gadolinium-enhanced magnetic resonance imaging scans in patients with early relapsing

remitting multiple sclerosis: implications for clinical trials and natural history. *Ann Neurol* 1991; 29:548-555

Healy BC, Arora A, Hayden MA, et al. Approaches to normalization of spinal cord volume: application to multiple sclerosis. *J Neuroimaging* 2012;22:e12-9

Hernan MA, Jick SS, Logroscino G, et al. Cigarette smoking and the progression of multiple sclerosis. *Brain* 2005; 128:1461-1465

Hernan MA, Olek MJ, Ascherio A. Cigarette smoking and incidence of multiple sclerosis. *Am J Epidemiol* 2001; 154:69-74

Hesseltine SM, Law M, Babb J, et al. Diffusion tensor imaging in multiple sclerosis: assessment of regional differences in the axial plane within normal-appearing cervical spinal cord. *AJNR Am J Neuroradiol.* 2006;27:1189-93

Heun R, Kappos L, Bittkau S, Städt D, et al. Magnetic resonance imaging and early diagnosis of multiple sclerosis. *Lancet* 1988; 2:1202-1203

Hickman SJ, Coulon O, Parker GJ, et al. Application of a B-spline active surface technique to the measurement of cervical cord volume in multiple sclerosis from three-dimensional MR images. *J Magn Reson Imaging* 2003;18(3):368-371

Hinks RS, Quencer RM. Motion artefacts in brain and spine MR. *Radiol Clin North Am* 1988; 26:737-53

Hobart J, Freeman J, Thompson A. Kurtzke scales revisited: the application of psychometric methods to clinical intuition. *Brain* 2000; 123:1027-1040

Holick MF. Sunlight and vitamin D for bone health and prevention of autoimmune diseases, cancers, and cardiovascular disease. *Am J Clin Nutr* 2004; 80:1678S-1688S

Horsfield MA, Sala S, Neema M, Absinta M, Bakshi A, Sormani MP, et al. Rapid semi-automatic segmentation of the spinal cord from the magnetic resonance images: Application in multiple sclerosis. *Neuroimage* 2010;50:446-455

Horton R, Wilming L, Rand V, Lovering RC, et al. Gene map of the extended human MHC. *Nat Rev Genet* 2004; 5:899-99

Hou P, Hasan KM, Sitton CW, et al. Phase-Sensitive T1 inversion recovery Imaging: A time-Efficient Interleaved Technique for Improve Tissue contrast in Neuroimaging. *AJNR Am J Neuroradiol* 2005; 26:1432-1438

Howell OW, Reeves CA, Nicholas R, Carassiti D, Radotra B, Gentleman SM, et al. Meningeal inflammation is widespread and linked to cortical pathology in multiple sclerosis. *Brain* 2011;134:2755-71

Hua K, Zhang J, Wakana S, et al. Tract probability maps in stereotactic spaces: analyses of white matter anatomy and tract-specific quantification. *Neuroimage* 2008; 39:336-347

- Huber, P.J. (1967). The behavior of maximum likelihood estimates under non-standard conditions. In Proceedings of the Fifth Berkeley Symposium on Mathematical Statistics and Probability. Berkeley, Ca: University of California Press, 1:221-233, 1967
- Hume AL, Waxman SG. Evoked potentials in suspected multiple sclerosis: diagnostic value and prediction of clinical course. *J Neurol Sci* 1988; 83:191-210.
- Hunter SF, Hafler DA. Ubiquitous pathogens: links between infection and autoimmunity and MS? *Neurology* 2000; 55:164-165
- Ikuta F, Zimmerman HM. Distribution of plaques in seventy autopsy cases of multiple sclerosis in the United States. *Neurology* 1976; 8:26-28
- International Multiple Sclerosis Genetics Consortium (IMSGC). Analysis of immune-related loci identifies 48 new susceptibility variants for multiple sclerosis. *Nat Genet* 2013;45:1353-60
- International Multiple Sclerosis Genetics Consortium (IMSGC). Risk Alleles for Multiple Sclerosis Identified by a Genomewide Study. *N Eng J Med* 2007; 357:851-862
- Jakkula E, Leppä V, Sulonen AM, Varilo T, *et al.* Genome-wide association study in a high-risk isolate for multiple sclerosis reveals associated variants in STAT3 Gene. *Am J Hum Genet* 2010; 86:285-291
- Junger SS, Stern BJ, Levine SR, Sipos E, Marti-Masso JF. Intramedullary spinal sarcoidosis: clinical and magnetic resonance imaging characteristics. *Neurology* 1993; 43:333-337
- Kalkers NF, Barkhof F, Bergers E, van Schijndel R, Polman CH. The effect of the neuroprotective agent riluzole on MRI parameters in primary progressive multiple sclerosis: a pilot study. *Mult. Scler.* 2002;8:532-533.
- Kampman MT, Brustad M. Vitamin D: a candidate for the environmental effect in multiple sclerosis – observations from Norway. *Neuroepidemiology* 2008; 30:140-6
- Kapoor R, Furby J, Hayton T, Smith KJ, Altmann DR, Brenner R, *et al.* Lamotrigine for neuroprotection in secondary progressive multiple sclerosis: a randomised, double-blind, placebo-controlled, parallel-group trial. *Lancet Neurol* 2010;9:681-688
- Kappos L, Moeri D, Radue EW, *et al.* for the Gadolinium MRI Meta-analysis Group. Predictive value of gadolinium-enhanced MRI for relapse rate and changes in disability or impairment in multiple sclerosis: a meta-analysis. *Lancet* 1999; 353:964-69
- Kappos L, Radue EW, O'Connor P, Polman C, Hohlfeld R, Calabresi P, *et al.* A placebo controlled trial of oral fingolimod in relapsing multiple sclerosis. *N Eng J Med* 2010;362:387-401

- Kebir H, Kreymborg K, Ifergan I, *et al.* Human T(H)17 lymphocytes promote blood brain barrier disruption and central nervous system inflammation. *Nat Med* 2007; 13:1173-1175
- Keiper MD, Grossman RI, Brunson JC, Schnall MD. The low sensitivity of fluid attenuated inversion recovery MR in the detection of multiple sclerosis of the spinal cord. *AJNR Am J Neuroradiol* 1997; 18:1035-39
- Kendi ATK, Tan FU, Kendi M, Huvaj S, Tellioglu S. MR spectroscopy of cervical spinal cord in patients with multiple sclerosis. *Neuroradiology* 2004; 46:764-769
- Kesselring J, Miller DH, Robb SA, *et al.* Acute disseminated encephalomyelitis. MRI findings and the distinction from multiple sclerosis. *Brain* 1990; 113:291-302
- Khaleeli Z, Ciccarelli O, Manfredonia F, Barkhof F, *et al.* Predicting progression in primary progressive multiple sclerosis: a 10-year multicentre study. *Ann Neurol* 2008; 63:790-793
- Kidd D, Thorpe JW, Thompson AJ, Kendall BE *et al.* Spinal cord MRI using multi-array coils and fast spin echo. II. Findings in multiple sclerosis. *Neurology* 1993; 43:2632-2637
- Kirkwood BR, Sterne JAC. *Essential medical statistics*, 2nd edition, Oxford, Blackwell Science; 2003. 37p, 364-365p.
- Klawiter EC, Schmidt RE, Trinkaus K, *et al.* Radial diffusivity predicts demyelination in ex vivo multiple sclerosis spinal cords. *Neuroimage*. 2011;55:1454-60
- Kremenutzky M, Rice GP, Baskerville J, Wingerchuck DM, Ebers GC. The natural history of multiple sclerosis: a geographically based study 9: observations on the progressive phase of the disease. *Brain* 2006; 129:584-594
- Krumbholz M, Theil D, Derfuss T, Rosenwald A, Schrader F, Monoranu CM, *et al.* BAFF is produced by astrocytes and up-regulated in multiple sclerosis lesions and primary central nervous system lymphoma. *J Exp Med* 2005;201:195-200
- Kurtzke JF. A Reassessment of the distribution of multiple sclerosis. *Acta Neurol Scandinav* 1975; 51:110-136
- Kurtzke JF. Epidemiologic Evidence for Multiple Sclerosis as an Infection. *Clin Microbiol Rev* 1993; 6:382-427
- Kurtzke JF. On the evaluation of disability in multiple sclerosis. *Neurology* 1961; 11:686-694
- Kurtzke JF. Rating neurologic impairment in multiple sclerosis: an expanded disability status scale (EDSS). *Neurology* 1983; 33:1444-52
- Kutzelnigg A, Lucchinetti CF, Stadelmann C, *et al.* Cortical demyelination and diffuse white matter injury in multiple sclerosis. *Brain* 2005; 128:2705-2712

- Lacour A, De Seze J, Revenco E, *et al.* Acute aphasia in multiple sclerosis: a multicentre study of 22 patients. *Neurology* 2004; 62:974-977
- Lang HLE, Jacobsen H, Ikemizu S, Andersson C, *et al.* A functional and structural basis for TCR cross-reactivity in multiple sclerosis. *Nat Immunol* 2002; 3:940-43
- Langrish CL, Chen Y, Blumenschein WM, *et al.* IL-23 drives a pathogenic T cell population that induces autoimmune inflammation. *J Exp Med* 2005; 201:233-40
- Lassmann H. The pathology of multiple sclerosis and its evolution. *Phil Trans R Soc Lond* 1999; 354:1635-1640
- Laurent D, Wasvary J, Yin J, Rudin M, Pellas TC, O'Byrne E. Quantitative and qualitative assessment of articular cartilage in the goat knee with magnetization transfer imaging. *Magn Reson Imaging*. 2001;19:1279-86
- Lavdas E, Vlychou M, Arikidis N, Kapsalaki E, Roka V, Fezoulididis I. Comparison of T1-weighted fast spin-echo and T1-weighted fluid-attenuated inversion recovery images of the lumbar spine at 3.0 Tesla. *Acta. Radiol.* 2010;51:290-5.
- Leary SM, Miller DH, Stevenson VL, Brex PA, Chard DT, Thompson AJ. Interferon beta-1a in primary progressive MS: an exploratory, randomized, controlled trial. *Neurology* 2003;60:44-51
- Le Bihan D, Turner R, Pekar J, Moonen CTW. Diffusion an perfusion imaging by gradient sensitisation: design, strategy and significance. *J Magn Reson Imaging* 1991; 1:7-8
- Lee JK, Choi HY, Lee SW, *et al.* Usefulness of T1-weighted image with fast inversion recovery technique in intracranial lesions: comparison with T1-weighted spin echo sequence. *Clin Imaging* 2000; 24:263-269
- Leibowitz U, Antonovsky A, Medalie JM, *et al.* Epidemiological study of multiple sclerosis in Israel. II. Multiple Sclerosis and level of sanitation. *J Neurol Neurosurg Psychiatry* 1966; 29:60-68
- Lennon VA, Wingerchuck DM, Kryzer TJ, Pittock SJ, *et al.* A serum antibody marker of neuromyelitis optica: distinction from multiple sclerosis. *Lancet* 2004; 364:2106-2112
- Leray E, Yaouanq J, Le Page E, *et al.* Evidence for a two-sage disability progression in multiple sclerosis. *Brain* 2010;133:1900-13
- Levy LM, Di Chiro G, Brooks RA, Dwyer AJ, Wener L, Frank J. Spinal cord artefacts from truncation errors during MR imaging. *Radiology* 1988; 166:479-83
- Lin X, Tench CR, Turner B, Blumhardt LD, Constantinescu CS. Spinal cord atrophy and disability in multiple sclerosis over four years: application of a reproducible automated technique in monitoring disease progression in a cohort of the interferon  $\beta$ -1a (Rebif) treatment trial. *J Neurol Neurosurg Psychiatry* 2003; 74:1090-1094

Loevner LA, Grossman RI, McGowan JC, Ramer KN, Cohen JA. Characterization of multiple sclerosis plaques with T1-weighted MR and quantitative magnetization transfer. *AJNR Am J Neuroradiol.* 1995;16:1473-9

Losseff N, Lai M, Miller DH, McDonald WI, Thompson AJ. The prognostic value of serial axial cord area measurement by magnetic resonance imaging (MRI) in multiple sclerosis (MS) (abstract) *J Neurol* 1995; 242 Suppl 2: S 110

Losseff NA, Webb SL, O'Riordan JI, Page R, *et al.* Spinal cord atrophy and disability in multiple sclerosis. A new reproducible and sensitive MRI method with potential to monitor disease progression. *Brain* 1996; 119:701-708

Lovas G, Szilágyi N, Majtényi K, *et al.* Axonal changes in chronic demyelinated cervical spinal cord plaques. *Brain* 2000;123:308-17

Lovato L, Willis SN, Rodig SJ, Caron T, Almendinger SE, Howell OW, *et al.* Related B cell clones populate the meninges and parenchyma of patients with multiple sclerosis. *Brain* 2011;134;534-41

Lublin FD, Reingold SC. Defining the clinical course of multiple sclerosis: results of an international survey. National Multiple Sclerosis Society (USA) Advisory Committee on Clinical Trials of New Agents in Multiple Sclerosis. *Neurology* 1996; 46:907-911

Lublin FD, Reingold SC, Cohen JA, Cutter GR, Sørensen PS, Thompson AJ, *et al.* Defining the clinical course of multiple sclerosis: The 2013 revisions. *Neurology.* 2014 May 28. [Epub ahead of print]

Lucchinetti CF, Popescu BF, Bunyan RF, Moll NM, Roemer SF, Lassmann H, *et al.* Inflammatory cortical demyelination in early multiple sclerosis. *N Engl J Med* 2011;365:2188-97

Lukas C, Sombekke MH, Bellenberg B, *et al.* Relevance of Spinal Cord Abnormalities to Clinical Disability in Multiple Sclerosis: MR Imaging Findings in a Large Cohort of Patients. *Radiology.* 2013;269(2):542-52

Lycklama à Nijeholt, Barkhof F, Scheltens P, Castelijns JA, *et al.* MR of the Spinal Cord in Multiple Sclerosis: Relation to clinical subtype and Disability. *AJNR Am J Neuroradiol* 1997; 18:1041-1048

Lycklama à Nijeholt GJ, Bergers E, Kamphorst W, *et al.* Post-mortem high resolution MRI of the spinal cord in multiple sclerosis. A correlative study with conventional MRI, histopathology and clinical phenotype. *Brain* 2001; 124:154-166

Lycklama à Nijeholt G, Thompson, Filippi M, Miller D, Polman C, Fazekas F, Barkhof F. Spinal-cord MRI in multiple sclerosis. *Lancet Neurol* 2003; 2:555-62

Lycklama à Nijeholt G, van Walderveen MA, Castelijns JA, *et al.* Brain and spinal cord abnormalities in multiple sclerosis: correlation between MRI parameters, clinical subtypes and symptoms. *Brain* 1998; 121:687-97

- Magliozzi R, Howell OW, Reeves C, Roncaroli F, Nicholas R, Serafini B, et al. A gradient of neuronal loss and meningeal inflammation in multiple sclerosis. *Ann Neurol* 2010;68:477-93
- Magliozzi R, Howell O, Vora A, Serafini B, Nicholas R, Puopolo M, et al. Meningeal B-cell follicle in secondary progressive multiple sclerosis associate with early onset of disease and severe cortical pathology. *Brain* 2007;130:1089-104
- Mainero C, Benner T, Radding A, et al. In vivo imaging of cortical pathology in multiple sclerosis using ultra-high field MRI. *Neurology* 2009;73:941-948
- Martin N, Malfair D, Zhao Y, et al. Comparison of MERGE and axial T2-weighted fast spin-echo sequences for detection of multiple sclerosis lesions in the cervical spinal cord. *AJR Am J Roentgenol.* 2012;199:157-162
- Mascalchi M, Dal Pozzo G, Bartolozzi C. Effectiveness of the short T1 inversion recovery (STIR) sequence in MR imaging of intramedullary spinal lesions. *Magn Reson Imaging* 1993; 11(1):17-25
- Maynard FM Jr, Bracken MB, Creasey G, Ditunno JF Jr, Donovan WH, Ducker TB, et al. International Standards for Neurological and Functional Classification of Spinal Cord Injury. American Spinal Injury Association. *Spinal Cord.* 1997;35:266-74
- McDonald I, Compston A. The symptoms and signs of multiple sclerosis. *McAlpine's Multiple Sclerosis*, 4<sup>th</sup> edition, Churchill Livingstone, Elsevier 2006.
- McDonald WI, Compston A, Edan G, *et al.* Recommended diagnostic criteria for multiple sclerosis: guidelines from the International Panel on the diagnosis of multiple sclerosis. *Ann Neurol* 2001; 50:121-127
- McDonnell GV, Hawkins SA. Clinical study of primary progressive multiple sclerosis in Northern Ireland, UK. *J Neurol Neurosurg Psychiatry* 1998;64:451-4
- McGavern DB, Murray PD, Rivera-Quiñones C, Schmelzer JD, Low PA, Rodriguez M. Axonal loss results in spinal cord atrophy, electrophysiological abnormalities and neurological deficits following demyelination in a chronic inflammatory model of multiple sclerosis. *Brain.* 2000;123:519-31
- Meinl E, Krumbholz M, Derfuss T, Junker A, Hohlfeld R. Compartmentalization of inflammation in the CNS: A major mechanism driving progressive multiple sclerosis. *J Neurol Sci* 2008; 274: 42-4
- Mezzapesa DM, Rocca MA, Falini A, Rodegher ME, Ghezzi A, Comi G, Filippi M. A preliminary diffusion tensor and magnetization transfer magnetic resonance imaging study of early-onset multiple sclerosis. *Arch Neurol.* 2004;61:366-8
- McFarland HF, Frank JA, Albert PS, *et al.* Using gadolinium enhanced magnetic resonance imaging lesions to monitor disease activity in multiple sclerosis. *Ann Neurol* 1992; 32:758-766

- Mikulis DJ, Wood MI, Zerodener OA, Poncelet BP. Oscillatory motion of the normal cervical spinal cord. *Radiology* 1994; 192:117-21
- Millen JW, Woollam DH. On the nature of the pia mater. *Brain* 1961;84:514-20
- Miller DH, Barkhof F, Nauta JJ. Gadolinium enhancement increases the sensitivity of MRI in detecting disease activity in multiple sclerosis. *Brain* 1993; 116:1077-1094
- Miller DH, McDonald WI, Blumhardt LD, *et al.* Magnetic resonance imaging in isolated non-compressive spinal cord syndromes. *Ann Neurol* 1987; 22:714-723
- Miller DH, Rudge P, Johnson G *et al.* Serial gadolinium enhanced magnetic resonance imaging in multiple sclerosis. *Brain* 1988; 111:927-939
- Miller DH, Soon D, Fernando KT, MacManus DG, Barker GJ, Yousry TA, *et al.* MRI outcomes in a placebo-controlled trial of natalizumab in relapsing MS. *Neurology* 2007;68:1390-1401
- Miller DH, Weinshenker BG, Filippi, Banwell BL, *et al.* Differential diagnosis of suspected multiple sclerosis: a consensus approach. *Mult Scler* 2008; 14: 1157-1174
- Moll NM, Cossoy MB, Fisher E, Staugaitis SM, Tucky BH, Rietsch AM, *et al.* Imaging correlates of leukocyte accumulation and CXCR4/CXCL12 in multiple sclerosis. *Arch Neurol.* 2009;66:44-53
- Molyneux PD, Barker GJ, Barkhof F, *et al.* for the European Study Group on Interferon beta-1b in secondary progressive MS. Clinical-MRI correlations in a European trial of interferon beta-1b in secondary progressive MS. *Neurology* 2001; 57:2191-97
- Montalban X, Sastre-Garriga J, Tintoré M, *et al.* A single-center, randomized, double-blind, placebo-controlled study of interferon beta-1b on primary progressive and transitional multiple sclerosis. *Mult Scler* 2009;15(10):1195-1205
- Montalban X, Tintoré M, Swanton J, Barkhof F, *et al.* MRI criteria for MS in patients with clinically isolated syndromes. *Neurology* 2010; 74:427-434
- Mottershead JP, Schmierer K, Clemence M, Thornton JS, *et al.* High field MRI correlates of myelin content and axonal density in multiple sclerosis. A post-mortem study of the spinal cord. *J Neurol* 2003; 250:1293-1301
- Mouritzen Dam A. Shrinkage of the brain during histological procedures with fixation in formaldehyde solutions of different concentrations. *J Hirnforsch* 1979;20:115-119
- Mowry EM, Deen S, Malikova I, Pelletier J, Bachetti P, Waubant E. The onset location of multiple sclerosis predicts the location of subsequent relapses. *J Neurol Neurosurg Psychiatry.* 2009; 80:400-403

Mugler JP III, Brookoeman JR. Three-Dimensional Magnetization-Prepared Rapid Gradient-Echo Imaging (3D MP RAGE). *Magn Reson Med* 1990; 15:152-157

Mumford CJ, Wood NW, Kellar-Wood H, Thorpe JW, *et al.* The British Isles survey of multiple sclerosis in twins. *Neurology* 1994; 44:11-5

Naismith RT, Xu J, Tutlam NT, *et al.* Radial diffusivity in remote optic neuritis discriminates visual outcomes. *Neurology*. 2010;74:1702-10

Naismith RT, Xu J, Klawiter EC, *et al.* Spinal cord tract diffusion tensor imaging reveals disability substrate in demyelinating disease. *Neurology*. 2013;80:2201-9

Nesbit GM, Forbes GS, Scheithauer BW, Okazaki H, *et al.* Multiple sclerosis: histopathologic and MR and/or CT correlation in 37 cases at biopsy and three cases at autopsy. *Radiology* 1991; 180:467-474

Nelson F, Poonawalla AH, Hou P, Huang F, *et al.* Improved Identification of Intracortical Lesions in Multiple Sclerosis with Phase-Sensitive Inversion Recovery in Combination with Fast Double Inversion Recovery MR Imaging. *AJNR Am J Neuroradiol* 2007; 28:1645-49

Nelson F, Poonawalla A, Hou P, Wolinsky JS, Narayana PA. 3D MPRAGE improves classification of cortical lesions in multiple sclerosis. *Multiple Sclerosis* 2008; 14:1214-1219

Nijeholt GJ, van Walderveen MA, Castelijns JA, *et al.* Brain and spinal cord abnormalities in multiple sclerosis. Correlation between MRI parameters, clinical subtypes and symptoms. *Brain*. 1998;121:687-97

Noseworthy J, Lucchinetti C, Rodriguez M, Weinshenker BG. Multiple Sclerosis. *N Engl J Med* 2000; 343(13):938-952

Oh J, Saidha S, Chen M, *et al.* Spinal cord quantitative MRI discriminates between disability levels in multiple sclerosis. *Neurology* 2013;80:540-7

Oh J, Zackowski K, Chen M, Newsome S, Saidha S, Smith SA, *et al.* Multiparametric MRI correlates of sensorimotor function in the spinal cord in multiple sclerosis. *Mult Scler* 2013;19:427-35

Olerup O, Hilbert J. HLA class II-associated genetic susceptibility in multiple sclerosis: a critical evaluation. *Tissue Antigens* 1991; 38:1-15

Oppenheimer DR. The cervical cord in multiple sclerosis. *Neuropathol Appl Neurobiol* 1978; 4:151-62

O'Riordan JI, Losseff NA, Phatouros C, Thompson AJ, *et al.* Asymptomatic spinal cord lesions in clinically isolated optic nerve, brain stem and spinal cord syndromes suggestive of demyelination. *J Neurol Neurosurg Psychiatry* 1998; 64:353-357

Ormerod IE, Miller DH, McDonald WI, *et al.* The role of NMR imaging in the assessment of multiple sclerosis and isolated neurological lesions: a quantitative study. *Brain* 1987; 110:1579-1616

- Orton SM, Herrera BM, Yee IM, Valdar W, *et al.* Sex ratio of multiple sclerosis in Canada: a longitudinal study. *Lancet Neurol* 2006; 5:932-36
- Pan JW, Krupp LB, Elkins LE, Coyle PK. Cognitive dysfunction lateralises with NAA in multiple sclerosis. *Appl Neuropsychol* 2001; 8:155-160
- Paty DW, Li DK, the UBC MS/MRI Study Group and the IFNB Multiple Sclerosis Study Group. Interferon beta-1b is effective in relapsing-remitting multiple sclerosis. II. MRI analysis results of a multicenter, randomized, double-blind, placebo controlled trial. *Neurology* 1993; 43:662-667
- Paty DW, Oger JFF, Kastrukoff LF, Hashimoto SA, *et al.* MRI in the diagnosis of MS: A prospective study with comparison of clinical evaluation, evoked potentials, oligoclonal banding, and CT. *Neurology* 1988; 38:180-185
- Peterson JW, Bö L, Mörk S, Chang A, Trapp BD. Transected neurites, apoptotic neurons, and reduced inflammation in cortical multiple sclerosis lesions. *Ann Neurol.* 2001;50:389-400
- Phadke JG, Best PV. Atypical and clinically silent multiple sclerosis: a report of 12 cases discovered unexpectedly at necropsy. *J Neurol Neurosurg Psychiatry* 1983; 46:414-420
- Pierrot-Deseilligny C and Souberbielle JC. Is hypovitaminosis D one of the environmental risk factors for multiple sclerosis? *Brain* 2010; 133:1869-1888
- Piperpaoli C, Jezzard P, Basser PJ, Barnett A, Di Chiro G. Diffusion tensor MR imaging of the human brain. *Radiology* 1996; 201:637-648
- Polman CH, O'Connor PW, Havrdova E, Hutchinson M, Kappos L, Miller DH, *et al.* A randomized, placebo-controlled trial of natalizumab for relapsing remitting multiple sclerosis. *N Eng J Med* 2006;354:899-910
- Polman C, Reingold S, Banwell B, Clanet M, Cohen JA, *et al.* Diagnostic Criteria for Multiple Sclerosis: 2010 Revisions to the McDonald Criteria. *Ann Neurol* 2011;69:292-302
- Polman C, Reingold S, Edan G, Filippi M, *et al.* Diagnostic Criteria for Multiple Sclerosis: 2005 Revisions to the 'McDonald Criteria'. *Ann Neurol* 2005; 58:840-846
- Poonawalla AH, Hou P, Nelson F, Wolinski JS, Narayana PA. Cervical Spinal Cord Lesions in Multiple Sclerosis: T1-weighted Inversion-Recovery MR imaging with Phase-Sensitive Reconstruction. *Radiology* 2008; 246:258-264
- Poser CM, Paty DW, Scheinberg L, McDonald WI, *et al.* New Diagnostic Criteria for Multiple Sclerosis: Guidelines for Research Protocols. 1983; 13:227-231
- Poskanzer DC, Walker AM, Yonkondy J, Sheridan JL. Studies in the epidemiology of multiple sclerosis in the Orkney and Shetland Islands. *Neurology* 1976; 26:14-17

- Provenzale JM, Barboriak DP, Gaensler EH, Robertson RL, Mercer B. Lupus related myelitis: serial MR findings. *Am J Neuroradiology* 1994; 15:1911-1917
- Radue EW, O'Connor P, Polman CH, Hohlfeld R, Calabresi P, Selmaj K, et al. Impact of Fingolimod Therapy on Magnetic Resonance Imaging Outcomes in Patients with Multiple Sclerosis. *Arch Neurol* 2012;2:1-11
- Ransohoff RM. Immunology: in the beginning. *Nature* 2009;492:41-2
- Rashid W, Davies GR, Chard DT, et al. Increasing cord atrophy in early relapsing-remitting multiple sclerosis: a 3 year study. *J. Neurol. Neurosurg. Psychiatry* 2006;77;51-55.
- Rao SM, Leo GJ, Bernardin L, et al. Cognitive dysfunction in multiple sclerosis. I. Frequency, patterns, and prediction. *Neurology* 1991;41:685-689
- Raz E, Bester M, Sigmund EE, et al. A better characterization of spinal cord damage in multiple sclerosis: a diffusional kurtosis imaging study. *AJNR Am J Neuroradiol.* 2013 Sep;34(9):1846-52
- Reich D, Ozturk A, Calabresi, Mori S. Automated vs conventional tractography in multiple sclerosis: variability and correlation with disability. *Neuroimage* 2010; 49:3047-3056
- Reid JD. Effects of flexion-extension movements of the head and spine upon the spinal cord and nerve roots. *J Neurol Neurosurg Psychiat* 1960;23:214-221
- Reina MA, De León Casasola Ode L, Villanueva MC, López A, Machés F, De Andrés JA. Ultrastructural findings in human spinal pia mater in relation to subarachnoid anesthesia. *Anesth Analg.* 2004;98:1479-85
- Rindfleisch E. Histologisches Detail Zur grauen Degeneration von Gehirn und Rueckenmark. *Arch Pathol Anat Physiol Klin Med (Virchow)* 1863; 26:474-483
- Robertson NP, O'Riordan JI, Chataway J, Kingsley DP, et al. Offspring recurrence rates and clinical characteristics of conjugal multiple sclerosis. *Lancet* 1997; 349:1587-90
- Robertson WD, Li D, Mayo J, Genton M, et al. Magnetic resonance imaging in the diagnosis of multiple sclerosis. *J Neurol* 1985; 232(suppl 1):58
- Rocca MA, Horsfield MA, Sala S, Copetti M, Valsasina P, Mesaros S, et al. A multicenter assessment of cervical cord atrophy among MS clinical phenotypes. *Neurology* 2011;76:2096-2102
- Rocca M, Mastronardo G, Mark A, Horsfield M, et al. Comparison of Three MR sequences for the Detection of Cervical Cord Lesions in Patients with Multiple Sclerosis. *AJNR Am J Neuroradiol* 1999; 20:1710-1716
- Roosendaal SD, Bendfeldt K, Vrenken H, et al. Grey matter volume in a large cohort of MS patients: relation to MRI parameters and disability. *Mult Scler* 2011;17:1098-106

- Rovaris M, Filippi M. Magnetic resonance techniques to monitor disease evolution and treatment trial outcomes in multiple sclerosis. *Curr Opin Neurol* 1999; 12:337-44
- Rovaris M, Gass A, Bammer R, Hickman SJ, *et al.* Diffusion MRI in multiple sclerosis. *Neurology* 2005; 65:1526-1532
- Rovaris M, Inglese M, Viti B, *et al.* The contribution of fast-FLAIR MRI for lesion detection in the brain of patients with systemic autoimmune diseases. *J Neurol* 2000; 247:29-33
- Rovaris M, Riccitelli, Judica E, *et al.* Cognitive impairment and structural brain damage in benign multiple sclerosis. *Neurology* 2008;71:1521-1526
- Rudick RA, Lee JC, Simon J, Fisher E. Significance of T2 lesions in multiple sclerosis: a 13-year longitudinal study. *Ann Neurol* 2006;60:236-242
- Samson RS, Cardoso MJ, Muhlert N, Sethi V, Wheeler-Kingshott CA, Ron M, *et al.* Investigation of outer cortical magnetisation transfer ratio abnormalities in multiple sclerosis clinical subgroups. *Mult Scler.* 2014 Feb 19. [Epub ahead of print]
- Sanna S, Pitzalis M, Zoledziowska M, Zara I, *et al.* Variants within the immunoregulatory CBLC gene are associated with multiple sclerosis. *Nat Genet* 2010; 42:495-497
- Sargsyan SA, Shearer AJ, Ritchie AM, Burgoon MP, *et al.* Absence of Epstein-Barr virus in the brain and CSF of patients with multiple sclerosis. *Neurology* 2010; 74:1127-1135
- Sarchielli P, Presciutti O, Pellicoli GP, *et al.* Absolute quantification of brain metabolites by proton magnetic resonance spectroscopy in normal appearing white matter of multiple sclerosis patients. *Brain* 1999; 122:513-21
- Sastre-Garriga J, Ingle GT, Rovaris M, Téllez N. Long-term clinical outcome of primary progressive MS: Predictive value of clinical and MRI data. *Neurology* 2005; 65:633-635
- Sawcer S. The complex genetics of multiple sclerosis: pitfalls and prospects. *Brain* 2008; 131:3118-3131
- Scalfari A, Neuhaus A, Daumer M, Muraro PA, Ebers GC. Onset of secondary progressive phase and long-term evolution of multiple sclerosis. *J Neurol Neurosurg Psychiatry* 2014;85:67-75
- Scalfari A, Neuhaus A, Degenhardt A, Rice GP, *et al.* The natural history of multiple sclerosis, a geographically based study 10: relapses and long-term disability. *Brain* 2010; 133:1914-1929
- Schirmer L, Antel JP, Brück W, Stadelmann C. Axonal loss and neurofilament phosphorylation changes accompany lesion development and clinical progression in multiple sclerosis. *Brain Pathol.* 2011;21:428-40

Schmierer K, Parkes HG, So PW, An SF, Brandner S, Ordidge RJ, et al. High field (9.4 Tesla) magnetic resonance imaging of cortical grey matter lesions in multiple sclerosis. *Brain*. 2010;133:858-67

Schmierer K, Scaravilli F, Altmann DR, et al. Magnetization transfer ratio and myelin in postmortem multiple sclerosis brain. *Ann Neurol*. 2004;56:407-15

Schmierer K, Wheeler-Kingshott CA, Boulby PA, et al. Diffusion tensor imaging of post mortem multiple sclerosis brain. *Neuroimage*. 2007;35:467-77

Schoenen J. Organisation cytoarchitectonique de la moelle épinière de différents mammifères et de l'homme. *Acta Neurol Belg* 1973; 73:348–358.

Schumacher GA, Beebe GW, Kibler RF, Kurland LT, et al. Problems of experimental trials of therapy in multiple sclerosis: report by the panel on the evaluation of experimental trials of therapy in multiple sclerosis. *Ann NY Acad Sci* 1965; 122:552-568

Serafini B, Rosicarelli B, Magliozzi R, Stigliano E, Aloisi F. Detection of ectopic B-cell follicles with germinal centers in the meninges of patients with secondary progressive multiple sclerosis. *Brain Pathol* 2004; 14:164-74

Sethi V, Muhlert N, Ron M, Golay X, et al. MS cortical lesions on DIR: not quite what they seem? *PLoS One* 2013;8:e78879

Sethi V, Yousry TA, Muhlert N, Ron M, et al. Improved detection of cortical MS lesions with phase-sensitive inversion recovery MRI. *J Neurol Neurosurg Psychiatry* 2012;83:877-82

Šidák, Z. K. Rectangular Confidence Regions for the Means of Multivariate Normal Distributions. *Journal of the American Statistical Association* 1967;62:626–633

Simmons ML, Frondoza GC, Coyle JT. Immunocytochemical localisation of N-acetyl-aspartate with monoclonal antibodies. *Neuroscience* 1991; 45:37-45

Simon KC, van der Mei IAF, Munger KL, Ponsonby A, et al. Combined effects of smoking, anti-EBNA antibodies, and *HLA-DRB1\*1501* on multiple sclerosis risk. *Neurology* 2010; 74:1365-1371

Smith ADM, Duckett S, Waters AH. Neuropathological changes in cyanide intoxication. *Nature* 1963; 200:179-181

Smith SA, Jones CK, Gifford A, Belegu V, et al. Reproducibility of tract-specific magnetisation transfer and diffusion tensor imaging in the cervical cord at 3 tesla. *NMR Biomed* 2010; 23:207-217

Smith SM, Jenkinson M, Johansen-Berg H, Rueckert D, Nichols TE, et al. Tract based spatial statistics: voxelwise analysis of multi-subject diffusion data. *Neuroimage* 2006; 31:1487-1505

Soilu-Hänninen M, Laaksonen M, Latinen I, Erälä JP, et al. A longitudinal study of serum 25-hydroxy vitamin D and intact parathyroid hormone levels indicate

- the importance of vitamin D and calcium homeostasis regulation in multiple sclerosis. *J Neurol Neurosurg Psychiatry* 2008; 79:152-7
- Sombekke M, Lukas C, Crusius BA, Tejedor D, *et al.* HLA-DRB1\*1501 and spinal cord magnetic Resonance Imaging Lesions in Multiple Sclerosis. *Arch Neurol.* 2009; 12:1531-1536
- Sombekke MH, Wattjes MP, Balk LJ, Nielsen JM, Vrenken H, Uitdehaag BM, *et al.* Spinal cord lesions in patients with clinically isolated syndrome: a powerful tool in diagnosis and prognosis. *Neurology.* 2013;80:69-75
- Sopori ML, Kozak W. Immunomodulatory effects of cigarette smoke. *J Neuroimmunol* 1998; 83:148-156
- Sormani MP, Li DK, Bruzzi P, Stubinski B, Cornelisse P, Rocak S, *et al.* Combined MRI lesions and relapses as a surrogate marker for disability in multiple sclerosis. *Neurology* 2011;77:1684-90
- Stevenson VL, Leary SM, Losseff NA, Parker GJM, *et al.* Spinal cord atrophy and disability in MS. A longitudinal study. *Neurology* 1998; 51:234-238
- Stevenson VL, Moseley IF, Phatouros CC, Macmanus D, Thompson AJ, Miller DH. Improved imaging of the spinal cord in multiple sclerosis using three-dimensional fast spin echo. *Neuroradiology* 1998; 40:416-19
- Striano P, Striano S, Carreieri PB, Bocella P. Epilepsia partialis continua as a first symptom of multiple sclerosis: electrophysiological study of one case. *Mult Scler* 2003; 9:199-203
- Stroman PW, Wheeler-Kingshott C, Bacon M, Schwab JM, Bosma R, Brooks J, *et al.* The current state-of-the-art of spinal cord imaging: Methods. *Neuroimage.* 2013 May 14. pii: S1053-8119(13)00500-4. doi: 10.1016/j.neuroimage.2013.04.124. [Epub ahead of print]
- Stromnes IM, Cerretti LM, Liggitt D, Harris RA, Goverman JM. Differential regulation of central nervous autoimmunity by T<sub>H</sub>1 and T<sub>H</sub>17 cells. *Nat Med.* 2008; 14(3):337-342
- Swanton JK, Fernando KT, Dalton CM, Miszkiel KA, *et al.* Early MRI in optic neuritis. The risk for disability. *Neurology* 2009; 72:542-550
- Swanton JK, Rovira A, Altmann DR, Barkhof F, *et al.* MRI criteria for multiple sclerosis in patients presenting with clinically isolated syndromes: a multicentre retrospective study. *Lancet Neurol* 2007; 6:677-86
- Tallantyre EC, Bø L, Al-Rawashdeh O, *et al.* Greater loss of axons in primary progressive multiple sclerosis plaques compared to secondary progressive disease. *Brain.* 2009;132:1190-9
- Tallantyre EC, Bø L, Al-Rawashdeh O, *et al.* Clinico-pathological evidence that axonal loss underlies disability in progressive multiple sclerosis. *Mult Scler.* 2010;16:406-11

- Tartaglino LM, Friedman DP, Flanders AE, Lublin FD, *et al.* Multiple sclerosis in the spinal cord: MR appearance and correlation with clinical parameters. *Radiology* 1995; 195:725-732
- Tench CR, Morgan PS, Constantinescu CS. Measurement of cervical spinal cord cross-sectional area by MRI using edge detection and partial volume correction. *J Magn Reson Imaging* 2003;18:368-371.
- Thacker EL, Mizaei F, Ascherio A. Infectious mononucleosis and the risk for multiple sclerosis: a meta-analysis. *Ann Neurol* 2006; 59:499-503
- Thompson AJ, Kermode AG, Wicks D, *et al.* Major differences in the dynamics of primary and secondary progressive multiple sclerosis. *Ann Neurol* 1991; 29:53-62
- Thompson AJ, Polman CH, Miller DH, *et al.* Primary progressive multiple sclerosis. *Brain* 1997;120:1085-96
- Thorogood M, Hannaford PC. The influence of oral contraceptives on the risk of multiple sclerosis. *Br J Obstet Gynaecol* 1998; 105:1296-1299
- Thorpe JW, Kidd D, Moseley IF, Kendall BE, *et al.* Serial gadolinium-enhanced MRI of the brain and spinal cord in early relapsing remitting multiple sclerosis. *Neurology* 1996; 46:373-378
- Thorpe JW, Kidd D, Moseley IF, Thompson AJ, *et al.* Spinal MRI in patients with suspected multiple sclerosis and negative brain MRI. *Brain* 1996; 119:709-714
- Thorpe JW, MacManus DG, Kendall BE, Tofts PS, *et al.* Short Tau inversion recovery fast spin-echo (fast STIR) imaging of the spinal cord in multiple sclerosis. *Magn Reson Imaging* 1994; 12(7):983-989
- Tintoré M, Rovira A, Martínez MJ, Rio J, *et al.* Isolated Demyelinating Syndromes: Comparison of Different MR Imaging Criteria to Predict Conversion to Clinically Definite Multiple Sclerosis. *AJNR Am J Neuroradiol* 2000; 21:702-706
- Trapp BD, Peterson JP, Ransohoff RM, Rudick R, Mörk S, Bö L. Axonal transection in the lesions of multiple sclerosis. *N Eng J Med* 1998;338:278-285
- Turano G, Jones SJ, Miller DH, *et al.* Correlation of SEP abnormalities with brain and cervical cord MRI in multiple sclerosis. *Brain* 1991; 114:663-681
- Udupa J.K, Samarasekera S. Fuzzy connectedness and object definition: theory, algorithms and applications in image segmentation. *Graph. Models Image Process.*, 58 (1996), pp. 246-261
- Ulvestad E, Williams K, Vedeler C, Antel J, *et al.* Reactive microglia in multiple sclerosis lesions have an increased expression of receptors for the Fc part of IgG. *J Neurol Sci* 1994; 121:125-131
- Vaithinanthar L, Tench CR, Morgan PS, Constantinescu CS. Magnetic resonance imaging of the cervical spinal cord in multiple sclerosis. A quantitative T1 relaxation time mapping approach. *J. Neurol.* 2003;250:307-315.

- Valsasina P, Agosta F, Benedetti B, Caputo D, *et al.* Diffusion anisotropy of the cervical cord is strictly associated with disability in ALS. *J Neurol Neurosurg Psychiatry* 2007; 78:480-4
- Valsasina P, Rocca MA, Agosta F, Benedetti B, *et al.* Mean diffusivity and fractional anisotropy histogram analysis of the cervical cord in MS patients. *Neuroimage* 2005; 26:822-8
- Van Hecke W, Nagels G, Emonds G, Leemans A, *et al.* A diffusion Tensor Imaging Group Study of the Spinal Cord in Multiple Sclerosis Patients With and Without T<sub>2</sub> Spinal Cord Lesions. *J Magn Res Med* 2009; 30:25-34
- Van Waesberghe JH, Kamphorst W, De Groot CJ, *et al.* Axonal loss in multiple sclerosis lesions: magnetic resonance imaging insights into substrates of disability. *Ann Neurol* 1999; 46:747-54
- Van Waesberghe JH, van Walderveen MA, Castelijns JA, Scheltens P, *et al.* Patterns of lesion development in multiple sclerosis: longitudinal observations with T1-weighted spin-echo and magnetization transfer MR. *AJNR Am J Neuroradiol* 1998; 19:675-683
- Vella A, Cooper JD, Lowe CE, *et al.* Localisation of a type I diabetes locus in the IL2RA/CD25 region by use of tag single-nucleotide polymorphisms. *Am J Hum Genet* 2005; 76:773-779
- Vercellino M, Plano F, Votta B, Mutani R, Giordana MT, Cavalla P. Grey matter pathology in multiple sclerosis. *J Neuropathol Exp Neurol.* 2005;64:1101-7
- Villard-Mackintosh L, Vessey MP. Oral contraceptives and reproductive factors in multiple sclerosis incidence. *Contraception* 1993; 47:161-168
- Von Essen MR, Kongsbak R, Schjerling P, Olgaard K, *et al.* Vitamin D controls T cell antigen receptor signalling and activation of human T cells. *Nature Immunol* 2010; 11:344-349
- Wattjes MP, Lutterbey GG, Gieseke J, Träber F, *et al.* Double Inversion Recovery Brain Imaging at 3T: Diagnostic Value in the Detection of Multiple Sclerosis Lesions. *AJNR Am J Neuroradiol* 2007; 28:54-59
- Webb AR, Kline L, Hollick MF. Influence of season and latitude of the cutaneous synthesis of vitamin D<sub>3</sub>: exposure to winter sunlight in Boston and Edmonton will not promote vitamin D<sub>3</sub> synthesis in human skin. *J Clin Endocrinol Metabol* 1988; 67:373-378
- Wegner C, Esiri MM, Chance SA, Palace J, Matthews PM. Neocortical neuronal, synaptic, and glial loss in multiple sclerosis. *Neurology* 2006;67(6):960-967
- Weier K, Mazraeh J, Naegelin Y, *et al.* Biplanar MRI for the assessment of the spinal cord in multiple sclerosis. *Mult Scler.* 2012;18(11):1560-9
- Weinshenker BG, Bass B, Rice GPA, Noseworthy J, *et al.* The Natural History of Multiple Sclerosis: A Geographically Based Study. 1. Clinical Course and Disability. *Brain* 1989; 112:133-46

Weinshenker BG, Bass B, Rice GPA, Noseworthy J, *et al.* The Natural History of Multiple Sclerosis: A Geographically Based Study. 2. Predictive Value of the Early Clinical Course. *Brain* 1989; 112:1419-1428

Wheeler-Kingshott CA, Cercignani M. About 'axial' and 'radial' diffusivities. *Magn Reson Med* 2009; 61:1255-1260

Wheeler-Kingshott CAM, Hickman SJ, Parker GJM, *et al.* Investigating cervical spinal cord structure using axial diffusion tensor imaging. *Neuroimage* 2002; 16:93-102

Wheeler Kingshott CAM, Parker GJM, Symms MR, *et al.* ADC mapping of the human optic nerve: increased resolution, coverage, and reliability with CSF-suppressed ZOOM-EPI. *Magn Reson Med* 2002; 47:24-31

White ML, Zhang Y, Healey K. Cervical spinal cord multiple sclerosis: evaluation with 2D multi-echo recombined gradient echo MR imaging. *J Spinal Cord Med* 2011;34:93-98

Willer CJ, Dymont DA, Sadovnick AD, Rothwell PM, *et al.* Timing of birth and risk of multiple sclerosis: population based study. *BMJ* 2005; 330:120-5

Williams & Warwick. *Gray's Anatomy* 36<sup>th</sup> Edition, Norwich: Churchill Livingstone; 1980 p864-p896

Willoughby EW, Grochowski E, Li DK, Oger J, *et al.* Serial magnetic resonance scanning in multiple sclerosis: a second prospective study in relapsing patients. *Ann Neurol* 1989; 25:43-9

Wilm BJ, Svensson J, Henning A, *et al.* Reduced field-of-view MRI using outer volume suppression for spinal cord diffusion imaging. *Magn Reson Med*. 2007;57:625-30

Woff SD, Balaban RS. Magnetisation transfer contrast (MTC) and tissue water relaxation in vivo. *Magn Reson Med* 1989; 10:135-144

Xu J, Shimony JS, Klawiter EC, *et al.* Improved in vivo diffusion tensor imaging of human cervical spinal cord. *Neuroimage*. 2013;67:64-76

Yiannakas MC, Kearney H, Samson RS, Chard DT, Ciccarelli O, Miller DH, *et al.* Feasibility of grey matter and white matter segmentation of the upper cervical cord in vivo: a pilot study with application to magnetisation transfer measurements. *Neuroimage* 2012;63:1054-9

Young AC, Saunders J, Ponsford JR. Mental change as an early feature of multiple sclerosis. *J Neurol Neurosurg Psychiatry* 1976; 39:1008-1013

Zackowski KM, Smith SA, Reich DS, Gordon-Lipkin E, *et al.* Sensorimotor dysfunction in multiple sclerosis and column-specific magnetisation transfer-imaging abnormalities in the spinal cord. *Brain* 2009; 132:1200-1209

Zajicek JP, Wing M, Scolding NJ, Compston DA. Interactions between oligodendrocytes and microglia. A major role for complement and tumour necrosis factor in oligodendrocyte adherence and killing. *Brain* 1992; 115:1611-1631

Zhang J, Jones M, DeBoy CA, et al. Diffusion tensor magnetic resonance imaging of Wallerian degeneration in rat spinal cord after dorsal root axotomy. *J Neurosci.* 2009;29:3160-71

Zhang H, Schneider T, Wheeler-Kingshott CA, Alexander DC. NODDI: practical in vivo neurite orientation dispersion and density imaging of the human brain. *Neuroimage.* 2012;61:1000-16

Zhao W, Cohen-Adad J, Polimeni JR, Keil B, Guerin B, Setsompop K, Serano P, Mareyam A, Hoecht P, Wald LL. Nineteen-channel receive array and four-channel transmit array coil for cervical spinal cord imaging at 7T. *Magn Reson Med.* 2013 Aug 20. doi: 10.1002/mrm.24911. [Epub ahead of print]

Zivadinov R, Banas AC, Yella V, Abdelrahman N, Weinstock-Guttman B, Dwyer MG. Comparison of three methods for measurement of cervical cord atrophy in multiple sclerosis. *AJNR Am J Neuroradiol*, 2008;29(2):319-325

Zollinger LV, Kim TH, Hill K, et al. Using diffusion tensor imaging and immunofluorescent assay to evaluate the pathology of multiple sclerosis. *J Magn Reson Imaging.* 2011;33:557-64